KARADENİZ TECHNICAL UNIVERSITY
THE GRADUATE SCHOOL OF NATURAL AND APPLIED SCIENCES

DEPARTMENT OF GEOMATICS ENGINEERING

INVESTIGATION OF THE EFFECTS OF CLIMATE CHANGE IN AFGHANISTAN USING REMOTE SENSING TECHNIQUES

MASTER THESIS

Abdul Baset YARASH

NOVEMBER 2024
TRABZON

KARADENİZ TECHNICAL UNIVERSITY

THE GRADUATE SCHOOL OF NATURAL AND APPLIED SCIENCES

DEPARTMENT OF GEOMATICS ENGINEERING

INVESTIGATION OF THE EFFECTS OF CLIMATE CHANGE IN AFGHANISTAN USING REMOTE SENSING TECHNIQUES

Abdul Baset YARASH

ORCID : - - -

This thesis is accepted to give the degree of

MASTER OF SCIENCE

By

The Graduate School of Natural and Applied Sciences at
Karadeniz Technical University

The Date of Submission : 25 / 10 /2024

The Date of Examination : 14 / 11 /2024

Supervisor : Assoc. Prof. Dr. Volkan YILMAZ

ORCID : - - -

Trabzon 2024

ACKNOWLEDGMENTS

I am very pleased to have spent a term of my life pursuing education. This thesis is a milestone on my way to obtaining a master's degree in Geomatics from Karadeniz Technical University.

I am grateful for everything my supervisor, Assoc. Prof. Dr. Volkan YILMAZ, has done to help me advance in my academic career. He has been a fantastic mentor and advisor to me. From the beginning of my studies, he was a huge advisor, and I consider myself fortunate to have had the opportunity to work under his wise supervision.

I would like to sincerely thank the respected members of the jury, Assoc. Prof. Dr. Saygın ABDIKAN and Assoc. Prof. Dr. Esra TUNÇ GÖRMÜŞ, for their valuable guidance and support in the completion of this thesis. Their precise advice and constructive feedback greatly enhanced the quality of the work and helped achieve the research objectives. I hope this work serves as a small token of our gratitude for their tireless efforts and sincere support.

I would like to sincerely thank my wonderful parents, my brother Muhammad Yusuf YARASH. They have continuously provided me with steadfast support and patience over the highs and lows of my academic career. Their unselfishness and belief in my potential form the basis of my strength and have a significant influence on my academic achievement. They have impacted my life in ways that go far beyond just helping.

Lastly, I would want to convey my sincere gratitude to the Republic of Turkey's government and the nation's generous citizens. I am particularly appreciative of Karadeniz Technical University's committed personnel and distinguished teachers, who throughout my academic career gave me every resource and support imaginable and never hesitated to lend a helping hand. I am so grateful for their unwavering commitment and generosity.

Abdul Baset YARASH

Trabzon 2024

DECLARATION

I hereby declare that I have completed this study entitled " Investigation of The Effects of Climate Change İn Afghanistan Using Remote Sensing Techniques ", which I submitted as a Master Thesis, under the supervision of my advisor, Assoc. Prof. Dr. Volkan YILMAZ, from start to finish. I confirm that I collected the data/samples myself, conducted the experiments/analyses in relevant laboratories or supervised them, and accurately presented any information obtained from other sources in both the text and the references. I further confirm that I complied with scientific research and ethical standards during the study process and acknowledge that I will accept any legal consequences in case of any violations discovered. 14/11/2024

Abdul Baset YARASH

TABLE OF CONTENTS

Page No

ACKNOWLEDGMENTS III
DECLARATION IV
TABLE OF CONTENTS V
SUMMARY VII
ÖZET VIII
LIST OF FIGURES X
LIST OF TABLES XV
ACRONYMS XVII
1. GENERAL INFORMATION 1
1.1. Introduction 1
1.2. Research Problem 2
1.3. Structure of the Thesis 3
1.4. Literature Review 4
2. MATERIALS AND METHOD 12
2.1. Study Area 12
2.1.1. Climate of Afghanistan 13
2.2. Climate Parameters Used in This Thesis 15
2.2.1. Normalized Difference Vegetation Index (NDVI) 15
2.2.2. Land Surface Temperature (LST) 15
2.2.3. VCI, TCI and VHI 16
2.2.4. Air Temperature (Ta) 17
2.2.5. Actual Evapotranspiration (AET) and Potential Evapotranspiration (PET) 18
2.2.6. Precipitation Parameter 19
2.2.7. Soil Moisture Parameter 20
2.2.8. Wind Speed Parameter 20
2.2.9. Exploration of Forest Loss 21
2.3. Data Collection and Software Used 21
2.3.1. Google Earth Engine Programing 23
2.4. Methodology 23
2.4.1. Statistical Analysis 25
2.4.2. Time Series Analysis 26
2.4.3. Type of Data for Time Series Analysis 26
2.4.4. Trend Analysis 26

2.4.5. Pearson’s Correlation Coefficient 27
2.4.6. Statistical Tests to Investigate the Trend 28
2.4.7. Trend Detection Using the Mann-Kendall Test 28
2.4.8. Homogeneity Test 30
2.4.9. ARIMA Model 30
2.4.10. Model Evaluation Metrics 32
3. RESULTS AND DISCUSSION 34
3.1. Results From the Monthly Trend Analysis 34
3.2. Results From the Seasonal Trend Analysis 57
3.3. Results From the Annually Trend Analysis 72
3.4. Examination Of Forests Change in Afghanistan 82
3.5. Results Based on Pearson's Correlation Coefficient 84
3.6. Results Based on The Mann-Kendall Test 101
3.7. Results Based on The Homogeneity Test 114
3.8. Results Based on ARIMA Model 138
3.8.1. Model Accuracy 139
3.8.2. Examining The Predicted Results of Climate Parameters 140
3.9. Drought Monitoring 154
3.10.Results Based on The Regional Scale 162
4. DISCUSSION 200
5. CONCLUSION 207
6. SUGGESTIONS 209
7. REFERENCE 210
RESUME

Master Thesis

SUMMARY

INVESTİGATİON OF THE EFFECTS OF CLİMATE CHANGE İN AFGHANİSTAN USİNG REMOTE SENSİNG TECHNİQUES

Abdul Baset YARASH

Karadeniz Technical University
The Graduate School of Natural and Applied Sciences
Department of Geomatics Engineering
Supervisor: Assoc. Prof. Dr. Volkan YILMAZ
2024, 216 Pages,

Afghanistan has not been immune from significant changes in climate parameters affected by climate change in recent decades. The main purpose of this study is to use remote sensing methods to investigate the effect of climate change in Afghanistan. In this study, data from various sensors on the Google Earth Engine platform between 2000 and 2023 were used to investigate the climate parameters such as NDVI, VCI, TCI, VHI, LST, air temperature (Ta), precipitation, soil moisture, AET, PET, wind speed, and forest loss. These climate parameters were examined on a monthly, seasonal, and annual basis for each of the eight areas that make up Afghanistan. The status of trends was analyzed using the Mann-Kendall and homogeneity tests, while Pearson's correlation coefficient examined parameter associations. The ARIMA model predicted trends (2024–2035) except for the forest loss parameter, with accuracy validated by R^2, RMSE, and MAE. The results showed that NDVI increased while LST decreased in most regions, except in the north, where NDVI declined despite its overall high values. Precipitation trends varied, but soil moisture decreased consistently across all regions due to insufficient rainfall and stony soils. The western region experienced the highest wind speeds, impacting vegetation and soil moisture. Agricultural drought was most severe in the north and west, while deforestation declined from 2000 to 2023, except for a rise in 2023. Lastly, seasonal maps were created for these parameters in the following years: 2000, 2012, and 2023.

Key Words: Climate Change, Remote Sensing, Climatic Parameters, Time Series Analyse, ARIMA Model

Yüksek Lisans

ÖZET

UZAKTAN ALGILAMA TEKNİKLERİ KULLANILARAK AFGANİSTAN'DA İKLİM DEĞİŞİKLİĞİNİN ETKİLERİNİN İNCELENMESİ

Abdul Baset YARASH

Karadeniz Teknik Üniversitesi
Fen Bilimleri Enstitüsü
Harita Mühendisliği Anabilim Dalı
Danışman: Doç. Dr. Volkan YILMAZ
2024, 216 Sayfa

Son yıllarda, iklim değişikliği dünya genelindeki çevresel göstergeler üzerinde önemli etkiler yaratmıştır ve Afganistan bu değişikliklerden muaf kalmamıştır. Bu tezin ana amacı, uzaktan algılama yöntemleri aracılığıyla Afganistan'daki iklim değişikliğinin etkilerini incelemek için çeşitli iklim parametreleri analiz edilmiştir. Bu çalışmada, NDVI, VCI, TCI, VHI, LST, Hava Sıcaklığı (Ta), Yağış, Toprak Nemi, Gerçek Buharlaşma (AET), Potansiyel Buharlaşma (PET), Rüzgar hızı ve Orman kaybı iklim parametreleri, 2000 ile 2023 yılları arasında Google Earth Engine platformunda farklı sensörlerden elde edilen verilerle incelenmiştir. Bu iklim parametreleri Afganistan'ın sekiz bölgesinde uygulanmıştır ve her bir bölge için aylık, mevsimsel ve yıllık analiz edilmiştir. Parametreler arasındaki ilişkileri incelemek için Pearson korelasyon katsayısı kullanılmış, Önemli eğilimleri kontrol etmek için Mann-Kendall testi ve homojenlik testi uygulanmıştır. Ayrıca orman kaybı parametresi harıc diğer iklim parametreleri de ARIMA modeli kullanılarak 2024-2035 yılları arasında trendin yönü tahmin edilmiştir. Model tahminlerini değerlendirmek için R^2, RMSE ve MAE kriterleri kullanılmış ve tatmin edici sonuçlar elde edilmiştir. Sonuçlar, Afganistan genelinde NDVI artışının ve LST düşüşünün kuzey bölgesi hariç her yerde gözlemlendiğini gösterdi. Kuzeyde, en yüksek NDVI değerlerine rağmen NDVI'nın benzersiz bir şekilde azaldığı tespit edildi. Yağış trendleri kuzey, kuzeydoğu ve batıda azalırken, diğer bölgelerde arttı; ancak yağış artışı, tüm bölgelerde düşüş gösteren toprak nemini yenilemek için yetersiz kaldı. Batı bölgesi, NDVI, toprak nemi ve AET'yi etkileyen en yüksek rüzgar hızını (11 m/s) kaydetti. Kuraklık indeksleri (VCI, TCI, VHI), kuzey ve batının en savunmasız bölgeler olduğunu, kuzeydoğu ve güneydoğunun ise zaman zaman tarımsal kuraklık yaşadığını ortaya koydu. PET parametresi doğuda belirgin mevsimsel ve yıllık dalgalanmalar gösterirken, diğer bölgelerde anlamlı bir yıllık eğilim bulunamadı. Toprak nemindeki düşüş,

taşlı ve kumlu topraklar ile kuzeydoğu ve merkezdeki uzun süreli kar örtüsüne bağlandı. Orman örtüsü en fazla doğu, güneydoğu ve kuzeydoğuda gözlemlenirken, ormansızlaşma 2000-2023 yılları arasında azalan bir eğilim sergiledi ancak 2023'te yeniden artış kaydedildi. Pearson korelasyon katsayısı, iklimsel parametreler arasında güçlü bir ilişki olduğunu göstererek verilerin yüksek güvenilirliğini doğruladı.

Anahtar Kelimeler: İklim Değişikliği, Uzaktan Algılama, İklim Parametreleri, Zaman Serisi Analizi, ARIMA Modeli

LIST OF FIGURES

Page No

Figure 1. Study Area. 12
Figure 2. The effects of climate on the living conditions of the people of Afghanistan. 14
Figure 3. Methodological framework in this study. 25
Figure 4. Structure of the ARIMA model. 32
Figure 5. Monthly mean NDVI time series trend analysis. 36
Figure 6. Monthly mean LST time series trend analysis. 38
Figure 7. Monthly mean Ta time series trend analysis. 40
Figure 8. Monthly Total AET time series trend analysis. 42
Figure 9. Monthly Total PET time series trend analysis. 44
Figure 10. Monthly mean Precipitation time series trend analysis. 46
Figure 11. Monthly mean Soil Moisture time series trend analysis. 48
Figure 12. Monthly mean Wind Speed time series trend analysis. 50
Figure 13. Monthly mean VCI time series trend analysis. 52
Figure 14. Monthly mean TCI time series trend analysis. 54
Figure 15. Monthly mean VHI time series trend analysis. 56
Figure 16. Seasonal trend analysis of NDVI, LST, Ta, AET, PET, Precipitation, Soil Moisture and Wind speed parameters in throughout Afghanistan. 58
Figure 17. Seasonal trend analysis of NDVI, LST, Ta, AET, PET, Precipitation, Soil Moisture and Wind speed parameters in North Region. 60
Figure 18. Seasonal trend analysis of NDVI, LST, Ta, AET, PET, Precipitation, Soil Moisture and Wind speed parameters in Northeastern region. 63
Figure 19. Seasonal trend analysis of NDVI, LST, Ta, AET, PET, Precipitation, Soil Moisture and Wind speed parameters in South Region. 64
Figure 20. Seasonal trend analysis of NDVI, LST, Ta, AET, PET, Precipitation, Soil Moisture and Wind speed parameters in Southeastern Region. 66
Figure 21. Seasonal trend analysis of NDVI, LST, Ta, AET, PET, Precipitation, Soil Moisture and Wind speed parametes in Western Region. 67
Figure 22. Seasonal trend analysis of NDVI, LST, Ta, AET, PET, Precipitation, Soil Moisture and Wind speed parameters in Eastern Region. 69
Figure 23. Seasonal trend analysis of NDVI, LST, Ta, AET, PET, Precipitation, Soil Moisture and Wind speed parameters in Central Region. 70
Figure 24. Seasonal trend analysis of NDVI, LST, Ta, AET, PET, Precipitation, Soil Moisture and Wind speed parameters in West Central Region. 72

Figure 25. Annually trend analysis of NDVI, LST, Ta, AET, PET, Precipitation, Soil Moisture, VCI, TCI, VHI and Wind speed parameter in throughout Afghanistan. 73
Figure 26. Annually trend analysis of NDVI, LST, Ta, AET, PET, Precipitation, Soil Moisture, VCI, TCI, VHI and Wind speed parameters in North region. 74
Figure 27. Annually trend analysis of NDVI, LST, Ta, AET, PET, Precipitation, Soil Moisture, VCI, TCI, VHI and Wind speed parameters in Northeastern region. 75
Figure 28. Annually trend analysis of NDVI, LST, Ta, AET, PET, Precipitation, Soil Moisture, VCI, TCI, VHI and Wind speed parameters in South region. 76
Figure 29. Annually trend analysis of NDVI, LST, Ta, AET, PET, Precipitation, Soil Moisture, VCI, TCI, VHI and Wind speed parameters in Southeastern region. 77
Figure 30. Annually trend analysis of NDVI, LST, Ta, AET, PET, Precipitation, Soil Moisture, VCI, TCI, VHI and Wind speed parameters in Western region. 78
Figure 31. Annually trend analysis of NDVI, LST, Ta, AET, PET, Precipitation, Soil Moisture, VCI, TCI, VHI and Wind speed parameters in Eastern region. 79
Figure 32. Annually trend analysis of NDVI, LST, Ta, AET, PET, Precipitation, Soil Moisture, VCI, TCI, VHI and Wind speed parameters in Central region. 80
Figure 33. Annually trend analysis of NDVI, LST, Ta, AET, PET, Precipitation, Soil Moisture, VCI, TCI, VHI and Wind speed parameters in West Central region. 81
Figure 34. Amount of forest loss (deforestation areas) between the 2000-2023 year. 83
Figure 35. Correlation Coefficient between the parameters in throughout Afghanistan. ... 85
Figure 36. Correlation Coefficient between the parameters in North region. 88
Figure 37. Correlation Coefficient between the parameters in Northeastern region. 90
Figure 38. Correlation Coefficient between the parameters in South region. 92
Figure 39. Correlation Coefficient between the parameters in Southeastern region. 94
Figure 40. Correlation Coefficient between the parameters in Western region. 96
Figure 41. Correlation Coefficient between the parameters in Eastern region. 97
Figure 42. Correlation Coefficient between the parameters in Central region. 99
Figure 43. Correlation Coefficient between the parameters in West Central region. 100
Figure 44. Significant change points based on the Pettitt's test in the mean of NDVI values for annually (2000–2023). 116
Figure 45. Significant change points based on the Pettitt's test in the mean of LST values for annually (2000–2023). 118
Figure 46. Significant change points based on the Pettitt's test in the mean of Ta values for annually (2000–2023). 120
Figure 47. Significant change points based on the Pettitt's test in the mean of AET values for annually (2000–2023). 122

Figure 48. Significant change points based on the Pettitt's test in the mean of PET values for annually (2000–2023). 124
Figure 49. Significant change points based on the Pettitt's test in the mean of Precipitation values for annually (2000–2023). 126
Figure 50. Significant change points based on the Pettitt's test in the mean of Soil Moisture values for annually (2000–2023). 128
Figure 51. Significant change points based on the Pettitt's test in the mean of Wind Speed values for annually (2000–2023). 130
Figure 52. Significant change points based on the Pettitt's test in the mean of VCI values for annually (2000–2023). 132
Figure 53. Significant change points based on the Pettitt's test in the mean of TCI values for annually (2000–2023). 133
Figure 54. Significant change points based on the Pettitt's test in the mean of VHI values for annually (2000–2023). 135
Figure 55. Significant change points based on the Pettitt's test in the mean of HGFC values for annually (2000–2023). 137
Figure 56. NDVI prediction values from 2024 to 2035. 141
Figure 57. LST prediction values from 2024 to 2035. 143
Figure 58. Ta prediction values from 2024 to 2035. 144
Figure 59. AET prediction values from 2024 to 2035. 147
Figure 60. PET prediction values from 2024 to 2035. 148
Figure 61. Precipitation prediction values from 2024 to 2035. 150
Figure 62. Soil moisture prediction values from 2024 to 2035. 152
Figure 63. Wind speed prediction values from 2024 to 2035. 153
Figure 64. VCI prediction values from 2024 to 2035. 156
Figure 65. TCI prediction values from 2024 to 2035. 160
Figure 66. VHI prediction values from 2024 to 2035. 161
Figure 67. Spatial distribution of NDVI for 2000 year: 2000-year(a), Spring(b), Summer(c), Fall(d), Winter(e). 163
Figure 68. Spatial distribution of NDVI for 2012 year: 2012-year(a), Spring(b), Summer(c), Fall(d), Winter(e). 164
Figure 69. Spatial distribution of NDVI for 2023 year: 2023-year(a), Spring(b), Summer(c), Fall(d), Winter(e). 165
Figure 70. Spatial distribution of LST for 2000 year: 2000-year(a), Spring(b), Summer(c), Fall(d), Winter(e). 166
Figure 71. Spatial distribution of LST for 2012 year: 2012-year(a), Spring(b), Summer(c), Fall(d), Winter(e). 167
Figure 72. Spatial distribution of LST for 2023 year: 2023-year(a), Spring(b), Summer(c), Fall(d), Winter(e). 168

Figure 73. Spatial distribution of AET for 2000 year: 2000-year(a), Spring(b), Summer(c), Fall(d), Winter(e). 169

Figure 74. Spatial distribution of AET for 2012 year: 2012-year(a), Spring(b), Summer(c), Fall(d), Winter(e). 170

Figure 75. Spatial distribution of AET for 2023 year: 2023-year(a), Spring(b), Summer(c), Fall(d), Winter(e). 171

Figure 76. Spatial distribution of PET for 2000 year: 2000-year(a), Spring(b), Summer(c), Fall(d), Winter(e). 172

Figure 77. Spatial distribution of PET for 2012 year: 2012-year(a), Spring(b), Summer(c), Fall(d), Winter(e). 173

Figure 78. Spatial distribution of PET for 2023 year: 2023-year(a), Spring(b), Summer(c), Fall(d), Winter(e). 174

Figure 79. Spatial distribution of precipitation for 2023 year: 2023-year(a), Spring(b), Summer(c), Fall(d), Winter(e). 175

Figure 80. Spatial distribution of precipitation for 2012 year: 2012-year(a), Spring(b), Summer(c), Fall(d), Winter(e). 176

Figure 81. Spatial distribution of Precipitation for 2023 year: 2023-year(a), Spring(b), Summer(c), Fall(d), Winter(e). 177

Figure 82. Spatial distribution of Soil Moisture for 2000 year: 2000-year(a), Spring(b), Summer(c), Fall(d), Winter(e). 178

Figure 83. Spatial distribution of Soil Moisture for 2012 year: 2012-year(a), Spring(b), Summer(c), Fall(d), Winter(e). 179

Figure 84. Spatial distribution of Soil Moisture for 2023 year: 2023-year(a), Spring(b), Summer(c), Fall(d), Winter(e). 180

Figure 85. Spatial distribution of Ta for 2000 year: 2000-year(a), Spring(b), Summer(c), Fall(d), Winter(e). 181

Figure 86. Spatial distribution of Ta for 2012 year: 2012-year(a), Spring(b), Summer(c), Fall(d), Winter(e). 182

Figure 87. Spatial distribution of Ta for 2023 year: 2023-year(a), Spring(b), Summer(c), Fall(d), Winter(e). 183

Figure 88. Spatial distribution of Wind Speed for 2000 year: 2000-year(a), Spring(b), Summer(c), Fall(d), Winter(e). 184

Figure 89. Spatial distribution of Wind Speed for 2012 year: 2012-year(a), Spring(b), Summer(c), Fall(d), Winter(e). 185

Figure 90. Spatial distribution of Wind Speed for 2023 year: 2023-year(a), Spring(b), Summer(c), Fall(d), Winter(e). 186

Figure 91. Spatial distribution of VCI for 2000 year: 2000-year(a), Spring(b), Summer(c), Fall(d), Winter(e). 187

Figure 92. Spatial distribution of VCI for 2012 year: 2012-year(a), Spring(b), Summer(c), Fall(d), Winter(e). 188

Figure 93. Spatial distribution of VCI for 2023 year: 2023-year(a), Spring(b), Summer(c), Fall(d), Winter(e). 189
Figure 94. Spatial distribution of TCI for 2000 year: 2000-year(a), Spring(b), Summer(c), Fall(d), Winter(e). 190
Figure 95. Spatial distribution of TCI for 2012 year: 2012-year(a), Spring(b), Summer(c), Fall(d), Winter(e). 191
Figure 96. Spatial distribution of TCI for 2023 year: 2023-year(a), Spring(b), Summer(c), Fall(d), Winter(e). 192
Figure 97. Spatial distribution of VHI for 2000 year: 2000-year(a), Spring(b), Summer(c), Fall(d), Winter(e). 193
Figure 98. Spatial distribution of VHI for 2012 year: 2012-year(a), Spring(b), Summer(c), Fall(d), Winter(e). 194
Figure 99. Spatial distribution of VHI for 2023 year: 2023-year(a), Spring(b), Summer(c), Fall(d), Winter(e). 195
Figure 100. Forest areas: Eastern region(a), Southeastern region(b). 196
Figure 101. Forest areas: North region(a), Northeastern region(b). 197
Figure 102. Forest areas: Central region(a), West Central region(b). 198
Figure 103. Forest areas: Western region(a), South region(b). 199
Figure 104. Mean LST difference in each region. 201
Figure 105. Mean Ta difference in each region. 202

LIST OF TABLES

Page No

Table 1. Drought Class based on VCI, TCI, and VHI values..... 17

Table 2. Type of Precipitation in mm/day..... 20

Table 3. Type of Wind Speed..... 21

Table 4. Remote sensing data used in this thesis..... 22

Table 5. Interpret of the Pearson correlation coefficient..... 28

Table 6. Z-value of the Mann-Kendall test for the monthly, seasonal and annual NDVI between the 2000-2023 years..... 102

Table 7. Z-value of the Mann-Kendall test for the monthly, seasonal and annual LST (C˚) between the 2000-2023 years..... 103

Table 8. Z-value of the Mann-Kendall test for the monthly, seasonal and annual Ta (C˚) between the 2000-2023 years..... 105

Table 9. Z-value of the Mann-Kendall test for the monthly, seasonal and annual AET between 2000-2023 years..... 106

Table 10. Z-value of the Mann-Kendall test for the monthly, seasonal and annual PET between the 2000-2023 years..... 107

Table 11. Z-value of the Mann-Kendall test for the monthly, seasonal and annual Precipitation between the 2000-2023 years..... 109

Table 12. Z-value of the Mann-Kendall test for the monthly, seasonal and annual Soil Moisture between the 2000-2023 years..... 110

Table 13. Z-value of the Mann-Kendall test for the monthly, seasonal and annual Wind speed between the 2000-2023 years..... 111

Table 14. Z-value of the Mann-Kendall test for the monthly, seasonal and annual VCI between the 2000-2023 years..... 112

Table 15. Z-value of the Mann-Kendall test for the monthly, seasonal and annual TCI between the 2000-2023 years..... 113

Table 16. Z-value of the Mann-Kendall test for the monthly, seasonal and annual VHI between the 2000-2023 years..... 114

Table 17. P-value of Homogeneity Test (Pettitt's test) for NDVI Values..... 115

Table 18. P-value of Homogeneity Test (Pettitt's test) for LST Values..... 117

Table 19. P-value of Homogeneity Test (Pettitt’s test) for Ta Values..... 119

Table 20. P-value of Homogeneity Test (Pettitt’s test) for AET Values..... 121

Table 21. P-value of Homogeneity Test (Pettitt’s test) for PET Values..... 123

Table 22. P-value of Homogeneity Test (Pettitt’s test) for Precipitation Values..... 125

Table 23. P-value of Homogeneity Test (Pettitt’s test) for Soil Moisture Values..... 127

Table 24. P-value of Homogeneity Test (Pettitt’s test) for Wind Speed Values..... 129

Table 25. P-value of Homogeneity Test (Pettitt's test) for VCI Values. 131
Table 26. P-value of Homogeneity Test (Pettitt's test) for TCI Values. 131
Table 27. P-value of Homogeneity Test (Pettitt's test) for VHI Values. 134
Table 28. P-value of Homogeneity Test (Pettitt's test) for HGFC Values. 136
Table 29. Parameters of the model (p,d,q)(sp,sd,sq) for NDVI, LST, Ta, AET and PET parameters. 138
Table 30. Parameters of the model (p,d,q)(sp,sd,sq) for precipitation, soil moisture, wind speed, VCI, TCI and VHI parameter. 138
Table 31. ARIMA model accuracy 139
Table 32. Average annual VCI value. 155
Table 33. Average annual TCI value. 158
Table 34. Average annual VHI value. 159

ACRONYMS

GEE	: Google Earth Engine
NDVI	: Normalized Difference Vegetation Index
LST	: Land Surface Temperature
Ta	: Air Temperature
AET	: Actual Evapotranspiration
PET	: Potential Evapotranspiration
Precipit	: Precipitation
S-M	: Soil Moisture
W-S	: Wind Speed
VCI	: Vegetation Condition Index
TCI	: Temperature Condition Index
VHI	: Vegetation Health Index
HGFC	: Hansen Global Forest Change
Eta	: Actual Evapotranspiration
ARIMA	: Autoregressive Integrated Moving Average
ERA5	: European Reanalysis 5th Generation
CHIRPS	: Climate Hazards Group InfraRed Precipitation with Station data
CC	: Coefficient of Determination
RMSE	: Root Mean Square Error
MAE	: Mean Absolute Error
GLEAM	: Global Land Evaporation Amsterdam Model
ASCAT	: Advanced SCAT terometer
SMOS	: Soil Moisture and Ocean Salinity
TG	: Ground Temperature
ACF	: Autocorrelation Function
PACF	: Partial Autocorrelation Functi

1. GENERAL INFORMATION

1.1. Introduction

Before the emergence of man, events such as floods, earthquakes, volcanic eruptions, storms, etc. caused the face of the earth to change. Even though these changes were destructive and did not involve humans, they played a crucial role in shaping the geomorphological evolution of the earth. The issue of change of use has taken on the color and smell of destruction since the time when man set foot on the earth. Burning the forest and allocating it to agricultural land to obtain its basic needs was the first human action to change the face of the earth. Although humans have always been changing the earth for many years, the current measurements of the earth's change indicate the highest rate of change in the entire history of human life. These changes, which include direct and indirect human interventions, can cause serious changes to about half of the earth's land surface at the end of this century, and terrestrial ecosystems will undergo many changes (Akbari et al., 2016). And in societies like Afghanistan that have limited water resources and do not have the ability to optimally manage resources and adapt to climate changes, it will suffer more.

Afghanistan is a country located in the heart of the Asian continent and is located in the arid and semi-arid regions of the world with a young and growing population. Most regions of this country have cold winters and very hot summers. About 63% of this country is mountainous, which is the source of the waters of the rivers, which mostly enter the neighboring countries after traveling. At the same time, Afghanistan has not been able to use its water resources properly due to the lack of infrastructure and stable governments. For this reason, the country has always been prone to droughts and floods (URL-1, 2024). This country is located far from the sea, and therefore it is not humid, and the relative humidity is low and clouds and fog form less during the year. Its winters are very cold up to -20 C˚, and its summers are very hot above 40 C˚. The weather varies from one province to another and from one city to another. Rainfall also varies in different places and fluctuates between 100-400 mm. This value is between 250-400 mm in the eastern regions and between 100-150 mm in the western and southwestern regions. In the central regions, due to higher altitudes and more rainfall, the air is colder than other regions, but in the southern and western regions, due to a little rainfall. The weather is warmer and has hot and dry summers and milder winters (URL-2, 2024).

In recent decades, increasing heat, frequent droughts, changes in rainfall, deforestation, unseasonal rains, floods caused by climate change, and increasing greenhouse gases have caused Afghanistan to witness major climate changes, and it has led to the displacement of people, the reduction of livestock, and the destruction of thousands of hectares of agricultural land in Afghanistan. To contain and investigate the consequences caused by climate change, the use of remote sensing is a suitable tool to investigate climate parameters. The use of remote sensing data to investigate and analyze climate parameters is a relatively new method that significantly reduces the cost of estimating by the classical method. Remote sensing images are a suitable tool for preparing maps of climatic indicators due to their wide and timely coverage as well as high accuracy. Today, the use of remote sensing technology to monitor changes has received major attention, and numerous studies were conducted in this field in Afghanistan and other parts of the world (Mehrabi, 2019). The research conducted to investigate climate change in Afghanistan will be reviewed in the literature review section.

Various climate parameters have been used to study climate change thus far. Research and dissertations in this field have predominantly focused on different climate parameters. In this thesis, several parameters were utilized to examine climate change across Afghanistan. These parameters were selected due to the significant relationships they share; a change in one can lead to alterations in the others. For instance, changes in air temperature not only affect land surface temperature but also influence soil moisture and nutrient levels, which, in turn, impact the physiological characteristics, community structure, and population dynamics of plants (Nabizada et al., 2022).

1.2. Research Problem

In recent years, significant research has been conducted on climate and environmental changes in Afghanistan using remote sensing techniques. However, much of this research has focused on specific regions, short-term periods, or individual environmental factors, leaving gaps in our understanding of the broader, long-term impacts of climate change (NUPI, 2021). Furthermore, Afghanistan's diverse topography and climatic zones-from arid deserts to mountainous regions-necessitate a more regionally nuanced analysis that takes into account the varied effects of climate change across different regions, such as the north, South, eastern, and central regions. Many past studies have not fully investigated the

complex interactions between the climate parameters that have had the most impact on climate change in Afghanistan over the past two decades (UNEP, 2023).

In this study, the effects of climate change across Afghanistan were investigated using a wide range of climate parameters such as Normalized Difference Vegetation Index (NDVI), Vegetation Condition Index (VCI), Temperature Condition Index (TCI), Vegetation Health Index (VHI), Land Surface Temperature (LST), Air Temperature (Ta), precipitation, soil moisture, Actual Evapotranspiration (AET), Potential Evapotranspiration (PET) and wind speed. The climate parameters were analyzed on monthly, seasonal, and annual scales, allowing for an in-depth study of environmental trends. Furthermore, deforestation between 2000 and 2023 is examined, providing insights into forest cover loss. To predict the trends of these climatic parameters up to 2035, the ARIMA model was used to forecast future changes and provide a broader understanding of Afghanistan's vulnerability to climate change.

1.3. Structure of the Thesis

This thesis consists of 7 parts. The first part includes general information about the use of remote sensing techniques for climate studies, the research problem, the structure of the thesis, and literature review. The second part of the thesis is materials and method, which includes the study area, climate of Afghanistan, climate parameters used in this thesis, data collection and software used, methodology, statistical analysis, and predictive model. The third part is the results of this thesis, and in this section, the data was analyzed in three time scales (monthly, seasonal, and seasonal) and in two spatial scales, and maps of each climate parameter were prepared for the 2000, 2012 and 2023 years. Also, in this section, the results of statistical tests, correlation coefficient and predictive model are included. The fourth part of the thesis is the discussion and comparison of the results with previous studies. The fifth section is a summary of the finding. The sixth part included the suggestions and limitations of this research, and the references used in the thesis were also included.

1.4. Literature Review

The literature review for this study is built upon an extensive examination of over 70 research articles, focussing on the use of remote sensing techniques to analyse climate and environmental changes in Afghanistan and globally. These studies cover a range of topics, including the application of climate parameters such as NDVI, LST, precipitation, soil moisture, ET, PET, and others, which are essential for assessing vegetation health, land surface temperature, and overall climatic conditions. Previous research has provided valuable insights into regional climate patterns, drought monitoring, and deforestation trends, but many have been limited to specific areas or time frames. This thesis builds upon the existing body of knowledge by integrating multiple agro-climatic parameters across broader spatial and temporal scales. The review highlights gaps in comprehensive studies that consider the effects of climate change on both vegetation and land degradation, setting the foundation for this research's contribution to a more holistic understanding of Afghanistan's changing environment.

The Food and Agriculture Organization of the United Nations and the International Institute for Applied Systems Analysis conducted research in cooperation with the government of Afghanistan (2019) regarding climate change in Afghanistan. In this research, temperature, precipitation, humidity, and evapotranspiration parameters were used in 8 regions of Afghanistan for investigation. The results of this study generally show that the weather conditions of Afghanistan will become hotter and drier in the future. As the average annual temperature from 1981-2010 and in the predicted years between 2041-2070 shows an increase of 2 to 2.8 C^0. It also shows the average annual rainfall of the period 1981-2010, which shows relatively moderate values in general and a pattern of decreasing rainfall along a section from the northeast to the southwest of Afghanistan. The projected future precipitation shows a similar spatial pattern, but the amount of annual precipitation may decrease slightly in the future. The results of this research show that rainfall amounts will change slightly in the northeast and northwest regions compared to 1981-2010, while the changes will be more significant in other regions. The decrease in rainfall will be more in the western-central and southern regions. It also shows the projected amount of annual moisture in the 2050s, indicating a worsening of the annual vertical water balance. In this research, the amount of actual evapotranspiration (ETa) is much lower than the reference

potential evapotranspiration (ETo), which indicates a very significant lack of seasonal or year-round moisture in the soil of Afghanistan.

Aich et al. (2017) conducted a study on climate change in Afghanistan using reanalysis and CORDEX-South Asia simulations. The study analyzed temperature, precipitation, standard evapotranspiration parameter and five additional climate parameters for extreme evaluations & used in agriculture. The results of research show that in addition to the already existing deficit in adaptation to current climate conditions, the situation will be aggravated in the future, particularly in the areas of water management and agriculture. Thus, the results of this study underline the importance of adaptation to climate change in Afghanistan. Nabizada et al. (2022) examined the dynamics of LST in Afghanistan between 2000 and 2021, evaluated the effect of factors such as soil moisture, precipitation and vegetation on LST. In this study, FLDAS, CHIRPS and MODIS data are used and the correlation between these data is analyzed using the regression method. The results of the research show that LST in Afghanistan during the studied period had a slightly decreasing but insignificant trend ($R = 0.2$, p-value = 0.25), while vegetation, precipitation and soil moisture had an increasing trend. It was found that soil moisture has the greatest effect on LST.

Salik and Karacabey (2019) carried out a study aimed at revealing NDVI changes that may indicate the phenological stages of agricultural products derived from Landsat 8 images. The research focused on the Balkh and Jawzjan regions of Afghanistan, analyzing NDVI variations from the beginning to the end of the growing season, which ultimately affect the final yield. Ganji and Kajisa (2019) researched the evaluation of the FAO-56 Penman-Monteith model using alternative climatic data in Afghanistan. The results of their study indicate that solar radiation, humidity, and wind speed have a direct effect on evapotranspiration. Mahasa et al. (2023) conducted a study to analyze the temporal changes of evapotranspiration (ET) between 2003 and 2021 in the Orange River Basin of South Africa-Lesotho, using a synergistic approach based on remote sensing. The research focused on assessing drought through ET, VCI, and precipitation parameters. The results demonstrated a direct correlation between ET, VCI, and precipitation. Additionally, Alahacoon and Edirisinghe (2022) explored drought using the Standardized Water Surface Index (SWSI). Their findings revealed a strong correlation between the Standardized Precipitation Index (SPI) and SWSI, with Pearson correlation coefficients ranging from 0.58 to 0.67, while the correlation between the VCI and SWSI ranged from 0.75 to 0.81.

A study by the National Environmental Protection Agency of the Islamic Republic of Afghanistan (n.d.) analyzed temperature and precipitation trends across Afghanistan from 1960 to 2008, with prediction extending from 2008 to 2090. The results indicate that the average annual temperature has risen by 0.6°C since 1960, with a decadal increase of approximately 0.13°C. Additionally, the average precipitation has slightly decreased, with a reduction of around 0.5 mm per month since 1960. The study also predicts that by the 2060s, the mean annual temperature will rise by 1.4°C to 4.0°C, and by the 2090s, it could increase by 2.0°C to 6.2°C. Precipitation projections for the 2090s suggest generally drier conditions, with changes ranging from a high of 40 mm to a mean decrease of 20 mm, and a low of -10 mm. The study further reveals that between 1990 and 2000, Afghanistan experienced an average loss of 29,400 hectares of forests annually, with a deforestation rate of 2.25%. This rate increased to 2.92% per year between 2000 and 2005, leaving forests to cover less than 2% of Afghanistan's land. Moreover, the conversion of pastures into dry wheat cultivation has exposed vast areas to wind and soil erosion.

In a study by Ganji and Kajisa (2018) the investigation of reference evapotranspiration using the Penman-Monteith Equation in the western basin of Afghanistan revealed that high temperature, low humidity, and wind speed significantly impact reference evapotranspiration. The results showed that evapotranspiration rates were highest from June to September, with the strongest relationship between error and wind speed compared to other variables. Additionally, a study by Prasad et al. (2023) examined actual evapotranspiration (ETa) in India over the period 1980–2018. The trend was analyzed using the Mann-Kendall test, and the results indicated an increase in ETa of 1.91 mm per year.

Also, research conducted by Dıkıcı and Aksel (2021) examined drought in Turkey using the NDVI and VCI indices, evaluating agricultural and forest areas separately. The findings indicated that the NDVI index was more suitable for drought monitoring in this region compared to the VCI index. Similarly, research by Qu and Hao (2018) analyzed agricultural drought in the African basin using the VCI, TCI, and VHI indices from 2000 to 2017. The study revealed an increase in drought and food insecurity, posing a significant threat to food security in the region. In another study, Ejaz et al. (2023) investigated drought in Saudi Arabia using VCI, TCI, VHI, SPEI, and evapotranspiration parameters. Pearson correlation analysis showed that VHI and SPEI are more effective for drought monitoring in ultra-arid regions with scarce data. Tehrani et al. (2022) conducted research using NDVI, SAVI, LST, VCI, TCI, VHI, and SPI indices to study drought, finding the highest correlation

between SPI, NDVI, and VCI. The results suggest that NDVI and VCI can be used as substitutes for SPI. In another study by GÜL (2023) the VCI, TCI and VHI indices were used to investigate drought in Turkey. The results of the study show that severe droughts occurred in Turkey between 2018 and 2021year.

In a separate investigation carried out by Zhao et al. (2021) the VCI, TCI, VHI, NDVI, LST, and TVDI parameters were used to examine drought. The results showed that the LST reconstructed by the ATC model significantly improved the accuracy of drought assessment. In most regions, the reconstructed TCI, VHI, and TVDI were found to be more reliable for monitoring drought conditions compared to the unreconstructed VCI. Additionally, the four drought parameters (TCI, VCI, VHI, and TVDI) demonstrated similar temporal and spatial patterns across the study area. In another research effort, Thilagaraj et al. (2021) investigated the drought situation, revealing that the area of healthy vegetation and drought-free land has significantly decreased from 934.29 to 107.83 square kilometers over the years, reaching alarming conditions. The findings indicated that the results of the VHI correlate with the agricultural drought compared to the Standard Precipitation Index (SPI), with both indices reflecting similar trends in precipitation dryness. Similarly, Mojaradi et al. (2020) utilized the Modified Standardized Precipitation Index (MSPI) and SPI index to examine drought conditions. Their results demonstrated that the accuracy of the MSPI was higher than that of the SPI, and subsequent evaluations with the VCI index showed a very strong correlation between the two. This indicates that the MSPI index largely corroborates the findings of the VCI index. Therefore, in areas where precipitation stations are scarce, the VCI index can be employed based on its acceptable level of accuracy.

Erdoğan (2023) performed an examination of various climatic parameters using the GEE platform. The analysis focused on regional trends, and a significant trend was established between 2000 and 2021 through the Mann-Kendall test. Additionally, research conducted by Bulut et al. (2019) investigated Turkish soil moisture values utilizing data from several sources, such as the Advanced Scatterometer (ASCAT), the Advanced Microwave Scanning Radiometer-Earth Observing System (AMSR-E), the European Space Agency Climate Change Initiative (ESA-CCI), the Antecedent Precipitation Index (API), and the Global Land Data Assimilation System (GLDAS). This analysis was supplemented by station-based calibrated soil moisture observations collected by the Turkish General Meteorological Department. The results demonstrated that the correlation between GLDAS

and ESA-CCI data with observational data was superior to that of the other datasets, with a correlation range of 0.57 to 0.87.

Yu et al., 2023 investigated soil moisture in Central Asia utilizing data from European Reanalysis-Interim (ERA5), Essential Climate Variables (ECV), the Famine Early Warning Systems Network (FEWS), and the Land Data Assimilation System (FLDAS). The findings revealed that ERA5 data demonstrated superior performance and greater potential for assessing soil moisture in the region. Similarly, Zha et al. (2022) conducted research on soil moisture in China, employing ERA5 and GLEAM data. Their results indicated that the performance of both datasets was compatible, with findings reported in pentad units. Additionally, Ahlmer et al. (2018) examined soil moisture in Sweden, focusing on rain-induced flooding. This research utilized ASCAT and SMOS data, and concluded that the approach of employing satellite-derived soil moisture data shows promise for enhancing flood reliability.

Abbas and Ahmad (2014) a study to investigate land surface temperature (LST) in Iraq using MODIS data. Their findings revealed a strong correlation between the daily average ground truth temperature (TG) and the daily average LST obtained from MODIS data. In another study, Zhao et al. (2020) examined LST in China for the period 2000-2017, utilizing MODIS data, which was subsequently evaluated against terrestrial data. The results demonstrated that MODIS data exhibited greater consistency with terrestrial observations, accurately depicting spatial and temporal changes in LST across annual, seasonal, and monthly scales. From 2003 to 2017, the overall annual average LST in China showed a weak upward trend, with significant uneven distribution across the country. Furthermore, Tang et al. (2024) investigated LST in China between 2000-2021 using MODIS data, comparing it with GLDAS and ERA5-Land datasets. Their results indicated that while MODIS shared similar spatial patterns with GLDAS and ERA5-Land, it offered higher image quality, greater spatial detail, and more apparent spatial discontinuity. Additionally, Alqasemi et al. (2020) researched LST and air temperature in the United Arab Emirates. Their analysis, which incorporated LST data from MODIS and air temperature data from ground stations, revealed a strong correlation between the two, with regression coefficients of $R^2 > 0.96$ for LSTd/Tmax and $R^2 > 0.94$ for LSTn/Tmin, and a Root Mean Square Error of approximately 1.75°C for LSTd/Tmax and 0.97°C for LSTn/Tmin.

In a study conducted by Nascimento et al. (2022), the air temperature and ground surface temperature were compared for the city of São Paulo, Brazil. The results indicated

that the mean mean absolute error (MAE) and mean root mean square error (RMSE) ranged from 1.2 to 1.9 ℃, with 83.0% of the values being less than or equal to 2.7 ℃. The coefficient of determination between air temperature and land surface temperature (LST) was found to be R = 0.81 during spring and summer, and R = 0.82 during autumn and winter.

Balas et al. (2023) investigated the effect of LST and land Ta on land use and land cover (LULC). The findings revealed a strong correlation between LST and air temperature, with a correlation coefficient of 0.97, and a temperature difference of 2.9°C between the maximum air temperature and LST. Additionally, the study by Gallo et al. (2011) examined the relationship between air and land surface temperature under clear and cloudy sky conditions. The results showed that the average difference between LST and Tair was less than 2°C in cloudy conditions, whereas minimum differences exceeding 2°C (and up to +7 °C) were observed under clear sky conditions. This study also considered factors such as wind speed, observation time of Tair and LST, season, the occurrence of rainfall at the time of observation, and NDVI values in evaluating the relationship between Tair and LST.

Mostarshed (2014) analyzed precipitation patterns over a 57-year period in Afghanistan, focusing on annual, seasonal, and monthly variations. The results indicated that the average annual precipitation is 256 mm; however, the annual time series did not reveal a significant trend at any meaningful level. This lack of significant change in annual rainfall is attributed to a shift in precipitation patterns from spring to summer. In a similar vein, McNally et al. (2022) recommended utilizing datasets for assessing rainfall in Central Asia and Afghanistan. Their research employed FLDAS and CHIRPS datasets, demonstrating their suitability for investigating precipitation in these regions. Another study by Suryavanshi et al. (2022) examined the precipitation characteristics of Afghanistan at the provincial scale using Climate Forecast System Reanalysis (CFSR) data and applied the Mann-Kendall test. The findings revealed that precipitation in Afghanistan is unevenly distributed both seasonally and annually, with the South and southwestern provinces being significantly drier compared to the relatively wetter north and northeastern regions. Notably, spring and winter account for approximately 80% of Afghanistan's annual rainfall; however, a significant decrease in precipitation during these seasons were observed. Additionally, the trend of declining annual rainfall has become evident across many provinces, and analyses of heavy rainfall parameter indicate a general trend toward drier conditions in Afghanistan.

Masood et al. (2023) conducted a study on rainfall in Pakistan utilizing the CHIRPS dataset. Additionally, Khan et al. (2023) investigated rainfall using data from the Tropical

Rainfall Measuring Mission (TRMM) for the period from 1998 to 2015. Their study employed various validation techniques, including the Mann-Kendall test, correlation coefficient, standard deviation, mean error (ME), mean absolute error (MAE), and root mean square error (RMSE), to assess the accuracy of the rainfall measurements.

Furthermore, Azad and Shabanzada (2020) conducted a study on wind speed in Iran, analyzing the data on both an annual and monthly basis. They applied the Mann-Kendall test to assess the trends in average wind speed, revealing a significant decreasing trend in the annual average wind speed. Moreover, Bazgir et al. (2018), performed a homogeneity analysis of temperature and precipitation data in Iran, utilizing homogeneity tests to evaluate the consistency of the data. Their findings indicated that 91.5% of the minimum temperature data and 88.5% of the maximum temperature data fell into the heterogeneity class, while the precipitation data were found to be homogeneous across all monitoring stations.

Modarresi et al. (2019) focusing on the regional analysis of climate change, utilized the Mann-Kendall test and homogeneity to examine trends, resulting in significant and reliable findings. In the research conducted by Kocsis et al. (2019) the authors illustrated the superior performance of both homogeneity and Mann-Kendall tests for trend analysis in precipitation time series in Keszthely, Western Hungary. Similarly, Ilori and Ajayi (2020) conducted a study aimed at change detection and trend analysis of future temperature and rainfall in West Africa, utilizing the Mann-Kendall and homogeneity tests to assess rainfall and temperature. Their findings indicate that, for the historical period (1961-2000), a turning point in the precipitation and temperature series occurred during the 1970s and 1980s, with a significant increasing trend in temperature observed across all climate regions.

The ARIMA model was widely utilised to forecast climate data in numerous studies and was acknowledged for its efficiency in time series analysis, where it was utilised to identify trends and seasonal patterns in the data (Zo et al., 2024). In research conducted by Sayah et al. (2020) the ARIMA model was employed to forecast temperature in Lebanon, with performance results demonstrating predictions at a 95% confidence level over three years. Another study by Sabzevari and Islamian (2024) applied the ARIMA model to temperature predictions in Iran, analyzing data from 1990 to 2021 and extending forecasts for the subsequent five years. The model was calibrated using the parameters (1,1,1), yielding improved results. Similarly, research by Dimri et al. (2020) employed the ARIMA model to investigate and predict rainfall and temperature in Uttarakhand, India. They used

the SARIMA seasonal model, achieving optimal results with parameters set as SARIMA (0,1,1) (0,1,1), which demonstrated high accuracy.

Zo et al. (2024) utilized the ARIMA model to predict climate changes and their subsequent impacts for decision-making in the insurance industry. The results of the model demonstrated its high performance in forecasting climatic parameters. In addition, a study by Gill et al. (2023) highlighted the ARIMA model's effectiveness, indicating its high accuracy in performance evaluations. Another study by Islami and Zari (2014) focused on predicting monthly precipitation and temperature using time series models, specifically the ARIMA model. The ARIMA model parameters, determined based on the Akaike Information Criterion (AIC) and variance, were found to be ARIMA (20,6,12) for precipitation and ARIMA (24,12,12) for temperature. The results indicated that the ARIMA model demonstrated higher accuracy in predicting monthly rainfall, with a correlation coefficient of 0.6 and a mean square error of 0.0003, compared to the predicted values for temperature

2. MATERIALS AND METHOD

2.1. Study Area

Afghanistan is a landlocked country between Central Asia and South Asia. It is located in the eastern hemisphere between 29° 31′ and 38°30′ north latitude and 75°31′ and 60°31′ east longitude from the Greenwich meridian (URL-14, 2024). Afghanistan has an area of 652,860 square kilometers, the 41st largest country in the world, and its population is about 40.5 million people, which ranks it 37th among countries in the world. Kabul is the capital of the country and largest city (URL-12, 2024). Afghanistan is divided into 8 regions (Figure1). They are North region, South region, Western region, Northeastern region, Eastern region, Southeastern region, Central region and West Central region (Akseer et al., 2016). The study areas in this thesis are the 8 regions of Afghanistan.

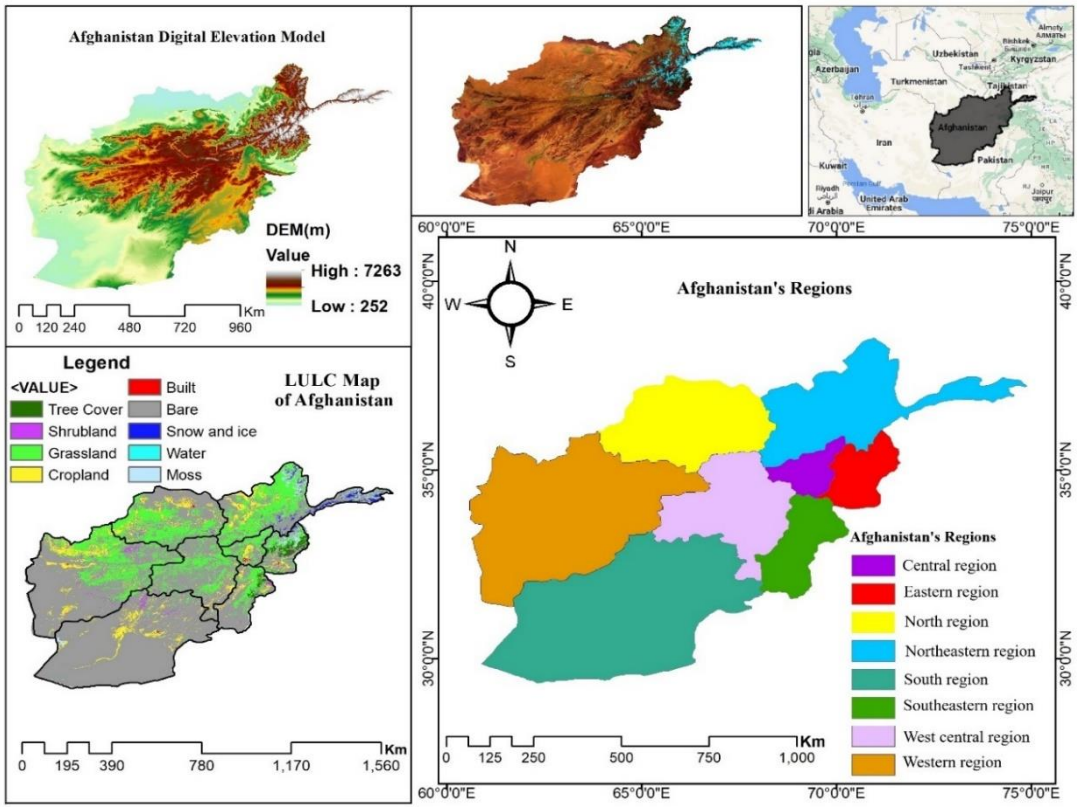

Figure 1. Study Area.

Afghanistan is a mountainous country, with most of the northeastern, central, and west-central regions covered by high mountains. As shown in the DEM image in Figure 1, this image is based on SRTM data with a spatial resolution of 30 meters and dates back to the year 2000. To understand the land cover types in Afghanistan, Figure 1 shows the land cover map of the country, prepared by ESA WorldCover with a spatial resolution of 10 meters, based on data from 2020-2021. In this map, Afghanistan's land is classified into different categories such as agricultural areas, urban areas, forests, grasslands, barren lands, water bodies, and snow or glacier-covered areas (URL-10, 2024).

2.1.1. Climate of Afghanistan

Global temperatures are rising due to human activities, and climate change is now posing a severe threat to all aspects of human life. If left unaddressed, humanity and the natural world will face catastrophic warming, exacerbated droughts, further sea level rise, uninhabitable residential areas, desertification of agricultural lands, and more frequent devastating floods. Developing nations are particularly vulnerable to the impacts of climate change, as they lack the resources and infrastructure to mitigate and manage its effects. As a result, they often bear the brunt of the climate crisis without the ability to adequately respond. Afghanistan, a country that has long grappled with the harsh consequences of climate change, continues to suffer from its ongoing impacts (shown in Figure 2).

In Afghanistan, meteorological data before 2001 is not fully available or reliable. Prior to 2000, most meteorological stations were damaged and ceased functioning due to the civil war. Although these stations were gradually reactivated after 2000, some regions still lacked operational weather stations until 2005 (URL-3, 2024). Even in active stations, only limited climatic parameters were collected, and some of the parameters used in this study were not recorded at all. Meteorological data in Afghanistan is mostly managed by government authorities, and accessing this data is often challenging. The time frame for this study spans from 2000 to 2023. However, data for the early years and some of the parameters analyzed in this research are incomplete or unavailable.

Decades of conflict have severely weakened Afghanistan’s ability to protect itself from natural disasters, leading to significant economic and human losses. Moreover, Afghanistan’s dry and semi-arid climate, characterized by stark seasonal temperature differences, heightens the risks of natural disasters. These disasters frequently inflict damage

on human lives, livelihoods, and both public and private property (URL-3, 2024). The country experiences cold winters and scorching summers in most regions, with an average annual rainfall of around 300 mm. In winter, snowfall in the central Hindu Kush and Pamir mountain ranges can reach up to one meter. Afghanistan's precipitation patterns are influenced by cold fronts from Siberia and warm fronts from the Indian Ocean (URL-6, 2024).

In this study, Afghanistan was divided into eight geographical regions to investigate the effects of climate change. The climate in each region varies significantly. The South and western regions experience hot, dry desert conditions with minimal relative humidity and low water vapor content. These areas receive very little rainfall, averaging only 70 to 80 mm annually, and snowfall is absent during the winter. Conversely, the northeastern and central regions have mild summers and very cold winters. Snowfall and frost in mountainous areas like the Pamirs, Baba Mountains, Hindu Kush, and Salang Pass can persist well into the summer. The altitude differences in these regions contribute to strong winds and fluctuating temperatures, with summers remaining cool (URL-15, 2024).

The eastern and southeastern regions experience dry, extremely hot summers and mild winters. Rainfall is concentrated in the winter months, with annual totals ranging from 250 to 400 mm, providing suitable conditions for forest growth. In contrast, the north region has a dry climate, with scorching summer temperatures exceeding 40°C and cold winters dropping below 0°C. The central region displays a diverse climate, with some areas resembling a Mediterranean climate, while others endure hot summers and cold winters (URL-15, 2024).

Figure 2. The effects of climate on the living conditions of the people of Afghanistan (URL-16, 2024).

2.2. Climate Parameters Used in This Thesis

2.2.1. Normalized Difference Vegetation Index (NDVI)

The NDVI is one of the most widely used indicators for assessing crop health in the agricultural sector. In recent years, NDVI has gained prominence among researchers across various fields, including vegetation classification, land cover change detection, vegetation phenology, continental land cover mapping, and the study of vegetation dynamics. This index provides crucial information about the presence and health of green vegetation by measuring leaf pigments. Healthy leaves reflect a significant amount of near-infrared radiation while absorbing a large portion of the visible spectrum (Nabizada et al., 2023). The $NDVI$ is calculated using the following formula:

$$NDVI = \frac{b_{nir} - b_{red}}{b_{nir} + b_{red}} \quad (1)$$

where b_{nir} is the reflectance in the red visible range (0.670–0.620 μm) and b_{red} is the infrared reflectance (0.876–0.841 μm). The range of $NDVI$ values is between −1 and 1(Nabizada et al., 2023).

2.2.2. Land Surface Temperature (LST)

Land Surface Temperature (LST) refers to the temperature of the earth's outermost surface layer and is influenced by surface emissivity, vegetation, and land cover types. LST provides crucial data on the physical characteristics of the earth's surface, ranging from local to global scales, and is vital in numerous applications. LST data is widely used for various studies such as geothermal energy exploration, water resource management, drought monitoring, agriculture, environmental geochemical processes, meteorological research, and understanding global surface temperature changes. Additionally, it aids in weather forecasting, hydrology, ecology, assessing plant conditions, urban climate studies, and environmental analysis. LST is also critical for estimating geophysical variables like evapotranspiration and soil moisture.

In many urban areas, LST is increasing due to changes in land cover and human activities. One key factor is the reduction of green spaces and vegetation, which influences

the absorption of solar radiation, surface temperatures, evaporation rates, stored heat, and wind patterns. These changes ultimately alter the atmospheric conditions near the earth's surface (Pahlevanzadeh et al., 2019). The LST is calculated using the following formula:

$$LST = \left[\frac{bt_{max} - bt}{bt_{max} - bt_{min}}\right] \times 100 \quad (2)$$

where bt is brightness temperature, bt_{max} and bt_{min} are the maximum and minimum brightness temperature values for a specific period in the long term.

2.2.3. VCI, TCI and VHI

In this study, three key indicators were used for drought monitoring, one of which is the VCI, introduced by Kogan in 1997. The VCI is calculated using the following relationship and is expressed as a percentage. A VCI value between 50 and 100 represents favorable vegetation conditions, while values closer to zero indicate the presence of drought in the region, reflecting severe stress on vegetation. The VCI effectively measures the health of vegetation relative to its historical maximum and minimum conditions, making it a valuable tool for assessing drought severity (Arekhi et al., 2022).

$$VCI = \left[\frac{NDVI_i - NDVI_{mn}}{NDVI_{mx} - NDVI_{mn}}\right] \times 100 \quad (3)$$

Where $NDVI_{mn}$ and $NDVI_{mx}$ values are respectively the minimum and maximum NDVI values for a period.

The TCI is used to estimate plant dryness in agricultural lands and is a critical parameter in the study of drought. TCI measures the relative temperature conditions affecting vegetation, where an increase in the TCI index over time indicates rising plant dryness and a reduction in moisture levels in crops. This gradual increase in plant dryness is one of the early indicators of drought conditions. Monitoring the TCI helps assess the stress level of plants due to high temperatures, contributing to more effective drought detection and management (URL-4, 2024). The TCI is calculated using the following formula.

$$TCI = \left[\frac{LST_{mx} - LST}{LST_{mx} - LST_{mn}}\right] \times 100 \quad (4)$$

Where LST_{mx} and LST_{mn} are the maximum and minimum land surface temperature in a certain period in the long term, respectively.

As previously discussed, the TCI and the VCI represent the temperature and humidity conditions of vegetation, respectively. Kogan (1995) introduced the VHI to provide a more comprehensive approach to drought monitoring. Kogan (1995) demonstrated that the TCI serves as a valuable complement to the VCI, and when used together, these two indices offer a highly reliable tool for monitoring drought conditions. The combination of TCI and VCI within the VHI allows for a more robust assessment of both thermal stress and vegetation health (Khodaee et al., 2017). The VHI is calculated using the following formula.

$$VHI = bVCI + (1 - b)TCI \quad (5)$$

Where b is the coefficient of the VHI equation, which was set to b = 0.5 due to the lack of more detailed information about the effect of VCI and TCI on VHI (Ejaz et al., 2023). Table 1 shows different drought conditions based on VCI, TCI, and VHI values.

Table 1. Drought Class based on VCI, TCI, and VHI values (Ejaz et al., 2023).

VHI/VCI/TCI Values	Drought Class
0 to 10	Extreme Drought
10 to 20	Severe Drought
20 to 30	Moderate Drought
30 to 40	Mild Drought
More than 40	No Drought

2.2.4. Air Temperature (Ta)

Air temperature refers to the warmth or coolness of the air in the external environment. It is a crucial parameter used in meteorological reports and weather forecasts to describe current weather conditions. This information is vital for humans and meteorological systems, as it informs decisions related to clothing, safety, agriculture, industry, and air travel. While both Land Surface Temperature (LST) and air temperature measure temperature, they differ

significantly in their definitions. Air temperature pertains to the temperature of the air at various altitudes above the ground, varying from one location to another. In contrast, LST is influenced by heat transfer from the air to the land surface, solar radiation, energy absorption, and other local factors associated with the Earth's surface (URL-5, 2024).

2.2.5. Actual Evapotranspiration (AET) and Potential Evapotranspiration (PET)

The total amount of water lost from a field through evaporation from the soil surface and transpiration from vegetation is referred to as evapotranspiration. Evaporation is an energy-dependent process that involves the transformation of liquid water into vapor. To encapsulate the concept of evapotranspiration, three key terms are commonly used (Hidarnejad et al., 2013):

- Eto (Reference Evapotranspiration): This measures the rate of evaporation and transpiration from a reference surface, typically a grass surface with specific characteristics.
- Eta (Actual Evapotranspiration): This refers to the total volume of water converted into vapor under natural conditions, either near or on the land surface.
- PET (Potential Evapotranspiration): This occurs when sufficient water is available for vegetation, allowing it to utilize water to its maximum capacity.

Actual evapotranspiration plays a crucial role as a component of the hydrological cycle, significantly impacting both regional and global climates (Akbari et al., 2011). Approximately 22% of atmospheric precipitation that falls on land and nearly 100% of precipitation over oceans and seas is lost to the atmosphere through evapotranspiration, thereby reintegrating into the hydrological cycle (Rahimpour et al., 2018).

While evapotranspiration is a vital component of the water balance, it is challenging to measure, and traditional methods for its determination are often limited. Conventional methods of estimating evapotranspiration tend to be point-based and cover only small areas, making it difficult to apply over larger fields. However, with advancements in remote sensing technology, calculating evapotranspiration has become more straightforward. The following formulas are used to calculate actual and potential evapotranspiration (Akbari et al., 2011). To calculate potential evapotranspiration, the following formula is employed:

$$ET_{f24} = \frac{R^*_{24}}{\partial \beta_y} 86400 \times 10^3 \quad (6)$$

The value of ∂ is calculated from this equation: $\partial = [2.0501 - (0.002361 \times Q_0)] \times 10^6$

Where ET_{f24} is the daily potential evapotranspiration (mm/day), ∂ is the Latent heat of evaporation (j/kg), β_y is the volume of water (kg/m^3) and Q_0 is the water temperature (°C).

In order to obtain the amount of Eta, the amount of moment evapotranspiration must be calculated, which is calculated from the following equation.

$$w = \frac{R^* - Gr_0 - U}{R^* - Gr_0} \quad (7)$$

Where w is moment evapotranspiration, R^* is the Momentary pure radiation on the surface of the earth, Gr_0 is Instantaneous soil heat flow and U is the Sensible heat flow and the actual evapotranspiration value can be calculated as.

$$AET = ET_{f24} \times w \quad (8)$$

2.2.6. Precipitation Parameter

Precipitation is the process through which water vapor condenses under atmospheric conditions and falls to the Earth's surface in either liquid or solid form due to the force of gravity. The primary forms of precipitation include drizzle, rain, snow, and hail (URL-6, 2024). As a landlocked country, Afghanistan's water resources are predominantly derived from rainfall, which exhibits significant temporal and spatial variability. The average annual precipitation in Afghanistan is approximately 256 mm; however, this amount is not evenly distributed across the country. The north regions experience higher levels of rainfall, while the western and South areas receive significantly less (Mostarshed, 2014). Daily precipitation can vary considerably depending on geographical region, seasonal changes, and prevailing weather conditions. To better understand this variability, daily precipitation can be classified based on these factors.

Table 2. Type of Precipitation in mm/day.

Type of Precipitation	Precipitation (mm/day)
Low precipitation	0 - 2
Average precipitation	2 - 10
High precipitation	10 – 50
Too much precipitation	50 - 100
Heavy precipitation	more than 100

2.2.7. Soil Moisture Parameter

Soil moisture is the amount of water in the space between soil grains. There are two types of soil moisture (URL-7, 2024):

- Surface Soil moisture: It is moisture that exists up to a depth of about 10 cm from the surface of the land.
- Undersurface Soil moisture: It is the amount of water that is 2 meters deep from the ground.

In this thesis, our goal is to investigate the Surface Soil moisture, because the Surface Soil moisture has a direct relationship with the growth of vegetables. Soil moisture is usually measured with the following units (URL-8, 2024):

1. cm or mm: It indicates that there is water up to several centimeters or millimeters from the surface of the earth to the interior of the soil. This unit is suitable for checking Soil moisture to the level of a country.

2. M3/M3: It shows how many cubic meters of soil contains water. This unit is usually suitable for checking the Soil moisture of any region or small areas.

3. Percentage (%): It shows how many percent of the soil contains water.

2.2.8. Wind Speed Parameter

Wind is the movement of air from areas of high pressure to areas of low pressure. The intensity of this airflow is directly proportional to the pressure gradient, which is the difference in atmospheric pressure between two points. Wind speed is typically measured in centimeters per second (cm/s). Various types of wind speeds can significantly impact the environment (URL-10, 2024).

Table 3. Type of Wind Speed.

Type of Wind Speed	Name of the Wind
(0 – 11) km/h	Calm weather
(12 – 29) km/h	moderate wind
(30 – 50) km/h	Semi strong or strong wind
(51 – 87) km/h	Strong storm
(88 – 118) km/h	A strong storm that uproots trees

2.2.9. Exploration of Forest Loss

Forests are among the most critical climatic parameters for maintaining the ecological balance of the environment. Forest cover is essential for every country, and monitoring changes in forest cover annually is crucial. This research utilizes Hansen's dataset to investigate the extent of deforestation in various regions of Afghanistan. Hansen's dataset, derived from Landsat bands, offers a spatial accuracy of 30 meters. In this research, the amount of deforestation was calculated using the Loss of (HGFC) dataset band on the Google Earth Engine platform for the years 2000 to 2023 at the regional level.

2.3. Data Collection and Software Used

In this thesis, Google Earth Engine (GEE) was employed to examine the climate parameters in the form of time series. For data analysis and prediction, software tools such as Excel, Origin, and SPSS were utilized, while QGIS and ArcGIS were used for map preparation. Initially, a literature review was conducted to select appropriate data for these climate parameters. Subsequently, each parameter was calculated at the regional level. This study utilized various sensors and datasets, and a summary of the remote sensing data sources is presented in Table 4.

Table 4. Remote sensing data used in this thesis.

parameters	Sensor and Dataset	Spatial Resolution	Period
NDVI	MODIS/061/MOD13Q1	250m	2000 – 2023
LST	MODIS/061/MOD11A2	1000m	2000 – 2023
VCI	MODIS/061/MOD13Q1	250m	2000 – 2023
TCI	MODIS/061/MOD11A2	1000	2000 – 2023
VHI	MODIS Dataset	250m and 1000m	2000 – 2023
AET	IDAHO Dataset	4638.3m	2000 – 2023
PET	IDAHO Dataset	4638.3m	2000 – 2023
Ta	ERA5 Dataset	11132m	2000 – 2023
Precipitation	CHIRPS Dataset	5566m	2000 – 2023
Soil Moisture	IDAHO Dataset	4638.3m	2000 – 2023
Wind Speed	FLDAS Dataset	11132m	2000 – 2023
Forest Loss	Hansen global forest change	31 m	2000 – 2023

This study employed MODIS data to analyze climate parameters, including NDVI, VCI, TCI, VHI, and LST. For the NDVI and VCI indices, the MODIS/061/MOD13Q1 dataset was employed, which has a spatial resolution of 250 meters and a temporal resolution of 16 days. The LST and TCI parameter were derived from the MODIS/061/MOD11A2 dataset, characterized by a spatial resolution of 1000 meters and a temporal resolution of 8 days. The VHI index, calculated as a combination of the VCI and TCI indices, utilizes the same data as those indices (Tehrani et al., 2022).

The IDAHO dataset has been used to check AET, PET, and soil moisture parameters. This dataset is called Monthly Climate and Climatic Water Balance for Global Terrestrial Surfaces, University of Idaho, which was collected by the University of Idaho. The data in this dataset is taken from the Terra sensor. Its spatial resolution is 4638.3 m, and its temporal resolution is one month. This dataset has available data from 1958 to 2023 years, and using the AET, PET, and soil bands, the above index was calculated. The unit used in these bands is the millimeter (State of Idaho, 2011).

For precipitation analysis, the Climate Hazards Group InfraRed Precipitation with Station (CHIRPS) dataset was used. This UCSB-CHG/CHIRPS/PENTAD dataset includes a precipitation band, measured in mm/pentad, where one pentad represents a five-day period. It offers precipitation data from 1981 to the present with a spatial resolution of 5566 meters, providing both daily and monthly information (McNally et al., 2022). Additionally, the ERA5 dataset was utilized for the Ta parameter, available from 1950 onwards. The

temperature_2m band records air temperature at a height of 2 meters above ground level, with a spatial resolution of 11132 meters and hourly data collection (Tang et al., 2024). The FLDAS dataset was employed to explore wind speed, offering a spatial resolution of 11132 meters and daily and monthly data availability since 1982. The Wind_f_tavg band calculates wind speed in m/s (McNally et al., 2022).

Finally, forest loss was analyzed using the Hansen Global Forest Change (HGFC) dataset, which is derived from Landsat bands. This dataset has a spatial resolution of 30 meters and provides data from 2000 to 2023. The lossyear band quantifies the amount of deforestation (Huacani et al., 2022). All data for the period from 2000 to 2023 was processed using the GEE programming platform.

2.3.1. Google Earth Engine Programing

Google Earth Engine (GEE) is a cloud-based platform for geographic data analysis that facilitates the visualization and analysis of various satellite images. Scientists and researchers leverage this platform for applications in remote sensing, disease outbreak prediction, natural resource management, and more (URL-11, 2024). GEE offers extensive capabilities for analyzing time series data.

As a cutting-edge technology platform based on JavaScript, Google Earth Engine enables users to execute operations quickly and at no cost, eliminating the need for storage. To access this platform, users simply need a Google account. Upon logging in, they can take advantage of the comprehensive features offered by GEE for free. Additionally, completed projects can be easily shared with other users through the unique URL generated by the platform (YAMAN, 2023).

2.4. Methodology

The methodology applied in this study involves selecting appropriate datasets and calculating each climate parameter as a time series for the period from 2000 to 2023 using Google Earth Engine (Figure 3). The climate parameters, including NDVI, LST, VCI, TCI, VHI, Ta, soil moisture, and wind speed, were calculated as averages, while precipitation, AET, PET and amount of deforestation were computed as totals. One of the key advantages

of using GEE is that the data provided is pre-processed for atmospheric and radiometric corrections, eliminating the need for further adjustments (Alahacoon and Edirisinghe, 2022).

After generating the time series for each climate parameter in GEE, the data was exported in Excel format for further statistical analysis. Initially, all climate parameters usage in this study (except HGFC) were calculated on a monthly basis in GEE, and then seasonal and annual averages were computed using Excel. Subsequently, the changes in each climate parameter across Afghanistan's regions were plotted to illustrate monthly, seasonal, and annual trends.

To assess the relationships between climate parameters, Pearson's correlation coefficient was applied. The Mann-Kendall test was utilized to evaluate the significance and direction of trends at monthly, seasonal, and annual scales. Additionally, the homogeneity test was performed to determine whether the data exhibited consistent patterns or if notable heterogeneities were present throughout the study period.

Following the trend analysis conducted with the Mann-Kendall test, it was determined that a forecast of the data up to the year 2035 would provide valuable insights. After extensive research and model comparison, the ARIMA model was selected as the most appropriate for predicting the direction of the data trend. By carefully assessing the behavior and patterns within the data, the ARIMA model's parameters were identified and adjusted for optimal performance. Each climate parameter was then forecasted using the SPSS software. To ensure the reliability and robustness of the predictions, the model's accuracy was evaluated using key statistical metrics: root mean square error (RMSE), coefficient of determination (R^2), and mean absolute error (MAE). These criteria confirmed that the model's predictions fell within acceptable limits, providing a solid foundation for forecasting future climate trends in Afghanistan. The methodological framework employed in this thesis is summarized as follows.

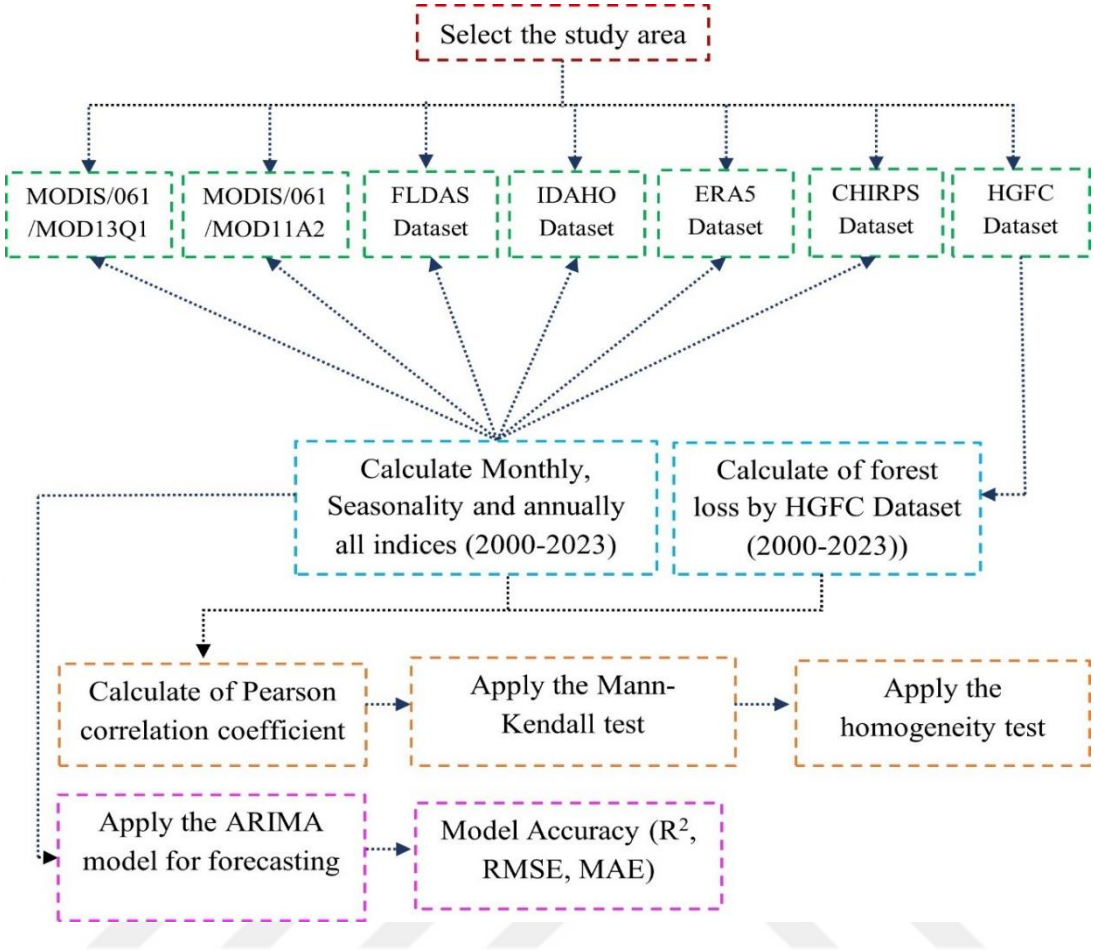

Figure 3. Methodological framework in this study.

2.4.1. Statistical Analysis

Statistics can be defined as the science of classifying data and information, facilitating logic-based decision-making, and enabling detailed planning and description. It encompasses both science and art of collecting and analyzing data to derive meaningful interpretations and conclusions. In contemporary research, interpreting and analyzing results without statistical analysis has become increasingly rare. A report that includes statistical tables, graphs, and their corresponding analyses and interpretations is referred to as a statistical analysis (Sarmento and Costa, 2019). Statistical analysis is generally divided into two main categories (Byrne, 2007):

- Descriptive Statistics: This branch is used to summarize and present data through measures such as mean, median, standard deviation, and range.

- Inferential Statistics: This branch focuses on drawing conclusions and making predictions based on tests, regression analysis, variance analysis, and parameter estimation.

In this thesis, after downloading the time series data from GEE, the data was analyzed and interpreted using statistical methods. The software utilized for these statistical analyses includes Excel, SPSS, Origin, and several auxiliary tools associated with Excel.

2.4.2. Time Series Analysis

Time series analysis is a crucial aspect of statistical analysis. A time series is created by organizing the observed values of an event chronologically. It enables the observation of past events and facilitates the prediction of future occurrences (YAMAN, 2023). Essentially, a time series consists of a collection of random observations arranged in chronological order. Statistical methods that utilize such data are referred to as time series analysis models (URL-12, 2024).

2.4.3. Type of Data for Time Series Analysis

Time series data is usually composed of various components that characterize the patterns and behavior of the data over time. For a time series analysis, the first step is to understand the type of data you are working with (URL-13, 2024). Time series data is divided into two parts (Jose, 2022):

- Metric: Data that was measured and collected at regular time intervals.
- Events: Data that is not measured and collected at regular time intervals.

2.4.4. Trend Analysis

Trend analysis is a fundamental concept in interpreting time series graphs. A trend represents the direction of a dataset based on its long-term increase or decrease. Trends do not always exhibit a linear pattern; some may show an upward trajectory that can suddenly reverse into a downward trend. The line representing this dataset's trend is referred to as the “trend of change” (YAMAN, 2023).

In this study, data was downloaded from Google Earth Engine and organized in Excel as monthly, seasonal, and annual time series. Linear trend analysis was then employed to examine these trends. This method, a branch of statistical science, is utilized for trend analysis and modeling time series data. The linear trend is represented as a straight line that helps to identify the primary direction of the dataset. One of the models applied in linear trend analysis is the linear model (Hess et al., 2001). The linear model used in this analysis is represented by the following equation:

$$F(x) = my + c \tag{9}$$

Where, $F(x)$ represents the dependent variable, y is the independent variable, m denotes the slope of the line, and ccc is the intercept of $F(x)$. According to this equation, a positive slope value (m) indicates an upward trend, while a negative slope value suggests a downward trend. To evaluate the model's performance with the data, the R-squared (R^2) value should be examined. A large and positive R^2 value indicates better model performance with an upward slope, whereas a large and negative R^2 value indicates better model performance with a downward slope. Conversely, a small R^2 value suggests that the model does not fit the data well (PEARCE and CRYER, 1986).

2.4.5. Pearson's Correlation Coefficient

Pearson's correlation coefficient is a statistically significant measure that examines the relationship between two variables. This relationship is visually represented by drawing a line through the data points of the two variables. The strength and direction of this linear relationship can be positive or negative, which is quantified using the Pearson correlation coefficient calculator. The coefficient is calculated using the following equation and is denoted by the letter (r) or (R). Its values range from -1 to 1 (Ejaz et al., 2023).

$$r = \frac{m\sum zx - (\sum z)(\sum x)}{\sqrt{[m\sum z^2 - (\sum z)^2][m\sum x^2 - (\sum x)^2]}} \tag{10}$$

Where, m represent the number of pairs of scores, $\sum zx$ the sum of the products of the paired scores, $\sum x$ the sum of the z scores, $\sum x$ the sum of x scores, $\sum z^2$ the sum of squared scores of z and $\sum x^2$ sum of squared x scores.

Pearson's correlation coefficient (r) measures the strength of the linear relationship between two variables. A stronger relationship will yield values closer to 1 or -1, indicating that all data points lie on a "best fit" straight line. This implies that changes in the factors of one variable do not diminish the correlation with the other variable. Conversely, values closer to zero suggest greater variability between the variables (Table 5) (URL-16, 2024).

Table 5. Interpret of the Pearson correlation coefficient.

Strength of association	Positive	Negative
Smal	0.1 to 0.3	-0.1 to -0.3
Medium	0.3 to 0.5	-0.3 to -0.5
Large	0.5 to 1.0	-0.5 to -1.0

2.4.6. Statistical Tests to Investigate the Trend

A statistical test is a method employed to draw conclusions about an event based on sample data. These tests are used to either accept or reject a null hypothesis and are applicable across various fields for data analysis (Neideen and Brasel, 2007). Statistical tests can be categorized into two types:

- Parametric tests: These require the assumption of a normal data distribution.
- Non-parametric tests: These do not assume a normal data distribution.

In this research, Mann-Kendall and homogeneity tests, which fall under the category of non-parametric tests, were utilized. A detailed explanation of each of these tests is provided in another section.

2.4.7. Trend Detection Using the Mann-Kendall Test

In this thesis, the Mann-Kendall test was employed to assess the presence of trends in the data. Initially developed by Mann in 1945 and further refined by Kendall in 1975, this method is particularly advantageous for analyzing time series data that do not conform to a

specific statistical distribution (Sayemuzzaman and Jha, 2014). The calculations for the Mann-Kendall test in this research were carried out using Excel. The procedure for calculating the test statistics involves determining the difference between each observation, applying the sign function, and extracting the L parameter as outlined below.

$$L = \sum_{i=1}^{m=1} \sum_{f=i+1}^{m} fng(z_f - z_i) \tag{11}$$

Where m is the number of series observations, and z_f and z_i are the i and f series data, respectively. The sign function (fng) can also be calculated as follows.

$$fng(z) = \begin{cases} +1 \;\; if \;\; (z_f - z_i) > 0 \\ 0 \quad if \;\; (z_f - z_i) = 0 \\ -1 \;\; if \;\; (z_f - z_i) < 0 \end{cases} \tag{12}$$

For the values of $m \geq 10$, L has a normal distribution with zero mean and the following standard deviation:

$$V_{var}(L) = \frac{m(m-1)(2m+5) - \sum_{k=1}^{n} k(k-1)(2k+5)}{18} \tag{13}$$

Where n represents the number of groups with nodes (equal data in a row creates a node), and k denotes the length of the k group of nodes. Finally, the Z value of the non-parametric Mann-Kendall test is calculated using the following equation.

$$Z = \begin{cases} \frac{L-1}{\sqrt{V_{var}(L)}} & if \quad L > 0 \\ 0 & if \quad L = 0 \\ \frac{L+1}{\sqrt{V_{var}(L)}} & if \quad L < 0 \end{cases} \tag{14}$$

The negative value of Z indicates a decreasing trend, while a positive value signifies an increasing trend in the data series. At a significance level of 95%, if $|Z| \geq 1{,}96$, the null hypothesis is rejected, indicating that the time series of the studied parameter has a significant trend. Conversely, if $|Z| < 1{,}96$, it is assessed as having no trend (Makari and

Abasnaya, 2020). Thus, the time series of the studied parameter exhibits a significant trend when the value of *Z* falls within the range of 1.96<Z<-1.96.

2.4.8. Homogeneity Test

The homogeneity test is a crucial statistical method used to assess the consistency of data in the time series. This test helps determine whether climate changes in a region are uniform over time or whether similar changes are observed across different regions. Homogeneity implies that there are no significant differences between the data, indicating that the variables are consistent (Modaresi et al., 2019).

In this study, the XLSTAT program was utilized to perform this test. It highlights significant climate changes over time. For instance, when examining climate variations from 2000 to 2023 in a specific area, we can identify the year when a significant change occurred and whether the changes have since increased or decreased. The statistical assumptions for the homogeneity test are as follows:

- H_0: There is homogeneity in the data.
- Ha : There is a point in time after which a significant change has occurred in the data, known as the change point date.

Several methods exist for conducting homogeneity tests. In this thesis, Pettitt's method was employed, which is a non-parametric test with a significance level of 0.05 (Modaresi et al., 2019):

- If the p-value > 0.05, the data is considered homogeneous, leading to the acceptance of H_0 and rejection of Ha.
- If the p-value < 0.05, the data is classified as heterogeneous, resulting in the rejection of H_0 and acceptance of Ha.

2.4.9. ARIMA Model

In this study, time series graphs for the NDVI, VCI, TCI, VHI, LST, Precipitation, Soil Moisture, Evapotranspiration, Potential Evapotranspiration, and Wind Speed parameter were created on a monthly, seasonal, and annual basis. Forecasting was conducted using the monthly data. Observations of the time series graphs indicate that these climate parameters

fluctuate over time and exhibit significant changes, demonstrating clear seasonality. According to the predictions, these data are compatible with the ARIMA model, which was employed in this study using the SPSS Modeler program.

The Autoregressive Integrated Moving Average (ARIMA) model, also known as the Box-Jenkins model, is widely used for predicting climate data. This model operates under the assumption that the data must be stationary. To utilize the model effectively, it is essential to ensure that a stationary process is established. In 1994, Bax and her colleagues introduced the ARIMA model, accounting for the differential order (d) in non-stationary conditions (Xu et al., 2024). If the data is not in a stationary form, it should be transformed accordingly. Stationary data refers to data that does not exhibit a trend (Sayah et al., 2020).

Before entering the variables into the model, steps were taken to ensure their stationarity. Subsequently, the stationarity in the mean and variance of the data was evaluated through autocorrelation (ACF) and partial autocorrelation (PACF) plots. The ARIMA model consists of three components:

- Autoregressive - AR: This component of the model determines how past values are used to predict current values. It is denoted by the (p), which represents the number of past observations (Xu et al., 2024). This component is calculated using the following formula.

$$Y_T = \varphi_1 Y_{T-1} + \varphi_2 Y_{T-2} + \cdots + \varphi_n Y_{T-n} + \theta_T \quad (15)$$

Where, $Y_T\ is$ time series value at T time, $\varphi_1, \varphi_2 \ldots . \varphi_n$ are the parameters of the Autoregressive, $Y_{T-1}, Y_{T-2} \ldots . Y_{T-n}$ are the past value of time series and θ_T is Random noise.

- Moving Average – MA: This component represents past error values (noise) used to predict current values. The moving average model is denoted by (q), which indicates the number of past noise observations (Islami and Zari, 2014).

$$Z_T = \theta_T + Z_1 \theta_{T-1} + Z_2 \theta_{T-2} + \cdots + Z_n \theta_{T-n} \quad (16)$$

Where, $\theta_T, \theta_{T-1}, \theta_{T-2} .. \theta_{T-n}$ are the past error terms and $Z_1, Z_2 .. Z_n$are are the parameters of the moving average part.

- Integrated – I: This section makes the data model static. It was shown to (d). The parameter (d) indicates the stationary number (GILL et al., 2023).

Finally, the ARIMA model is represented as ARIMA(p, d, q), and its general formula is given in Equation (17). The overall structure of the ARIMA model is illustrated in Figure 4.

$$X_T = \varphi_1 Y_{T-1} + \varphi_2 Y_{T-2} + \ldots + \varphi_n Y_{T-n} + \theta_T + \theta_T + Z_1\theta_{T-1} + Z_2\theta_{T-2} + \ldots + Z_n\theta_{T-n} \quad (17)$$

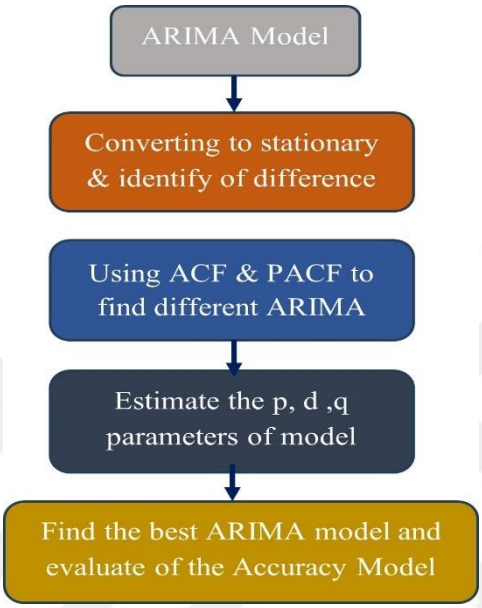

Figure 4. Structure of the ARIMA model.

2.4.10. Model Evaluation Metrics

To evaluate the accuracy of the models, various error criteria are employed. In this model, the following criteria, which are among the most significant for error evaluation, are used (Khan et al., 2023):

- Root Mean Squared Error (RMSE): RMSE measures the difference between the predicted values and the actual values. A lower RMSE value indicates better model performance. The RMSE should be less than the mean of the data and can be calculated using the following formula:

$$RMSE = \sqrt{\frac{1}{m}\sum_{j=1}^{m}(X_T - Y_T)^2} \quad (18)$$

Where, X_T is the actual value, Y_T forecasting value at T time and (m) is the number of observations.

- Mean Absolute Error (MAE): MAE calculates the mean of the absolute differences between the actual and forecasted values. Its formula is as follows:

$$MAE = \frac{1}{m}\sum_{j=1}^{m}(X_T - Y_T)^2 \quad (19)$$

- R-squared (R2): This value indicates the variance of the actual data used by the model. Its range is between 0 and 1, with values closer to 1 signifying better model performance. It is calculated using the following equation:

$$R^2 = 1 - \frac{\sum_{i=1}^{m}(X_T - Y_T)^2}{\sum_{i=1}^{m}(X_T - Z_T)^2} \quad (20)$$

Where, Z_T is the average of observed data.

3. RESULTS AND DISCUSSION

In this section, the results of the work done are included. At first, trend analysis was done on three scales (monthly, seasonally, and annually) by linear trend, and then statistical tests were used to investigate the trends. Also, after the examination of trends, the results of the model that was selected for prediction are included. In the examination of monthly time series data, the linear trend of each climate parameters for throughout Afghanistan and the 8 regions were examined as an average and total. And some regions have an increasing trend and some regions decreasing trend was observed. To observe the seasonal trend, NDVI, LST, AET, PET, precipitation, soil moisture, Ta, and wind speed parameters were examined. The linear trend of each parameter used in this thesis for the purpose of investigating climate change was observed on an annual basis. Its results are included in the following titles. The results of the forest loss were also calculated annually for each region between 2000 and 2023, and its trend was observed linearly. The VCI, TCI, and VHI indices were used for drought monitoring and the trend of these climate parameters was observed annually. The results were included in the form of plots and tables.

The Mann-Kendall test was employed to identify trends in climate parameters, while correlation coefficients were used to explore relationships between data in each region. The homogeneity test was applied to assess the homogeneity and heterogeneity of the data on both seasonal and annual scales. After analyzing the trends, ARIMA model forecasts were incorporated. Initially, model parameters were identified and recorded in tables. The model then predicted the data on a monthly basis with both actual and forecasted values plotted in graphs. RMSE, MAE, and R^2 metrics were used to evaluate the model's performance. The results for each parameter and region were presented in the tables.

3.1. Results From the Monthly Trend Analysis

According to Figure 5, the NDVI data from 2000 to 2023 reveals distinct patterns of vegetation health across various regions of Afghanistan. Most areas, including the Northeastern, Eastern, Southeastern, South, Western, West Central, and Central regions, show an overall increasing trend in NDVI values, while the North region experiences a decline.

Vegetation typically peaks in spring, particularly in April and May, with significant declines noted in 2008, reflecting periods of poor conditions. Regions like the South and Southeastern areas display robust growth during the growing season, particularly from 2010 onwards, indicating favorable climatic conditions. Notably, the Western region maintains a stable pattern of vegetation health, with consistent NDVI peaks during spring and summer, and only minor fluctuations observed in recent years.

In contrast, the North region demonstrates considerable seasonal fluctuations, with notable peaks in spring months, including a high of 0.414 in April 2003. Despite a drop in NDVI values to -0.01 in January 2008, recovery is seen in 2009 with a peak at 0.413 in April. Over the following decade, the North region continues to exhibit similar fluctuations, though recent data indicate a more balanced performance in 2023. The Northeast region mirrors these trends, showing initial rises in NDVI values during spring, a notable decline in 2008, and subsequent recovery from 2009 to 2015, reflecting improvements during the summer months.

The Western region of Afghanistan exhibits a relatively stable NDVI pattern throughout the year, with peaks occurring in spring and early summer. Early years show consistent NDVI values, with significant increases noted in 2005, 2015, and 2016, suggesting improved vegetation growth. However, winter months consistently demonstrate lower NDVI values due to dormant vegetation. The West Central region reflects typical seasonal fluctuations, with low values in winter and notable peaks during spring and summer. The data across all regions highlights a complex interaction between seasonal patterns and climatic conditions, with varying degrees of vegetation health improvements over time.

In accordance with Figure 5, the monthly NDVI data from Afghanistan shows a complex interplay between vegetation health and climatic conditions over the years. The seasonal peaks and troughs in NDVI highlight the importance of timely agricultural interventions and environmental management strategies to mitigate the adverse effects of climate variability.

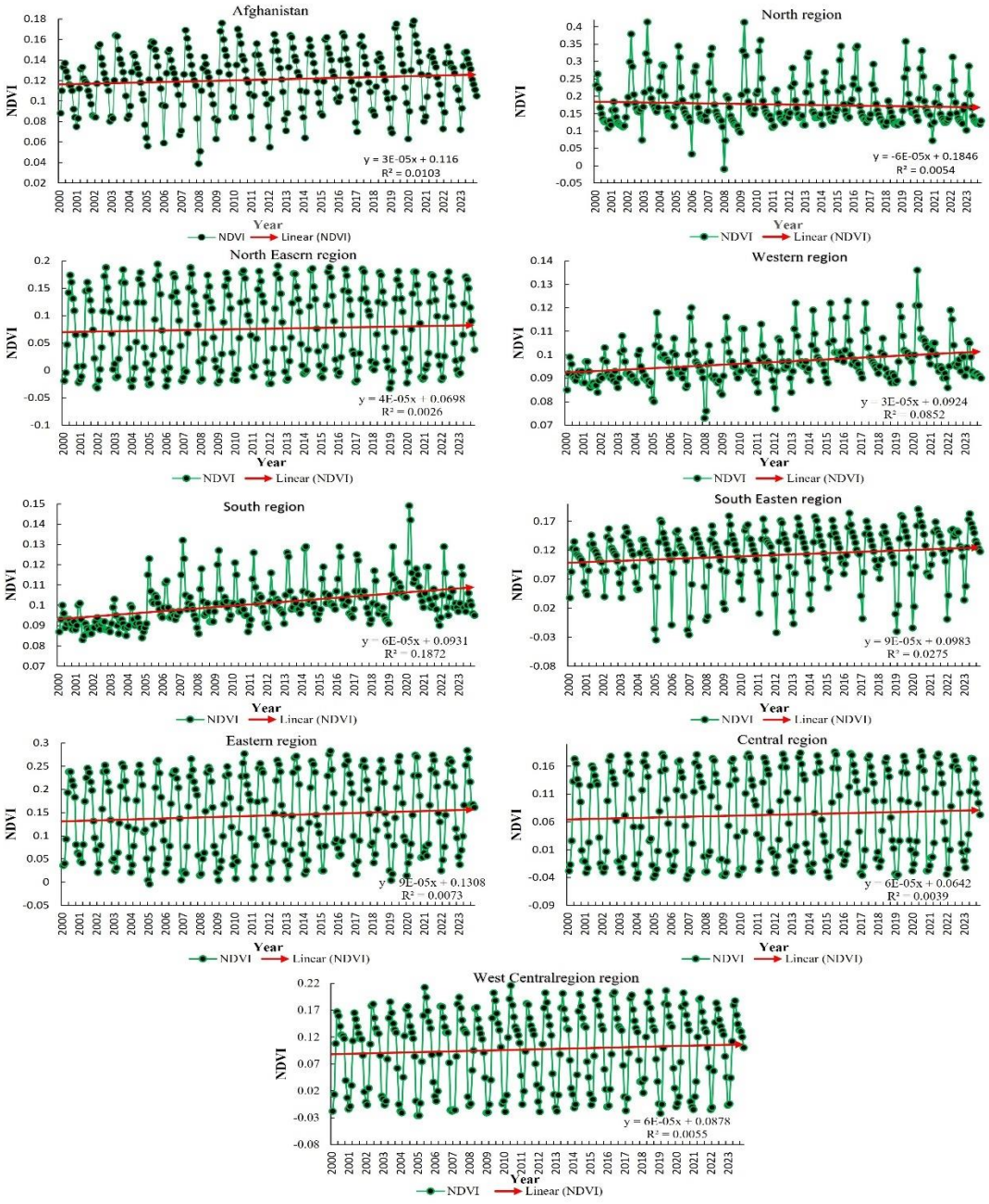

Figure 5. Monthly mean NDVI time series trend analysis.

As shown in Figure 6, the monthly data for the LST parameter throughout Afghanistan and in all regions show a very slight decreasing trend. The Land Surface Temperature (LST) data for Afghanistan from 2000 to 2023 reveals significant seasonal and annual temperature variations across the country. Summer months (June to August) consistently record high temperatures, often exceeding 44°C, while winter months (January and February) experience considerably lower temperatures, frequently dropping below 10°C. An upward trend in LST

noted since around 2005, particularly during the growing season, with extreme temperatures recorded in 2008 and 2019 highlighting substantial fluctuations.

In the north region of Afghanistan, summer temperatures can surpass 46°C, while winter temperatures typically range from 1.8°C to 5.7°C. This dataset indicates a warming trend, especially since 2005, which could have significant implications for local ecosystems and agricultural practices. The northeastern region experiences winter temperatures that can plummet to -11.5°C, contrasting sharply with summer peaks around 34.4°C. The discernible warming trend suggests shifts in climate patterns that may affect agriculture and water resources.

The western and south regions also show considerable seasonal variation, with winter temperatures often falling below 10°C and summer peaks exceeding 50°C. For example, July 2021 recorded temperatures around 52.658°C in the south. A gradual warming trend is evident, particularly during the summer months, reinforcing the necessity for adaptive strategies to tackle climate change challenges. The temperature data for these regions points to the urgency of implementing effective measures to manage the impacts of rising temperatures on agriculture and local ecosystems.

In the southeastern and eastern regions, significant temperature fluctuations are also observed, with winter lows around -2.36°C and summer highs nearing 43.43°C. These temperature changes emphasize the importance of developing adaptive strategies to enhance climate resilience throughout Afghanistan. Monitoring LST variations across different regions will provide valuable insights for future planning and resource management, ensuring that the country can effectively respond to the challenges posed by climate change.

Figure 6. Monthly mean LST time series trend analysis.

As depicted in Figure 7, the time series data of the Ta parameter throughout Afghanistan and across all regions exhibit a very slight upward trend. The analysis of average Ta data across various regions of Afghanistan from 2000 to 2023 reveals distinct seasonal patterns, highlighting the diverse climatic conditions that can significantly impact agriculture and water resources. Throughout the entire country, winter months (January and February) consistently show Ta below freezing, particularly in regions like the north and central areas, where severe cold spells can drop Ta as low as -15°C. Conversely, the summer months (June to August) generally record high temperatures, often exceeding 25°C, with the South region reaching extremes above 30°C.

In the north region, characterized by cold winters with average Ta falling below freezing, significant warming trends are evident in summer, peaking at 27.683°C in July 2019. The fluctuations in winter temperatures raise concerns about the region's water resources and agricultural productivity. The northeastern region exhibits notably cold winters, with lows reaching -15.634°C, contrasting with moderate summer averages around 18°C. The significant variability in winter temperatures suggests challenges for agricultural practices during the colder months. The western region, exhibiting moderate winter temperatures ranging from -4.335°C to 2.178°C, records summer peaks around 27.409°C. The consistent warmth during summer promotes agricultural activities, although the rapid temperature drop in autumn poses potential risks for crop viability.

The South region displays a mild winter and extreme summer, with temperatures reaching 33.402°C. The smooth transition from summer to autumn suggests a stable agricultural environment; however, the high summer temperatures could stress water resources. The southeastern and eastern regions both exhibit cold winters with lows around -7°C and relatively mild summers, averaging between 17°C and 23°C. The cooling trend in autumn highlights challenges for agriculture as temperatures drop toward the freezing mark. In the central region, extremely cold winters with temperatures below -13°C contrast with moderate summer temperatures of 14°C to 18°C, significantly impacting livelihoods and agricultural practices and necessitating adaptive strategies.

The west-central region, like the central area, experiences harsh winters with averages around -13°C in January, while summer temperatures remain conducive to agriculture, averaging between 16°C and 19°C. The sharp decline in temperatures during autumn emphasizes the need for careful planning in agricultural cycles. Overall, while all regions face the challenge of extreme winter temperatures, the degree of summer warmth varies significantly, with an overall warming trend suggesting potential long-term implications for agricultural productivity and water resource management, urging the need for adaptive strategies in the face of climate change.

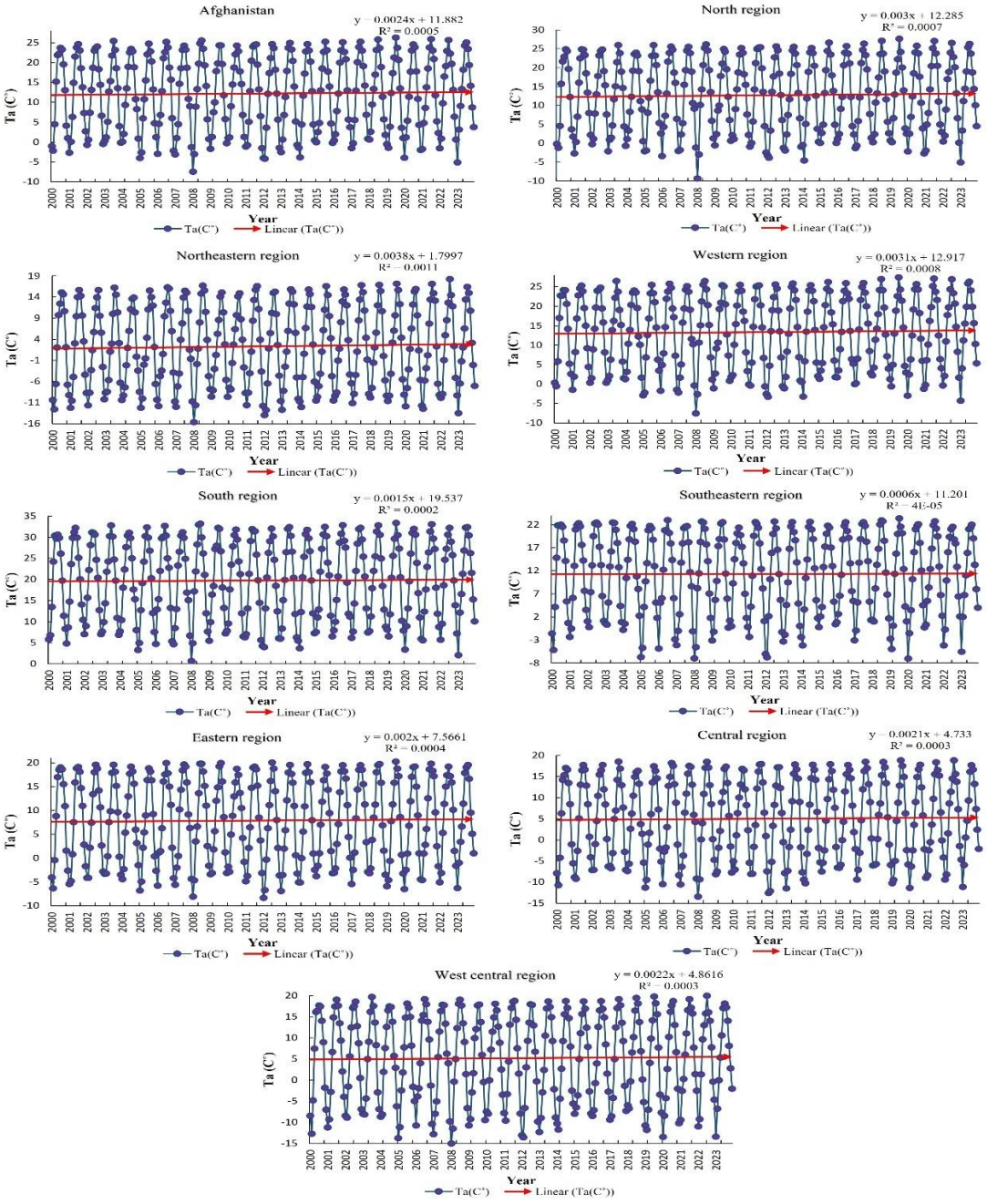

Figure 7. Monthly mean Ta time series trend analysis.

As illustrated in Figure 8, the time series data of the AET parameter throughout Afghanistan and across all regions shows a very slight increasing trend. The AET data for Afghanistan from 2000 to 2023 reveals significant seasonal variability influenced by diverse climatic conditions across different regions. In the north region, winter months such as January and February show extremely low AET values, with January 2008 recording no evapotranspiration due to freezing conditions. In contrast, spring months witness a notable

surge in AET, peaking in April at 59.704 mm in 2002, which underscores the region's favorable conditions for plant growth. However, summer months typically see a drop in AET, often falling below 2 mm, reflecting limited moisture availability despite high evaporation rates. This pattern indicates the region's vulnerability to climate variability, emphasizing the need for adaptive water management strategies.

Comparatively, the northeastern region exhibits a similar trend of low AET in winter, with minimal evapotranspiration recorded in January 2008. However, this region maintains relatively higher AET during the summer months, peaking at 43.457 mm in June 2002, showcasing ongoing water demand from vegetation. Notably, AET trends in this region show an increasing pattern in spring and summer months compared to earlier years, suggesting potential shifts in climate dynamics. The western region, on the other hand, demonstrates a more variable pattern, with January 2001 recording only 4.306 mm. The spring peak occurs at 66.817 mm in April 2019, but summer values fluctuate dramatically, indicating inconsistent moisture availability, particularly with a drop to 1.554 mm in June 2006.

In the South region, AET trends reveal significant year-to-year variability, with a peak of 36.026 mm in April 2019. The region experiences notable fluctuations, exemplified by an unusually high AET of 35.416 mm in February 2022. Despite high temperatures in summer, AET values remain lower, indicating limited moisture availability, which impacts vegetation health. This contrasts with the southeastern region, where spring months show substantial peaks, with March 2012 reaching 84.757 mm, emphasizing high moisture conditions. Here, AET levels in summer can reach 46.566 mm in July 2023, indicating relatively better moisture conditions compared to the south.

Lastly, the eastern region showcases the most pronounced seasonal variability, with AET peaking above 70 mm in spring months, particularly reaching 78.482 mm in April 2003. The summer also sees exceptionally high values, such as 85.34 mm in July 2010, reflecting robust evapotranspiration driven by temperature and solar radiation. Conversely, winter months demonstrate lower moisture availability, with AET values dropping below 5 mm in January. This contrasts with the central region, where AET peaks in spring and early summer, reaching 82.358 mm in May 2015. However, both regions illustrate significant interannual variability and highlight the critical importance of understanding AET trends for effective water resource management and agricultural planning across Afghanistan.

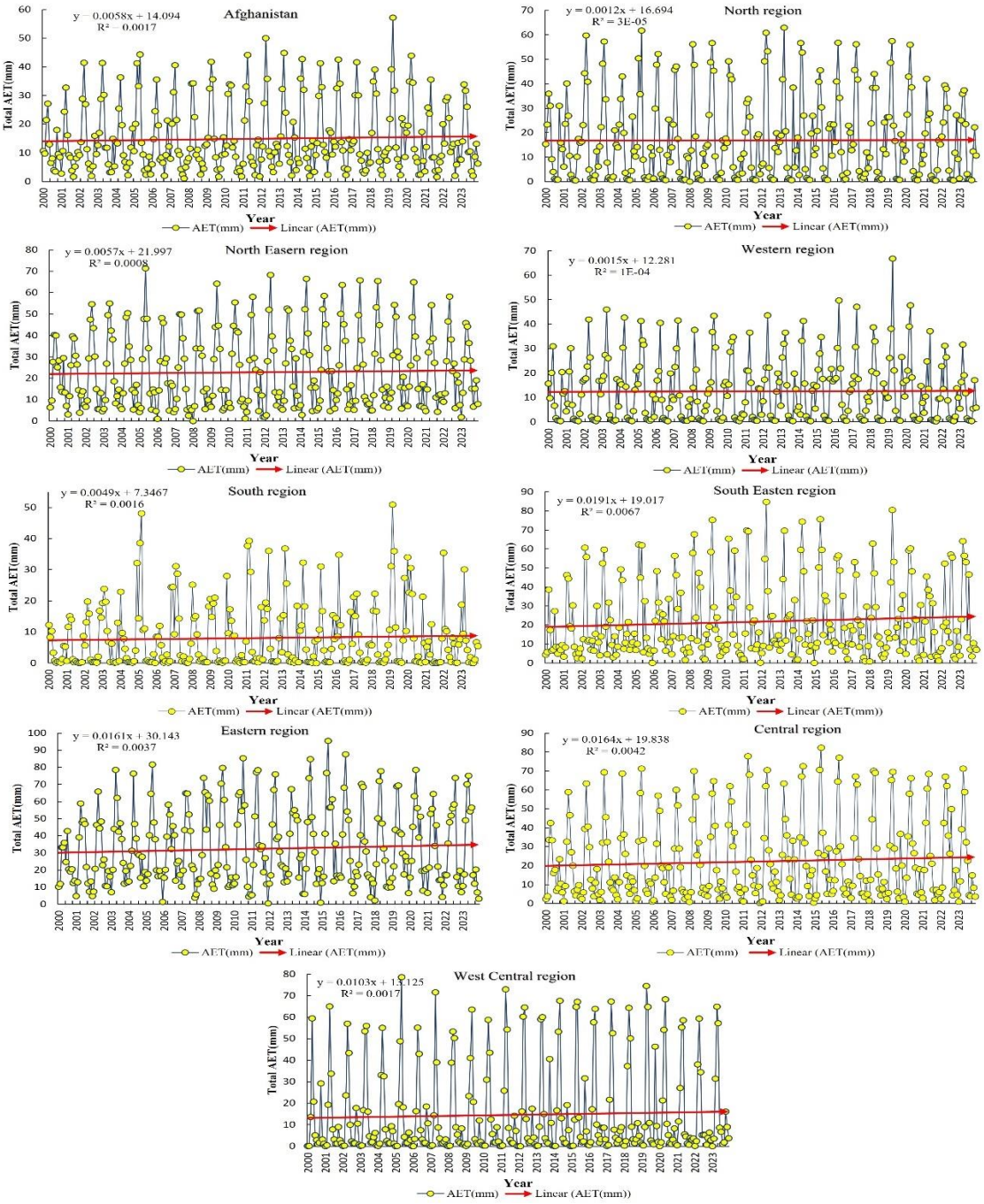

Figure 8. Monthly Total AET time series trend analysis.

As indicated in Figure 9, the PET parameter shows a slight decreasing trend in the Eastern region and a very slight increasing trend on a monthly basis in other regions. The potential evapotranspiration (PET) data for Afghanistan from 2000 to 2023 illustrates significant seasonal variations influenced by the country's diverse climatic conditions. Overall, winter months consistently show low PET values, with January 2000 recording 25.071 mm at the national level. The north region specifically begins at a lower 17.873 mm

in January 2000, while the northeastern region shows even lower values of 7.27 mm during the same period. In contrast, the South region, starting with a relatively higher PET of 48.945 mm, demonstrates a more substantial baseline moisture level. These initial differences underscore the climatic disparities across regions, which lead to varied responses as the seasons transition.

As spring progresses, PET values in all regions show notable increases, reflecting the shift in climatic conditions. Nationally, PET peaks at 127.511 mm in April 2021, while the north region experiences a peak of 130.02 mm in April 2001. The northeastern region, although reaching a lower peak of 75.322 mm in April 2022, still indicates an upward trend as it moves from winter to spring. This upward trend is particularly crucial for agricultural planning, as the timing of water availability can significantly impact crop growth. The South region's peak in April and May often exceeds 170 mm, revealing critical months for agricultural water demand, highlighting the importance of seasonal management strategies.

In the summer months, PET values across all regions consistently reach their highest levels, reflecting the increased evaporation rates due to higher temperatures. The national peak of 232.302 mm in July 2010 exemplifies this trend, while the north region surpasses this with a record of 247.316 mm in July 2019. The western region records an even higher maximum of 265.667 mm in July 2000. The South region stands out with peaks reaching 291.708 mm in July 2001 and 280.573 mm in July 2023, emphasizing the critical need for effective water resource management during this period of high demand. The significant fluctuations in summer PET values across regions highlight the need for tailored agricultural practices that respond to local climatic conditions.

Throughout the years, fluctuations in PET data reveal distinct interannual variability, posing challenges for effective water management and agricultural planning. For example, the northeastern region saw a notable dip in January 2023 to just 1.879 mm, while the central region experienced a dramatic decrease to 1.051 mm in January 2020. Similarly, the western region recorded a dip to 17.362 mm in January 2023. These fluctuations necessitate ongoing monitoring and adaptive strategies to manage water resources effectively and ensure agricultural sustainability.

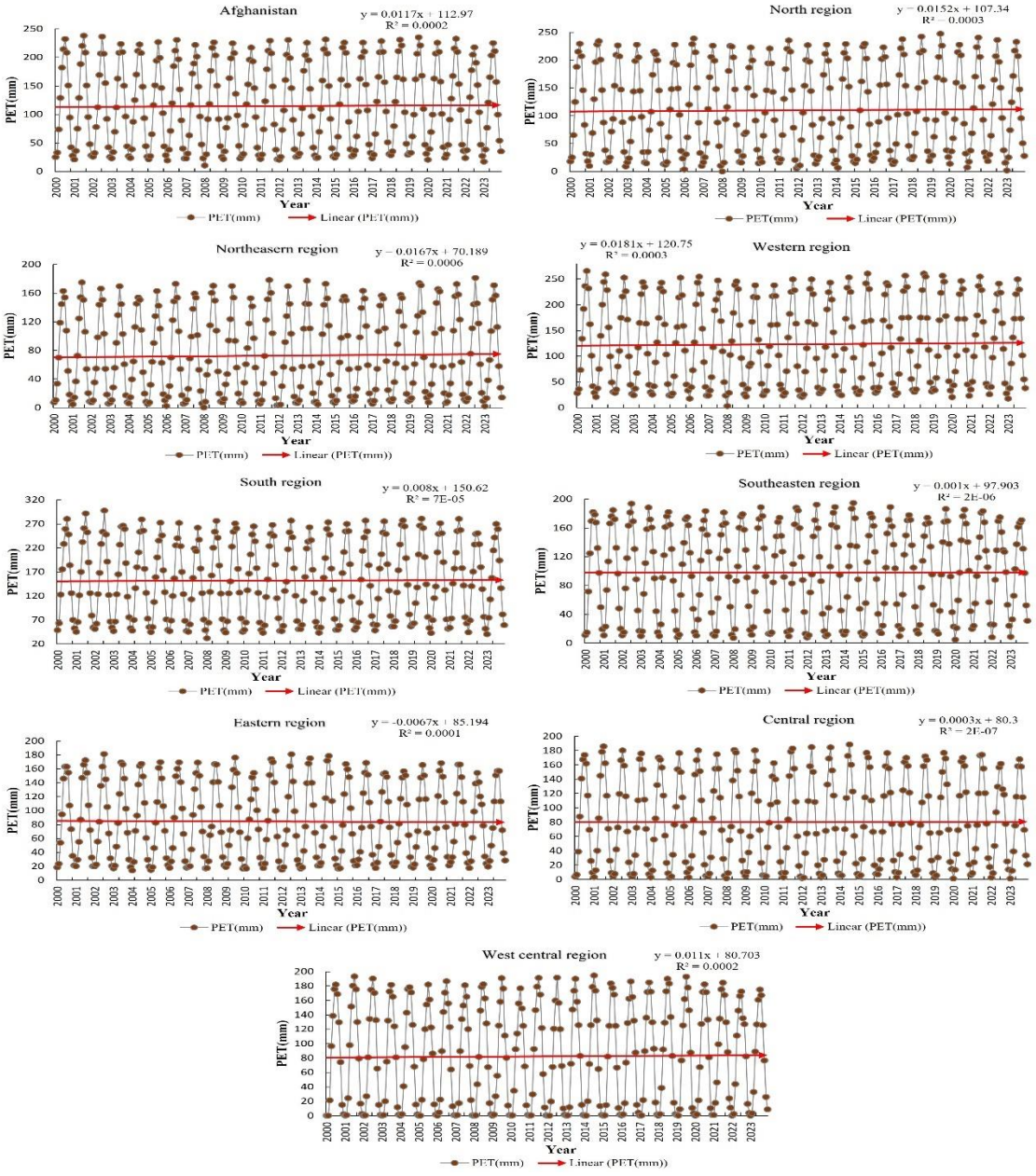

Figure 9. Monthly Total PET time series trend analysis.

The precipitation values are illustrated in Figure 10. The time series data for the precipitation parameter across Afghanistan show a very slight decreasing trend in the North, Northeastern, and Western regions, while the Eastern, Southeastern, South, Central, and West Central regions exhibit a very slight monthly increasing trend. The precipitation data for Afghanistan from 2000 to 2023 indicates distinct seasonal variability across different regions, influencing agricultural practices and water resource management. The eastern and northeastern regions experience the highest rainfall during spring, with March consistently

showing peaks over 100 mm. For instance, March 2021 in the northeastern region recorded an exceptional 159.81 mm, while the eastern region witnessed similar patterns in years like 2007 and 2019. This trend contrasts sharply with the western and South regions, where winter months see lower precipitation levels, such as January averages often below 40 mm, with the highest recorded in January 2020 at 72.15 mm in the west. This disparity underscores the need for adaptive water management strategies that cater to the unique rainfall patterns of each region.

While spring months are critical for water replenishment in the eastern and northeastern regions, the central region also exhibits significant peaks, particularly in March and April, with notable rainfall exceeding 130 mm in both months in 2020 and 2016. In comparison, the north region shows a significant peak in March 2003 at 125.47 mm, indicating a strong reliance on spring rains. In contrast, the western and South regions experience notable dryness during the summer months, averaging around 1-2 mm, with only occasional spikes like 1.47 mm in the west during July 2019. This variability in precipitation levels necessitates tailored agricultural practices and water management strategies to address the seasonal fluctuations.

The interannual variability observed in precipitation also highlights the challenges faced by the South and southeastern regions. For instance, February 2020 recorded high rainfall in the south at 89.13 mm, contrasting sharply with the generally lower averages in summer months. Meanwhile, southeastern Afghanistan shows distinct seasonal patterns, with significant rainfall typically occurring in spring and monsoon-influenced summer months. In contrast, the western region sees a pronounced drop in rainfall during summer, often below 2 mm, necessitating effective water management to ensure agricultural sustainability during these dry periods.

Overall, while regions like the northeastern and eastern areas benefit from substantial spring rainfall, leading to effective irrigation practices, other regions such as the western and South areas face considerable challenges due to lower rainfall in critical growing seasons. The variability in precipitation across Afghanistan from 2000 to 2023 emphasizes the importance of adaptive strategies that consider the unique climatic patterns of each region, ultimately ensuring the sustainable management of water resources and agricultural practices throughout the country.

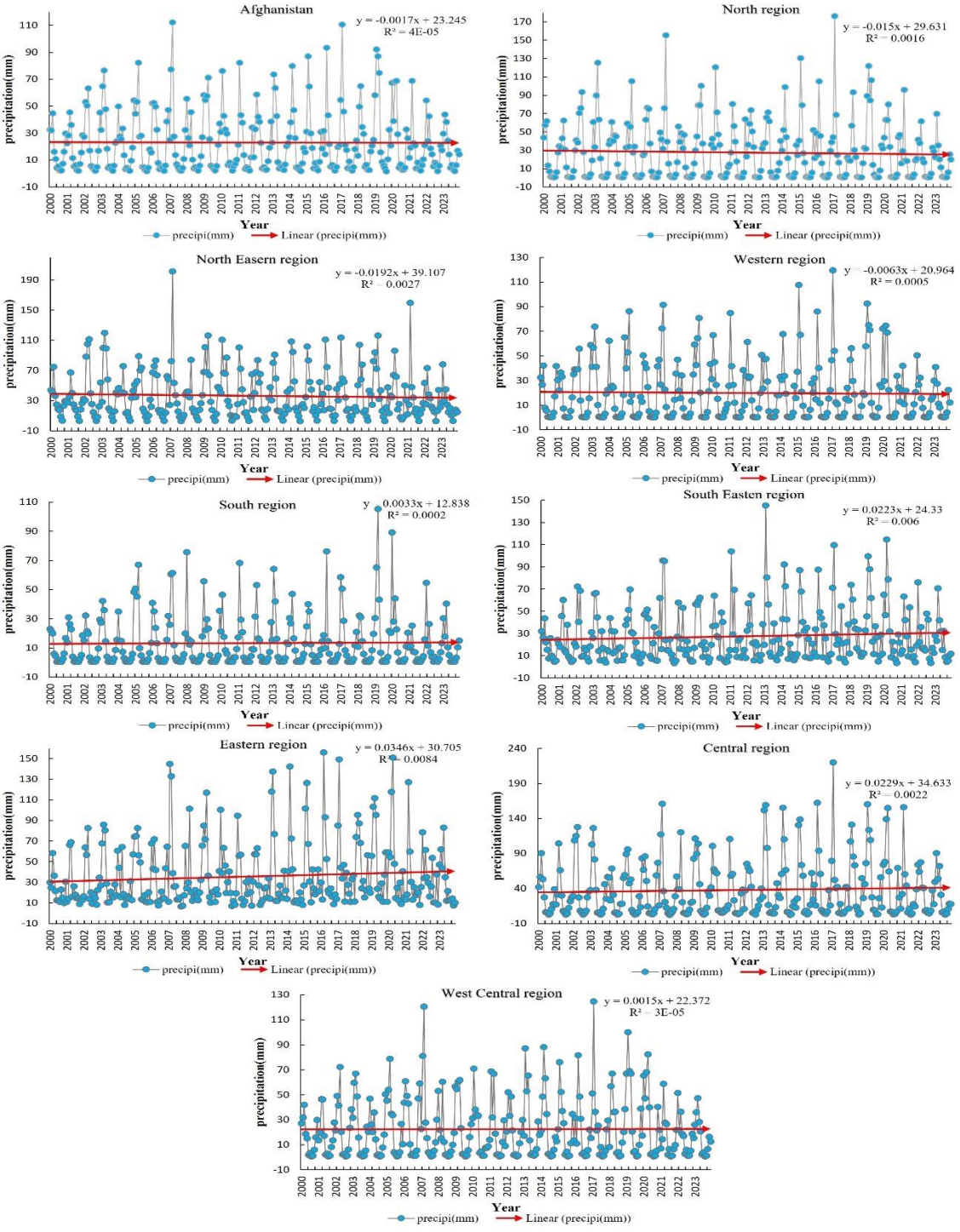

Figure 10. Monthly mean Precipitation time series trend analysis.

The soil moisture values are illustrated in Figure 11. The time series data for the soil moisture parameter across Afghanistan and in all regions demonstrate a decreasing monthly trend. The analysis of soil moisture data across various regions of Afghanistan from 2000 to 2023 reveals significant seasonal variability and distinct patterns that greatly influence

agricultural practices and water resource management. In general, winter months consistently demonstrate higher moisture levels across most regions, with north Afghanistan peaking at 21.75 mm in January 2005 and northeastern Afghanistan reaching an impressive 41.38 mm in January 2000. This trend is critical as these winter moisture levels provide essential water resources for agricultural activities, setting a foundation for crop growth as the seasons transition.

As spring approaches, regions such as northeastern Afghanistan and the central region witness notable peaks in moisture, with northeastern Afghanistan reaching 58.51 mm in April 2002 and the central region recording a maximum of 30.12 mm in April 2019. However, this increase is often followed by a substantial decline in moisture levels during the summer months, particularly from June to August. In north Afghanistan, for instance, moisture drops to an average of 4.32 mm in July 2020, while the western region consistently records values below 4 mm during the same months. Such declines signal critical challenges for agricultural sustainability, necessitating adaptive water management strategies to mitigate drought impacts.

In contrast, the South region exhibits persistently low moisture levels throughout the year, with the highest value recorded at just 6.75 mm in March 2003 and summer averages often below 2 mm. This stark reduction underscores the severe water scarcity challenges faced in this region, reinforcing the need for effective irrigation and conservation practices. Similarly, the southeastern region reflects variable moisture levels, peaking at 19.78 mm in March 2020 but still exhibiting significant declines during the hotter months, highlighting the necessity for targeted water management interventions.

Lastly, the east and west-central regions show fluctuations that reflect similar trends, with the eastern region peaking at 54.60 mm in April 2014, while the west-central region recorded a low of 2.93 mm in January 2022. Both regions experience critical low moisture levels in the summer, emphasizing the importance of seasonal monitoring and strategic management to optimize agricultural productivity. The variability in soil moisture data across Afghanistan underscores the necessity for region-specific water resource management strategies to ensure sustainable agricultural practices and address the pressing challenges posed by climate variability and arid conditions.

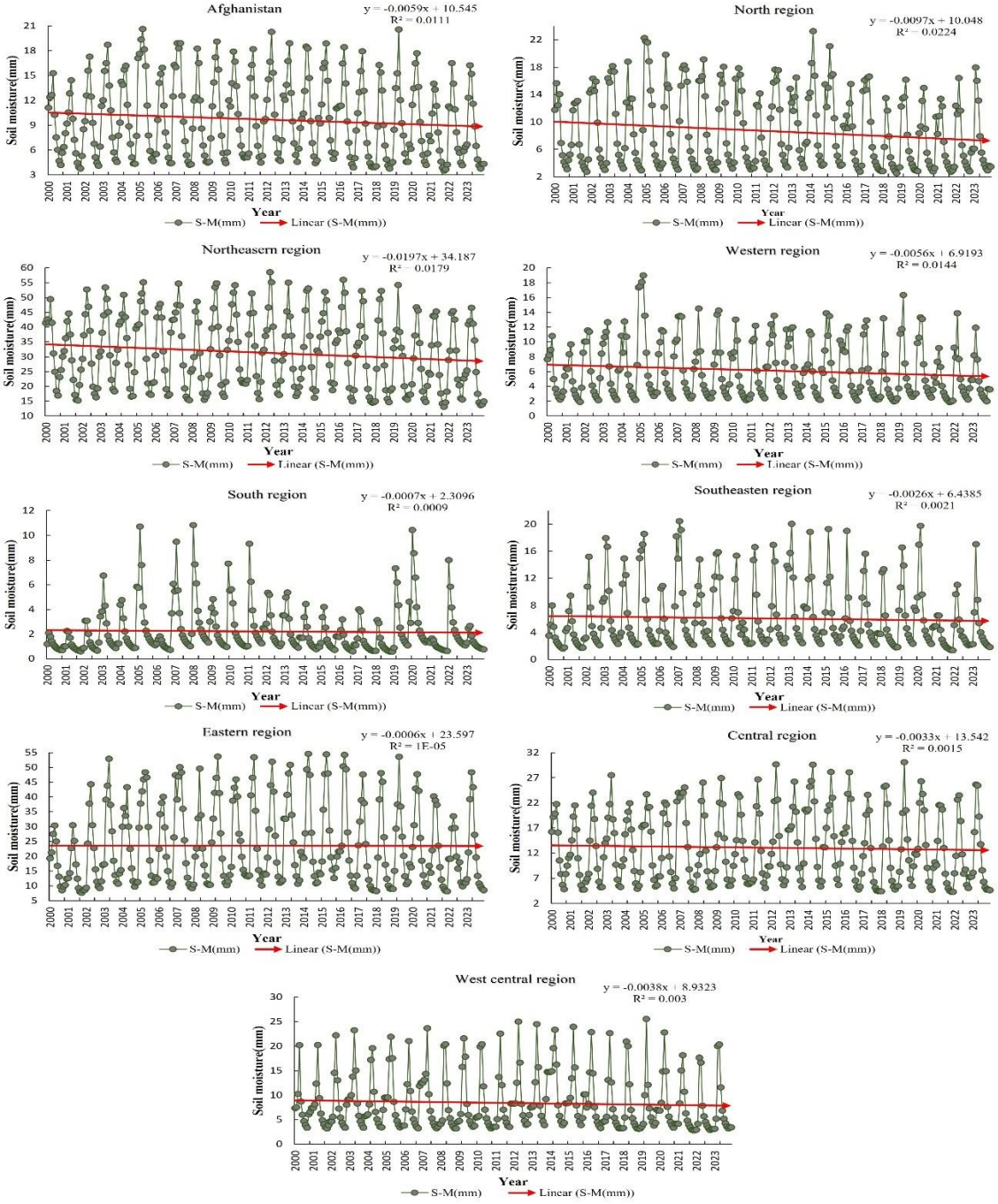

Figure 11. Monthly mean Soil Moisture time series trend analysis.

Figure 12 illustrates the wind speed trends, showing a very low increasing trend in the South and Western regions, while a very low decreasing trend is observed throughout Afghanistan and in other regions. The analysis of wind speed data across Afghanistan from 2000 to 2023 reveals distinct seasonal variations and regional differences that are crucial for understanding agricultural and environmental dynamics. In general, wind speeds peak during the summer months across most regions, particularly in July, with notable averages

recorded in the Western region, where speeds can reach as high as 9.34 m/s. The South region also demonstrates significant summer peaks, averaging between 6.74 m/s, which is essential for considering impacts on agriculture and local infrastructure. In contrast, winter months consistently exhibit lower wind speeds across all regions, with averages dropping below 4 m/s, indicating a seasonal shift that affects various ecological and agricultural processes.

Regionally, North Afghanistan exhibits a marked seasonal pattern with winter lows around 3.30 m/s and summer peaks of approximately 6.03 m/s. The consistency in wind speeds during spring, particularly in April, provides favorable conditions for agricultural activities, making it vital for farmers to adapt their practices accordingly. Conversely, the Northeastern region maintains relatively low averages, typically ranging between 2.40 to 3.69 m/s. While this stability can be beneficial for agriculture, it may pose challenges for air quality management during winter months, where lower wind speeds may lead to stagnation.

The Central and West Central regions also show moderate wind speeds, with the Central region ranging from 2.85 to 6.29 m/s and the West Central region fluctuating between 2.69 and 5.74 m/s. Both regions experience peak wind speeds during summer months, though the West Central region demonstrates a noticeable increase in speeds in recent years, especially in 2021 and 2023, suggesting potential climatic shifts that require further investigation. This upward trend necessitates proactive management strategies to mitigate the impacts of higher wind speeds on agriculture and energy production.

Understanding wind speed variations across Afghanistan is essential for effective agricultural planning, resource management, and environmental monitoring. Each region's unique wind patterns not only influence agricultural productivity but also highlight the need for adaptive strategies in the face of changing climatic conditions. By recognizing these trends, stakeholders can better prepare for the challenges and opportunities presented by wind dynamics, ultimately contributing to enhanced resilience in agricultural practices and environmental stewardship across the country.

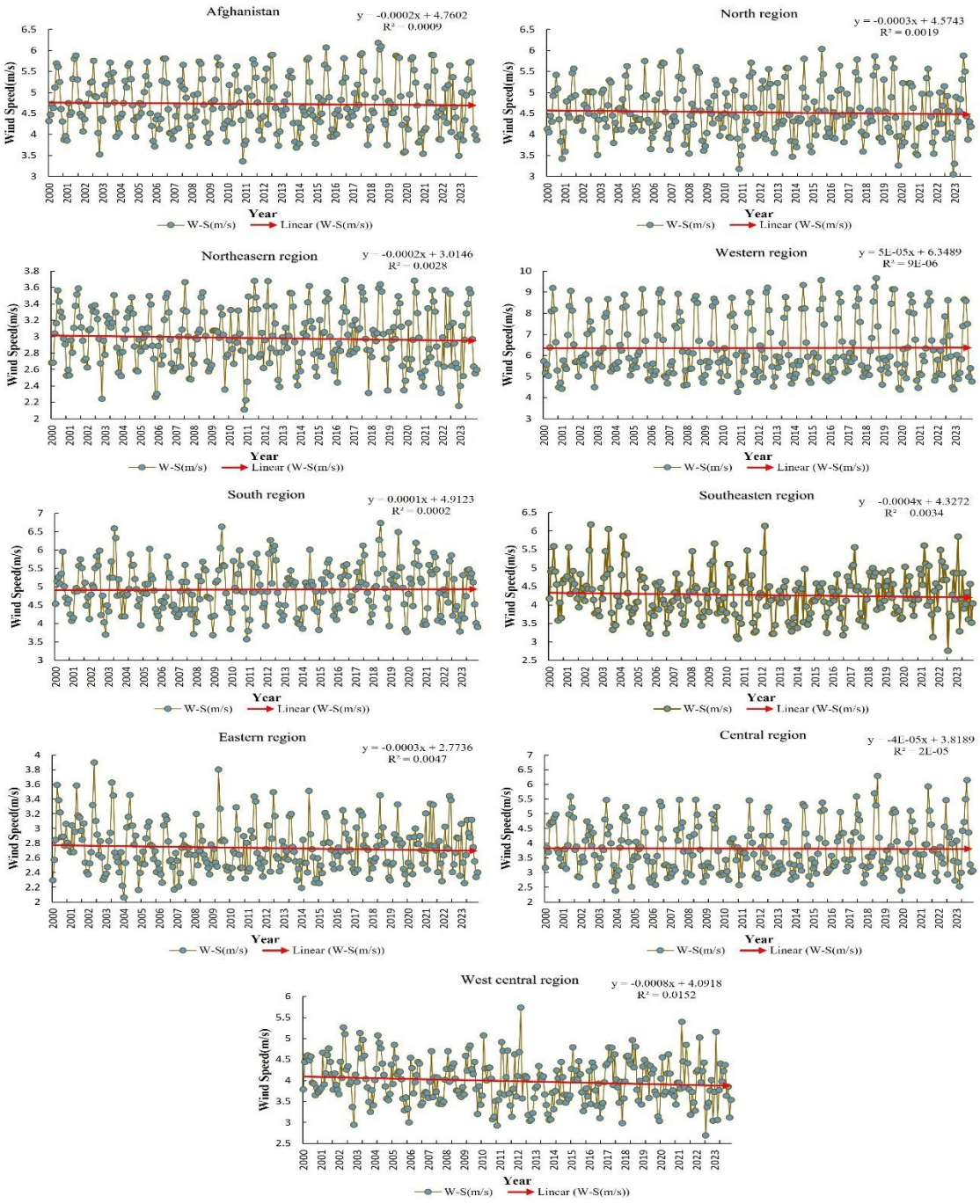

Figure 12. Monthly mean Wind Speed time series trend analysis.

The values of the VCI are presented in Figure 13. The time series data of the VCI show a very low increasing trend in the Southeastern, Eastern, and Central regions, while a very low decreasing trend is observed throughout Afghanistan and in the other regions. The VCI across different regions of Afghanistan from 2000 to 2023 reveals both similarities and significant variances in seasonal patterns and overall vegetation health. Spring months, particularly April and May, consistently show elevated VCI values across regions, often

exceeding 0.70, indicating favorable growth conditions. Notably, the years 2008 and 2011 emerge as periods of optimal vegetation health across several regions, highlighting the responsiveness of vegetation to climatic conditions. However, winter months consistently present lower VCI values across all regions, particularly in January and February, underscoring the stress imposed by colder temperatures.

In North Afghanistan, VCI values typically exceed 0.70 during spring, but notable declines below 0.20 in some years, such as 2006 and 2020, highlight periods of climatic adversity. Similarly, the Northeast region shows fluctuations with a marked decline to 0.04 in 2006 and stress in early 2020, suggesting vulnerabilities that require adaptive management strategies. Meanwhile, the Western and South regions demonstrate higher spring values but experience significant stress in the summer months, particularly in July, where values often dip below 0.40.

The Southeast region stands out with exceptionally high VCI values in May 2005, reaching 0.93, while the Eastern region shows resilience with a peak of 0.91 in August 2010. However, both regions also exhibit challenges during the winter, with values frequently dropping below 0.30. In contrast, the Central region maintains relatively high VCI values in the growing season, with peaks in May, while experiencing severe winter lows below 0.10, indicating a need for continuous monitoring and sustainable practices.

Overall, the data underscores a common theme across regions: the necessity for ongoing vegetation health monitoring and adaptive management to bolster resilience against climate variability. While spring and early summer months consistently reflect optimal growth conditions, the recurring winter stress and periodic droughts necessitate targeted interventions to enhance agricultural productivity and ensure ecological stability in Afghanistan.

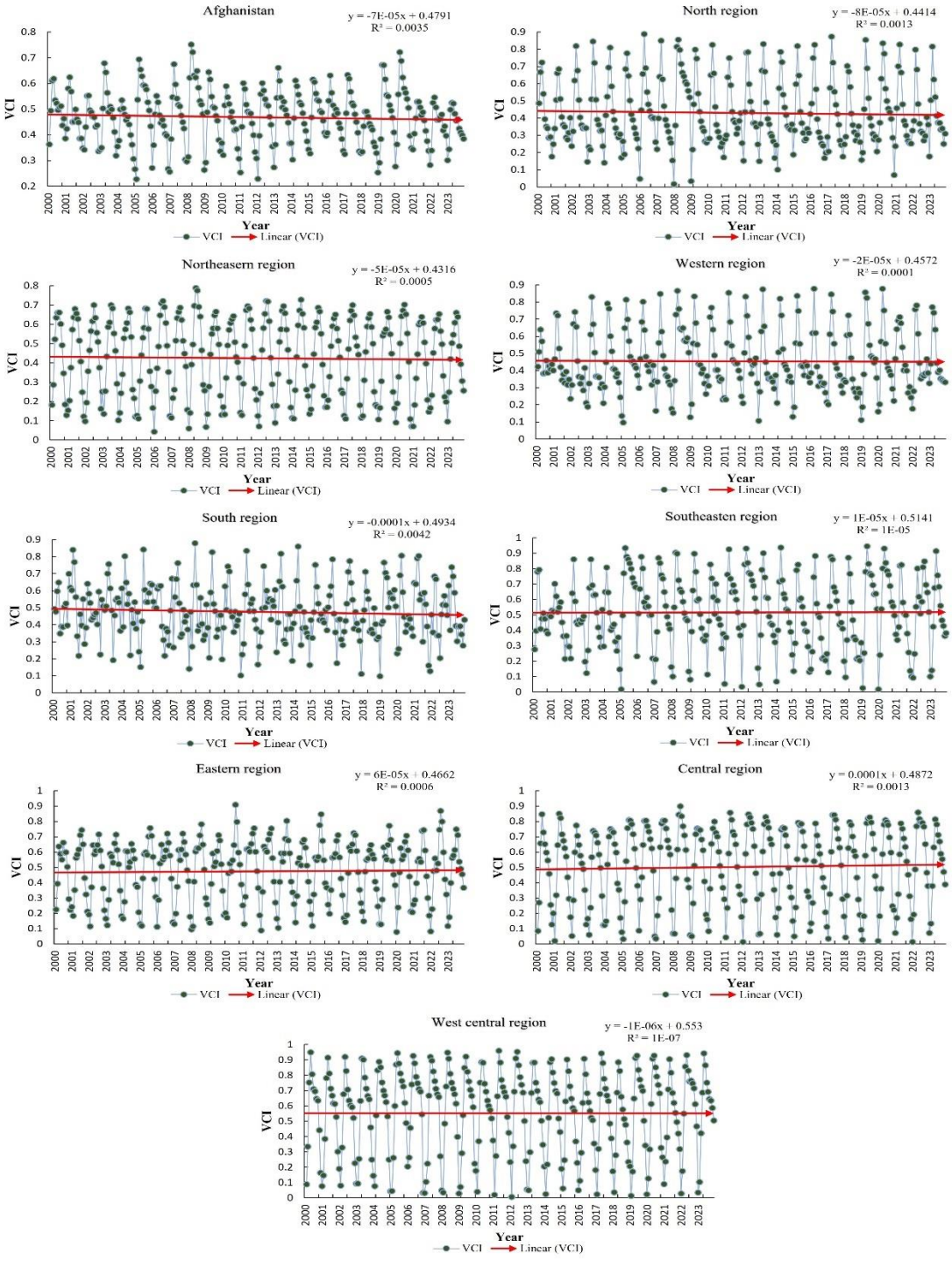

Figure 13. Monthly mean VCI time series trend analysis.

Figure 14 presents the TCI, which shows an increasing monthly trend throughout Afghanistan and in all regions. The TCI data across Afghanistan from 2000 to 2023 reveals notable seasonal variations in vegetation health, with distinct trends observed in different regions. Generally, winter months, particularly January and February, showcase favorable

TCI values across all regions, often exceeding 0.70. This indicates optimal conditions for plant growth, with the western and north regions recording peak TCI values, such as 0.92 in January 2008. However, the onset of spring marks a significant decline in TCI values in almost all areas, with some regions, like the western and South regions, experiencing critical lows of 0.07 and 0.08 in April 2000. These trends highlight a common vulnerability during the transitional period from winter to spring, where thermal stress poses a threat to vegetation health.

As the summer progresses, TCI values tend to dip further, reflecting adverse thermal conditions for vegetation across Afghanistan. Notably, the western and South regions exhibit some of the lowest recorded TCI values, with measurements of 0.04 in June 2001 and 0.09 in June 2010, respectively. In contrast, the northeastern region experiences significant thermal stress in June 2023, where TCI drops to 0.13, indicating heightened challenges for plant survival. Despite these low values, the majority of regions demonstrate some recovery during the autumn months, suggesting a potential for vegetation resilience as temperatures begin to cool.

Comparative analyses of TCI data also reveal that the northeastern region tends to experience greater fluctuations than others, indicating a heightened sensitivity to temperature changes. The peaks and troughs in TCI throughout the year, particularly the dramatic drops observed in spring and summer, emphasize the need for effective agricultural management practices tailored to regional climatic conditions. In the eastern and southeastern regions, while there are notable declines in TCI during summer, a recovery is often seen in the fall, indicating a critical window for improving vegetation health before winter sets in.

The TCI data across various regions of Afghanistan illustrates a complex interplay of seasonal temperature variations affecting vegetation health. While winter months provide generally favorable conditions for plant growth, the critical transitions into spring and summer expose vulnerabilities across all regions. Continuous monitoring and adaptive agricultural strategies will be essential to mitigate the impacts of climate variability and enhance the resilience of vegetation health in the face of changing thermal conditions.

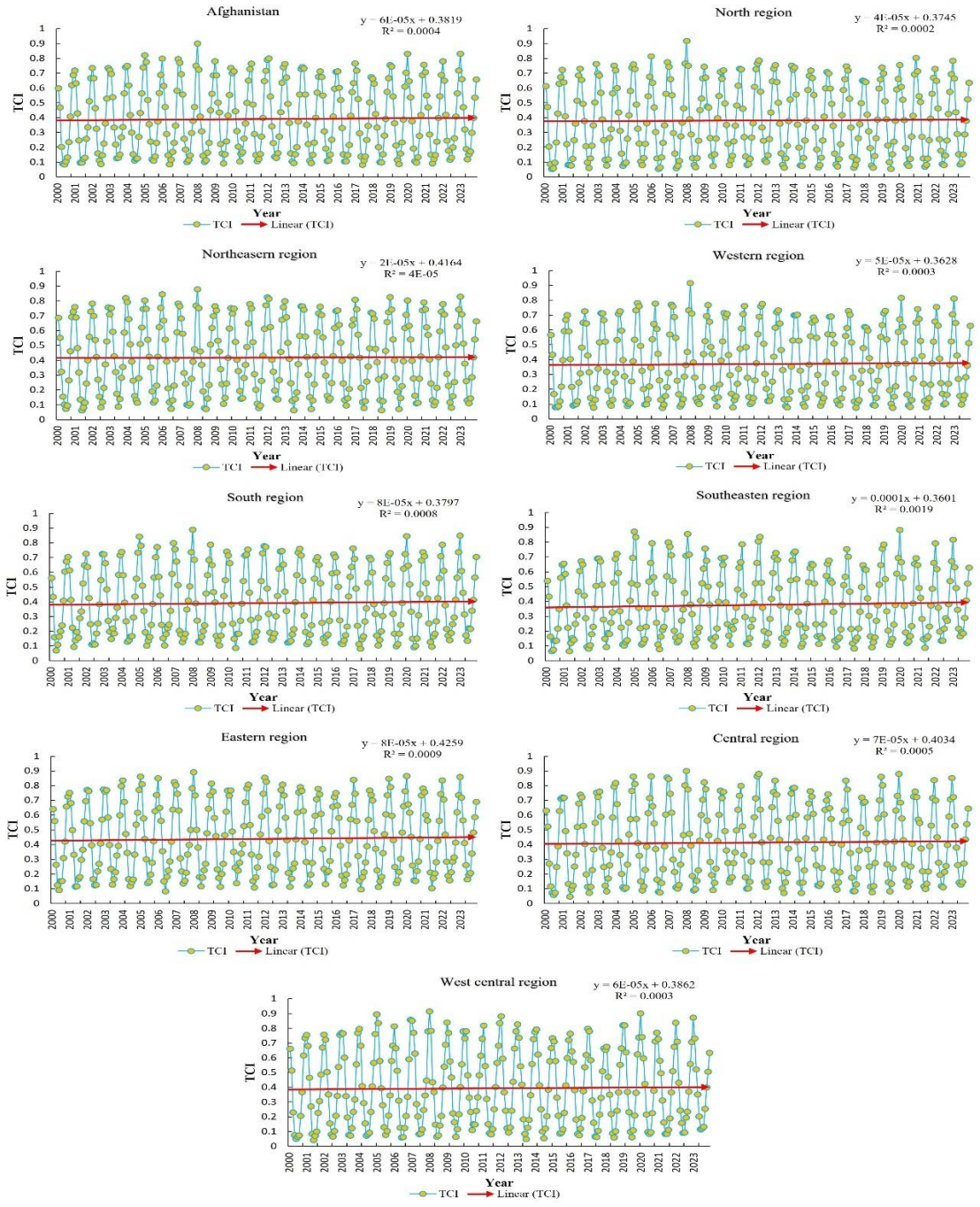

Figure 14. Monthly mean TCI time series trend analysis.

The VHI values are illustrated in Figure 15. The VHI, which combines both indices, indicates a slight increase in the trends for the Western, Southeastern, Eastern, Central, and West Central regions, while it shows a low decrease throughout Afghanistan and in the North, South, Western, and Northeastern regions. VHI data across Afghanistan from 2000 to 2023 illustrates distinct regional variations in vegetation health. In the South region, VHI values showed remarkable resilience, peaking at 0.74 in January 2023, despite experiencing

severe drops to 0.16 during summer months, particularly in July 2016. This indicates the region's capacity to recover from climatic stress, particularly in spring and winter. Similarly, the western region also demonstrated variability, starting from 0.49 in January 2000 and achieving a peak of 0.60 in March 2023. However, it faced significant declines during summer months, with values dropping to 0.20 in July 2016, reflecting similar challenges in moisture availability and thermal stress.

Comparatively, the north region exhibited a strong recovery trend with VHI reaching a high of 0.63 in March 2023. This region consistently showed favorable conditions in winter, highlighting the importance of these months for vegetation health. In contrast, the northeastern and eastern regions recorded generally lower VHI values, with the northeastern region peaking at 0.48 in February 2023 and the eastern region reaching a maximum of 0.58 in May 2005. Both regions also experienced significant declines during summer months, emphasizing the persistent challenges they face due to rising temperatures and limited moisture.

The central region displayed a notable recovery trend, peaking at 0.56 in October 2005 and stabilizing around 0.50 in 2023. Despite some fluctuations, it reflects an overall improvement in vegetation health, particularly in late spring and early summer. In comparison, the southeastern region demonstrated gradual improvement, particularly in early spring, with values reaching up to 0.59 in April 2012. However, it faced declines during mid-summer, indicating the critical need for effective land management strategies to mitigate climatic impacts.

Overall, the analysis of VHI data across different regions reveals varying degrees of resilience and stress in vegetation health. Regions like the south and west show strong recovery potential, while the north region stands out for its consistently favorable conditions. Conversely, the northeastern and eastern regions face ongoing challenges that necessitate effective management practices to enhance vegetation resilience. Continuous monitoring of VHI trends across all regions is essential to inform agricultural practices and support sustainable land management strategies amid changing climatic conditions.

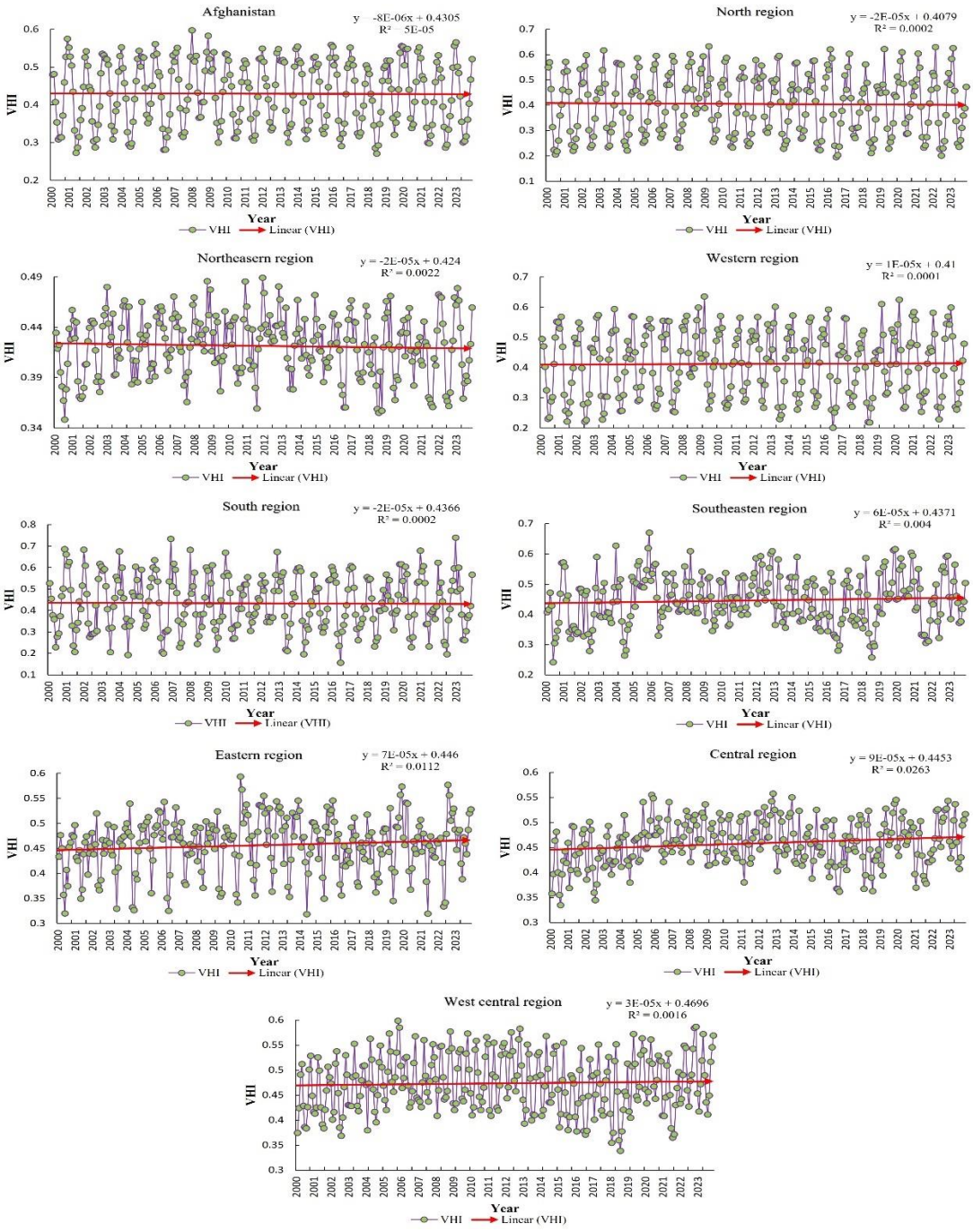

Figure 15. Monthly mean VHI time series trend analysis.

3.2. Results From the Seasonal Trend Analysis

This section analyzes the linear trends of various climate parameters including NDVI, LST, Ta, AET, PET, precipitation, soil moisture, and wind speed on a seasonal basis across Afghanistan. The country experiences distinct seasonal variations: spring spans March to May, summer from June to August, fall from September to November, and winter from December to February. Notably, the NDVI has shown a consistent upward trend throughout Afghanistan on a monthly scale, as depicted in Figure 16. Seasonal average NDVI data from 2000 to 2023 indicates significant growth, particularly in spring, where increased rainfall contributes to widespread vegetation cover. This surge in NDVI during spring is followed by a moderate increase in summer, largely due to rice cultivation in the northeastern region and extensive forests in the eastern and southeastern areas. However, a contrasting pattern emerges in winter, where NDVI levels are comparatively lower.

The analysis further reveals that the peak vegetation growth in spring was recorded in 2020, while the lowest growth levels were observed in the springs of 2000 and 2001. Interestingly, there was a noticeable decline in vegetation growth during the springs of 2021, 2022, and 2023, raising concerns about potential climatic or environmental stressors impacting vegetation health. Such fluctuations emphasize the importance of continuous monitoring and adaptive management strategies to address the challenges posed by climate variability in Afghanistan. By understanding these seasonal trends, stakeholders can develop targeted interventions to enhance vegetation resilience and ensure sustainable land use practices in the face of changing climatic conditions.

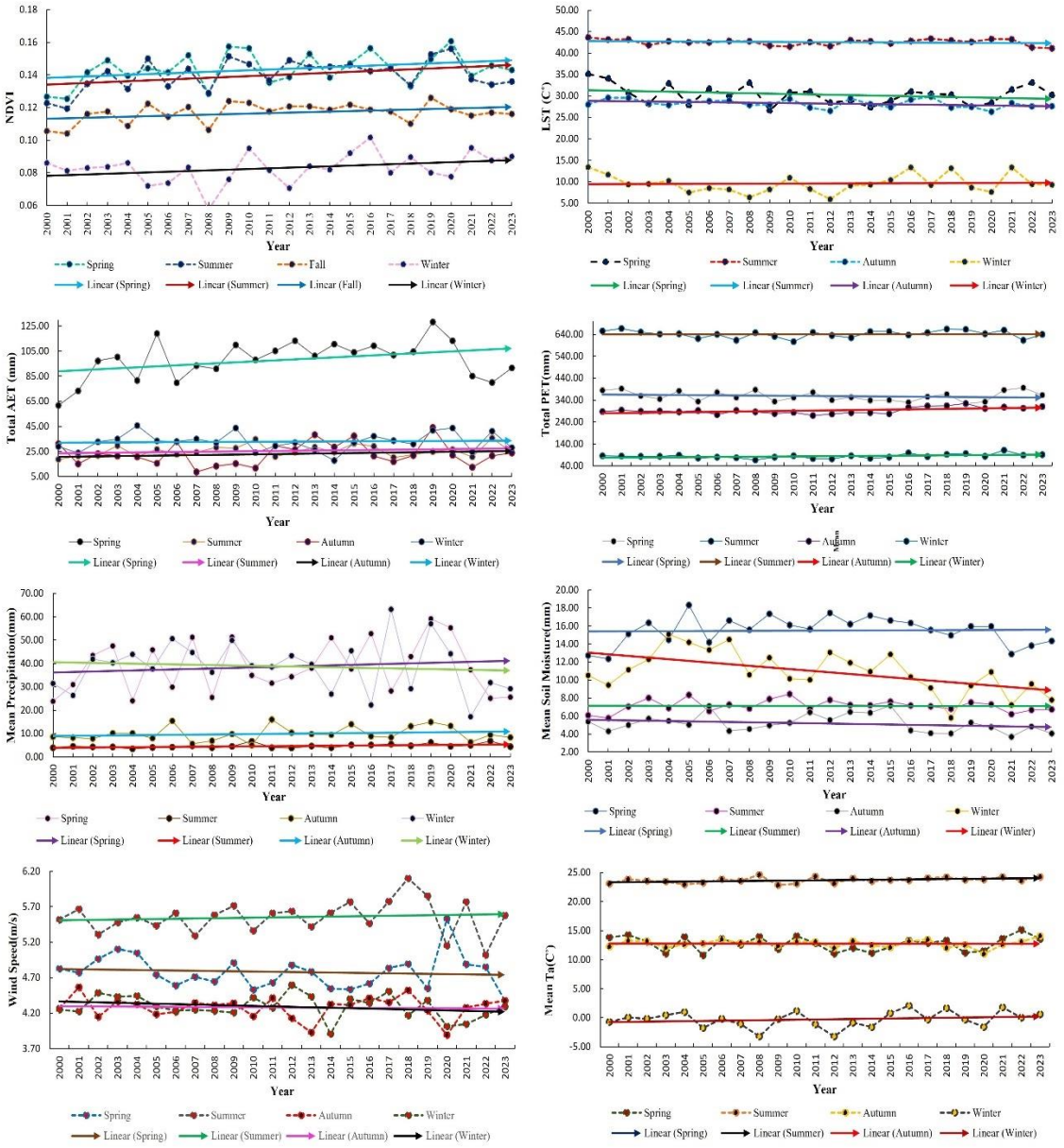

Figure 16. Seasonal trend analysis of NDVI, LST, Ta, AET, PET, Precipitation, Soil Moisture and Wind speed parameters in throughout Afghanistan.

According to Figure 16, the LST data averaged for seasonal analysis shows a decreasing trend throughout Afghanistan in all seasons. This trend may be influenced by NDVI, which has exhibited an increasing trend from 2000 to 2023 on both monthly and seasonal scales. The highest mean surface temperature reaches up to 45 °C in the summer season, while the lowest mean LST is around 15 °C in the winter season. The total AET values for each season, also depicted in Figure 16, show an increasing trend across all four seasons, with the highest actual evapotranspiration occurring in the spring. This can be attributed to the rising NDVI during this period. Furthermore, Figure 16 indicates that PET

data exhibits a constant trend in summer and winter, a decreasing trend in spring, and an increasing trend in autumn. In Afghanistan, the highest temperatures occur in the summer, leading to elevated levels of PET during this season due to its direct relationship with LST. Additionally, the maximum precipitation is recorded in spring and winter, with an increasing trend observed in spring and a decreasing trend in winter. Conversely, precipitation levels in the summer and autumn seasons are significantly low across Afghanistan.

As illustrated in Figure 16, the Soil Moisture levels throughout Afghanistan exhibit varying trends across the seasons. There is a relative increase during the spring season; however, a significant decrease is observed in winter, likely due to reduced precipitation, which shows a declining trend during this season. Conversely, both summer and autumn display a relatively increasing trend in Soil Moisture, attributed to a rise in precipitation. On average, the highest wind speeds in Afghanistan occur during the summer, peaking at nearly 6 m/s in the summer of 2018. While summer shows an increasing trend in wind speed, the other seasons exhibit a decreasing trend, with the highest wind speeds recorded in the western and South regions.

Additionally, Figure 16 presents Ta values calculated for each season, revealing a trend where summer has the highest average temperatures and winter has the lowest. Air temperature demonstrates a relatively increasing trend in both summer and winter, while spring and autumn show a relatively low trend, which may be linked to the increase in vegetation and precipitation observed across Afghanistan in recent years.

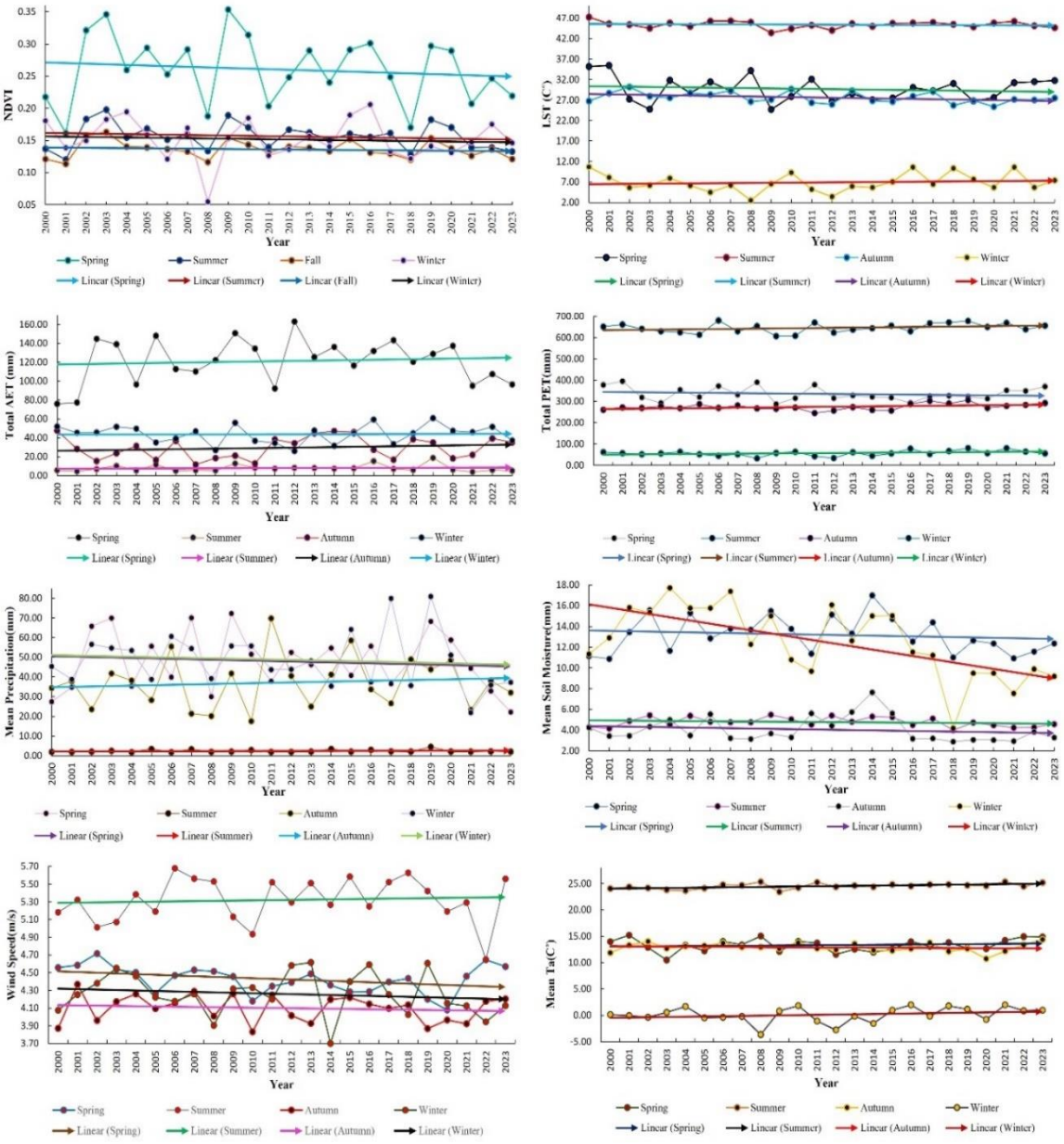

Figure 17. Seasonal trend analysis of NDVI, LST, Ta, AET, PET, Precipitation, Soil Moisture and Wind speed parameters in North Region.

The climate parameters examined on a seasonal scale in the North region are illustrated in Figure 17. In this area, the maximum value of NDVI fluctuated up to 0.3 during the spring season but has shown a decreasing trend throughout all four seasons. The decline in NDVI during spring may be attributed to low levels of precipitation and soil moisture, as the North region experiences a dry climate. Additionally, the LST trend during the summer, spring, and autumn seasons shows a relative decrease, while a slight increase is observed in the winter season. Notably, in the springs of 2021, 2022, and 2023, there is a relative increase

in LST, which likely contributes to the overall decrease in NDVI during these years. The AET values have also been analyzed in this region on a seasonal scale. Here, AET exhibits an increasing trend across all four seasons, with the highest actual evapotranspiration occurring in the spring season. However, the amount of AET has decreased in recent years during spring. The maximum PET in this region occurs in the summer, with a relatively increasing trend observed during the summer, fall, and winter seasons, while a relatively decreasing trend is noted in spring.

The amount of precipitation in this region, as shown in Figure 17, occurs primarily in spring, winter, and autumn, with little to no precipitation during the summer. Consequently, the differences in precipitation among these three seasons are minimal. A decreasing trend is observed in the spring and winter seasons, while an increasing trend is noted in autumn; however, no significant trend is evident during the summer. Between 2000 and 2023, the highest levels of soil moisture in this region were recorded in the spring and winter seasons, but in recent years, there was a notable decrease in soil moisture during both the winter and spring. The decrease in soil moisture has become more pronounced in the winter, while the trend in the spring has remained relatively stable. Most areas in this region consist of dry and waterless lands, with only a small portion irrigated using groundwater during the summer and autumn.

As illustrated in Figure 17, the highest wind speed in the North region between 2000 and 2023 occurs during the summer season. Most areas in this region consist of flat plains, which contributes to the higher wind speeds. The increase in wind speed during the summer is attributed to the decline in vegetation cover, actual evapotranspiration (AET), and other factors. This rise in wind speed has also led to an increase in potential evapotranspiration (PET). In this region, the highest air temperature (Ta) is recorded in the summer season. Although the land surface temperature (LST) in this region averages up to 47°C during summer, the average Ta level reaches about 25°C. This discrepancy can be primarily attributed to the increase in wind speed, and no significant trend is observed for the Ta parameter across the seasons.

As depicted in Figure 18, the climate parameters were analyzed on a seasonal scale in the Northeastern region. In this area, the NDVI exhibits an increasing trend across all seasons, with notable growth in recent years attributed to effective groundwater management. The highest NDVI values are observed during the summer season, primarily

due to rice cultivation in certain parts of the region, where growth peaks in June and July. Additionally, plant growth in the Pamir areas also reaches its zenith during the summer.

According to Figure 18, the LST parameter shows a consistent trend across all four seasons, with the highest values recorded in summer and the lowest in winter. Meanwhile, the AET value has demonstrated an increasing trend throughout all seasons. This increase may explain the relative rise in LST observed in some years, as the AET values have also risen. Changes in vegetation types have contributed to this increase in AET. And PET data has a relatively increasing trend in winter, autumn, and summer and a slightly decreasing trend in spring. In this region, the maximum amount of PET is created in the summer season, due to the low LST, the total maximum amount of PET reaches up to 500 mm during the summer season. Also, the highest amount of precipitation that occurs in spring and winter decreased. Especially, the amount of precipitation has decreased a lot in recent years, the reason for this can be the change in atmospheric and precipitation patterns in the region.

Also, as shown in Figure 18, the Soil Moisture values exhibit a decreasing trend throughout the seasons, likely due to the decline in Precipitation. The highest levels of humidity are observed in spring; however, the humidity levels are generally higher in summer than in autumn. This is attributed to the Pamir Mountains, which are covered with snow that melts during the summer months, contributing to increased humidity in these areas. Most of the land in this region is covered by mountains, which results in very low wind speeds.

As illustrated in Figure 18. However, the highest wind speeds occur during the summer season, with a notable increase observed in this period. Conversely, a decreasing trend in wind speed was recorded in the other seasons. Additionally, Figure 18 indicates that the air temperature exhibits a relatively increasing trend throughout the year. In this region, the average air temperature reaches a maximum of 15 °C in summer, while the lowest temperature can drop to -15 °C in winter.

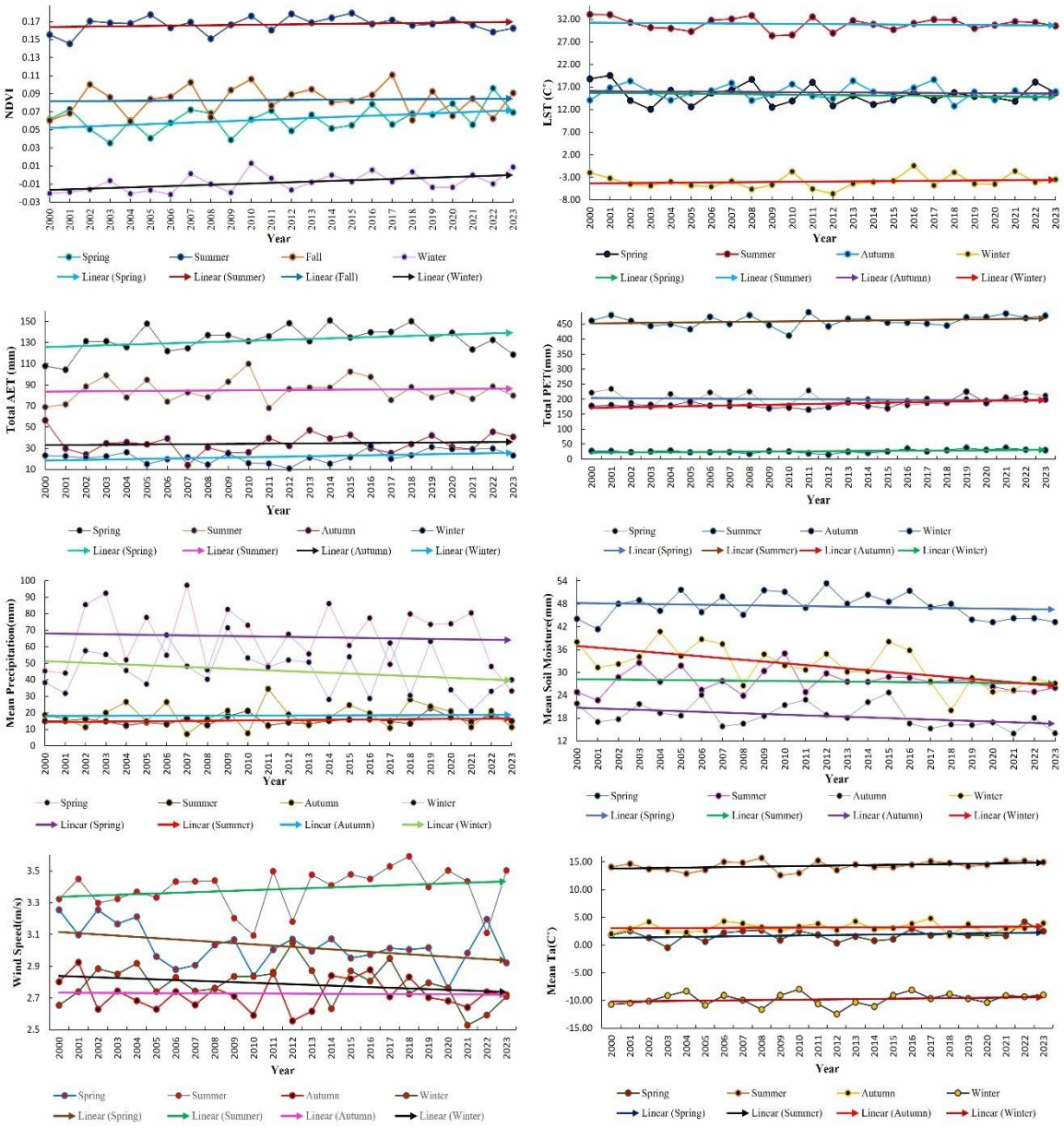

Figure 18. Seasonal trend analysis of NDVI, LST, Ta, AET, PET, Precipitation, Soil Moisture and Wind speed parameters in Northeastern region.

Figure 19 illustrates the climate parameters on a seasonal scale. The NDVI data shows an increasing trend throughout the seasons, with the highest values observed in spring. This is primarily because the LST does not fall below zero in this region during winter, resulting in minimal differences in NDVI levels across summer, autumn, and winter. Residents in this region have utilized solar panels to extract groundwater, enabling the cultivation of various crops, which has contributed to the rise in NDVI. The peak NDVI was recorded in the spring of 2020, reaching 0.15; however, in 2021, 2022, and 2023, the growth rate of NDVI declined.

Meanwhile, LST shows a slight increase during the summer but decreases in winter, spring, and autumn. This decrease in LST is attributed to the rising NDVI in the region, with LST levels exceeding 50 °C during the summer months.

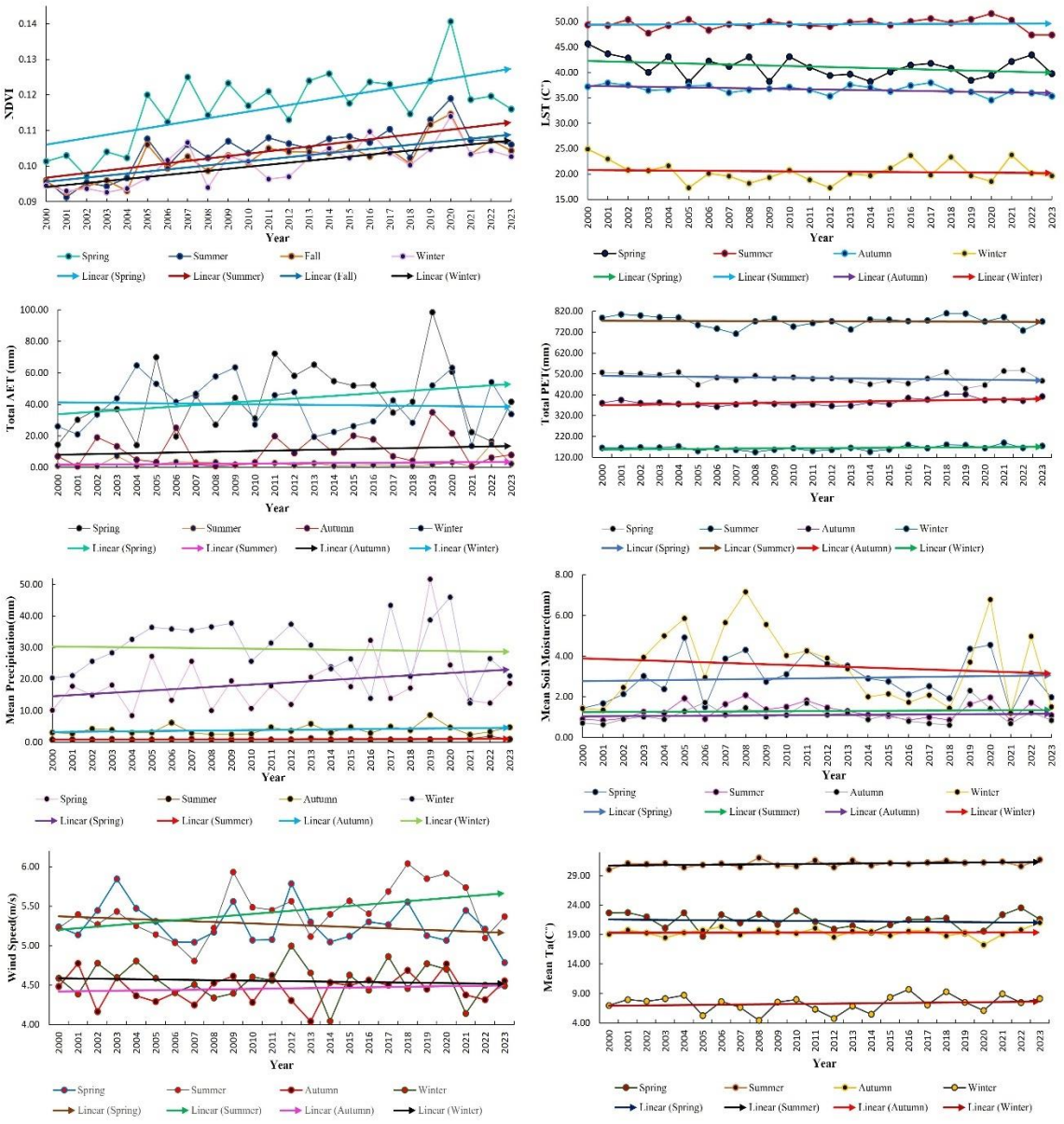

Figure 19. Seasonal trend analysis of NDVI, LST, Ta, AET, PET, Precipitation, Soil Moisture and Wind speed parameters in South Region.

According to Figure 19, the AET parameter exhibits an increasing trend in spring, summer, and autumn, while showing a decreasing trend in winter. In this region, the low vegetation cover, loss of surface water, and limited rainfall contribute to lower AET levels. The highest amount of AET occurs in spring, reaching up to 80 mm. Due to the elevated

LST in this area, the PET parameter peaks during the summer, but no significant trend is observed across the seasons. Additionally, the precipitation parameter demonstrates an increasing trend in spring and autumn, while a decreasing trend is noted in winter. The summer season does not show a significant trend due to the loss of precipitation, with winter precipitation levels being very low, typically around 40 to 50 mm.

As the precipitation decreases in winter, soil moisture levels also decline in the South region. Surface moisture is notably low in this area, ranging from 3 to 7 mm during winter and spring, primarily due to insufficient rainfall and vegetation. This region experiences high wind speeds due to its flat plains, with the highest wind speeds occurring in spring and summer, reaching up to 5-6 m/s. Wind speed trends show an increase in summer and autumn but a decrease in spring and winter. Furthermore, air temperatures in this region are generally higher than in other areas, with the average temperature peaking in summer. However, there is no significant trend in air temperature across any of the seasons, as illustrated in Figure 19.

The climate parameters for the southeastern region are examined in Figure 20. In this area, the growth of NDVI remains relatively stable across spring, summer, and autumn due to the prevalence of forest cover. NDVI values exhibit an increasing trend throughout the year. Conversely, LST values demonstrate a decreasing trend in all seasons, with the highest temperatures occurring in the summer. The density of forest cover in this region contributes to higher AET levels, which also show an increasing trend across all four seasons, peaking in spring. The maximum amount of PET is recorded in the summer season, reaching up to 600 mm, but it exhibits a decreasing trend throughout the year, which is related to the decline in LST. Additionally, precipitation in this region shows an increasing trend in spring, summer, and autumn, while a decreasing trend is observed in winter. The highest precipitation levels are recorded in spring and winter, with the Mediterranean climate also contributing to occasional summer rainfall.

According to Figure 20, the Soil Moisture levels in this region exhibit an increasing trend in spring, summer, and autumn, while a decreasing trend is observed in winter, similar to precipitation patterns. The wind speed is most prominent in the spring season, showing a decreasing trend, while an increasing trend is noted in the other seasons. Although wind speed has significantly decreased in recent years during spring, there was a slight increase in the other seasons. The air temperature shows a slight decreasing trend in summer and spring, whereas it exhibits a slight increasing trend in winter and autumn.

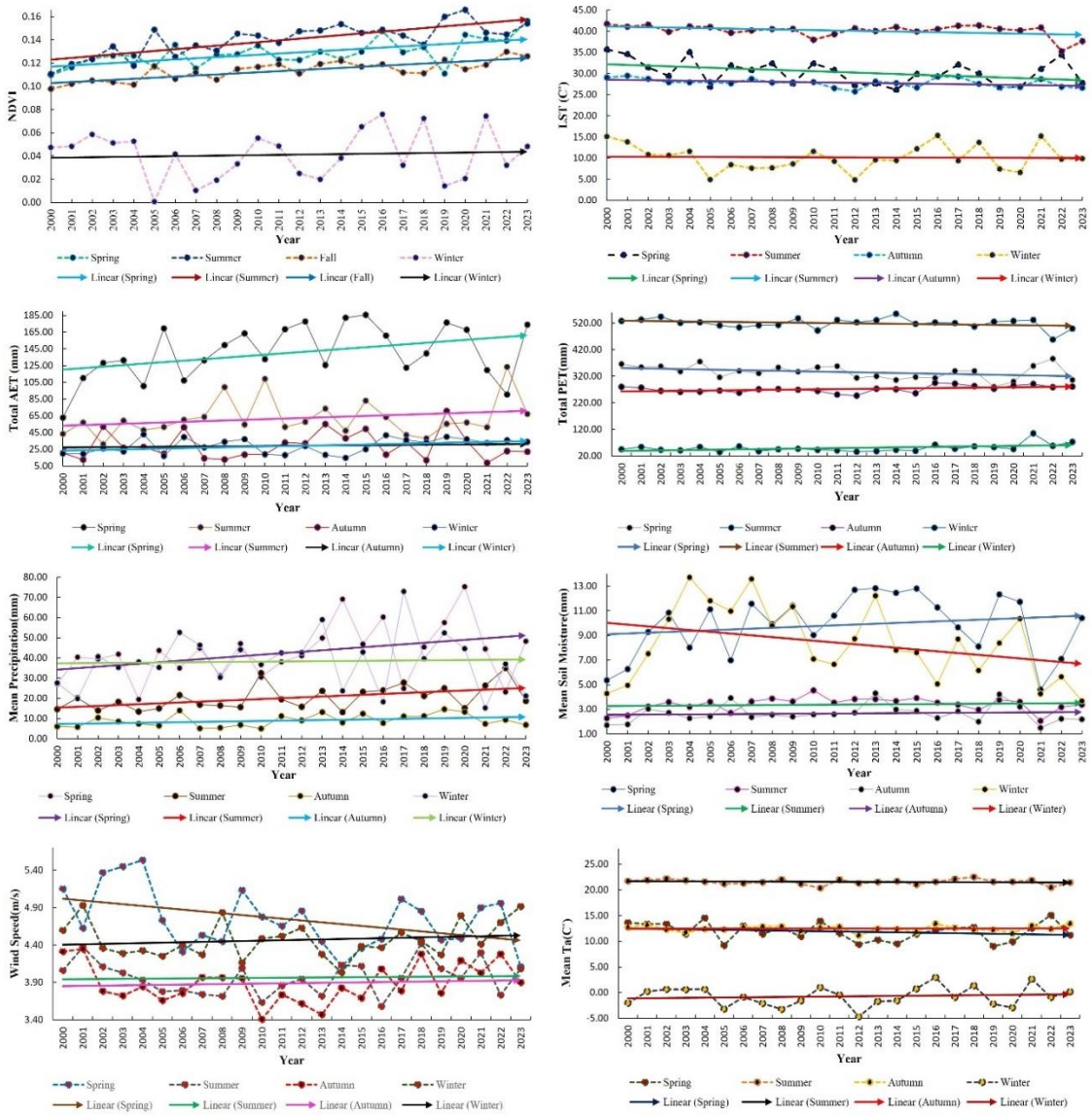

Figure 20. Seasonal trend analysis of NDVI, LST, Ta, AET, PET, Precipitation, Soil Moisture and Wind speed parameters in Southeastern Region.

Figure 21 illustrates the climate parameters of the western region. In this area, the NDVI has shown an increase during all seasons from 2000 to 2023. The local population utilizes solar panels to extract underground water, contributing to the rise in NDVI; however, the overall NDVI value in this region remains quite low. The LST has decreased during spring, summer, and autumn between 2000 and 2023, with a slight increase observed in winter. The highest LST is recorded in summer, reaching up to 47 °C. The AET in spring peaks at around 120 mm and has exhibited an increasing trend, but it has decreased since

2019. Due to the dryness prevalent in the summer, the AET is significantly low during that season. Additionally, the highest PET occurs in summer, reaching up to 750 mm, while the lowest levels are observed in winter.

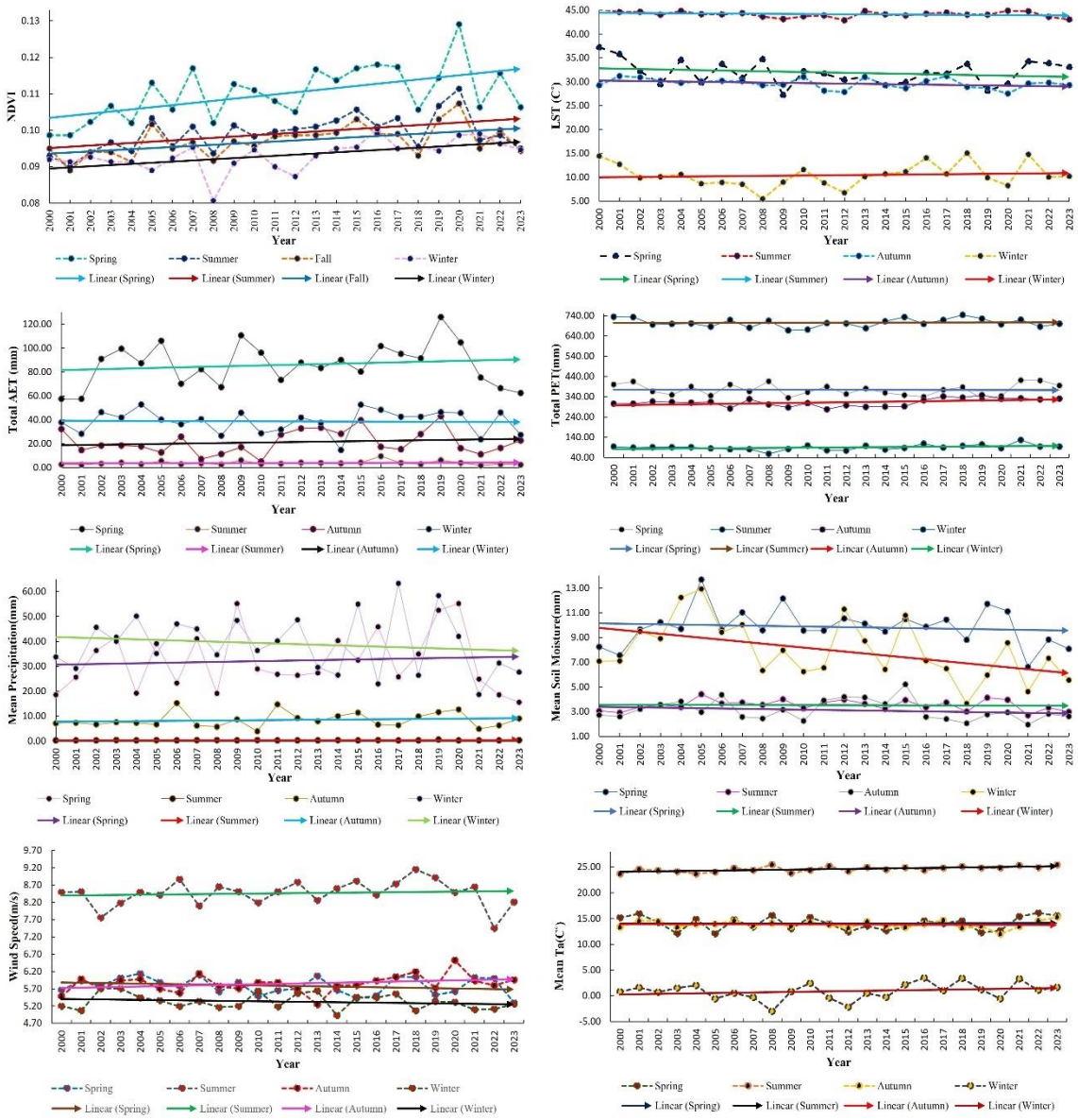

Figure 21. Seasonal trend analysis of NDVI, LST, Ta, AET, PET, Precipitation, Soil Moisture and Wind speed parameters in Western Region.

The mean values of precipitation in Figure 21 illustrate seasonal variations, with the highest amounts occurring in spring and winter. Notably, the peak precipitation was recorded in winter 2017. However, due to a decline in rainfall in recent years, winter precipitation has started to decrease, while spring precipitation has shown a slight upward trend. Soil moisture levels have declined across all seasons, particularly in winter. This decrease was gradual

starting in 2005 during both winter and spring. The western region of Afghanistan experiences the highest wind speeds in the country. As depicted in Figure 21, the highest wind speed in spring exceeds 9 m/s, and this region exhibits consistent wind speeds that do not fluctuate significantly throughout the seasons. The relatively high wind speeds can be attributed to the flat and sandy plains. Additionally, the mean air temperature in summer surpasses 25°C and has generally increased in spring, summer, and winter from 2000 to 2023.

As shown in Figure 22, the eastern region of Afghanistan has significant forest cover, and between 2000 and 2023, the growth of horticulture and the increasing interest in agriculture have contributed to the rise in NDVI in this area. In this region, NDVI displays an upward trend throughout all four seasons, with the highest values observed in summer, followed by autumn. During these seasons, the forests reach their peak growth. The amount of LST has decreased during summer, spring, and autumn, which can be attributed to the rise in NDVI. However, in winter, LST has shown a slight increase due to the Mediterranean climate of the region, which prevents temperatures from falling below zero. Additionally, AET has risen in spring and summer, with the lowest recorded AET in 2000, after which it has steadily increased.

According to Figure 22, PET exhibits an increasing trend in spring and summer, while a decreasing trend is observed in the other seasons. The rise in PET during spring and summer is attributed to the decline in LST. Precipitation shows an increasing trend across all four seasons in this region, with the highest amounts recorded in spring and winter. Due to the Mediterranean climate, this area occasionally experiences rainfall in the summer; however, precipitation has decreased in 2021, 2022, and 2023. Soil moisture has increased in spring and summer; conversely, during winter, when precipitation slightly rises, soil moisture significantly decreases. This reduction can be attributed to the high permeability of the soil, the steep slopes in the region, and the fact that a large portion of rainwater is absorbed by plants before it can be stored in the soil. The eastern region experiences low wind speeds due to its mountainous terrain, with maximum average wind speeds not exceeding 4 m/s, and this figure has decreased during the spring season. Additionally, air temperature increases in spring and summer but decreases in winter and autumn.

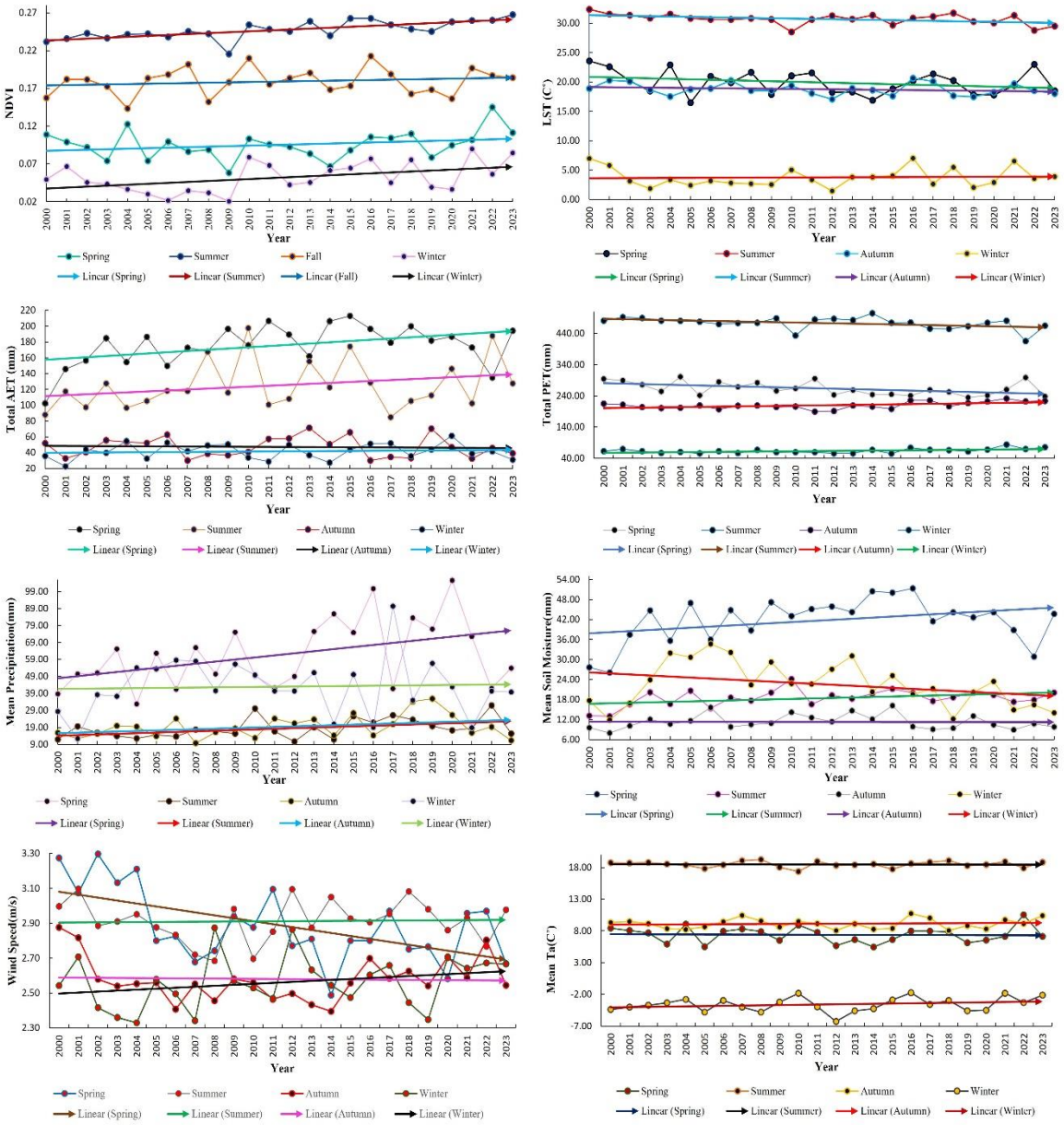

Figure 22. Seasonal trend analysis of NDVI, LST, Ta, AET, PET, Precipitation, Soil Moisture and Wind speed parameters in Eastern Region.

As illustrated in Figure 23, NDVI exhibits an increasing trend in all seasons. However, NDVI remains very weak in this region, as very few lands are used for agriculture and gardens, with most of the land being mountainous and devoid of vegetation. The highest growth of NDVI was observed in the summer season, followed by autumn, as the melting snow during this time provides plants with access to water sources. The amount of LST shows a decreasing trend in spring, summer, and autumn, while a slight increasing trend is noted in winter. Conversely, the highest amount of AET is observed in the spring season,

with an increasing trend throughout the year. In this region, the average LST in spring exceeds 35 °C, and the PET fluctuates up to 500 mm during the summer season.

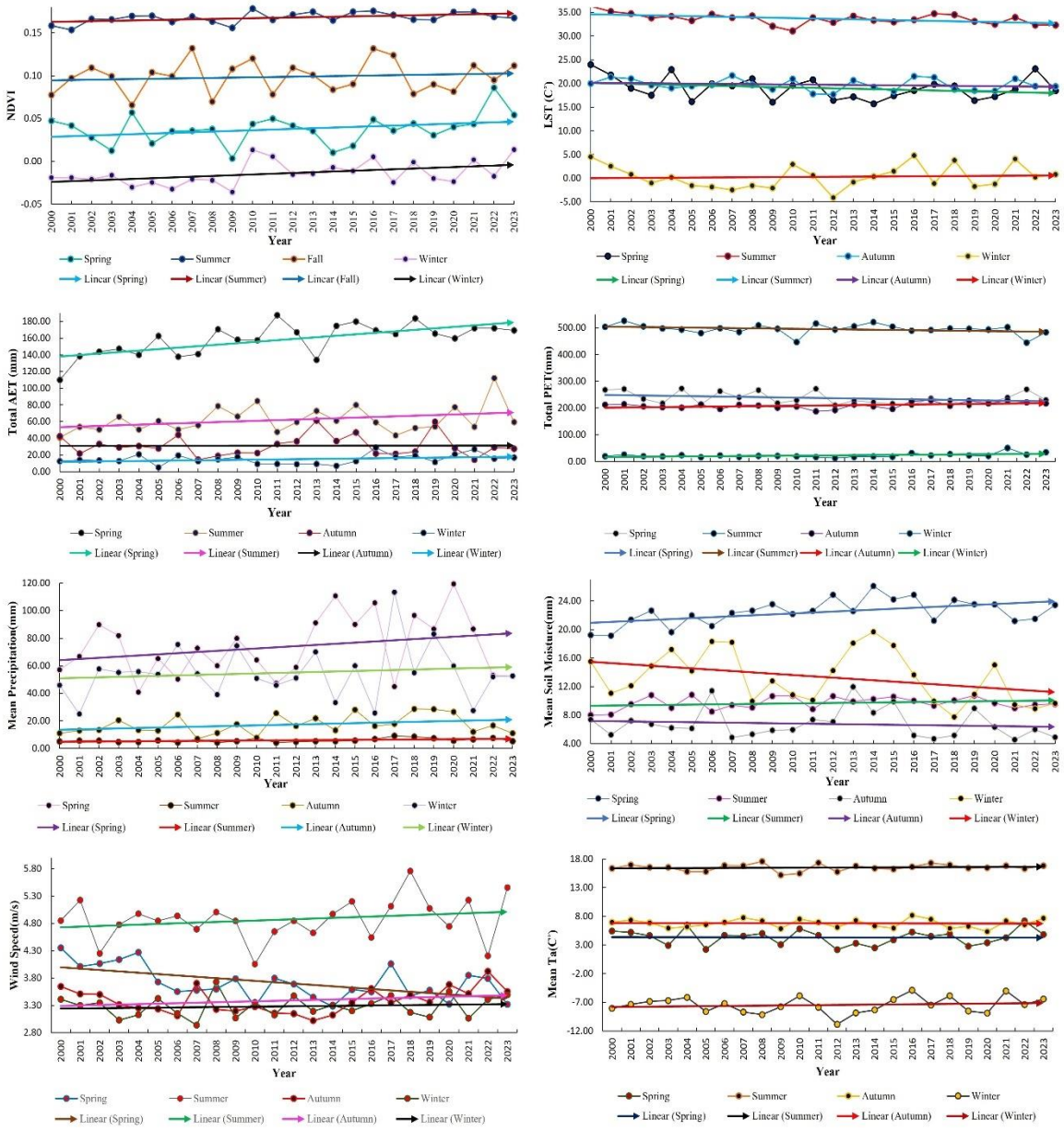

Figure 23. Seasonal trend analysis of NDVI, LST, Ta, AET, PET, Precipitation, Soil Moisture and Wind speed parameters in Central Region.

As illustrated in Figure 23, the amount of precipitation shows an increasing trend in spring, winter, and autumn. However, while Soil Moisture in the spring season is on the rise, it exhibits a decreasing trend in winter, which may be attributed to the slopes of the mountains. Between 2000 and 2023, wind speed values in summer, winter, and autumn have

shown an increasing trend, although a decrease was noted during the winter season. In this region, the highest wind speed is observed in summer, reflecting an upward trend, whereas it has started to decline in spring. The decrease in wind speed during spring correlates with increases in soil moisture and AET, while LST has decreased. This is due to the inverse relationship between wind speed and soil moisture/AET and the direct relationship between wind speed and LST. Additionally, the highest air temperature in this region can reach up to 20 °C in summer, while it drops below 0 °C in winter.

Figure 24 illustrates the climate parameters of the West Central region. In this area, the NDVI has shown an increase throughout all seasons from 2000 to 2023. The highest NDVI values were observed in summer and autumn, primarily because much of the land in this region is mountainous and covered with snow during spring and winter. As the snow melts in summer, it enhances plant growth. On the other hand, the increase in NDVI has led to a decrease in LST during spring, summer, and autumn. In spring, the decline in wind speed and the increase in precipitation have contributed to a rise in AET. Additionally, the reduction in wind speed during this season has resulted in higher soil moisture levels.

As indicated in Figure 24, the highest amount of PET is observed during the summer season; however, it exhibits a decreasing trend, likely due to the reduction in LST during this period. Additionally, while precipitation levels are increasing in spring, they have decreased in winter, possibly due to lower AET. In this mountainous region, air temperatures in winter can drop below 0°C due to snowfall. Conversely, Ta has increased in summer and winter but decreased in spring and autumn.

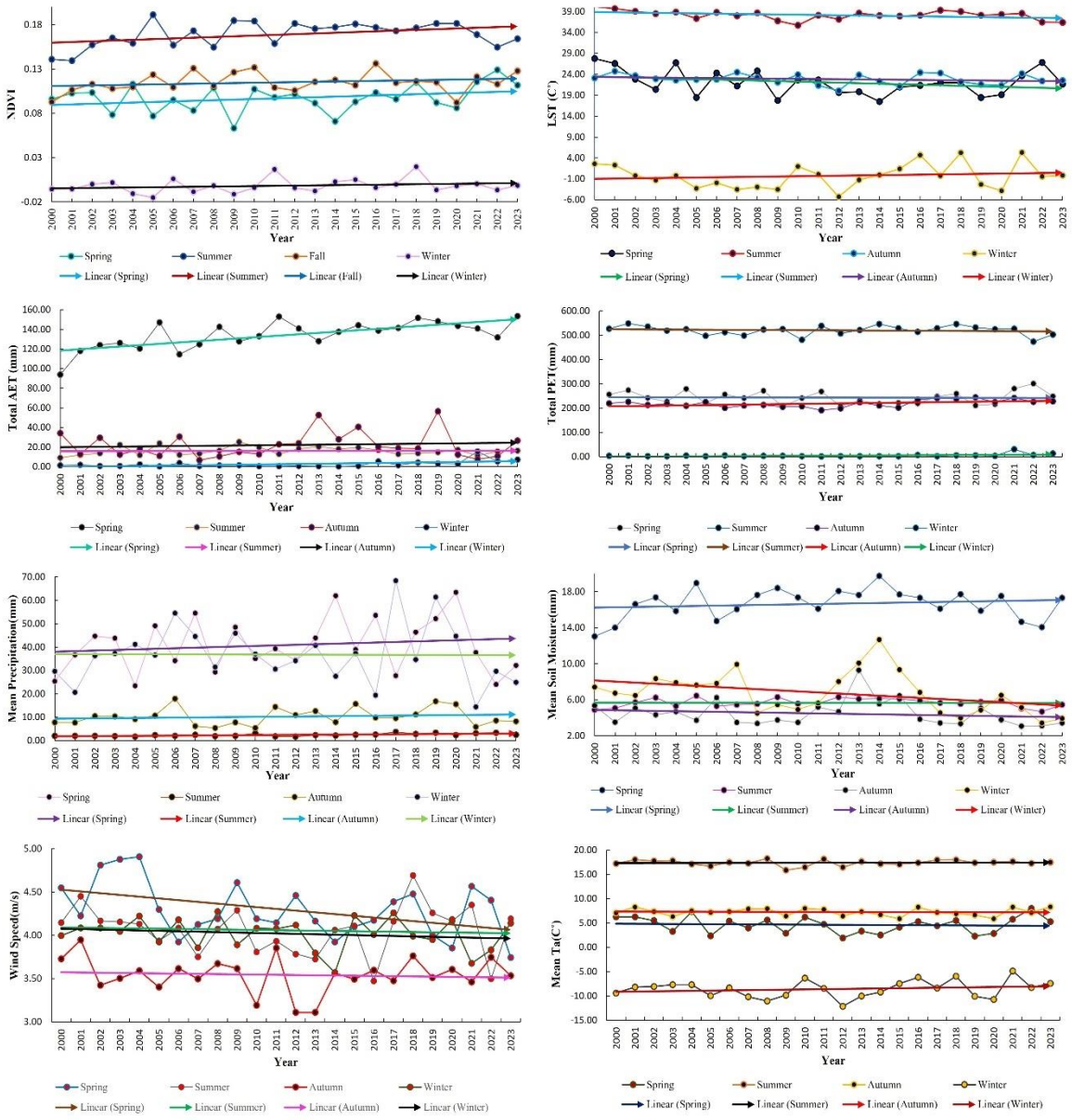

Figure 24. Seasonal trend analysis of NDVI, LST, Ta, AET, PET, Precipitation, Soil Moisture and Wind speed parameters in West Central Region.

3.3. Results From the Annually Trend Analysis

In this section, the results of the linear trend analysis for the climate parameters (NDVI, LST, VCI, TCI, VHI, Ta, AET, PET, precipitation, soil moisture, and wind speed) were examined on an annual scale. As illustrated in Figure 25, among the clımate parameters analyzed annually in Afghanistan, the NDVI, TCI, AET, PET, and Ta parameters exhibit a

linearly increasing trend. In contrast, the LST, VCI, soil moisture, and wind speed parameters show a decreasing trend, while precipitation and VHI demonstrate stable trends.

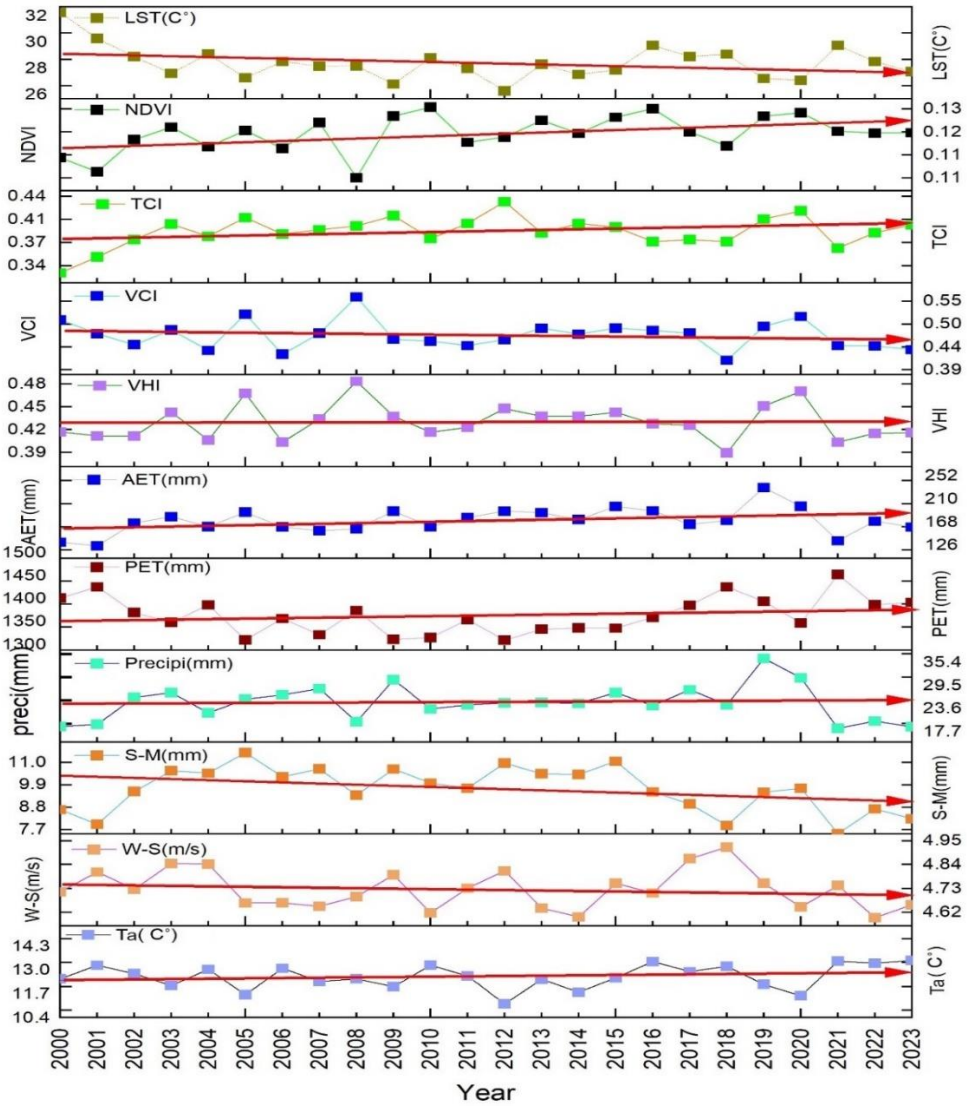

Figure 25. Annually trend analysis of NDVI, LST, Ta, AET, PET, Precipitation, Soil Moisture, VCI, TCI, VHI and Wind speed parameter in throughout Afghanistan.

As shown in Figure 25, there is a notable increase in the NDVI, which corresponds with a decrease in LST. This trend indicates that as land surface temperatures decline, vegetation health and coverage, as represented by NDVI, improve. Additionally, the TCI has risen, influenced by a reduction in soil moisture levels. The increase in AET further supports this trend, highlighting that higher evapotranspiration rates are contributing to enhanced vegetation growth. Furthermore, the air temperature has displayed an increasing trend, which

has led to a rise in PET, underscoring the complex interplay between temperature, moisture availability, and plant growth in the region.

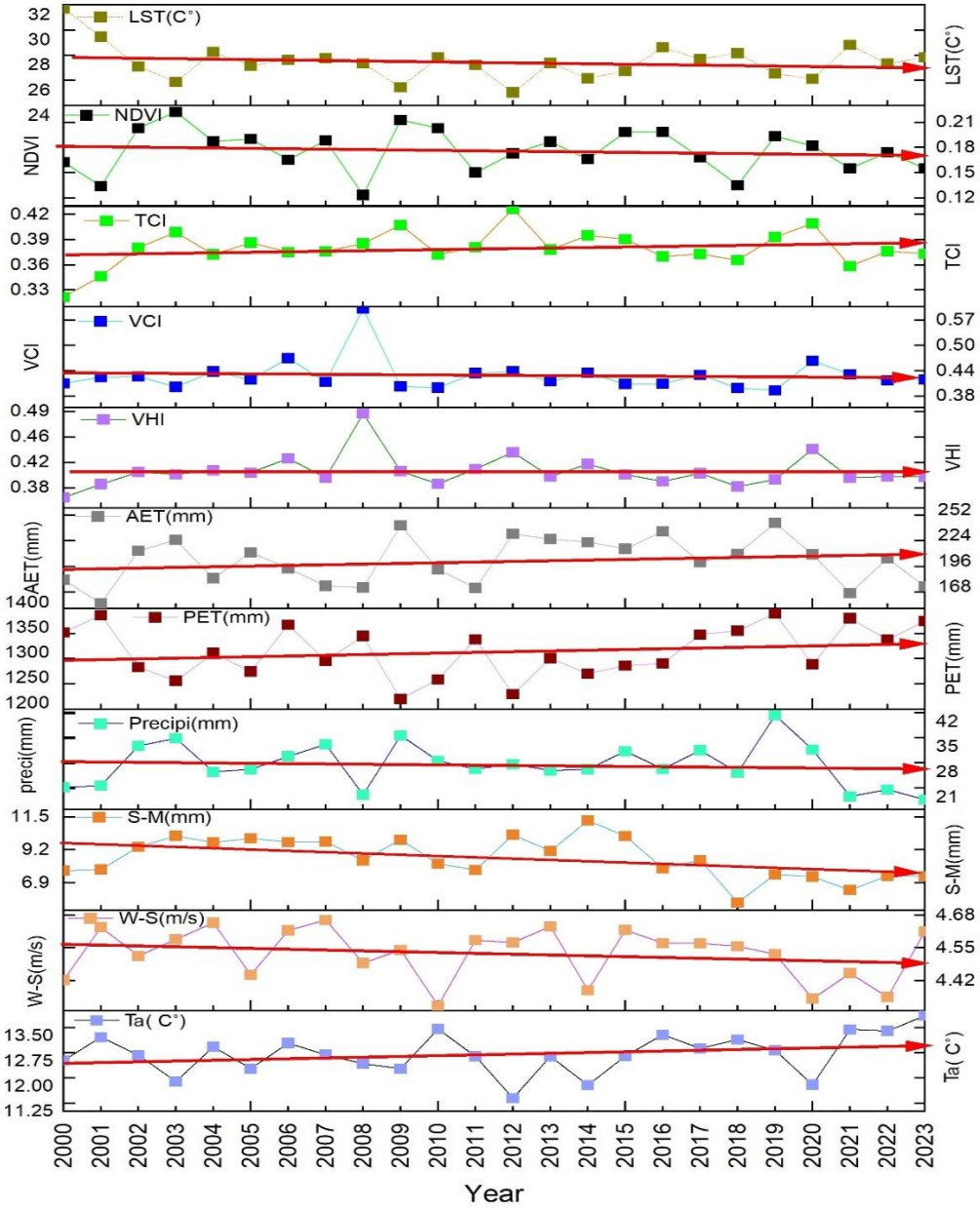

Figure 26. Annually trend analysis of NDVI, LST, Ta, AET, PET, Precipitation, Soil Moisture, VCI, TCI, VHI and Wind speed parameters in North region.

According to Figure 26, the indices for TCI, AET, PET, and Ta show a distinct increasing trend, while NDVI, LST, precipitation, soil moisture, and wind speed indices exhibit a declining trend. Additionally, the trends for TCI and ET indices remain relatively constant. In the north region, LST demonstrates a notably low decreasing trend, in contrast to the rising trend observed in air temperature. The decline in NDVI is attributed to

reductions in precipitation and soil moisture. However, both AET and PET are on the rise, indicating an increase in evapotranspiration despite the challenges posed by decreasing moisture levels.

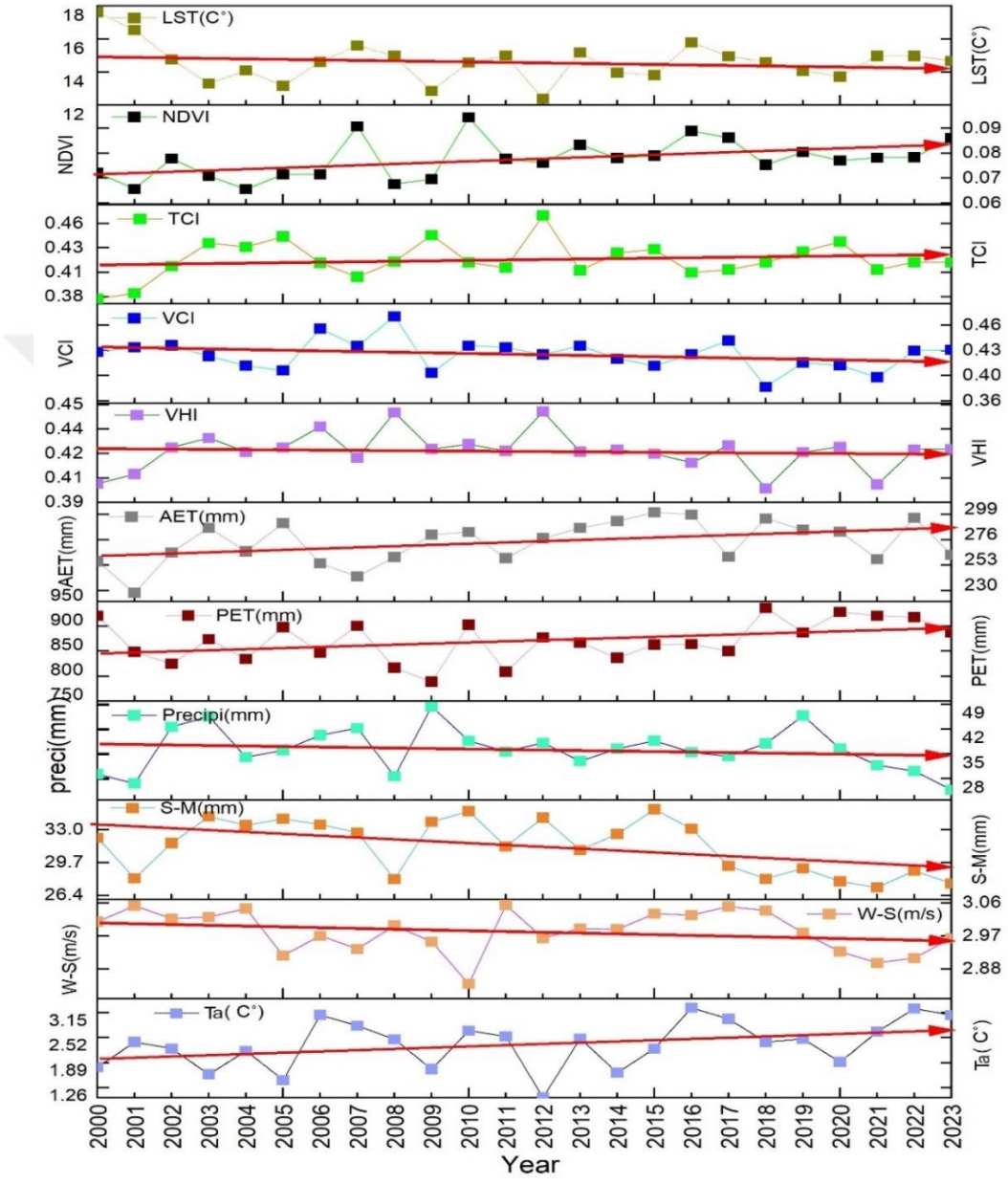

Figure 27. Annually trend analysis of NDVI, LST, Ta, AET, PET, Precipitation, Soil Moisture, VCI, TCI, VHI and Wind speed parameters in Northeastern region.

As illustrated in Figure 27, the NDVI, AET, PET, TCI, and Ta parameters exhibit an increasing trend, while the LST, precipitation, soil moisture, VCI, VHI, and wind speed parameter demonstrate a decreasing trend. In the northeast region, the decline in LST correlates with an increase in NDVI, indicating a rise in AET. However, both precipitation

and soil moisture levels have decreased. Conversely, the amount of Ta has increased, suggesting higher PET levels. Additionally, while TCI has risen, both VCI and VHI have shown a decline.

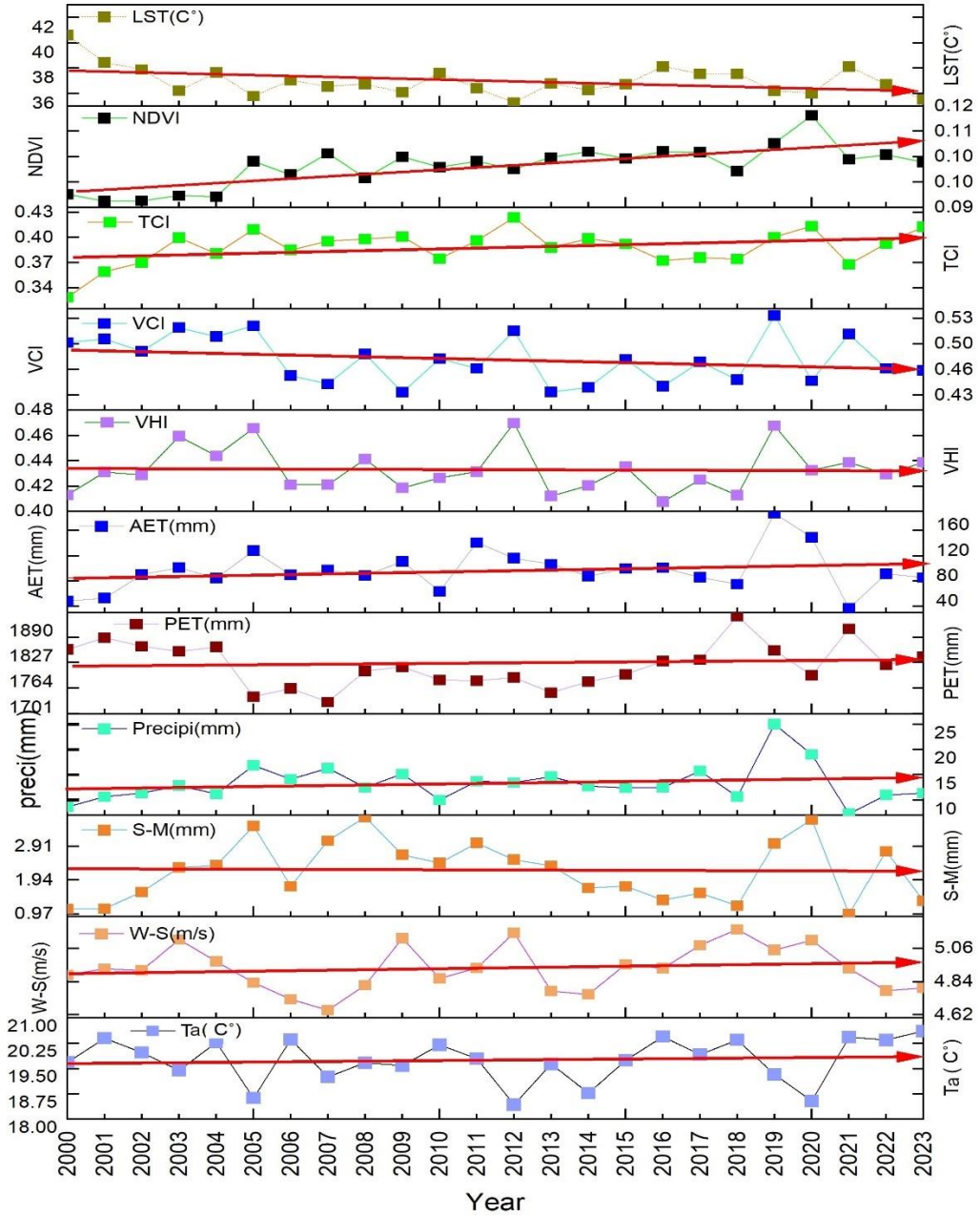

Figure 28. Annually trend analysis of NDVI, LST, Ta, AET, PET, Precipitation, Soil Moisture, VCI, TCI, VHI and Wind speed parameters in South region.

As depicted in Figure 28, the NDVI, AET, PET, TCI, precipitation, wind speed, and Ta parameters show an increasing trend in the South region, while the LST, soil moisture, VCI, and VHI parameters exhibit a decreasing trend. In this area, the decline in LST is

associated with an increase in NDVI, which subsequently leads to a rise in AET. This increase in AET has contributed to a slight uptick in precipitation levels. Additionally, the TCI is on the rise, whereas the VCI is declining, primarily influenced by low soil moisture levels and a corresponding increase in air temperature.

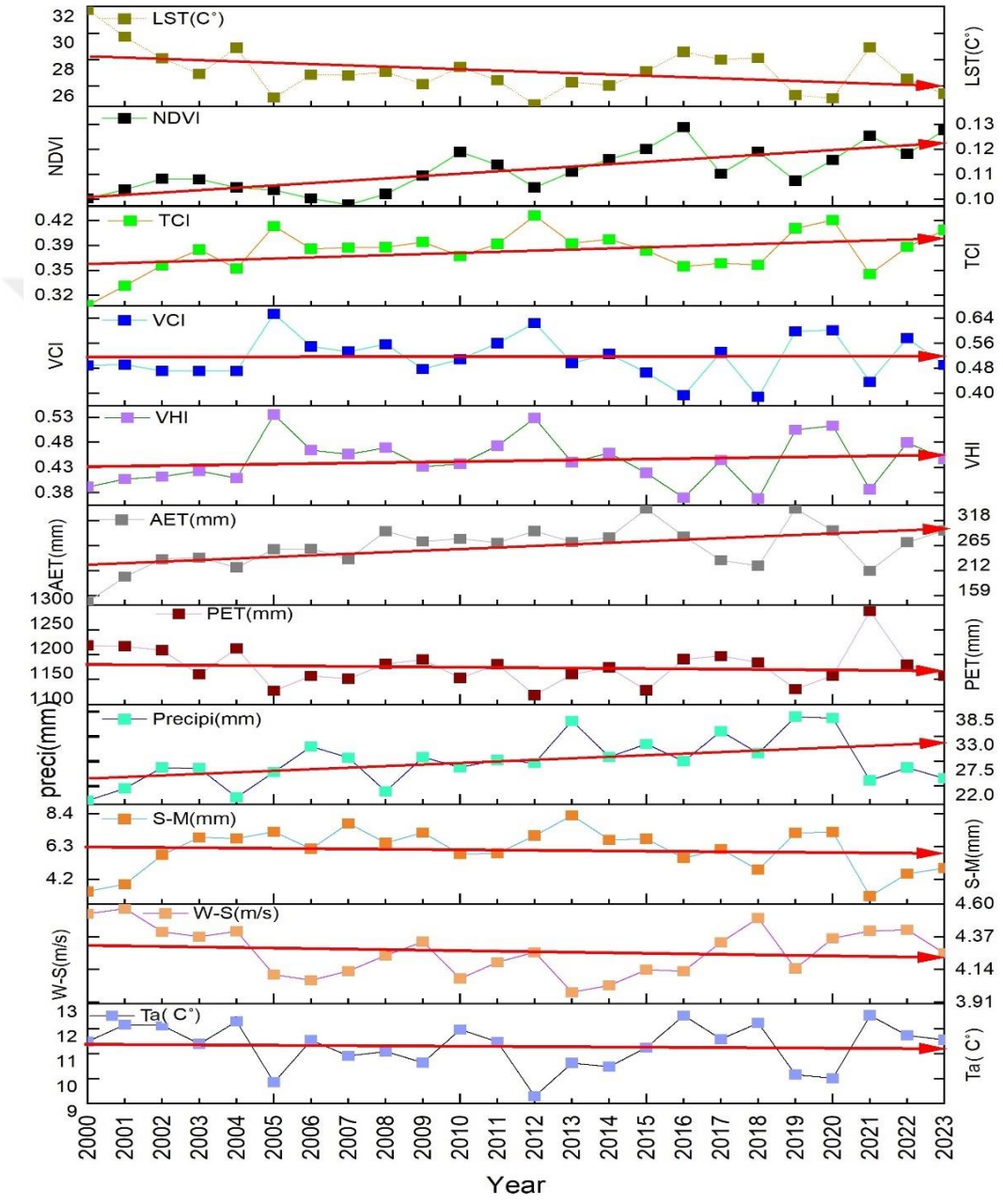

Figure 29. Annually trend analysis of NDVI, LST, Ta, AET, PET, Precipitation, Soil Moisture, VCI, TCI, VHI and Wind speed parameters in Southeastern region.

As illustrated in Figure 29, the NDVI, AET, TCI, VHI, and precipitation parameters exhibit an increasing trend, while the LST, soil moisture, VCI, PET, wind speed, and Ta

parameters show a decreasing trend in the southeastern region. In this area, the decline in LST correlates with an increase in NDVI, which subsequently elevates AET and contributes to localized rainfall, resulting in higher precipitation levels. Conversely, due to the relative soil permeability, soil moisture has decreased, leading to a decline in VCI, while TCI and VHI have increased. Additionally, in this region, the reductions in LST, Ta, and wind speed have contributed to a slight decrease in PET.

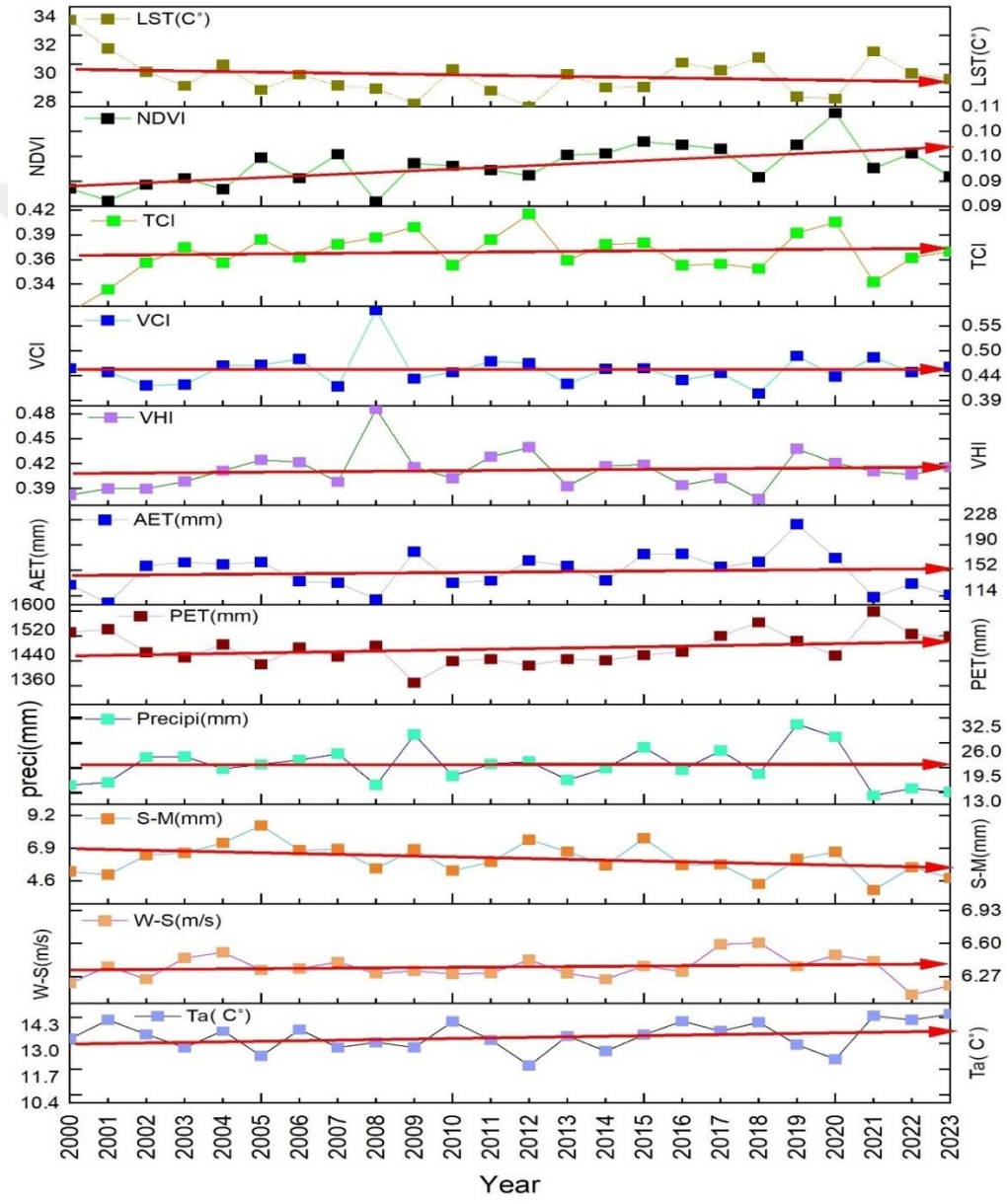

Figure 30. Annually trend analysis of NDVI, LST, Ta, AET, PET, Precipitation, Soil Moisture, VCI, TCI, VHI and Wind speed parameters in Western region.

As shown in Figure 30, the NDVI, AET, PET, TCI, VHI, Ta, and wind speed parameters exhibit an increasing trend, while the LST, soil moisture, VCI, and precipitation

parameters demonstrate a decreasing trend in the western region. In this area, the reduction in LST corresponds with an increase in NDVI, which, in turn, contributes to a slight rise in AET. However, both precipitation and soil moisture levels have decreased, resulting in an increase in TCI and a decline in VCI. The rise in PET may be attributed to the increase in Ta.

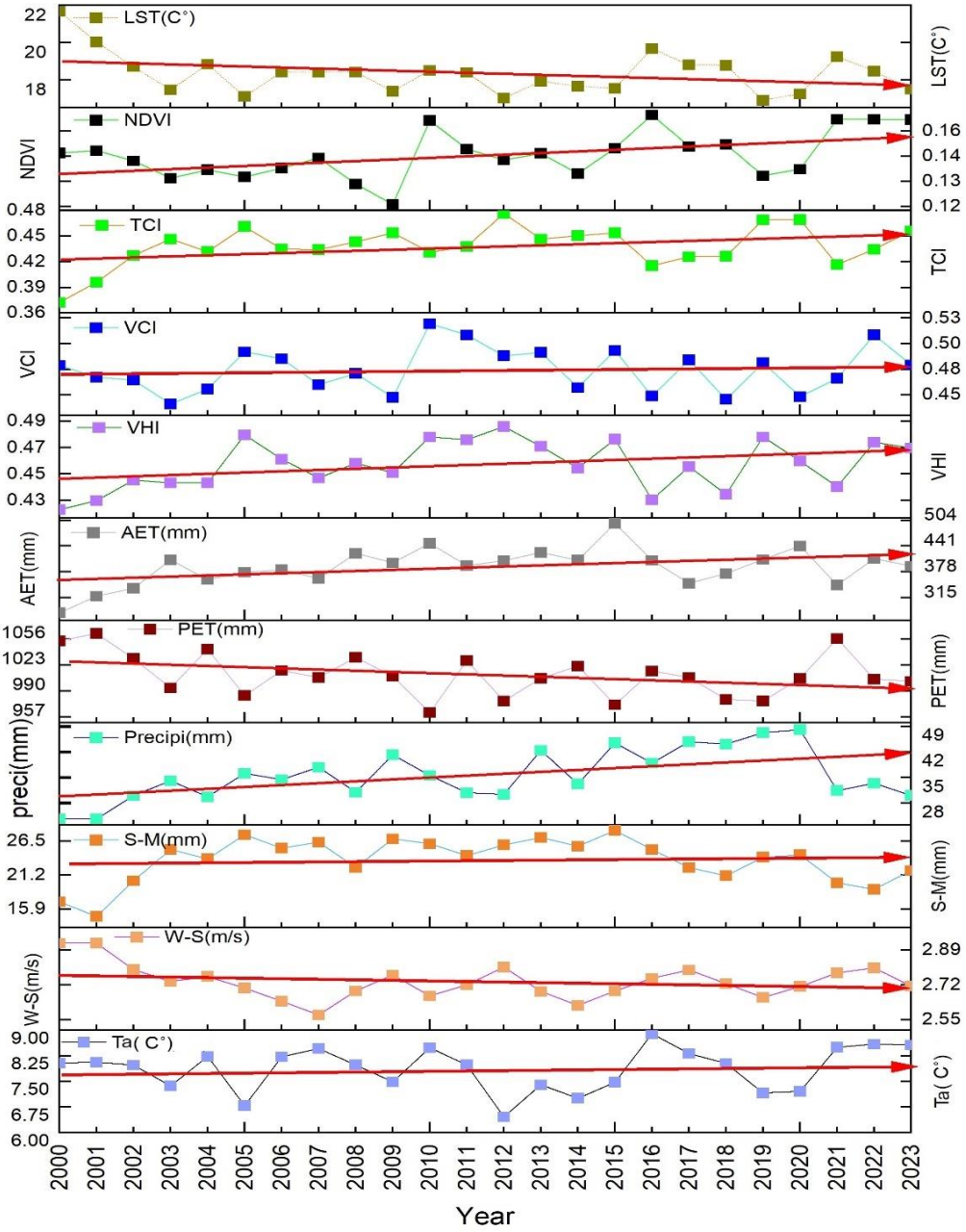

Figure 31. Annually trend analysis of NDVI, LST, Ta, AET, PET, Precipitation, Soil Moisture, VCI, TCI, VHI and Wind speed parameters in Eastern region.

As illustrated in Figure 31, the NDVI, AET, TCI, VCI, VHI, precipitation, soil moisture, and Ta parameters show an increasing trend, while the LST, PET, and wind speed parameters exhibit a decreasing trend in the eastern region. In this area, the significant decline in LST has led to a marked reduction in PET from 2000 to 2023, although other climate parameters have experienced growth. Despite the increase in the Ta parameter, it has not significantly impacted the rise in PET.

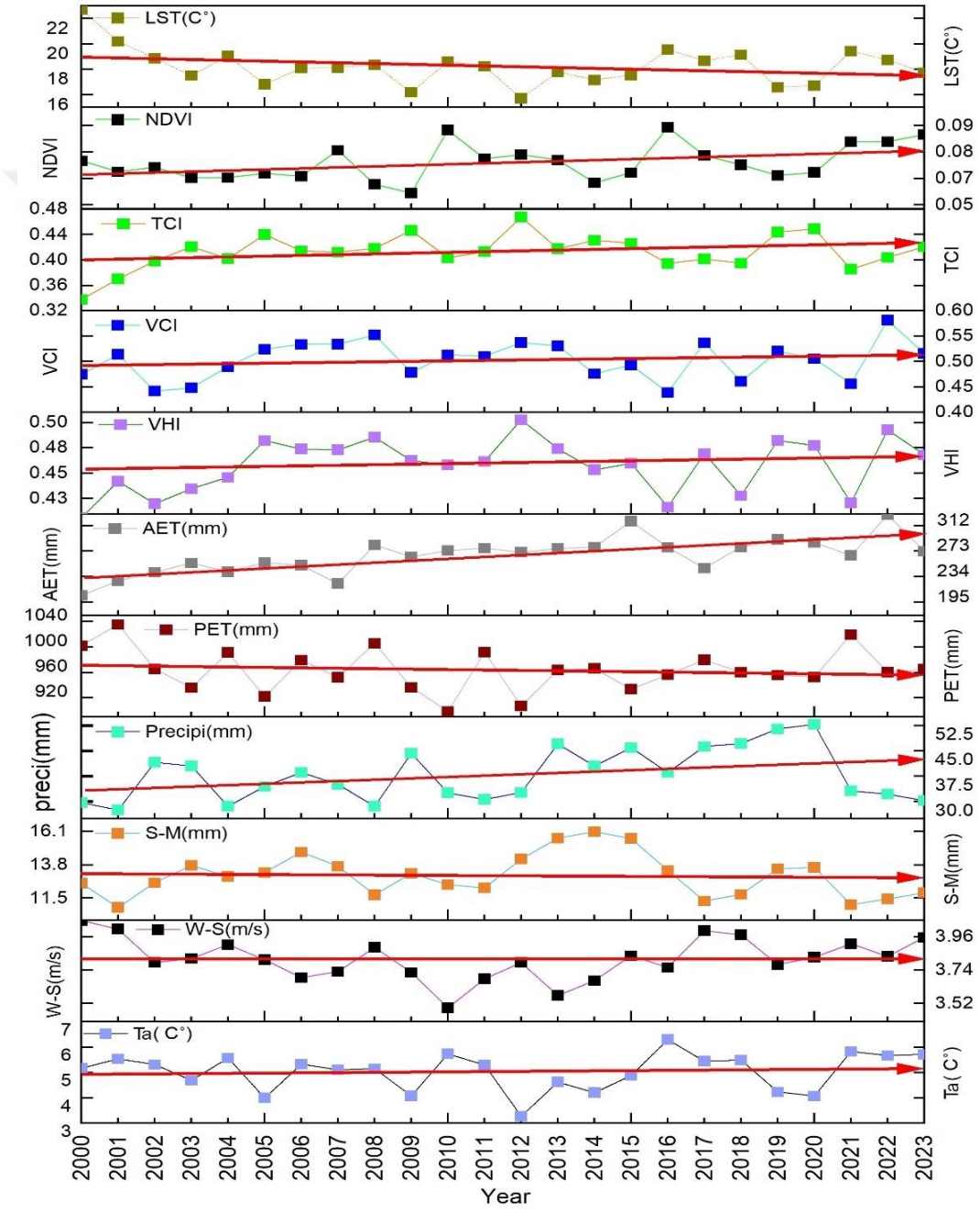

Figure 32. Annually trend analysis of NDVI, LST, Ta, AET, PET, Precipitation, Soil Moisture, VCI, TCI, VHI and Wind speed parameters in Central region.

As shown in Figure 32, the NDVI, AET, TCI, VCI, VHI, precipitation, and Ta parameters exhibit an increasing trend, while the LST, PET, soil moisture, and wind speed parameters show a decreasing trend in the central region. In this area, the reduction in LST has led to an increase in NDVI, which in turn has contributed to a rise in AET. Furthermore, the increase in AET is indicative of greater precipitation. However, the amount of soil moisture has decreased, which may be attributed to the soil's permeability in this region.

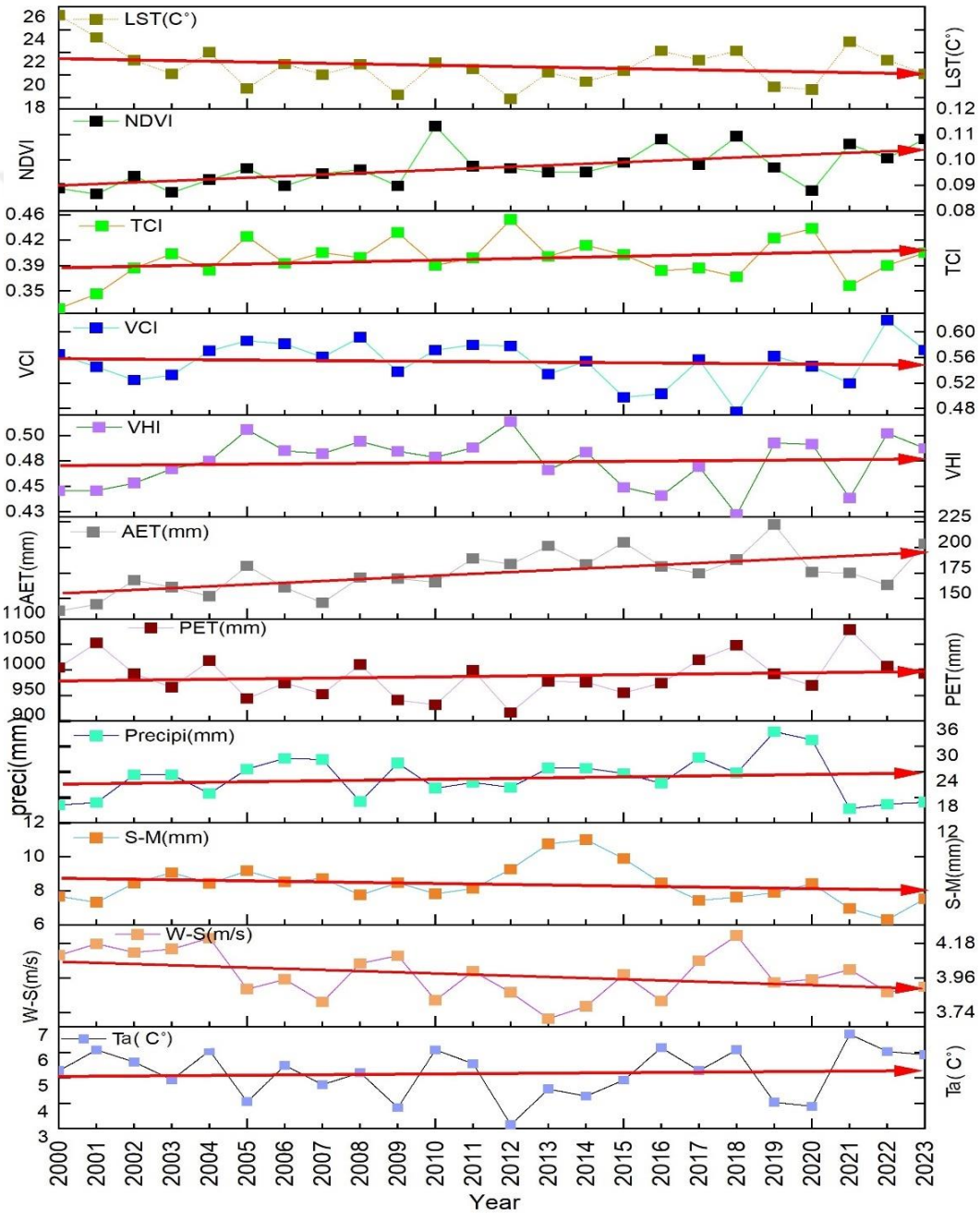

Figure 33. Annually trend analysis of NDVI, LST, Ta, AET, PET, Precipitation, Soil Moisture, VCI, TCI, VHI and Wind speed parameters in West Central region.

As illustrated in Figure 33, the NDVI, AET, PET, TCI, VHI, precipitation, and Ta parameters show an increasing trend, while the LST, VCI, soil moisture, and wind speed parameters exhibit a decreasing trend in the central region. In this area, the decrease in LST has led to an increase in NDVI, which has consequently raised the amount of AET. This rise in AET indicates an increase in precipitation. Additionally, as Ta increases, the amount of PET also rises. However, due to the permeability of the soil in this region, soil moisture has decreased, resulting in an increase in TCI and a decrease in VCI.

3.4. Examination Of Forests Change in Afghanistan

In the analysis of forest changes in Afghanistan, the Hansen Global Forest Change (HGFC) dataset was utilized through Google Earth Engine (GEE). This analysis assessed deforestation trends using the "Loss" band to examine forest loss from 2000 to 2023 in various regions. The forested areas in Afghanistan are mainly concentrated in the eastern, southeastern, and scattered northeastern regions. In these areas, deforestation occurs as people cut down trees for fuel.

As shown in Figure 34a, the highest deforestation across Afghanistan occurred in 2003, 2005, and 2007, while the lowest was recorded in 2014. However, the rate of deforestation increased again in 2023. Overall, from 2001 to 2023, the trend of forest loss decreased, with a correlation coefficient (CC) of -0.577, indicating a significant negative trend. The total deforested area in Afghanistan between 2000 and 2023 was 2,431.6 ha.

The eastern region holds the most extensive forest cover in Afghanistan. In this region, the highest deforestation occurred in 2003, while the lowest was in 2013 and 2014. The correlation coefficient in this region is -0.413, with total deforestation from 2000-2023 amounting to 804.35 hectares (as shown in Figure 34b). In the northeastern region, deforestation peaked in 2001 and has shown a declining trend since. The CC value in this region is -0.515, with total deforestation reaching 417.42 ha (Figure 34c).

In the southeastern region, deforestation was highest in 2004, with a subsequent decreasing trend. The correlation coefficient is -0.396, and the total deforested area between 2000-2023 was 873.47 ha (Figure. 34d). Additionally, deforestation trends in the South, central, and west-central regions are increasing, while the north and western regions show a decreasing trend. However, due to limited forest cover in the South, north, western, central, and west-central regions, the overall deforested area in these regions is relatively low.

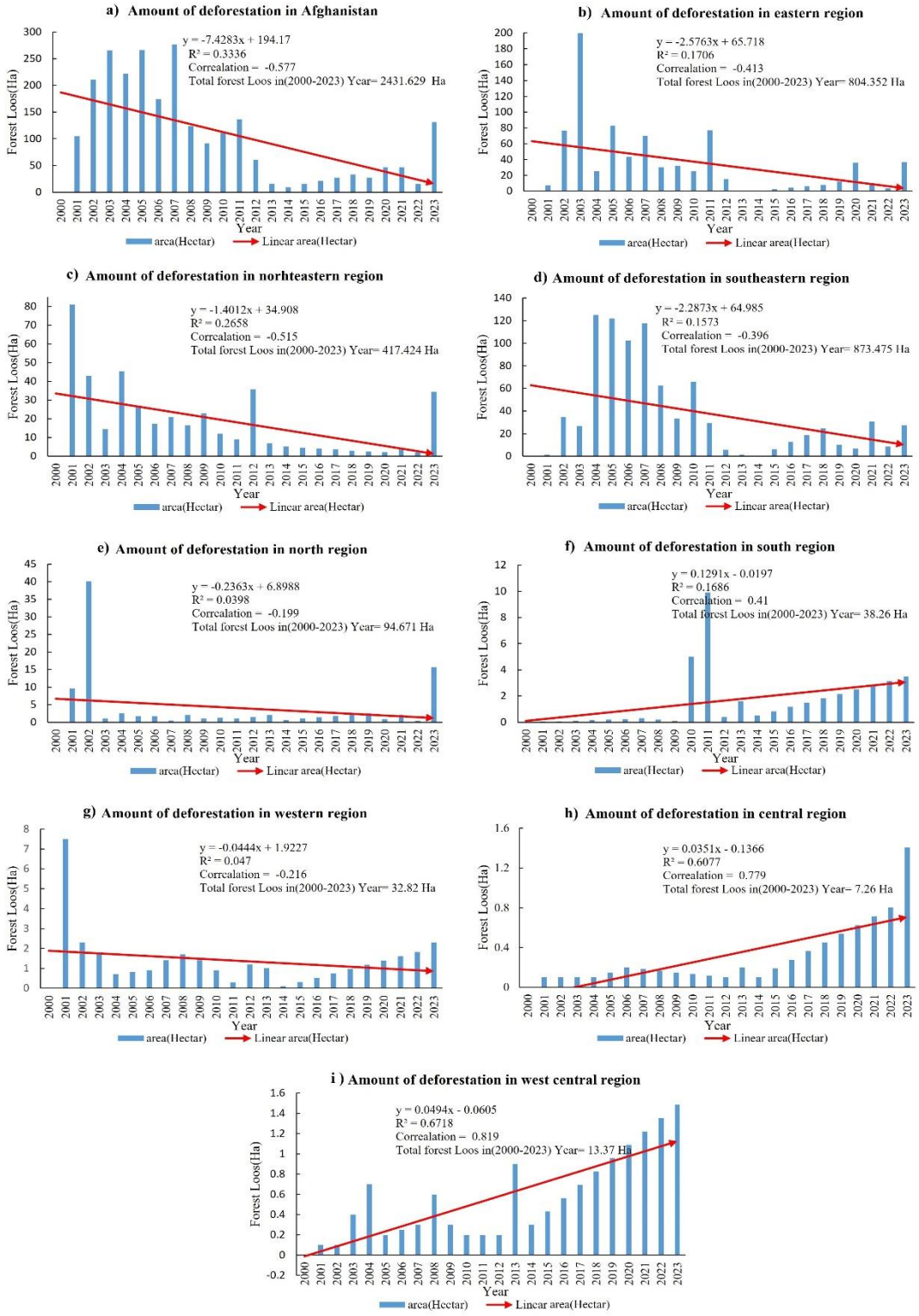

Figure 34. Amount of forest loss (deforestation areas) between the 2000-2023 year.

3.5. Results Based on Pearson's Correlation Coefficient

The linear relationships between NDVI, LST, VCI, TCI, VHI, Ta, precipitation, soil moisture, AET, PET, and wind speed parameters were evaluated annually from 2000 to 2023 for each region using the Pearson Correlation Coefficient (r). To calculate the correlation coefficient, the mean values of the data were used, and then anomalies between the indices were compared to analyze these correlations. The climate parameters applied to Afghanistan's climate and environmental data, along with the correlation coefficients (r) between them, are presented in Figure 35.

As shown in Figure 35, the correlation coefficient between LST and Ta is 0.61, indicating a strong, direct relationship between these two climate parameters. On the other hand, the correlation between LST and NDVI is -0.4, showing an inverse relationship, while the correlation between NDVI and Ta is -0.15. This suggests that the relationship between LST and NDVI is stronger and more inversely correlated than that of NDVI with Ta. Additionally, the correlation between TCI and LST is -0.98, indicating a very strong inverse relationship. As temperatures increase, TCI levels drop, contributing to drought conditions. The relationship between TCI and Ta is also strong and inverse, with a correlation of -0.65. TCI also shows a direct relationship with NDVI, meaning that higher TCI values contribute to an increase in NDVI.

As presented in Figure 35, VCI demonstrated a relatively strong and inverse relationship with Ta, with a correlation value of -0.49. However, the correlation between VCI and LST was weaker at -0.07, as favorable air temperatures generally promote better plant growth. VCI showed a weak correlation with NDVI across Afghanistan, with a correlation value of -0.07. This weak correlation occurs because, if NDVI increases generally but unevenly across a region, the VCI decreases, resulting in a loss of correlation. The correlation between VHI and LST, as well as VHI and Ta, was -0.56 and -0.72, respectively, indicating that as VHI increases, both LST and Ta decrease, showing a strong inverse correlation. Additionally, VHI showed a strong direct correlation with both VCI and TCI, with correlation values of 0.86 and 0.62, respectively. Furthermore, the relationship between LST and AET was strongly inverse, with a correlation value of -0.7. This is because increased LST, if accompanied by decreased soil moisture and plant stomata closure, leads to a reduction in AET. Similarly, the correlation between LST and soil moisture was also inverse, with a value of -0.59.

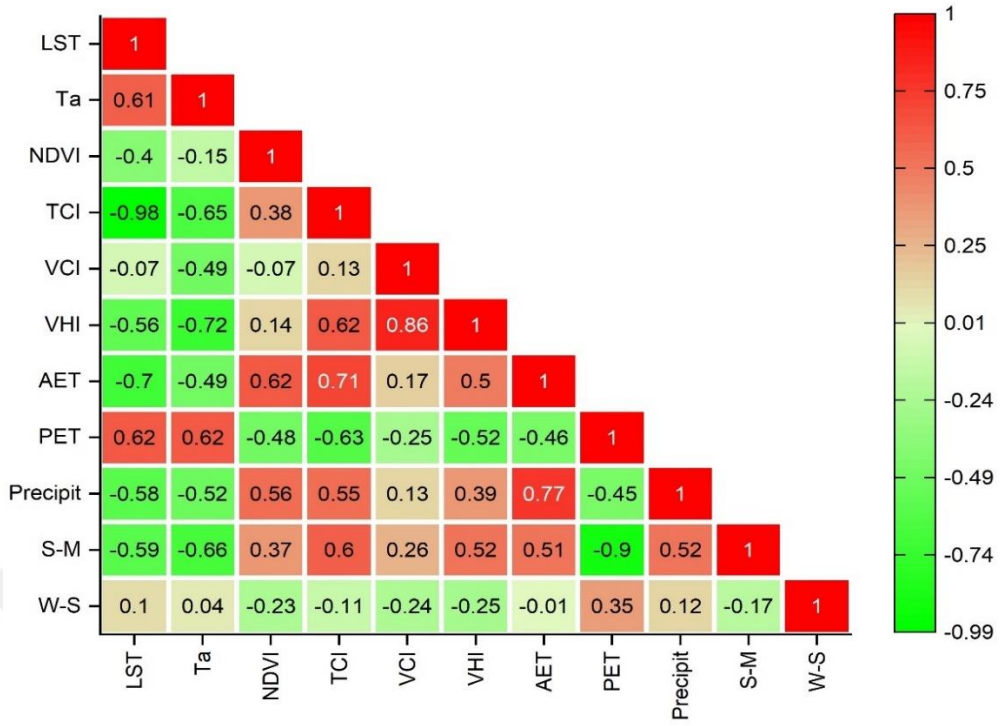

Figure 35. Correlation Coefficient between the parameters in throughout Afghanistan.

As shown in Figure 35, VCI demonstrated a relatively strong inverse relationship with Ta, with a correlation value of -0.49. However, the correlation between VCI and LST was much weaker at -0.07, since suitable air temperatures generally promote better plant growth. VCI also exhibited a weak correlation with NDVI across Afghanistan, with a correlation value of -0.07. This weak correlation occurs because when NDVI increases unevenly across regions, the VCI tends to decrease, diminishing the overall correlation. The correlation between VHI and LST, as well as VHI and Ta, was -0.56 and -0.72, respectively. This indicates that as VHI increases, LST and Ta both decrease, showing a strong inverse relationship. VHI also displayed a strong direct correlation with both VCI and TCI, with values of 0.86 and 0.62, respectively.

Furthermore, the relationship between LST and AET was strongly inverse, with a correlation value of -0.7. This is because higher LST, combined with reduced soil moisture and plant stomata closure, leads to a decrease in AET. Similarly, the correlation between LST and soil moisture was also inverse, with a value of -0.59. The AET parameter displays a strong and direct correlation with the NDVI, VCI, TCI, and VHI indices, as higher values of NDVI, VCI, TCI, and VHI correspond to higher AET levels. Additionally, both LST and

Ta exhibit a direct and strong correlation with PET, with a value of 0.62, as an increase in LST leads to a rise in PET.

According to Figure 35, the correlation between PET and NDVI is -0.48, indicating a strong inverse relationship. This is because, with an increase in PET, evapotranspiration from plants rises, potentially reducing plant growth, which in turn lowers NDVI. PET also has an inverse relationship with VCI, TCI, and VHI. Specifically, the correlation between PET and TCI is -0.63, as higher PET causes a reduction in TCI. Similarly, the correlation between PET and VHI is -0.52, signifying that as PET draws more water from plants, it leads to plant stress and dryness. Furthermore, an inverse correlation exists between PET and AET, with a value of -0.46. Due to widespread water shortages across Afghanistan, as PET increases, AET tends to decrease. There is also an inverse correlation between LST and precipitation, with a value of -0.58, as higher LST reduces precipitation. On the other hand, precipitation shows a strong and direct relationship with NDVI (0.56), as increased rainfall fosters better vegetation growth. Moreover, precipitation has a strong positive correlation with TCI, and as precipitation rises, so does TCI, ultimately contributing to an increase in the VHI.

As illustrated in Figure 35, a strong and direct correlation exists between AET and precipitation, with a value of 0.77, indicating that AET increases as precipitation rises. Additionally, there is an inverse correlation of -0.45 between precipitation and PET, reflecting a strong negative relationship. This is because precipitation is typically accompanied by a drop in LST, which reduces evaporation and consequently lowers PET. The correlation between soil moisture and Ta is -0.66, showing a strong inverse relationship. As air temperature increases, soil moisture tends to decrease.

Moreover, soil moisture shares a very strong and direct correlation with NDVI, TCI, VCI, and VHI indices, signifying that plant growth is heavily dependent on increased soil moisture. AET also shows a strong direct correlation with soil moisture, valued at 0.51, as AET is closely tied to soil moisture levels-higher soil moisture leads to more evapotranspiration. On the contrary, the correlation between PET and soil moisture is -0.9, reflecting a strong inverse relationship. This occurs because an increase in PET typically results in a decrease in soil moisture due to higher evaporation rates. The relationship between precipitation and soil moisture is also strong and direct, with a value of 0.52. Furthermore, there is an inverse correlation between wind speed and the NDVI, VCI, TCI, and VHI indices, as higher wind speeds contribute to plant dryness and reduce both AET

and soil moisture. Conversely, wind speed shares a direct relationship with PET, with a correlation of 0.35. This means that as wind speed increases, PET rises as well, because moisture is transferred more rapidly from plant and soil surfaces to the atmosphere.

Figure 36 presents the correlation values in the north region of Afghanistan. The correlation coefficient between LST and Ta is 0.56, indicating a strong and direct relationship. In this region, the correlation between NDVI and Ta is -0.23, while the correlation between LST and NDVI is -0.4, suggesting that the relationship between LST and NDVI is stronger, and inverse compared to Ta. Furthermore, there is a highly inverse correlation of -0.98 between TCI and LST, reflecting that as temperatures rise, TCI levels drop, leading to drought. Similarly, the correlation between TCI and Ta is strongly inverse at -0.63. A direct relationship is observed between TCI and NDVI, where higher TCI values result in increased NDVI.

The correlation between VCI and Ta is weak at -0.07, while VCI and LST show a moderately inverse relationship at -0.2, indicating that suitable air temperatures typically promote better plant growth. VCI and NDVI exhibit a strong correlation of -0.52 in this region, suggesting that rising temperatures have negatively impacted plant growth rates. Additionally, there is a strong inverse correlation between VHI and both LST (-0.49) and Ta (-0.44), demonstrating that as VHI increases, LST and Ta values tend to decrease.

As seen in Figure 36, there was a strong and high correlation between the VHI and the TCI and VCI. The correlation between the VHI and VCI reached 0.9, while the correlation between the VHI and TCI was 0.55. Furthermore, a substantial inverse relationship of -0.61 exists between LST and AET, as a decrease in soil moisture and plant stomata closure, combined with an increase in LST, causes a drop in AET. There is also an inverse correlation of -0.48 between soil moisture and LST. The AET parameter shows a strong and direct correlation with the NDVI and TCI indices; higher values of the NDVI and TCI indices lead to higher AET. However, due to the high LST in this region, AET has a weak and inverse relationship with the VCI and VHI indices.

Additionally, as seen in figure 36, LST and Ta demonstrate a direct and strong correlation with PET, with values of 0.69 and 0.62, respectively, indicating that an increase in LST causes an increase in PET. Similarly, there is a high inverse correlation of -0.67 between PET and NDVI, as a rise in PET increases plant evapotranspiration, which may lead to decreased plant growth and a decline in NDVI. Moreover, there is an inverse relationship between PET and the TCI and VHI indices; the correlation between the two is -0.63,

indicating that as PET increases, TCI decreases. The correlation between PET and VHI is -0.14, meaning that as PET removes more water from the plants, the plants become drier.

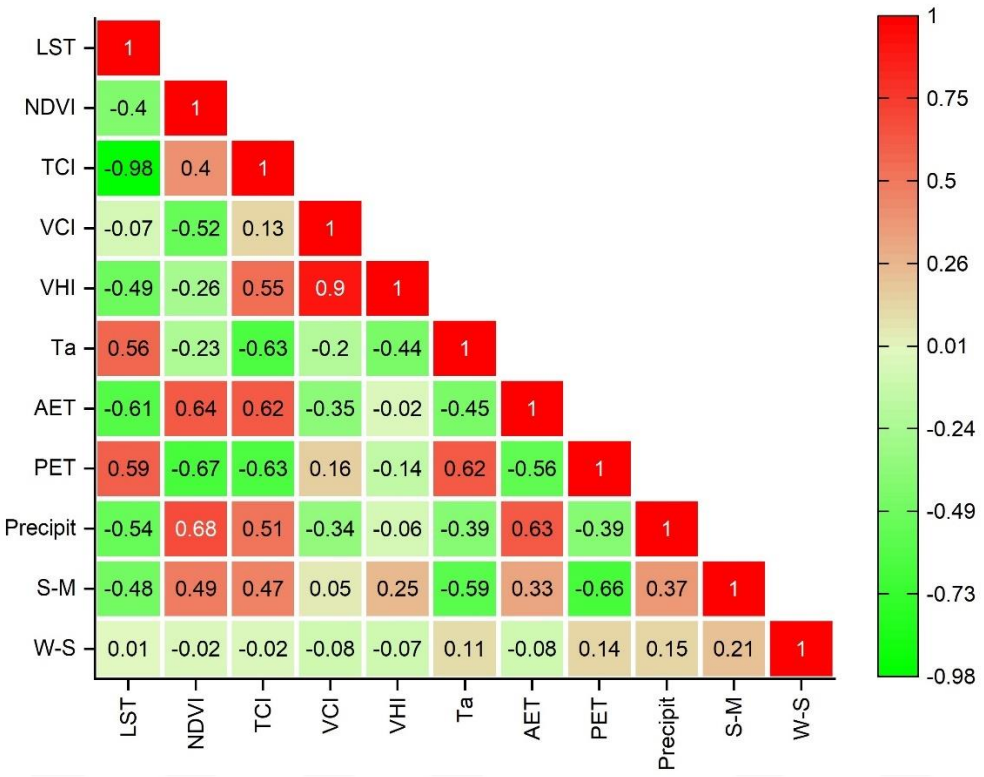

Figure 36. Correlation Coefficient between the parameters in North region.

As shown in Figure 36, the PET and AET parameters exhibit an inverse relationship with a value of -0.56. In the north region, increased water scarcity leads to a decline in AET as PET rises. Furthermore, there is a decrease in precipitation accompanying an increase in LST, resulting in an inverse correlation of -0.54. A strong and direct correlation of 0.68 exists between precipitation and NDVI, indicating that as precipitation increases, plant growth also improves. Additionally, there is a significant positive relationship between TCI and precipitation, where higher TCI levels correspond to increased precipitation. The relationship between AET and precipitation is strong and direct, reaching 0.63, demonstrating that AET levels rise in tandem with precipitation levels.

Figure 36 illustrates a strong inverse relationship of -0.39 between precipitation and PET. This relationship can be explained by the fact that precipitation typically leads to a decrease in LST, resulting in less evaporation and lower PET due to cooler temperatures. Additionally, a strong inverse relationship of -0.59 exists between soil moisture and Ta, indicating a decrease in soil moisture as air temperature rises. Conversely, a strong and direct

association between NDVI, TCI, and soil moisture highlights that higher soil moisture levels are essential for promoting increased plant growth.

According to Figure 36, the soil moisture parameter has a strong correlation with AET, reaching 0.33. AET increases under high soil moisture conditions due to the greater availability of water for evapotranspiration. However, the correlation between soil moisture and PET is -0.66, indicating a strong inverse relationship. As more water evaporates from the soil, an increase in PET typically results in a decrease in soil moisture. There is also a significant direct correlation of 0.37 between soil moisture and precipitation. Furthermore, wind speed exhibits an inverse relationship with NDVI, VCI, TCI, and VHI indices, as higher wind speeds lead to drier plants, resulting in lower soil moisture and AET levels. Additionally, there is a direct association of 0.14 between wind speed and PET, suggesting that as wind speed increases, the movement of moisture from soil and plant surfaces to the atmosphere accelerates, leading to higher PET.

The correlation values in Afghanistan's northeast are displayed in Figure 37. There is a significant direct relationship between the LST and Ta parameters, indicated by a correlation coefficient of 0.51. The correlation between NDVI and LST in this region is 0.14, reflecting the positive correlation due to the direct influence of vegetation on surface temperature and surrounding environmental conditions. Furthermore, there is a strong negative relationship of -0.97 between the TCI and LST, as dryness increases with rising temperature and a decline in TCI levels. Additionally, a correlation coefficient of -0.56 demonstrates a strong inverse relationship between the TCI and Ta.

Figure 37 indicates a correlation of -0.18 between the NDVI and TCI indices, reflecting a weak inverse relationship, as an increase in temperature typically leads to a decrease in plant growth. The relationship between the VCI and both Ta and LST is direct, with a correlation of 0.35, suggesting that rising air temperatures have contributed to plant dryness in this region. Additionally, the correlation between NDVI and VCI is very weak, likely due to the influence of short-term, localized factors on NDVI, while VCI is more sensitive to long-term changes and historical comparisons.

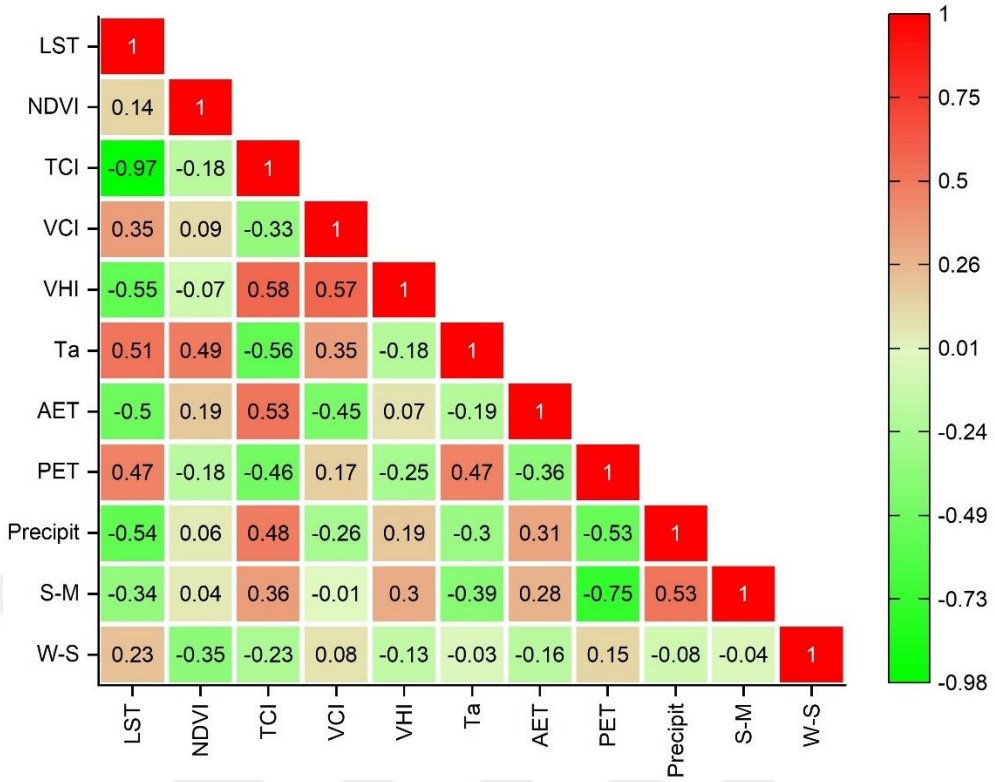

Figure 37. Correlation Coefficient between the parameters in Northeastern region.

As shown Fig 37, Furthermore, there is a strong inverse relationship between the VHI and LST, as well as between the VHI and Ta, with correlation coefficients of -0.55 and -0.18, respectively. This indicates that increases in temperature correspond to a decrease in the VHI, signaling drought conditions in the region. A strong positive correlation was also observed between the VHI and both TCI and VCI, with coefficients of 0.58 and 0.57, respectively. The relationship between LST and AET demonstrates a significant inverse correlation of -0.5, where an increase in LST, combined with reduced soil moisture and plant stomatal closure, results in decreased AET. Additionally, the correlation between soil moisture and LST is -0.34, indicating an inverse relationship. There is a direct and substantial relationship between the AET parameter and both the TCI and NDVI indices; as AET increases, so do the values of these indices. However, due to the high LST in this region, the relationships between AET and both the VCI and VHI indices are weak and inverse.

Figure 37 reveals a strong and significant correlation of 0.47 between LST and both Ta and PET, indicating that increases in LST and Ta lead to a rise in PET. In contrast, the NDVI and PET exhibit an inverse correlation of -0.18, which suggests that higher PET levels increase evapotranspiration in plants, potentially resulting in reduced plant growth and a

decline in NDVI. Additionally, a significant inverse relationship of -0.46 is observed between the PET and TCI indices, signifying that as PET increases, TCI decreases. The relationship between PET and VHI is also negative, at -0.25, indicating that plants become dryer as more water is extracted by PET. Similarly, the correlation between the PET and AET parameters are inverse, with a value of -0.36, suggesting that AET decreases as PET rises due to increasing water scarcity in the northeastern region. Finally, a correlation of-0.54 exists between precipitation and LST, demonstrating that as precipitation increases, LST decreases in this area.

Figure 37 illustrates a significant and positive relationship between precipitation and TCI, indicating that as TCI increases, so does the amount of precipitation. The direct correlation between AET and precipitation, with a coefficient of 0.31, demonstrates that AET values rise in tandem with precipitation values. Additionally, a strong inverse relationship exists between precipitation and PET, with a correlation coefficient of -0.53. This inverse relationship can be attributed to the fact that precipitation typically results in a decrease in LST; lower temperatures lead to less PET and reduced evaporation. Furthermore, as air temperatures rise, the moisture content in the soil tends to decrease.

In this context, Figure 37 also highlights a strong and significant correlation between soil moisture and both NDVI and TCI indices, suggesting that increased soil moisture is crucial for enhanced plant development. The correlation between AET and soil moisture is 0.28, indicating that higher soil moisture levels provide more water for evapotranspiration, thereby increasing AET. Conversely, the correlation between soil moisture and PET is -0.75, reflecting a strong inverse relationship; as PET increases due to higher evaporation rates, soil moisture diminishes. Additionally, a direct correlation of 0.53 exists between soil moisture and precipitation. An inverse relationship is observed between wind speed and the NDVI, TCI, and VHI indices, where higher wind speeds lead to drier vegetation, lower soil moisture, and reduced AET levels. Lastly, there is a correlation of 0.15 between wind speed and soil moisture, as increased wind speed facilitates the transfer of moisture from the soil to the atmosphere, thereby elevating PET.

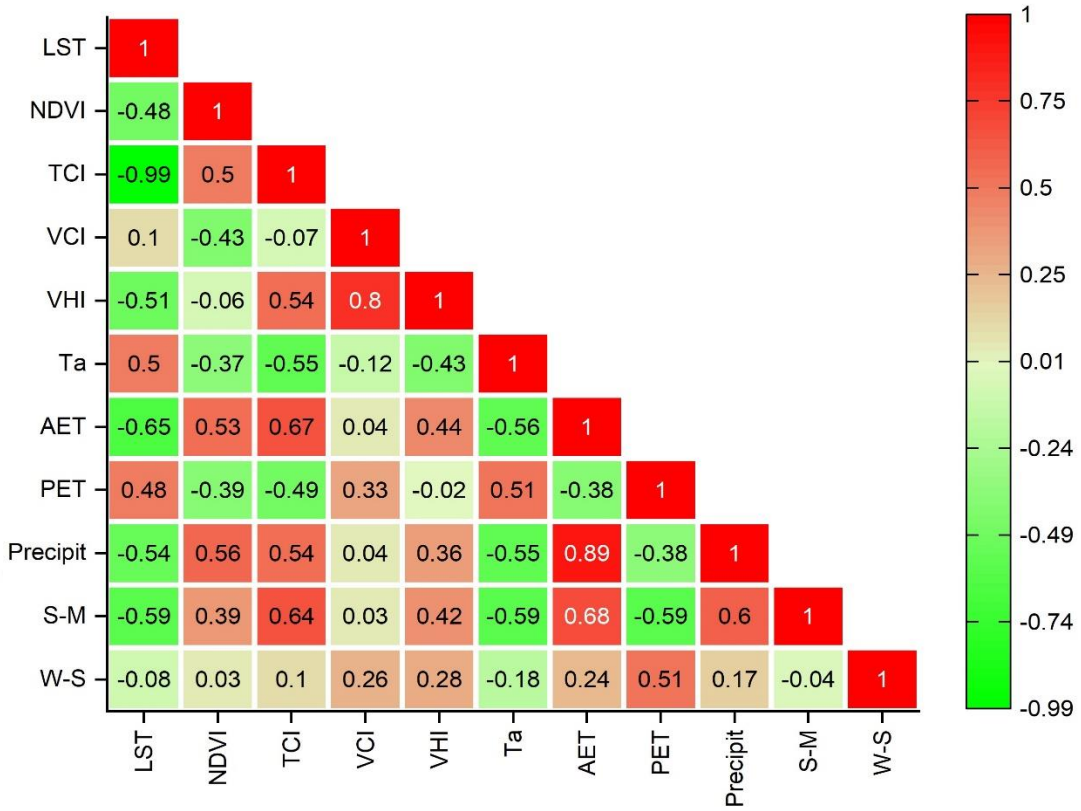

Figure 38. Correlation Coefficient between the parameters in South region.

The correlation coefficient values among the climate parameters in the South region are presented in Figure 38. NDVI in this region exhibits an inverse correlation of -0.48 with LST, indicating that NDVI decreases as LST increases. Additionally, LST demonstrates a strong inverse relationship with TCI, with a correlation of -0.99. Conversely, LST also shows an inverse relationship with the VHI, resulting in a correlation of -0.51. The correlation between Ta and LST is positive at 0.5. Moreover, the relationship between AET and LST is -0.65, suggesting that as LST increases, AET levels in this region decline. LST has a correlation of 0.48 with PET.

According to Figure 38, there is also an inverse correlation between LST and precipitation, with a coefficient of -0.54, alongside a strong inverse relationship between LST and soil moisture, measured at -0.59. This indicates that increases in precipitation and soil moisture lead to a decrease in LST. Furthermore, there is a positive correlation of 0.5 between NDVI and TCI, suggesting that while temperatures remain high, the improvement in vegetation is not sufficient to alleviate thermal stress. Additionally, the correlation between NDVI and VCI is -0.43, highlighting an inverse relationship due to the high

temperatures in this region, which contribute to VCI dryness despite relatively high NDVI values.

As illustrated in Figure 38, the correlation between NDVI and AET in this region is direct and measures 0.53. Conversely, the relationship between NDVI and PET is inverse, with a correlation coefficient of -0.39, which can be attributed to insufficient moisture availability and rising temperatures. Additionally, NDVI shows a direct relationship with both precipitation and soil moisture. A strong positive correlation of 0.54 was observed between the TCI and VHI, indicating favorable temperature conditions for the overall health of vegetation. However, a correlation of -0.55 exists between the TCI and Ta. The correlation between the TCI and AET is notably high at 0.76, reflecting the positive relationship under favorable temperature conditions. Conversely, the correlation between the TCI and PET is -0.49, indicating that high temperatures in the region have caused severe thermal stress in plants.

Furthermore, Figure 38 demonstrates that both TCI and VHI indices have strong positive relationships with precipitation and soil moisture parameters. In contrast, the VCI exhibits a weak relationship with both precipitation and soil moisture. Additionally, VHI has a strong negative relationship with Ta, while maintaining a positive correlation with AET. Also the air temperature has an inverse correlation of -0.56 with AET and a direct correlation of 0.51 with PET. Also, air temperature has a negative relationship with precipitation and soil moisture, the correlation of which was -0.55 for precipitation and -0.59 for soil moisture. And AET has an inverse relationship with PET, and the correlation between them is -0.38. And AET has a direct relationship with precipitation and soil moisture, and a strong correlation is observed between them. But PET has an inverse relationship with precipitation and soil moisture. And there is a direct and strong correlation between precipitation soil moisture. Also, a positive relationship was observed between wind speed with PET, VHI and VCI, which shows a significant correlation between them.

As illustrated in Figure 39, the correlation between NDVI and LST in this region is weak, measuring -0.07. This weak inverse relationship can be attributed to the high soil moisture values that coincide with lower temperatures; indeed, the correlation between LST and soil moisture is a strong -0.67. Conversely, a very strong inverse correlation of -0.99 exists between LST and TCI. Additionally, both the VCI and VHI indices demonstrate a strong inverse correlation with LST, indicating that LST decreases as vegetation cover increases in this region. In contrast, the Ta parameter shows a strong positive correlation of

0.74 with LST, signifying a direct relationship between the two. Moreover, the correlation between LST and AET is -0.77, indicating a strong inverse relationship; as LST increases, AET decreases. Similarly, there is an inverse relationship of -0.54 between LST and precipitation, suggesting a noteworthy connection between these variables. However, the relationship between LST and PET is direct and positive, with a correlation coefficient of 0.73.

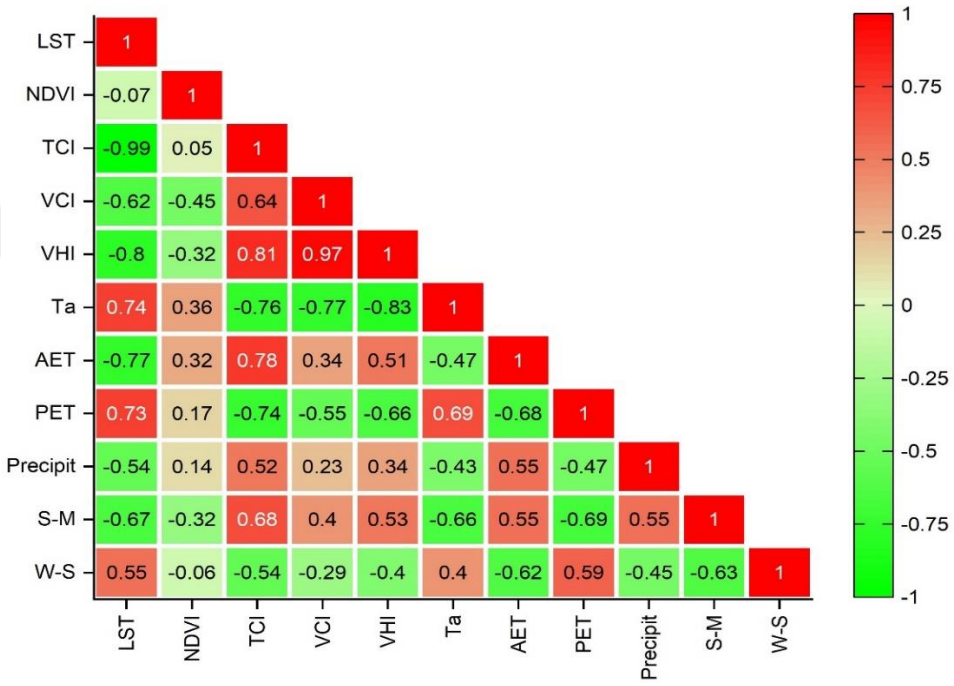

Figure 39. Correlation Coefficient between the parameters in Southeastern region.

According to Figure 39, the high temperatures in this region lead to dryness in the VCI, even when NDVI remains relatively high. Consequently, the correlation between the two measures is -0.45. A similar situation is observed between the NDVI and the VHI index. A significant relationship of 0.17 exists between the NDVI and PET, along with a direct correlation of 0.32 between the NDVI and AET. Additionally, there is a strong correlation between the NDVI, soil moisture, and precipitation. A robust positive correlation of 0.81 was discovered between the TCI and the VHI, indicating favorable temperature conditions for overall vegetation health. Furthermore, a strong correlation of 0.65 exists between the TCI and VCI. A strong inverse correlation of -0.76 was observed between TCI and the Ta parameter, indicating a significant relationship. The correlation between the TCI and AET is 0.78, reflecting that LST is inversely related to the TCI index. However, TCI shows a negative correlation of -0.74 with the PET parameter, emphasizing their significant

relationship. In this region, LST and wind speed also have a direct correlation of 0.55, demonstrating that increased wind speed directly affects LST. Additionally, TCI shows a direct relationship with precipitation and soil moisture parameters, which typically increase with rising precipitation and soil moisture levels. The correlation between TCI and wind speed is -0.54, as increased wind speed elevates surface temperature and dryness, thus reducing TCI.

As illustrated in Figure 39, the VCI index has a direct and significant relationship with the VHI. Conversely, VCI and VHI exhibit a strong inverse relationship. On the other hand, VCI and VHI are positively correlated with the AET parameter, but their relationship with PET is negative. VCI and VHI also maintain a direct and significant correlation with precipitation and soil moisture parameters. However, their relationship with wind speed is inverse, as increased wind speed has caused plant dryness in this region, reducing both VCI and VHI. The Ta parameter shows an inverse and significant relationship with the AET, precipitation, and soil moisture parameters, while its correlation with the PET parameter is 0.69, indicating a direct and significant relationship.

As shown in figure 39, in this region, the correlation between AET and PET is negative, possibly due to climate change or changes in land use. Additionally, a correlation of -0.62 exists between wind speed and AET, indicating an inverse relationship. This unusual finding may be attributed to high wind speed sometimes causing extreme soil dryness, negatively impacting AET. In contrast, a direct relationship of 0.59 between wind speed and PET indicates a strong and common correlation. Furthermore, PET shows an inverse and significant relationship with precipitation and soil moisture parameters, revealing a strong correlation between them.

The correlation values between the climate parameters in the western region are shown in Figure 40. In the western region of Afghanistan, the LST parameter has established a strong inverse correlation with NDVI, TCI, VCI, VHI, AET, precipitation, and soil moisture parameters. However, direct and strong correlations between LST and the Ta and PET parameters were observed. Additionally, NDVI has established a direct and strong correlation with AET, precipitation, and soil moisture parameters, which have contributed to their increase. Conversely, NDVI exhibits an inverse relationship with the PET and Ta parameters. A direct relationship of 0.64 was observed between VHI and TCI, indicating an unusual correlation. Furthermore, TCI maintains a direct relationship with AET,

precipitation, and soil moisture, which also reflects an unusual type of correlation. This phenomenon may result from unique climatic effects or other underlying reasons.

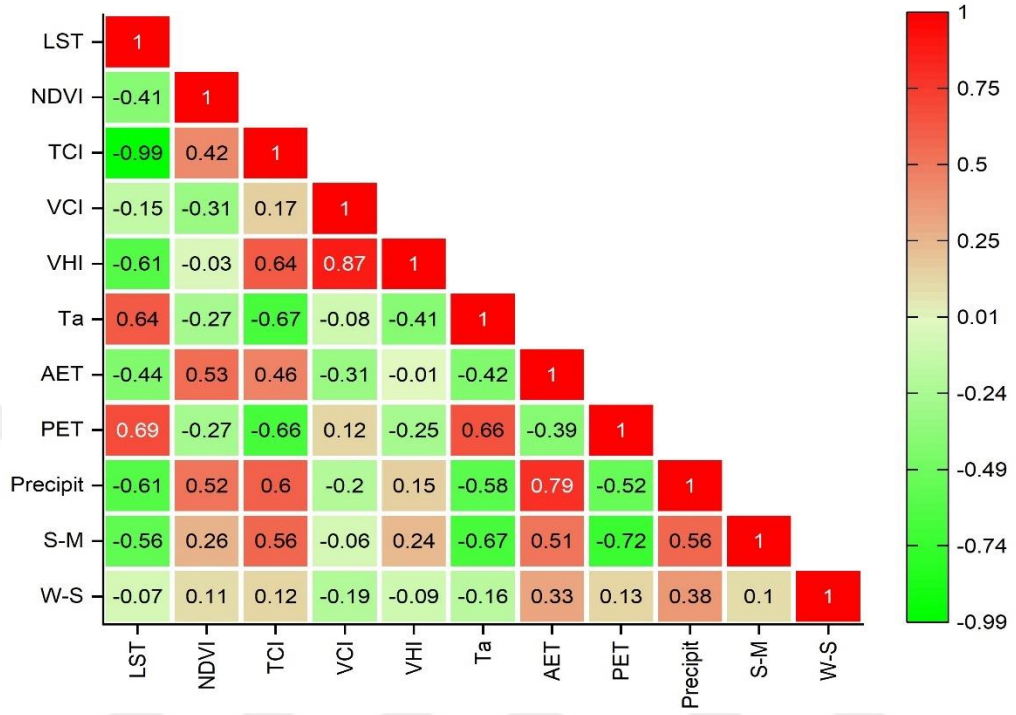

Figure 40. Correlation Coefficient between the parameters in Western region.

As illustrated in Figure 40, the correlation between VCI and VHI is 0.87, indicating a strong and significant relationship between these two indices. However, VCI and VHI exhibit weak relationships with other climate parameters due to insufficient vegetation, precipitation, and soil moisture in this region. The Ta parameter has established a correlation of -0.42 with the AET parameter, which is considered a normal relationship. Additionally, Ta has a correlation of 0.66 with the PET parameter, reflecting a typical association. Furthermore, Ta has inverse relationships with precipitation and soil moisture parameters, demonstrating a strong correlation between them. Like this, AET has a correlation of 0.79 with the precipitation parameter, indicating a very significant and strong relationship. Moreover, AET shows a positive and significant correlation with the soil moisture parameter in this region. AET also correlates positively with wind speed, highlighting the impact of high wind speeds on AET. In contrast, PET demonstrates a negative relationship with both precipitation and soil moisture, revealing a strong inverse correlation between these climate parameters.

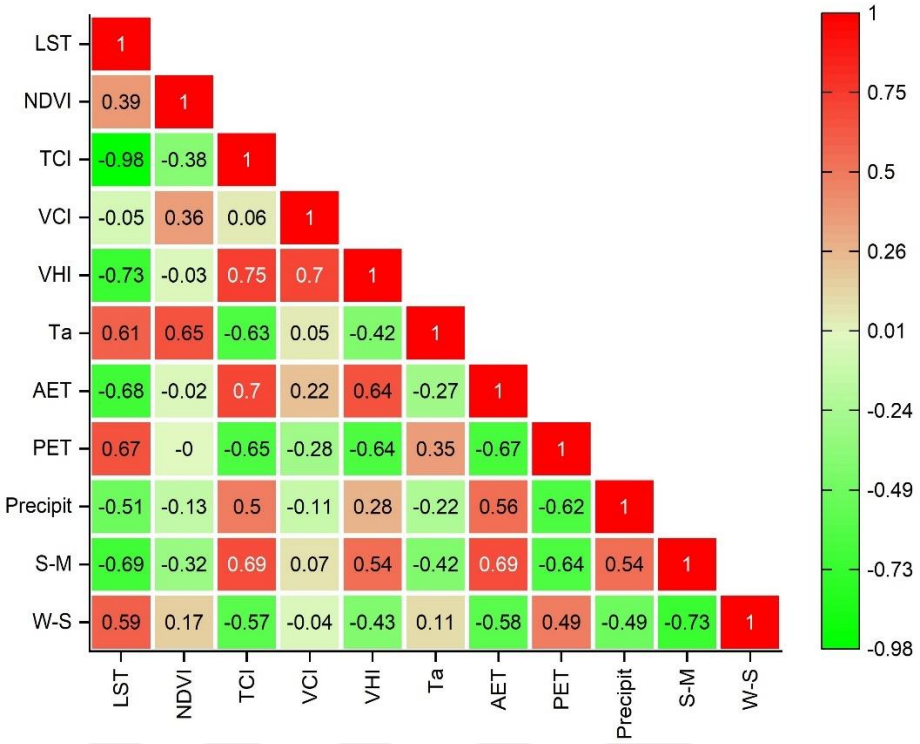

Figure 41. Correlation Coefficient between the parameters in Eastern region.

Figure 41 illustrates the correlation values among climate parameters in the Eastern region. In this area, NDVI exhibits a positive relationship with LST, with a correlation of 0.39. This trend is attributed to the region's forest cover, where NDVI tends to increase at higher temperatures, a pattern also observed with the Ta parameter. LST demonstrates a strong inverse relationship with the TCI and VHI indices, indicating a positive growth of NDVI in this region. Additionally, LST has a direct and robust correlation of 0.61 with the Ta parameter. An inverse relationship of -0.68 is observed between LST and AET, while a strong correlation of 0.67 exists between LST and the PET parameter. LST also shows a significant inverse correlation with precipitation and soil moisture. Furthermore, there is a positive relationship between LST and wind speed, which contributes to increasing temperatures.

Also, in the Eastern region an inverse relationship between the TCI and NDVI is common in this region, whereas a strong direct correlation is noted between NDVI and VCI. The relationship between NDVI and PET is found to be 0, suggesting no significant correlation. A strong correlation of 0.75 was observed between the TCI and VHI indices. Conversely, TCI has a significant inverse relationship with the Ta parameter. In this region, the TCI exhibits a direct relationship with AET, precipitation, and soil moisture parameters,

which is unusual. Additionally, a negative correlation was established between TCI and PET, which is also atypical.

As illustrated in Figure 41, high wind speed significantly influences the TCI index, resulting in a correlation of -0.57, indicating a strong inverse relationship. The VCI index also demonstrates a significant correlation with the VHI index. Furthermore, the VCI index has a notable correlation of 0.22 with the AET index and -0.28 with the PET index, establishing a significant relationship between these variables. The VHI index shows a strong correlation of 0.64 with the AET parameter, while it exhibits a correlation of -0.64 with the PET parameter, both of which are significant.

In the Eastern region Significant relationships have also been observed between the VHI index and precipitation, soil moisture, and wind speed parameters. Conversely, the relationship between AET and PET is inverse, with a correlation of -0.67, possibly due to high soil moisture levels that do not reach sufficient temperatures. The AET parameter has established strong direct relationships with both precipitation and soil moisture, indicating a significant correlation. Similarly, the PET parameter has created strong inverse relationships with rainfall and soil moisture, reflecting a significant correlation. Wind speed, in turn, has a negative relationship with precipitation and soil moisture parameters, although a strong correlation was observed.

Figure 42 also presents the correlation values among the climate parameters in the Central region. Similar to the Eastern region, a positive relationship between the NDVI index and LST were observed in this area, indicating comparable conditions. The LST parameter exhibits a significant inverse relationship with the TCI, VCI, and VHI indices. Furthermore, LST has a strong correlation of 0.71 with the Ta parameter, indicating a significant relationship. There is also an inverse and significant correlation between LST and the AET, precipitation, and soil moisture parameters, while its relationship with the PET parameter is direct and significant. Additionally, LST has a direct relationship with wind speed, showing a correlation of 0.48, which suggests that an increase in wind speed leads to a rise in temperature in this region.

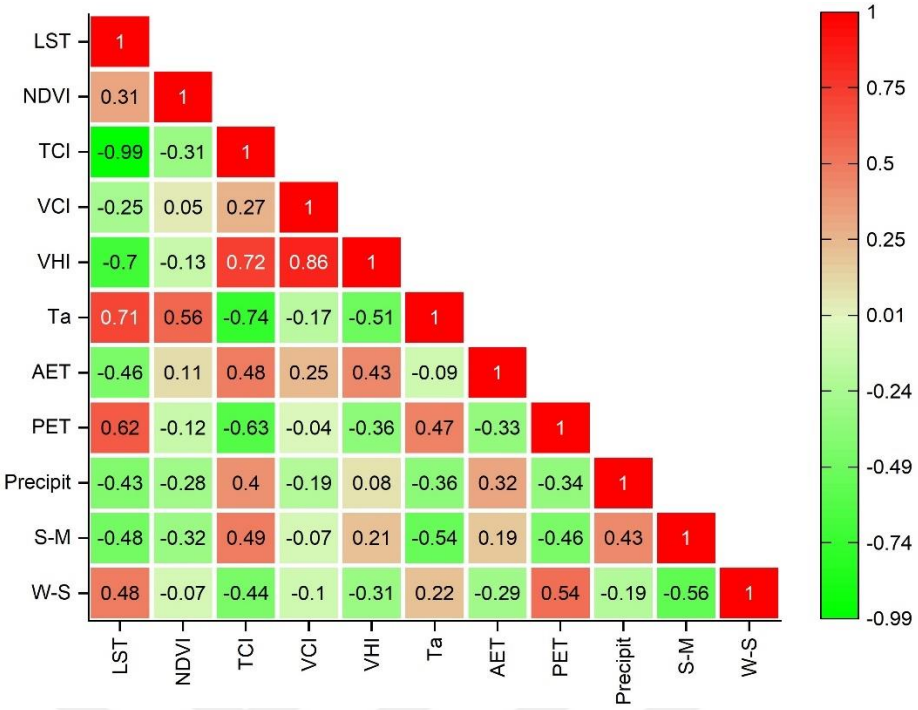

Figure 42. Correlation Coefficient between the parameters in Central region.

Likewise, as indicated in Figure 42, the relationship between the NDVI and VCI indices with the PET, precipitation, soil moisture, and wind speed parameters are weak and negative, suggesting a poor correlation among them. In contrast, the AET index shows a direct correlation with the NDVI, TCI, VCI, and VHI indices. Additionally, a significant correlation of 0.72 was observed between the TCI and VHI indices. In this region, there is a negative correlation between TCI and PET, while TCI exhibits a positive correlation with the AET, precipitation, and soil moisture parameters. Although these relationships are strong, they are not common, likely due to the high soil moisture levels in these areas.

According to Figure 42, VCI has a close relationship with the VHI index, showing a correlation of 0.86, which is expected. Similarly, the VHI index has a correlation of -0.51 with the Ta parameter and a correlation of 0.43 with the AET parameter, indicating a normal relationship. Furthermore, the correlation between Ta and PET is 0.47, while the correlations between Ta and precipitation, as well as soil moisture, are inverse and significant. A high inverse correlation has also been observed between the PET parameter and wind speed, indicating the impact of high PET on wind speed in this area. Additionally, a correlation of -0.56 was established between wind speed and soil moisture, suggesting that an increase in wind speed contributes to surface drying in this region.

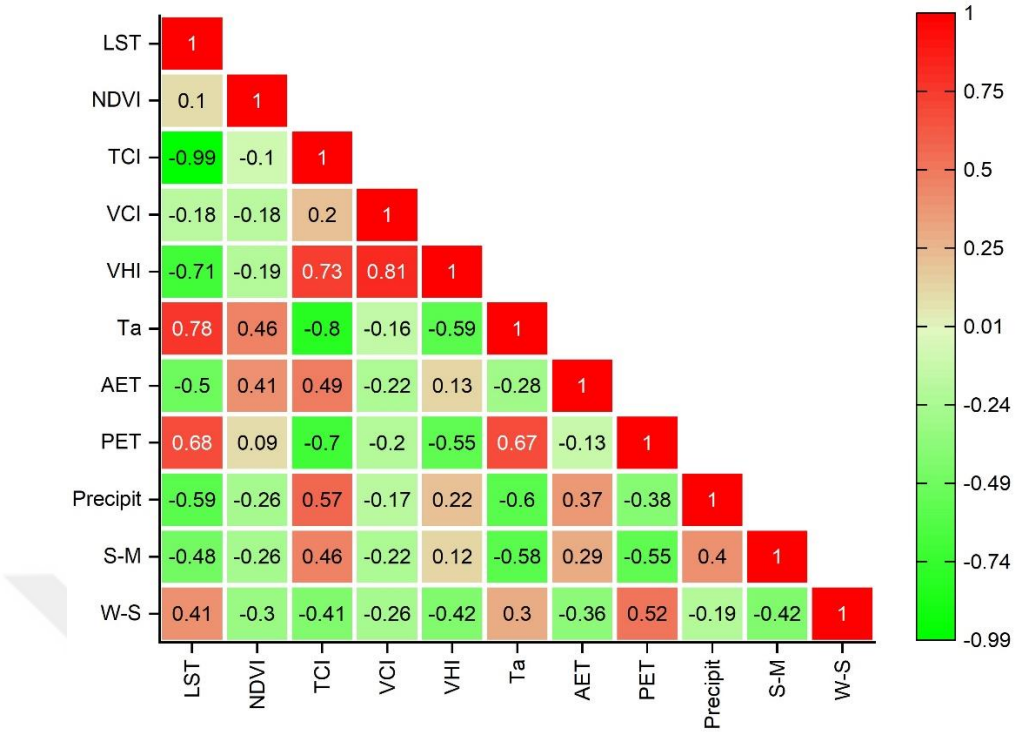

Figure 43. Correlation Coefficient between the parameters in West Central region.

Figure 43 displays the correlation values of the climate parameters for the west-central region. In this area, due to limited vegetation, the NDVI has a weak relationship with LST, although it shows a close direct correlation with the Ta parameter. LST has established strong inverse relationships with the TCI, VCI, and VHI indices, which mirrors the behavior of the Ta parameter with these indices. The correlation between LST and Ta is significant, recorded at 0.78. Additionally, the relationship between LST and the PET parameters is direct and strong. In contrast, the relationships between LST and the AET, precipitation, and soil moisture parameters are inverse and significant, which is typical for this region. Furthermore, increased wind speed has a direct effect on LST, with a correlation of 0.41. The NDVI exhibits a very weak correlation with the TCI, VCI, and VHI indices due to their low levels in this area, and its relationships with precipitation and soil moisture parameters are not significant. However, a significant correlation of 0.41 exists between NDVI and AET.

According to Figure 43, the TCI index has a significant direct relationship with the VCI and VHI indices, demonstrating a strong correlation. A notable correlation of -0.8 was observed between TCI and the Ta parameter, indicating a significant inverse relationship. The correlation between TCI and AET is 0.49, reflecting a significant and direct relationship,

whereas an unusual inverse correlation of -0.7 was noted between TCI and PET. Moreover, a strong direct relationship exists between TCI and both precipitation and soil moisture, likely due to the high levels of precipitation in this region, where temperature is less significant compared to moisture levels. Aside from VHI, the VCI shows weak relationships with other indices. The Ta parameter has a negative correlation with AET but a significant positive correlation of 0.67 with PET. Additionally, Ta exhibits an inverse and significant relationship with precipitation and soil moisture parameters. In this region, a direct but weak correlation exists between AET and precipitation and soil moisture parameters, attributed to the high precipitation throughout the year, despite slightly lower temperatures.

3.6. Results Based on The Mann-Kendall Test

In this section, the linear trend of the data analysed on a monthly, seasonal, and annual scale is assessed using the Mann-Kendall test to determine whether there is a significant trend. The Mann-Kendall test, as explained in previous sections, employs the condition of $1.96<Z<-1.96$. The resulting Z-values will be included in the tables for each parameter and analysed accordingly, and the red values in the table indicate the presence of a significant trend. The Mann-Kendall test was applied to the average monthly, seasonal, and annual data. Table 7 lists the Z-values of NDVI for each region on a monthly, seasonal, and annual basis. It indicates that the monthly NDVI for December, as well as the annual NDVI across Afghanistan, demonstrates a linear and significant increasing trend. However, no significant seasonal trend is observed. According to Table 6, the confidence level for the annual NDVI trend is approximately 95%, which is marked with a star. Conversely, the NDVI in the north region does not exhibit any significant trend on a monthly, seasonal, or annual basis. In the northeastern region, the NDVI for the months of March, April, July, and December shows a significant positive trend with confidence levels of 95%. Additionally, the NDVI displays a significant positive trend seasonally in winter and annually, with a confidence level of 95%.

According to Table 7, the NDVI in the western region has shown a significant trend on a monthly basis, except for January. It also exhibits a significant seasonal trend across all seasons and an annual trend with confidence levels reaching 95%. In the South region, the NDVI has demonstrated a significant trend monthly, seasonally, and annually from 2000 to 2023, indicating consistent growth since 2000, as discussed in previous sections. Furthermore, the NDVI in the eastern region has shown remarkable growth in the months of

July, August, September, and December, which is statistically significant. It also displays a significant seasonal trend during the summer and an annual trend, reflecting the overall growth of NDVI in this region. In the southeastern region, the NDVI exhibits a significant monthly trend, except for January, February, and March. Seasonally, it has a significant trend in spring, summer, and autumn, with an annual significance level above 95%. In the central region, a monthly trend is observed in December; however, no significant seasonal or annual trends are noted. In the west-central region, the NDVI has a significant monthly trend in May, October, and December, but no significant seasonal trends are observed. Overall, the NDVI in Afghanistan has demonstrated an increasing trend from 2000 to 2023, with no indications of decline.

Table 6. Z-value of the Mann-Kendall test for the monthly, seasonal and annual NDVI between the 2000-2023 years.

Z-value of M-K Test For each Region	Temporal Scale																
	Monthly												Seasonal				Annual
	Jan	Feb	Mar	Apr	May	Jun	Jul	Agu	Sep	Oct	Nov	Dec	Spring	Summer	Autumn	Winter	Years
Afghanistan	0.21	1.07	1.27	1.09	1.47	1.37	1.49	1.54	1.37	0.97	1.27	2.64	1.39	1.54	0.97	1.29	1.96
North	-0.77	-0.55	-0.32	-0.67	-0.42	-0.77	-0.70	-0.79	-1.34	-1.17	-0.12	0.72	-0.92	-0.79	-1.22	-0.52	-0.82
Northeastern	1.16	1.89	2.59	2.04	0.74	1.96	-0.40	0.17	0.30	0.37	0.00	2.83	1.74	0.10	0.42	2.48	2.55
Western	1.30	2.47	2.56	2.49	2.56	2.24	2.27	2.99	2.82	2.10	2.27	2.71	2.83	2.51	2.83	2.96	3.08
South	3.11	3.29	3.38	2.39	2.02	2.87	3.69	4.52	3.97	3.53	3.22	2.36	2.83	3.60	3.65	3.62	3.45
Eastern	0.79	0.82	1.37	1.37	0.00	1.57	4.05	3.38	2.41	0.35	0.47	2.36	1.14	4.15	0.77	1.59	2.26
Southeastern	0.00	0.57	1.24	3.40	3.20	2.78	4.22	4.62	4.65	4.13	2.89	2.18	3.25	3.84	4.05	0.27	3.57
Central	0.95	1.72	1.66	1.24	-0.12	1.09	1.15	1.32	1.86	0.45	-0.10	2.78	1.29	1.94	0.77	1.79	1.76
West Central	0.50	1.42	0.55	0.55	2.73	1.66	1.19	1.66	1.89	1.97	0.27	2.58	1.17	1.19	1.71	1.04	3.47
Positive Trend	1	2	3	4	4	4	4	4	4	4	3	8	3	4	3	3	7
Negative Trend	0	0	0	0	0	0	0	0	0	0	0	0	0	0	0	0	0
No Trend	8	7	6	5	5	5	5	5	5	5	6	1	6	5	6	6	2

The Z values of the LST parameter from the Mann-Kendall test are presented in Table 8. Throughout Afghanistan, the LST parameter does not exhibit a significant trend on a monthly, seasonal, or annual basis. However, in the north region, there is a significant decreasing trend in the monthly LST parameter observed in August, though no significant trends are noted seasonally or annually. Similarly, in the northeastern region, no significant trends are detected on a monthly, seasonal, or annual basis. In the western region, a significant monthly decreasing trend is observed in August, but there is no significant trend on a seasonal or annual basis. In the South region, the monthly LST shows a significant decrease in October, with a significant seasonal trend noted in autumn; however, no significant annual trend is found.

Table 7. Z-value of the Mann-Kendall test for the monthly, seasonal and annual LST (C°) between the 2000-2023 years.

Z-value of M-K Test For each Region	Temporal Scale																
	Monthly												Seasonal				Annual
	Jan	Feb	Mar	Apr	May	Jun	Jul	Agu	Sep	Oct	Nov	Dec	Spring	Summer	Autumn	Winter	Years
Afghanistan	-0.05	0.00	-0.37	-1.12	-1.12	-0.47	0.00	-1.81	-0.92	-1.81	-0.92	1.36	-0.97	-0.67	-1.61	0.07	-1.07
North	-0.21	-0.02	-0.52	-0.27	-0.62	0.62	-0.82	-2.51	-1.41	-1.91	-1.27	1.41	-0.17	-0.52	-1.66	0.37	-0.32
Northeastern	-0.48	0.02	0.12	-0.07	-0.07	-0.17	-0.32	-1.81	-0.67	-0.87	-0.62	1.66	-0.17	-0.87	-0.12	0.87	-0.47
Western	0.42	-0.22	-0.72	-0.92	-1.27	0.67	-0.77	-2.55	-0.77	-1.56	-0.62	1.56	-0.82	-1.27	-1.66	0.57	-0.72
South	-0.37	0.07	-0.82	-1.46	-1.61	0.47	1.22	-0.02	-0.82	-2.16	-1.07	-0.12	-1.41	1.07	-2.55	-0.52	-1.46
Eastern	-0.63	0.32	-0.17	-0.97	-1.91	-1.07	-2.51	-1.02	-0.72	-1.31	-0.22	0.97	-1.27	-2.41	-1.46	0.67	-1.27
Southeastern	-0.37	-0.17	-1.27	-1.56	-2.65	-1.91	-1.76	-0.92	-0.47	-2.21	-0.97	0.82	-1.76	-1.46	-2.11	-0.07	-1.61
Central	-0.79	0.07	-0.62	-0.67	-1.51	-1.27	-2.11	-2.41	-0.62	-1.76	-0.07	1.56	-1.22	-2.41	-1.27	0.27	-0.82
West Central	-0.21	-0.17	-0.72	-0.92	-1.41	-1.31	-1.96	-1.41	-0.32	-1.66	-0.27	1.96	-1.17	-2.06	-1.41	0.32	-0.82
Positive Trend	0	0	0	0	0	0	0	0	0	0	0	0	0	0	0	0	0
Negative Trend	0	0	0	0	1	0	2	3	0	2	0	0	0	3	2	0	0
No Trend	9	9	9	9	8	9	7	6	9	7	9	9	9	6	7	9	9

As indicated in table 8, In the eastern region, significant decreasing trends are observed monthly in July and seasonally during the summer, with a confidence level of 99%, although no annual trend is detected. The southeastern region exhibits significant decreasing trends in May and October, as well as a seasonal trend in autumn, but no significant annual trend is present. In the central region, significant decreasing trends are observed in July and August, along with a seasonal trend in summer, but no significant annual trend is noted. Similarly, in the central western region, a significant monthly decrease is seen in December and a seasonal decrease in summer, yet there is no significant annual trend. Overall, the LST parameter shows a significant decreasing trend across all regions of Afghanistan, with no indications of a significant increasing trend.

The Z values for the Ta parameter are provided in Table 9. The Ta parameter shows a significant increasing trend in July on a monthly scale for all of Afghanistan, but no significant trend is observed on a seasonal or annual basis. In the north region, a significant increasing trend was noted in July and during the summer season, while no significant annual trend is present. Similarly, in the northeastern region, the Ta parameter shows a significant increasing trend in March, July, and August, though no significant trend is observed seasonally or annually.

As depicted in table 9, in the western region, the Ta parameter exhibits a significant upward trend in June, July, and the summer season, but no significant annual trend is noted. Additionally, in the South region, a significant increasing trend was recorded in July and during the summer, but there is no annual trend. In the eastern region, while there is no significant seasonal or annual trend, significant trends are noted in February and September. Similarly, in the southeastern region, a significant downward trend is observed in May, but there is no significant trend on a seasonal or annual scale. The central region does not display any significant monthly, seasonal, or annual trend. Moreover, in the west-central region, a significant trend is only observed in July, while no significant seasonal or annual trend is present. Therefore, the Ta parameter shows no significant annual trend in any region between 2000 and 2023.

Table 8. Z-value of the Mann-Kendall test for the monthly, seasonal and annual Ta (C˚) between the 2000-2023 years.

Z-value of M-K Test For each Region	Temporal Scale																
	Monthly												Seasonal				Annual
	Jan	Feb	Mar	Apr	May	Jun	Jul	Agu	Sep	Oct	Nov	Dec	Spring	Summer	Autumn	Winter	Years
Afghanistan	-0.17	1.31	1.02	-0.42	-1.17	1.31	2.88	-0.22	1.41	-0.52	-0.57	0.92	-0.02	2.26	0.02	0.87	1.12
North	0.02	1.41	1.56	0.17	-0.32	1.61	3.40	-1.61	0.47	-0.52	-0.42	1.41	0.62	2.70	-1.27	1.31	1.51
Northeastern	-0.47	1.31	2.01	0.15	0.42	0.57	3.20	0.77	1.96	0.00	-0.32	0.42	0.72	1.81	0.92	1.22	1.81
Western	0.07	1.36	0.92	-0.52	-0.87	2.11	3.50	-0.72	0.77	-0.62	-0.27	1.27	0.22	3.25	-0.37	1.07	1.31
South	0.27	0.97	0.42	-1.12	-1.51	1.66	2.16	-0.22	0.82	-0.05	-0.60	0.27	-0.72	1.96	0.17	0.52	0.72
Eastern	-0.62	2.01	0.97	-0.27	-1.12	-0.82	0.32	0.60	2.06	-0.72	0.07	0.12	-0.77	-0.02	0.22	1.22	0.82
Southeastern	-0.47	0.97	0.07	-0.82	-2.08	-0.97	0.42	0.37	1.61	-0.92	-0.62	0.92	-1.27	-0.69	-0.07	0.47	-0.17
Central	-0.72	1.12	0.97	-0.07	-0.97	0.00	1.86	-0.42	1.61	-1.07	-0.42	0.92	-0.32	0.42	-0.07	0.52	0.67
West Central	-0.50	1.27	0.57	-0.47	-1.31	-0.27	2.11	-0.55	1.22	-1.17	-0.37	1.07	-0.67	0.02	-0.22	0.77	0.02
Positive Trend	0	1	1	0	0	1	6	0	2	0	0	0	0	3	0	0	0
Negative Trend	0	0	0	0	1	0	0	0	0	0	0	0	0	0	0	0	0
No Trend	9	8	8	9	8	8	3	9	7	9	9	9	9	6	9	9	9

The Z values of the AET parameter are listed in Table 10. The Z-value for the AET parameter shows a significant increasing trend in March and May across Afghanistan. However, no significant trend is observed on a seasonal or annual basis. In the north region, there is no significant trend on a monthly, seasonal, or annual scale. Similarly, in the northeastern region, while no significant monthly or seasonal trends are noted, a positive significant trend is observed annually. In the western region, a significant increasing trend is noted in March, but there are no significant trends seasonally or annually. Likewise, in the South region, no significant seasonal or annual trends are observed, though May shows a significant increasing trend. In the eastern region, significant increasing trends are observed in March, May, and September on a monthly scale, as well as during the spring season and annually.

Similarly, according to results (Table 10), in the southeastern region, significant increasing trends are noted in February, May, and September, and annually, though there is no significant seasonal trend. The central region displays a significant increasing trend in May and a significant decreasing trend in September, along with a significant increasing trend on both a seasonal and annual scale. Additionally, the west-central region shows significant increasing trends in January, February, May, July, and December, as well as in the spring and winter seasons and annually.

Table 9. Z-value of the Mann-Kendall test for the monthly, seasonal and annual AET between 2000-2023 years.

Z-value of M-K Test For each Region	Temporal Scale																
	Monthly												Seasonal				Annual
	Jan	Feb	Mar	Apr	May	Jun	Jul	Agu	Sep	Oct	Nov	Dec	Spring	Summer	Autumn	Winter	Years
Afghanistan	0.42	0.72	2.01	0.87	1.96	0.62	0.87	0.42	-1.02	0.17	0.87	-0.77	1.76	1.07	0.62	0.17	1.61
North	0.27	0.22	-0.62	0.12	1.22	0.00	-0.32	0.47	0.52	1.07	0.87	-1.02	0.02	0.07	0.97	-0.07	0.42
Northeastern	0.72	1.66	0.27	1.61	1.41	0.42	-0.72	0.22	0.32	0.52	1.81	1.27	1.36	0.52	0.87	1.46	2.01
Western	-0.62	0.77	2.36	0.00	0.82	0.27	0.62	0.42	0.72	1.17	0.47	-0.92	0.52	0.37	0.47	0.27	0.87
South	0.77	-0.12	1.12	0.52	2.6	0.07	-0.02	-0.07	-0.17	0.82	0.82	-0.57	1.17	0.17	0.82	0.07	0.52
Eastern	1.41	1.51	2.01	0.02	2.31	1.22	0.97	0.57	-0.57	0.00	0.07	-0.67	2.11	1.41	-0.22	0.22	2.16
Southeastern	0.77	2.55	0.67	1.22	2.8	0.22	0.32	1.07	-2.06	-0.07	0.62	-0.07	1.76	1.02	0.27	1.36	2.70
Central	0.47	1.71	1.12	1.86	2.75	1.22	1.41	0.37	-2.21	-0.32	0.42	0.25	3.10	1.36	-0.17	0.97	3.84
West Central	2.03	2.36	0.87	1.12	2.21	-0.22	2.46	0.94	-0.10	-0.22	1.46	2.16	3.50	0.37	0.02	2.16	3.10
Positive Trend	1	2	3	0	6	0	1	0	0	0	0	1	3	0	0	1	5
Negative Trend	0	0	0	0	0	0	0	0	2	0	0	0	0	0	0	0	0
No Trend	8	7	6	9	3	9	8	9	7	9	9	8	6	9	9	8	4

The results of Kendall's test for the PET parameter are presented in Table 11. The PET parameter does not show a significant seasonal or annual trend across Afghanistan, but a significant increasing trend is observed on a monthly scale in September, October, and

December. Similarly, in the north region, no significant seasonal or annual trend is present, though there is a significant increasing trend in September and December. In the northeastern region, significant trends are observed seasonally in autumn and winter, as well as monthly in September, October, and December, with no significant trend on an annual scale. In the western region, while no annual trend is noted, a significant increasing trend is observed in autumn and October. Likewise, the South region does not display any significant seasonal or annual trends, but significant increasing trends are noted in May and October.

Table 10. Z-value of the Mann-Kendall test for the monthly, seasonal and annual PET between the 2000-2023 years.

Z-value of M-K Test For each Region	Temporal Scale																
	Monthly												Seasonal				Annual
	Jan	Feb	Mar	Apr	May	Jun	Jul	Agu	Sep	Oct	Nov	Dec	Spring	Summer	Autumn	Winter	Years
Afghanistan	0.87	0.67	-0.47	-0.52	-0.87	-0.52	-0.47	1.46	2.11	2.11	1.27	2.06	-0.97	0.02	1.61	1.56	0.97
North	0.77	0.77	-0.77	-0.47	-0.52	0.27	1.76	0.97	2.41	1.31	0.57	2.01	-0.42	1.36	1.71	1.41	1.17
Northeastern	1.36	0.97	-0.32	-0.67	-0.17	0.37	0.82	1.51	2.70	2.16	1.56	2.31	0.07	1.17	2.16	2.13	1.31
Western	1.02	0.47	-0.07	0.07	-0.52	-0.32	-0.27	0.77	1.91	2.06	1.56	1.61	-0.37	0.17	1.96	1.17	1.12
South	0.17	1.07	-0.57	-1.07	-2.16	-0.52	-0.82	1.02	1.46	2.95	1.91	1.71	-1.71	-0.62	1.76	1.41	0.42
Eastern	0.92	1.41	-0.87	-2.21	-2.06	-1.86	-1.81	-0.07	2.26	1.12	2.01	2.65	-2.46	-2.36	1.96	1.71	-2.06
Southeastern	0.07	1.56	-1.07	-1.46	-2.75	-1.71	-0.52	0.22	1.22	1.91	0.97	2.36	-1.91	-0.92	2.01	1.71	-0.92
Central	-0.47	0.97	-0.32	-1.31	-1.02	-0.94	-1.56	0.27	1.22	1.31	1.17	2.21	-1.17	-1.61	1.86	1.56	-0.47
West Central	1.02	1.46	0.17	-0.27	-0.72	-0.72	-0.52	0.00	1.12	1.81	0.17	1.64	-0.47	-0.27	1.76	1.76	0.47
Positive Trend	0	0	0	0	0	0	0	0	4	4	1	6	0	0	4	1	0
Negative Trend	0	0	0	1	3	0	0	0	0	0	0	0	1	1	0	0	1
No Trend	9	9	9	8	6	9	9	9	5	5	8	3	8	8	5	8	8

According to the results in Table 11, a significant decreasing trend is observed seasonally during the spring and summer, while a significant increasing trend is noted in autumn and winter. Additionally, significant trends are observed monthly in April, May,

September, November, and December, as well as on an annual basis. In the southeast region, no significant annual trend is present, but significant trends are observed during the autumn season and in May and December. Similarly, in the central region, a significant trend is noted only in December, with no significant seasonal or annual trends. The west-central region also lacks significant trends on a monthly, seasonal, or annual scale. Therefore, the PET parameter exhibited a significant decreasing trend only in the eastern region annually, with a confidence level of 99%, while no significant annual trends were observed in the other regions.

Table 12 presents the Z-values for the precipitation parameter. Across Afghanistan, no significant annual trend is observed for the precipitation parameter, but there is a notable trend during the summer season, particularly in July and December. In the north region, no significant annual or seasonal trends were detected, but significant trends emerged in the months of July, August, and December. Similarly, the northeastern region also lacks significant annual or seasonal trends, though it displays significant trends in July and December.

As indicated in table 12, in the west and south regions, no significant seasonal or annual trends are observed. However, the west region shows significant trends in July, August, September, and December, while the south region experiences a significant trend in May. The east and southeast regions share similar patterns, with significant annual and seasonal trends in spring and summer, as well as in the months of May and July. The central and west-central regions exhibit no annual trends, but the central region shows a significant trend in July, and the west-central region displays significant trends in May, July, and August. Therefore, while a significant annual increase in precipitation is noted in two regions, no significant annual trends are observed in the remaining regions.

Table 11. Z-value of the Mann-Kendall test for the monthly, seasonal and annual Precipitation between the 2000-2023 years.

Z-value of M-K Test For each Region	Temporal Scale																
	Monthly												Seasonal				Annual
	Jan	Feb	Mar	Apr	May	Jun	Jul	Agu	Sep	Oct	Nov	Dec	Spring	Summer	Autumn	Winter	Years
Afghanistan	0.27	0.17	0.72	-0.27	1.31	0.27	2.80	1.12	0.42	0.22	1.02	-2.21	0.97	2.46	0.62	-0.37	0.27
North	-0.52	0.07	-0.22	-0.72	0.42	-0.62	3.03	3.59	1.84	0.17	0.32	-2.36	-0.22	1.07	0.42	-1.07	-0.57
Northeastern	-0.27	-0.27	-0.22	-0.67	-0.02	0.00	2.55	1.17	-0.30	-0.27	0.02	-2.41	-0.07	1.12	0.27	-0.97	-1.02
Western	-0.37	0.42	0.47	-0.37	1.56	-0.67	3.05	3.86	2.81	0.92	0.47	-2.61	0.32	1.32	0.57	-0.72	-0.12
South	0.37	-0.27	1.56	0.00	2.60	0.92	1.24	1.54	1.52	0.82	0.87	-0.87	1.07	1.59	0.97	0.22	0.32
Eastern	0.47	0.52	1.27	0.82	2.21	0.42	2.95	1.17	0.32	0.82	1.02	-1.31	2.01	2.11	1.46	-0.27	2.65
Southeastern	0.42	0.07	1.51	0.07	2.90	1.46	2.01	1.31	-0.02	1.31	1.31	-1.02	2.11	2.51	1.56	0.42	2.41
Central	0.02	0.72	0.57	0.37	1.66	0.57	3.08	1.61	-0.32	0.77	1.27	-0.77	1.02	2.31	1.61	0.17	1.91
West Central	0.32	0.27	0.62	-0.25	2.06	1.56	2.80	2.41	1.74	0.27	0.67	-1.56	0.62	2.95	0.82	-0.37	0.77
Positive Trend	0	0	0	0	4	0	8	3	1	0	0	0	2	5	0	0	2
Negative Trend	0	0	0	0	0	0	0	0	0	0	0	4	0	0	0	0	0
No Trend	9	9	9	9	5	9	1	6	8	9	9	5	7	4	9	9	7

Table 13 presents the Z-values for the soil moisture parameter. Across Afghanistan, no significant annual trend is observed for soil moisture. However, a significant negative trend is evident in December and throughout the winter season. In the north region, significant decreasing trends are observed in January, December, and during the winter season, as well as annually. Similarly, in the northeastern region, significant trends are observed in January, February, September, October, and December, along with significant trends in the fall and winter seasons and annually. The western region shows no significant annual trend, though a significant trend is present in December and during the winter season. In the south region, no significant monthly, seasonal, or annual trends are detected. The eastern and southeastern regions also lack significant seasonal and annual trends. However, in the east, significant trends are observed in May and August, while in the southeast region, a significant trend is found in December. Additionally, no significant annual trends are

observed in the central and west-central regions. Yet, in the central region, significant trends appear in May, as well as during the spring and winter seasons. Similarly, the west-central region shows significant trends in December and during the winter season.

Table 12. Z-value of the Mann-Kendall test for the monthly, seasonal and annual Soil Moisture between the 2000-2023 years.

Z-value of M-K Test For each Region	Temporal Scale																
	Monthly												Seasonal				Annual
	Jan	Feb	Mar	Apr	May	Jun	Jul	Agu	Sep	Oct	Nov	Dec	Spring	Summer	Autumn	Winter	Years
Afghanistan	-1.61	-1.66	-0.27	0.00	0.12	-0.37	-0.07	0.30	-0.67	-1.12	-1.12	-2.36	-0.27	-0.47	-1.31	-2.70	-1.66
North	-2.01	-1.41	-0.17	-0.50	-0.82	-1.17	-1.34	-1.27	-1.09	-1.17	-1.46	-2.55	-0.92	-1.31	-1.36	-3.45	-2.11
Northeastern	-2.11	-2.36	-1.07	-0.47	-0.22	-0.67	-0.72	-0.72	-2.26	-2.31	-1.81	-2.41	-0.82	-0.82	-2.11	-2.95	-2.36
Western	-1.91	-0.12	0.87	-0.37	-0.32	-0.02	0.02	0.27	0.27	-0.45	-1.17	-2.46	-0.42	-0.07	-1.07	-2.26	-1.22
South	-0.22	-0.12	0.27	0.17	0.17	0.07	0.07	0.22	0.20	0.12	-0.05	-1.81	0.32	0.17	0.02	-0.97	-0.27
Eastern	-0.92	-1.51	0.92	1.17	2.41	1.07	1.86	2.06	1.27	-0.12	-0.47	-1.17	1.12	1.56	-0.02	-1.86	-0.42
Southeastern	-0.52	-0.82	1.46	0.92	0.97	0.77	0.65	0.67	0.45	0.25	0.22	-2.01	1.17	0.52	0.42	-1.71	-0.42
Central	-1.51	-1.46	1.86	1.36	2.70	0.57	0.27	1.76	1.46	-0.72	-1.46	-1.66	2.16	0.62	-1.07	-1.96	-0.27
West Central	-1.91	-1.17	1.46	0.37	0.02	0.02	0.00	0.10	0.10	-1.12	-1.66	-2.01	0.42	0.07	-1.56	-1.96	-1.12
Positive Trend	0	0	0	0	2	0	0	1	0	0	0	0	1	0	0	0	0
Negative Trend	2	1	0	0	0	0	0	0	1	1	0	6	0	0	1	6	2
No Trend	7	8	9	9	7	9	9	8	8	8	9	3	8	9	8	3	7

In Table 14, the results of the wind speed parameter derived from the Mann-Kendall test are shown. According to the data, annual wind speed does not show a significant trend across any region in Afghanistan. Similarly, no significant seasonal trends are observed throughout the country, with significant trends detected only in the months of May, August, and December. In the north region, no significant monthly or seasonal trends are noted.

In contrast, the northeast region exhibits significant trends in May, August, and during the summer season. The western region shows a significantly increasing trend in August,

although no seasonal trend is observed. Likewise, the South region records significant trends in August and during the summer season, while the eastern region shows significant trends in April, May, and throughout the spring season. In the southeast region, no significant seasonal trends are detected, though a significant trend is observed in May. Additionally, the central region shows significant trends in April, May, and in the spring season, while the west-central region displays a significant trend in May.

Table 13. Z-value of the Mann-Kendall test for the monthly, seasonal and annual Wind speed between the 2000-2023 years.

Z-value of M-K Test For each Region	Temporal Scale																
	Monthly												Seasonal				Annual
	Jan	Feb	Mar	Apr	May	Jun	Jul	Agu	Sep	Oct	Nov	Dec	Spring	Summer	Autumn	Winter	Years
Afghanistan	0.97	-0.57	-0.12	-0.47	-2.06	0.82	0.72	2.31	0.37	0.12	-0.12	-2.01	-1.02	1.12	0.22	-1.22	-0.87
North	0.07	-0.52	-0.42	-1.31	-1.17	0.07	1.31	0.77	1.41	-0.72	-0.57	-1.27	-1.91	0.72	-0.77	-0.62	-1.22
Northeastern	0.72	-0.22	-0.77	-1.31	-2.65	1.31	0.97	1.96	0.52	-0.67	0.07	-1.56	-1.81	2.06	-0.22	-0.92	-1.22
Western	-0.47	-0.12	-0.42	-0.37	-1.36	0.07	0.12	3.1	1.46	1.02	-0.17	-1.76	-1.22	1.12	1.41	-1.22	0.22
South	0.42	0.17	0.72	-0.97	-1.31	0.87	1.81	3.50	1.07	1.61	-0.82	-1.46	-0.87	2.01	0.72	-0.17	0.52
Eastern	1.66	0.47	-1.17	-2.06	-2.51	0.67	-0.82	0.77	0.17	-0.17	1.07	-0.22	-2.55	0.00	0.32	1.41	-0.57
Southeastern	1.61	0.42	-0.77	-1.02	-2.11	0.27	-0.07	0.92	0.02	1.12	-0.02	-0.67	-1.46	0.12	0.57	0.92	-0.22
Central	1.81	-0.12	-0.62	-2.16	-2.41	1.02	0.52	0.87	1.56	-0.02	1.81	-0.82	-2.41	0.92	0.87	0.77	0.07
West Central	1.17	-0.42	-0.17	-1.17	-2.80	0.12	0.12	-0.47	-0.72	1.07	-0.22	-1.86	-1.86	-0.17	-0.22	-0.72	-1.66
Positive Trend	0	0	0	0	0	0	0	4	0	0	0	0	0	2	0	0	0
Negative Trend	0	0	0	2	6	0	0	0	0	0	0	1	2	0	0	0	0
No Trend	9	9	9	7	3	9	9	5	9	9	9	8	7	7	9	9	9

The values of the Mann-Kendall test for the VCI index are listed in Table 15. This index had a significant trend only in the month of December in the northeast region, but it did not have a significant monthly, seasonal and annual trend in other regions.

Table 14. Z-value of the Mann-Kendall test for the monthly, seasonal and annual VCI between the 2000-2023 years.

Z-value of M-K Test For each Region	Temporal Scale																
	Monthly												Seasonal				Annual
	Jan	Feb	Mar	Apr	May	Jun	Jul	Agu	Sep	Oct	Nov	Dec	Spring	Summer	Autumn	Winter	Years
Afghanistan	-0.61	-0.22	-0.84	-0.82	-0.62	0.17	0.05	0.07	-0.22	-0.67	-0.37	0.89	-0.97	0.32	-0.37	-0.42	-0.67
North	0.00	-0.27	0.57	-0.07	-0.02	-0.22	-0.22	-0.07	-0.42	-0.57	-0.07	0.67	0.32	-0.12	0.17	0.02	-0.37
Northeastern	-0.85	-0.07	0.67	0.02	-0.07	-0.82	-0.77	-1.31	-1.56	-1.17	-0.97	1.96	0.37	-1.27	-1.41	-0.62	-1.27
Western	0.00	-1.17	-0.27	1.51	1.76	0.97	0.27	-0.02	-0.17	-0.12	-0.47	0.02	1.27	0.42	-0.57	-0.62	0.42
South	-0.63	-0.82	0.72	0.47	0.00	0.57	-0.17	-0.02	0.17	-0.77	-1.41	-1.51	0.42	0.37	-1.41	-1.31	-1.31
Eastern	-0.42	0.77	0.57	-1.46	-0.77	-0.17	1.71	0.67	-0.02	0.00	0.62	1.41	-0.82	1.36	0.12	1.12	0.27
Southeastern	-1.37	-0.72	-0.27	0.72	1.07	0.77	1.17	0.37	0.32	0.42	0.32	-0.42	0.47	0.87	0.32	-1.86	0.22
Central	-1.85	0.47	0.47	-0.97	0.97	0.87	0.89	1.31	1.07	0.77	0.07	1.56	-0.02	1.12	0.27	0.92	0.62
West Central	-0.53	-0.52	-0.07	-0.82	-0.02	0.22	-0.02	-0.02	0.02	-0.12	-1.41	1.81	-0.27	-0.07	-0.52	1.56	-0.47
Positive Trend	0	0	0	0	0	0	0	0	0	0	0	1	0	0	0	0	0
Negative Trend	0	0	0	0	0	0	0	0	0	0	0	0	0	0	0	0	0
No Trend	9	9	9	9	9	9	9	9	9	9	9	8	9	9	9	9	9

Likewise, according to Table 16, the TCI index has no significant monthly, seasonal and annual trends throughout Afghanistan and in the northeastern region. And in the north and west regions, only in the month of August, a significant trend is observed, but seasonally and annually, no significant trend is observed. Also, no significant monthly or annual trend is observed in the south region, and there is a significant trend only in the autumn season. There is a significant trend in the east and southeast region in May, but the annual trend is not observed, and there is a significant trend in the east region in the summer season and in the southeast region in the autumn season. The same, there is a significant trend in the central region in the summer season, but it is not significant on a monthly and yearly basis. And in the west central region, there is a significant trend in the summer season and in June, and

there is no annual trend. Therefore, the TCI index has not a significant annual trend in all regions of Afghanistan.

Table 15. Z-value of the Mann-Kendall test for the monthly, seasonal and annual TCI between the 2000-2023 years.

Z-value of M-K Test For each Region	Temporal Scale																
	Monthly												Seasonal				Annual
	Jan	Feb	Mar	Apr	May	Jun	Jul	Agu	Sep	Oct	Nov	Dec	Spring	Summer	Autumn	Winter	Years
Afghanistan	0.05	0.00	0.70	1.04	0.82	0.60	-0.02	1.69	1.29	1.22	0.69	-1.19	1.12	1.09	1.22	-0.17	1.02
North	-0.11	-0.07	0.57	0.22	0.07	0.42	0.72	2.11	1.31	1.41	0.92	-1.71	-0.02	1.07	1.27	-1.02	0.37
Northeastern	0.37	-0.62	-0.22	-0.27	0.17	0.32	0.00	1.91	0.07	0.47	0.77	-1.36	-0.07	0.77	0.42	-0.72	0.57
Western	-0.48	0.22	0.72	0.97	0.82	0.00	0.92	2.31	1.12	1.02	0.52	-1.17	1.07	1.41	1.17	-0.42	0.77
South	0.26	-0.02	0.77	1.51	0.87	-1.41	-0.77	0.17	1.14	1.46	0.92	0.02	1.36	-1.12	1.96	0.67	1.27
Eastern	0.58	-0.37	0.57	1.07	2.06	1.17	1.56	1.36	0.52	1.36	0.37	-1.12	1.46	2.16	1.36	-0.22	1.51
Southeastern	0.37	0.07	1.31	1.36	2.60	1.27	0.82	1.02	0.72	1.91	0.77	-0.62	1.76	1.12	2.06	0.12	1.81
Central	0.63	-0.07	0.57	1.07	1.41	1.91	1.91	1.66	0.32	1.17	0.02	-1.41	1.17	2.46	1.02	-0.52	1.07
West Central	0.26	0.12	0.62	1.22	1.56	2.06	1.17	1.17	0.42	1.36	0.12	-1.56	1.27	1.96	1.07	-0.37	0.97
Positive Trend	0	0	0	0	2	1	0	2	0	0	0	0	0	3	2	0	0
Negative Trend	0	0	0	0	0	0	0	0	0	0	0	0	0	0	0	0	0
No Trend	9	9	9	9	7	8	9	7	9	9	9	9	9	6	7	9	9

Likewise, according to Table 17, the VHI index in the central region has a significant monthly trend in May and seasonally in spring. This index has not shown a significant trend in other regions.

Table 16. Z-value of the Mann-Kendall test for the monthly, seasonal and annual VHI between the 2000-2023 years.

Z-value of M-K Test For each Region	Temporal Scale																
	Monthly												Seasonal				Annual
	Jan	Feb	Mar	Apr	May	Jun	Jul	Agu	Sep	Oct	Nov	Dec	Spring	Summer	Autumn	Winter	Years
Afghanistan	-0.26	-0.84	-0.22	0.22	0.02	0.12	0.32	1.07	-0.17	0.20	0.62	-0.92	-0.32	0.37	0.32	-0.62	0.17
North	-0.11	-0.77	1.86	-0.12	-0.07	-0.22	-0.07	0.57	0.02	0.42	0.47	-0.27	-0.67	0.17	0.62	-0.67	-0.07
Northeastern	-0.32	-1.76	1.27	0.32	0.32	-1.07	-1.02	-0.87	-0.97	-0.22	-1.27	0.22	1.12	-0.62	-1.31	-0.22	-0.47
Western	-0.11	-1.51	-0.22	0.87	1.46	0.77	0.62	0.47	0.27	0.07	0.00	-0.82	1.27	0.62	0.07	-0.87	1.12
South	-0.74	-0.92	1.27	0.77	0.37	0.57	0.02	0.62	0.12	-0.67	-1.02	-1.56	1.51	0.17	-0.82	-1.76	0.12
Eastern	-0.21	-0.17	0.17	0.02	1.71	0.32	1.61	1.17	-0.27	0.77	0.77	1.51	0.72	1.61	0.57	1.36	1.56
Southeastern	-1.06	-1.91	0.02	1.71	1.51	1.12	1.41	0.52	0.57	0.72	0.37	-0.82	1.41	1.07	0.62	-1.86	1.07
Central	-1.00	0.92	1.02	0.77	3.45	1.56	1.56	1.56	0.92	1.02	0.52	1.31	2.11	1.46	0.47	0.77	1.36
West Central	-0.48	-0.17	0.52	0.57	1.91	0.67	0.27	0.22	0.17	0.17	-0.77	1.56	1.56	0.47	-0.37	0.87	0.72
Positive Trend	0	0	0	0	1	0	0	0	0	0	0	0	1	0	0	0	0
Negative Trend	0	0	0	0	0	0	0	0	0	0	0	0	0	0	0	0	0
No Trend	9	9	9	9	8	9	9	9	9	9	9	9	8	9	9	9	9

3.7. Results Based on The Homogeneity Test

In this section, the results of the homogeneity test to examine the trend of homogeneity and heterogeneity of the climate parameters used in this thesis are included seasonally and annually between 2000-2023 years. As described in the material and method section, the homogeneity test is used to obtain the point of the change of climatic parameters over time, and the significance level in this test is 5% (Bazgir et al., 2018). In this thesis, Pettitt's homogeneity test method is used in XLSTAT program. The results of this test for each parameter are included in the table on a seasonally and annual basis and are also shown annually in the charts, and the red values in the tables explain the heterogeneity of the data.

As illustrated in Table 17 and Figure 44, the NDVI across Afghanistan and in the north region shows no change point for a significant trend, indicating that the NDVI data is homogeneous. As a result, the alternative hypothesis (Ha) is rejected, and the null hypothesis (H0) is accepted. However, other regions exhibit seasonal and annual change points. Similarly, in the northeast region, NDVI remains homogeneous during the spring, summer, and autumn seasons. Yet, in the winter season and on an annual scale, the data is heterogeneous, as the P-value <0.05, indicating a change point. According to Figure 44, this change point occurred in 2009, after which NDVI in the northeast region has shown an increasing trend.

Table 17. P-value of Homogeneity Test (Pettitt's test) for NDVI Values.

Regions		Afghanistan	North	Northeastern	Western	South	Eastern	Southeastern	Central	West Central
Spring	P-value	0.739	0.763	0.300	**0.027**	**0.014**	0.220	**0.046**	0.520	0.515
	significant	H0	H0	H0	Ha	Ha	H0	Ha	H0	H0
	change point at year				2012	2006		2014		
Summe	P-value	0.101	0.653	0.616	0.068	**0.005**	**0.000**	**0.001**	0.059	0.127
	significant	H0	H0	H0	H0	Ha	Ha	Ha	H0	H0
	Change point at year					2010	2009	2011		
Fall	P-value	0.196	0.956	0.511	**0.05**	**0.003**	0.957	**0.002**	0.282	0.452
	significant	H0	H0	H0	Ha	Ha	H0	Ha	H0	H0
	Change point at year				2010	2010		2008		
Winter	P-value	0.341	0.893	**0.024**	**0.000**	**0.004**	**0.027**	0.525	**0.006**	0.810
	significant	H0	H0	Ha	Ha	Ha	Ha	H0	Ha	H0
	Change point at year			2009	2013	2012	2009		2009	
Annual	P-value	0.109	0.557	**0.010**	**0.005**	**0.008**	**0.031**	**0.000**	0.083	**0.002**
	significant	H0	H0	Ha	Ha	Ha	Ha	Ha	H0	Ha
	Change point at year			2009	2012	2012	2009	2009		2009

Likewise, NDVI according to Table 18 in the western region in the summer season, the Ha hypothesis is rejected and H0 is accepted that the data is homogeneous, but in the spring, fall, and winter seasons and annually, the P-value<0.05, which has a change point. NDVI in this region in the spring season after 2011, in the autumn season after 2010, and in the winter season after 2013, and according to Figure 44, after 2013, it increased annually. In the south region, NDVI data are heterogeneous in all seasons and annually, and the H0 hypothesis is rejected, and Ha is accepted, with a P-value <0.05. The change point of NDVI

was in the spring of 2006, in the summer and fall of 2010, and in the winter of 2012. Also, according to Figure 44, NDVI in this region increased since 2012. In the eastern region, the spring and autumn seasons, NDVI is homogeneous, and the hypothesis Ha is rejected and H0 is accepted, but in other seasons and annually, the P-value <0.05, and the hypothesis H0 is rejected, and Ha is accepted.

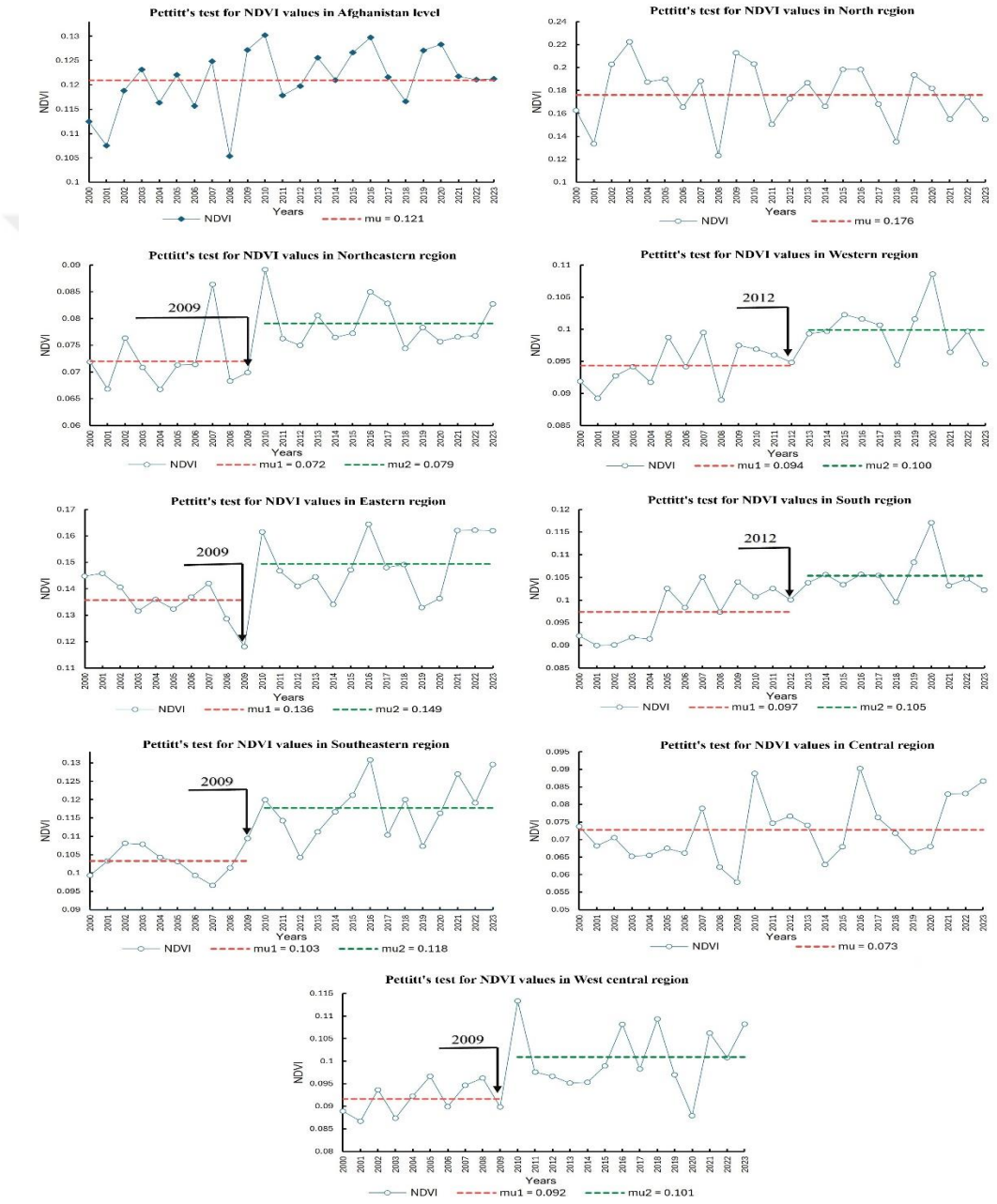

Figure 44. Significant change points based on the Pettitt's test in the mean of NDVI values for annually (2000–2023).

In reference to Table 18, the NDVI in the eastern region exhibited a change point in the summer and winter seasons in 2009, showing an increasing trend. Additionally, Figure 44 indicates that the NDVI had an annual change point in 2009, also reflecting an upward trend. In the southeastern region, NDVI remains homogeneous during the winter season, leading to the rejection of the alternative hypothesis (Ha) and acceptance of the null hypothesis (H0). However, in other seasons and on an annual basis, NDVI is heterogeneous, resulting in the rejection of H0 and acceptance of Ha. Specifically, NDVI in this region showed change points in the spring season of 2014, the summer season of 2011, and the autumn season of 2008, all indicating an increasing trend.

Figure 44 also demonstrates that NDVI experienced a change point annually in 2009, following an upward trajectory. In the central region, NDVI is homogeneous in the spring, summer, and fall seasons, as well as on an annual basis, leading to the rejection of Ha and acceptance of H0. Only in the winter season of 2009 does NDVI exhibit a change point, indicating heterogeneity. Similarly, the NDVI in the west-central region remains homogeneous across all seasons, resulting in the rejection of Ha and acceptance of H0. However, Figure 44 reveals that there was an annual change point in the west-central region in 2009, accompanied by an increasing trend.

Table 18. P-value of Homogeneity Test (Pettitt's test) for LST Values.

Regions		Afghanistan	North	Northeastern	Western	South	Eastern	Southeastern	Central	West Central
Spring	P-value	0.782	0.939	0.708	0.689	0.485	0.728	0.228	0.482	0.481
	significant	H0	H0	H0	H0	H0	H0	H0	H0	H0
	change point at year									
Summe	P-value	0.938	0.600	0.934	0.300	0.857	0.142	0.306	0.076	0.179
	significant	H0	H0	H0	H0	H0	H0	H0	H0	H0
	Change point at year									
Fall	P-value	0.336	0.187	0.242	0.325	0.057	0.759	0.249	0.546	0.414
	significant	H0	H0	H0	H0	H0	H0	H0	H0	H0
	Change point at year									
Winter	P-value	0.697	0.693	0.451	0.418	0.420	0.852	0.621	0.890	0.903
	significant	H0	H0	H0	H0	H0	H0	H0	H0	H0
	Change point at year									
Annual	P-value	0.600	0.719	0.873	0.621	0.557	0.765	0.238	0.678	0.700
	significant	H0	H0	H0	H0	H0	H0	H0	H0	H0
	Change point at year									

As shown in Table 19 and Figure 45, the LST index is homogeneous for all regions and in all seasons and annually, and the hypothesis Ha is rejected and H0 is accepted. In this index, the P-value>0.05 in all regions, and the Ha hypothesis is rejected, and no heterogeneity is observed in the LST data from 2000 to 2023.

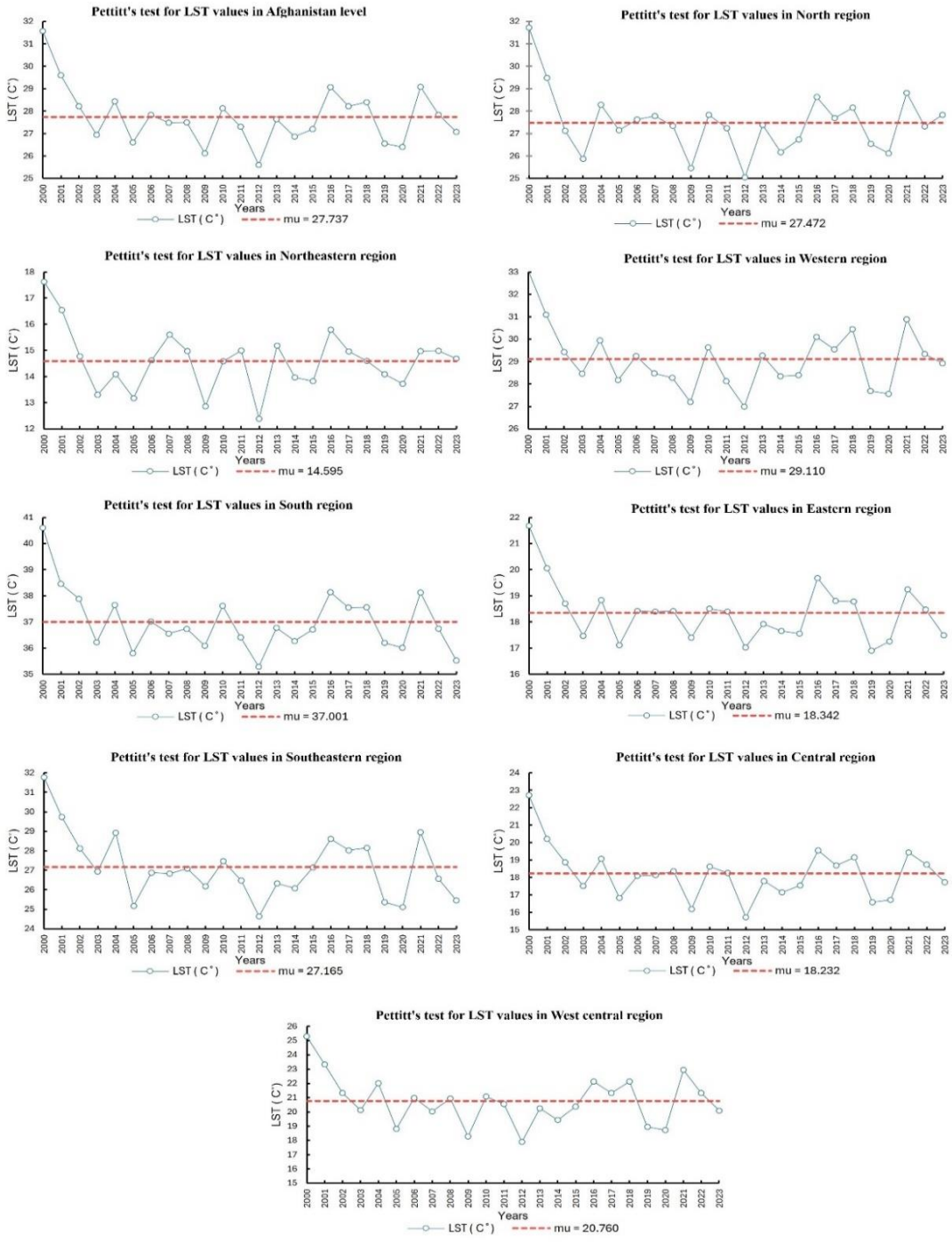

Figure 45. Significant change points based on the Pettitt's test in the mean of LST values for annually (2000–2023).

Table 19. P-value of Homogeneity Test (Pettitt's test) for Ta Values.

Regions		Afghanistan	North	Northeastern	Western	South	Eastern	Southeastern	Central	West Central
Spring	P-value	0.561	0.956	0.803	0.772	0.770	0.817	0.530	0.527	0.767
	significant	H0	H0	H0	H0	H0	H0	H0	H0	H0
	change point at year									
Summe	P-value	0.180	**0.043**	0.387	**0.024**	0.275	0.112	0.928	0.416	0.279
	significant	Ha	Ha	H0	Ha	H0	Ha	H0	Ha	Ha
	Change point at year		2005		2010					
Fall	P-value	0.071	0.784	0.903	0.432	0.521	0.358	0.279	0.068	0.505
	significant	H0	H0	H0	H0	H0	H0	H0	H0	H0
	Change point at year									
Winter	P-value	0.335	0.137	0.386	0.156	0.432	0.610	0.878	0.762	0.613
	significant	H0	H0	H0	H0	H0	H0	H0	H0	H0
	Change point at year									
Annual	P-value	0.448	0.222	0.203	0.492	0.724	0.589	0.792	0.579	0.832
	significant	H0	H0	H0	H0	H0	H0	H0	H0	H0
	Change point at year									

The Ta parameter is homogeneous across Afghanistan and specifically in the North-East, South, South-East, West, East, Central, and West Central regions during all seasons and on an annual basis, as indicated by Table 20 and Figure 46. Consequently, the alternative hypothesis (Ha) is rejected, and the null hypothesis (H0) is accepted, given that the P-value is greater than 0.05. The Ta data for these regions from 2000 to 2023 show no evidence of heterogeneity. However, in the North region, a change point was observed in the summer of 2005, indicating heterogeneity. Following this change point, the Ta parameter in this region exhibited an increasing trend. In other seasons and on an annual basis, the alternative hypothesis (Ha) is rejected, and the null hypothesis (H0) is accepted.

Additionally, Per Table 20, in the West region, a change point in the Ta parameter was noted during the summer of 2010, after which a significantly increasing trend began. Yet, in other seasons and annually in the Western region, the alternative hypothesis (Ha) is rejected, confirming that the data remains homogeneous. Overall, the Ta parameter was homogeneous annually without any significant change points, with noticeable increases only in the North and West regions during the summer season.

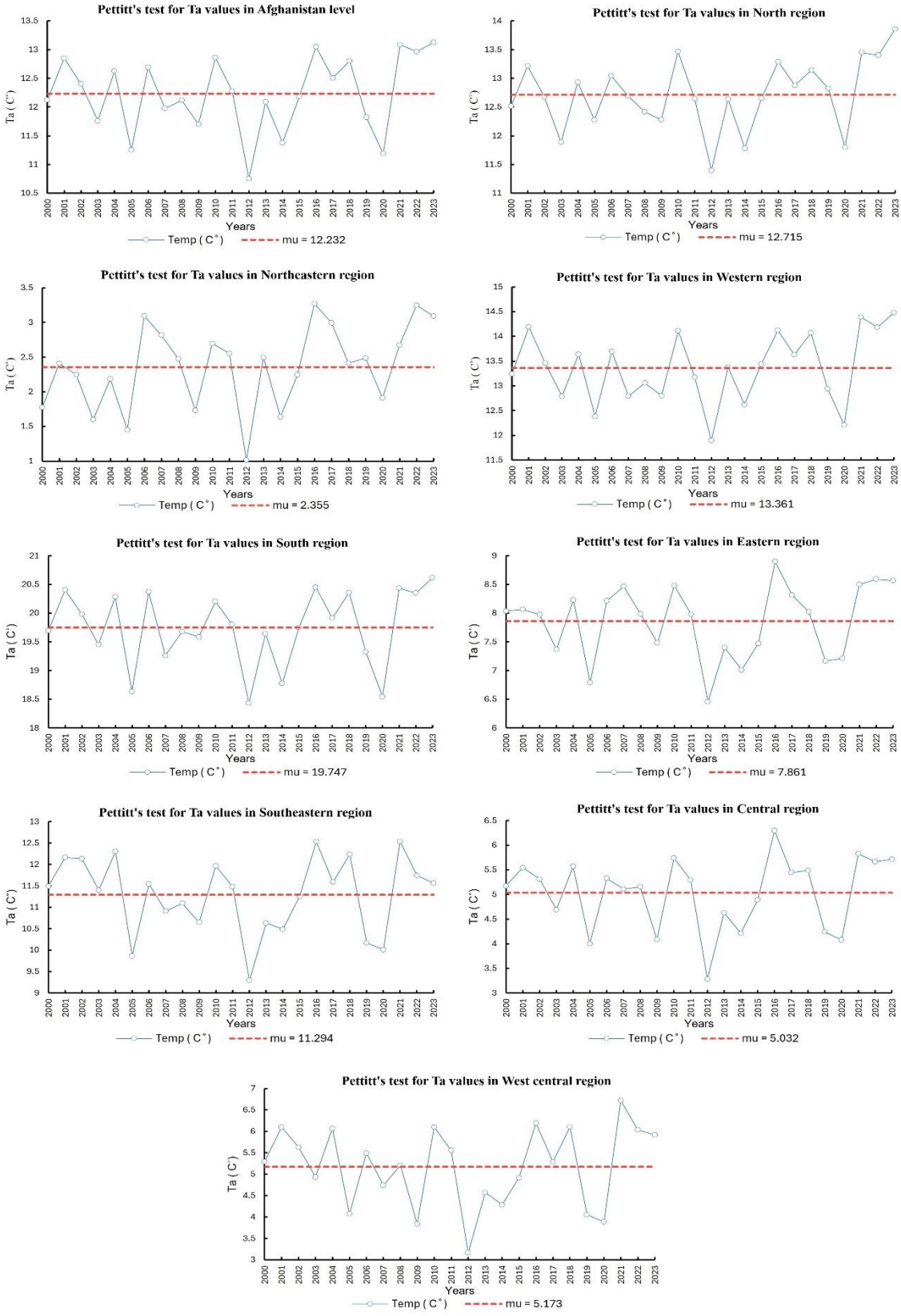

Figure 46. Significant change points based on the Pettitt's test in the mean of Ta values for annually (2000–2023).

Table 20. P-value of Homogeneity Test (Pettitt's test) for AET Values.

Regions		Afghanistan	North	Northeastern	Western	South	Eastern	Southeastern	Central	West Central
Spring	P-value	0.126	0.717	0.173	0.770	0.211	**0.030**	0.188	**0.006**	**0.007**
	significant	H0	H0	H0	H0	H0	Ha	H0	Ha	Ha
	change point at year						2008		2010	2010
Summe	P-value	0.929	0.693	0.516	0.783	0.776	0.578	0.723	0.454	0.972
	significant	H0	H0	H0	H0	H0	H0	H0	H0	H0
	Change point at year									
Fall	P-value	0.252	0.231	0.677	0.314	0.379	0.809	0.674	0.712	0.967
	significant	H0	H0	H0	H0	H0	H0	H0	H0	H0
	Change point at year									
Winter	P-value	0.412	0.557	**0.022**	0.856	0.880	0.166	0.072	0.103	**0.002**
	significant	H0	H0	Ha	H0	H0	H0	H0	H0	Ha
	Change point at year			2015						2015
Annual	P-value	0.151	0.647	0.094	0.947	0.767	0.062	**0.028**	**0.001**	**0.001**
	significant	H0	H0	H0	H0	H0	H0	Ha	Ha	Ha
	Change point at year							2007	2007	2010

As shown in table 21 and figure 47, the AET parameter data for Afghanistan and the North, West, and South regions are homogeneous both seasonally and annually. Consequently, the alternative hypothesis (Ha) is rejected, and the null hypothesis (H0) is accepted, as the P-value is greater than 0 in the calculations of Pettitt's test. In the North-East region, a change point in AET was observed during the winter season, leading to the rejection of the null hypothesis (H0) and acceptance of the alternative hypothesis (Ha). This change occurred continuously in 2015, followed by an increasing trend. However, in other seasons and on an annual basis, the data remains homogeneous, as no change points are observed.

Similarly, based on table 21, in the Eastern region, a change point occurred in the spring of 2008, indicating heterogeneity and an increasing trend; however, in other seasons and annually, the AET data is homogeneous with no change points detected. In the Southeastern region, the data is homogeneous seasonally, leading to the rejection of the alternative hypothesis (Ha) and acceptance of the null hypothesis (H0). Nonetheless, as shown in Figure 47, the AET data is heterogeneous annually, with a change point observed in 2007, after which the AET parameter exhibited an increasing trend. Additionally, the Central and West Central regions showed a change point in the spring season, indicating

heterogeneity. This change point, observed in both regions in 2010, corresponds to an increasing trend, while the data is homogeneous in these regions during the summer and autumn seasons. Furthermore, the Central region was homogeneous in the winter season but heterogeneous annually, whereas the West Central region exhibited heterogeneity both in the winter season and annually.

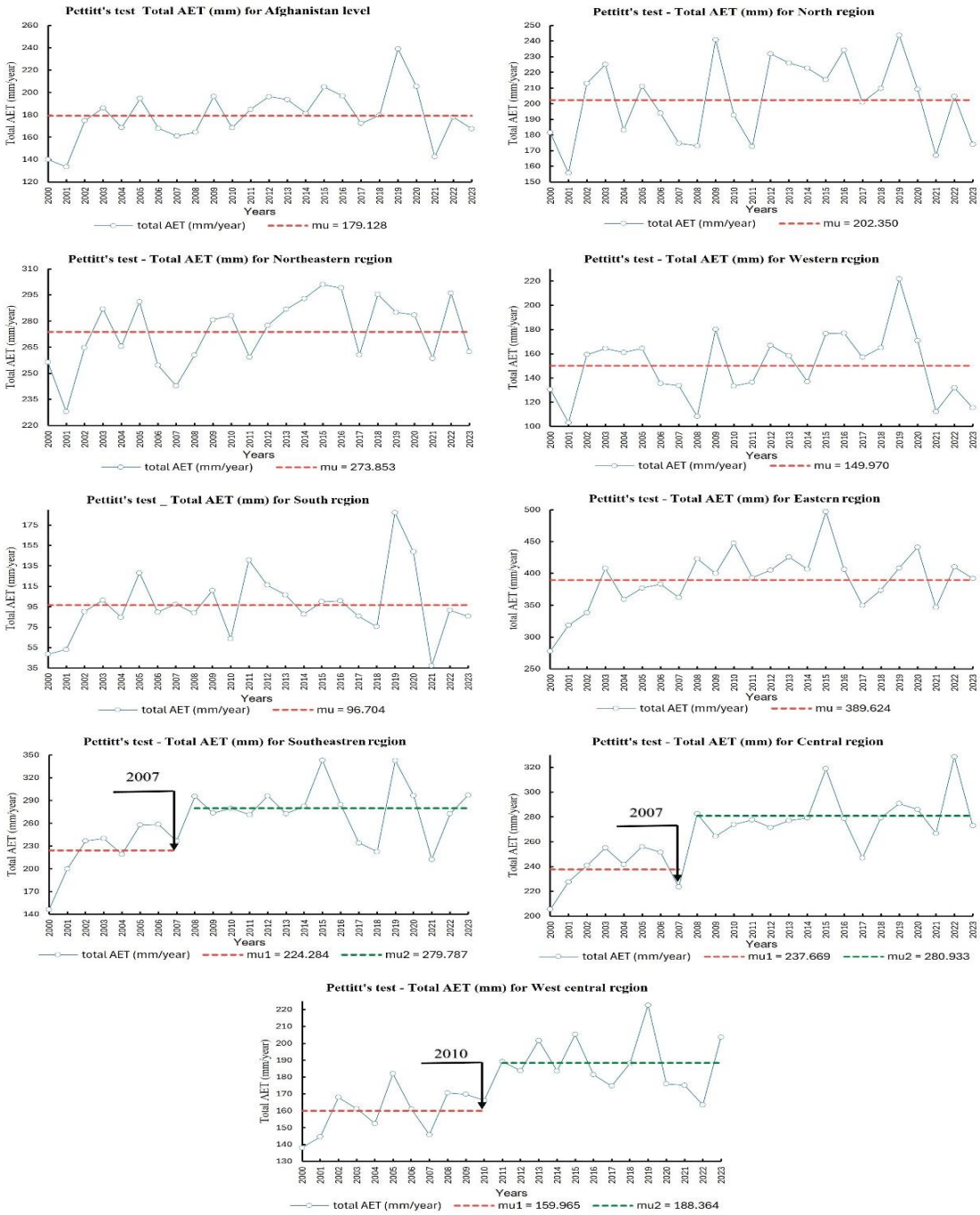

Figure 47. Significant change points based on the Pettitt's test in the mean of AET values for annually (2000–2023).

As shown in Table 22 and Figure 48, the results of the homogeneity test for the PET parameter indicate that the data is homogeneous across all regions on an annual basis, with no change points identified. This homogeneity also applies to the summer season. However, in the spring season, the Eastern region rejects the null hypothesis (H0) and accepts the alternative hypothesis (Ha) due to a change point observed in 2011, which marks a heterogeneous trend. In contrast, the other regions remain homogeneous during the spring season. Furthermore, in the fall season, the PET parameter is heterogeneous across all regions, with a change point identified in 2015. Following this year, an increasing trend was observed, leading to the acceptance of the alternative hypothesis (Ha). In the winter season, the PET parameter shows heterogeneity throughout Afghanistan and in the North-East, South, East, South-East, Central, and West-Central regions. The change point for the North-East region is identified in 2014, while for the other regions, it is in 2015. After these change points, an increasing trend was noted.

As illustrated in Figure 48, the PET parameter does not exhibit an annual change point in any of the regions and is considered homogeneous. However, seasonal heterogeneity was observed.

Table 21. P-value of Homogeneity Test (Pettitt's test) for PET Values.

Regions		Afghanistan	North	Northeastern	Western	South	Eastern	Southeastern	Central	West Central
Spring	P-value	0.860	0.759	0.873	0.781	0.430	**0.037**	0.134	0.258	0.958
	significant	H0	H0	H0	H0	H0	Ha	H0	H0	H0
	change point at year						2011			
Summe	P-value	0.805	0.249	0.484	0.900	0.321	0.055	0.874	0.395	0.661
	significant	H0	H0	H0	H0	H0	H0	H0	H0	H0
	Change point at year									
Fall	P-value	**0.000**	**0.010**	**0.001**	**0.001**	**0.001**	**0.002**	**<0.0001**	**0.002**	**0.000**
	significant	Ha	Ha	Ha	Ha	Ha	Ha	Ha	Ha	Ha
	Change point at year	2015	2015	2015	2015	2015	2015	2015	2015	2015
Winter	P-value	**0.017**	0.093	**0.002**	0.091	**0.037**	**0.014**	**0.009**	**0.010**	**0.010**
	significant	Ha	H0	Ha	H0	Ha	Ha	Ha	Ha	Ha
	Change point at year	2015		2014		2015	2015	2015	2015	2015
Annual	P-value	0.118	0.175	0.124	0.067	0.256	0.216	0.320	0.770	0.376
	significant	H0	H0	H0	H0	H0	H0	H0	H0	H0
	Change point at year									

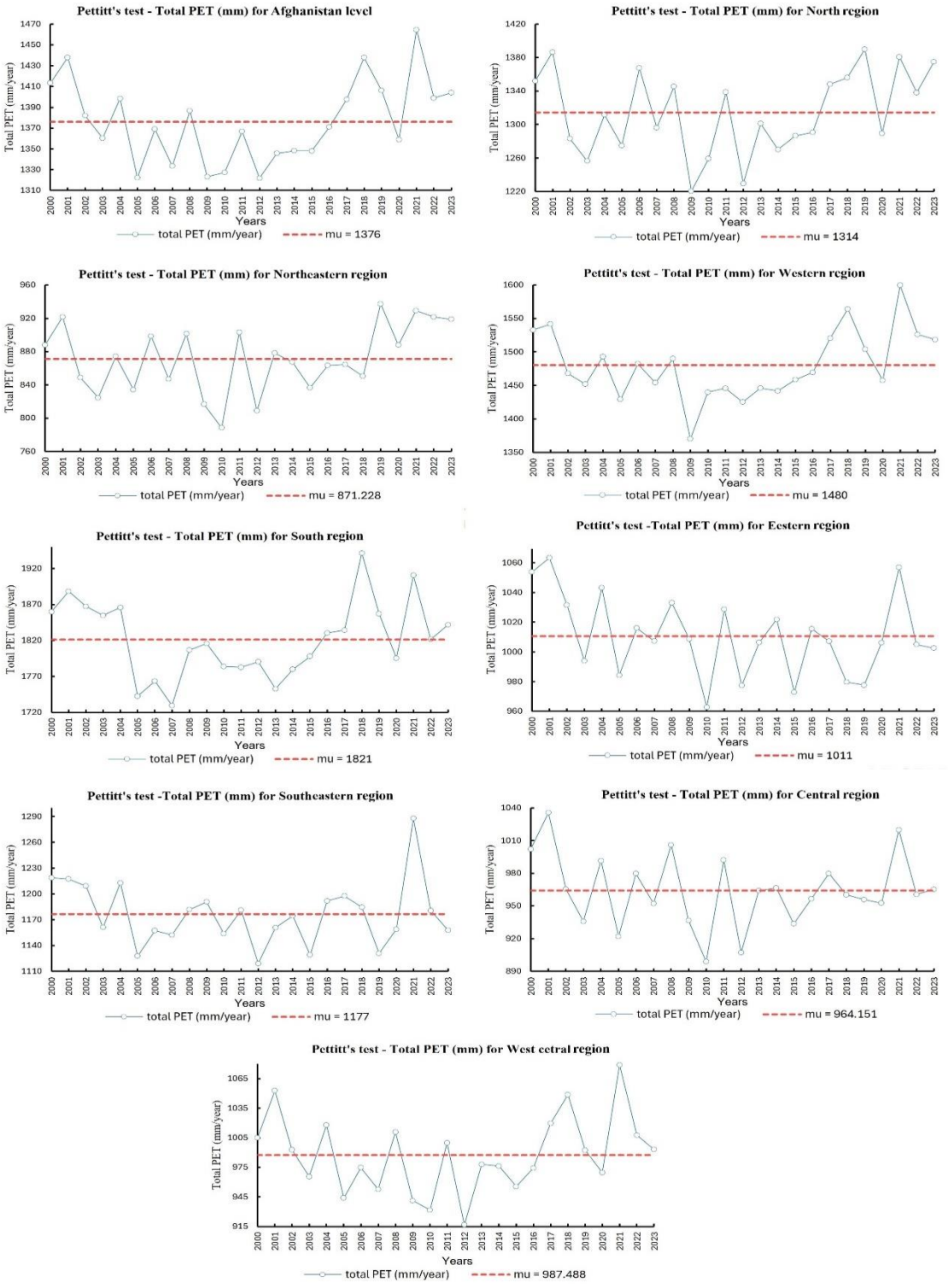

Figure 48. Significant change points based on the Pettitt's test in the mean of PET values for annually (2000–2023).

Similarly, the results of the homogeneity test for the precipitation parameter are presented in Table 23 and Figure 49. As indicated in Table 23 and Figure 49, the annual

precipitation parameter is homogeneous across all regions, with no observed change point. Consequently, the null hypothesis (H_0) is accepted, suggesting that the data does not exhibit a significant trend from the perspective of the homogeneity test. In the spring season, however, the eastern region shows a change point in precipitation, indicating heterogeneity, with an increasing trend observed after 2012. In contrast, the precipitation data for other regions remains homogeneous, with no change points detected. During the summer season, the precipitation data in the north, northeastern, western, South, and southeastern regions is also homogeneous, as indicated by a P-value greater than 0. However, throughout Afghanistan and in the eastern, central, and western-central regions, the data is heterogeneous, featuring a change point recorded in 2014, which reflects a significant increasing trend. Additionally, in the fall season, the southeastern region exhibits heterogeneity with a change point in 2010, after which a significant increasing trend is observed. In other regions, the precipitation data remains homogeneous.

Table 22. P-value of Homogeneity Test (Pettitt's test) for Precipitation Values.

Regions		Afghanistan	North	Northeastern	Western	South	Eastern	Southeastern	Central	West Central
Spring	P-value	0.454	0.652	0.516	0.859	0.766	**0.047**	0.074	0.201	0.366
	significant	H0	H0	H0	H0	H0	Ha	H0	H0	H0
	change point at year						2012			
Summe	P-value	**0.008**	0.936	0.893	0.648	0.575	**0.031**	0.066	**0.017**	**0.002**
	significant	Ha	H0	H0	H0	H0	Ha	H0	Ha	Ha
	Change point at year	2014					2014		2014	2014
Fall	P-value	0.419	0.973	0.143	0.767	0.366	0.269	**0.042**	0.143	0.410
	significant	H0	H0	H0	H0	H0	H0	Ha	H0	H0
	Change point at year							2010		
Winter	P-value	0.855	0.749	0.500	0.870	0.626	0.646	0.835	0.251	0.865
	significant	H0	H0	H0	H0	H0	H0	H0	H0	H0
	Change point at year									
Annual	P-value	0.680	0.553	0.936	0.473	0.846	0.075	0.064	0.089	0.683
	significant	H0	H0	H0	H0	H0	H0	H0	H0	H0
	Change point at year									

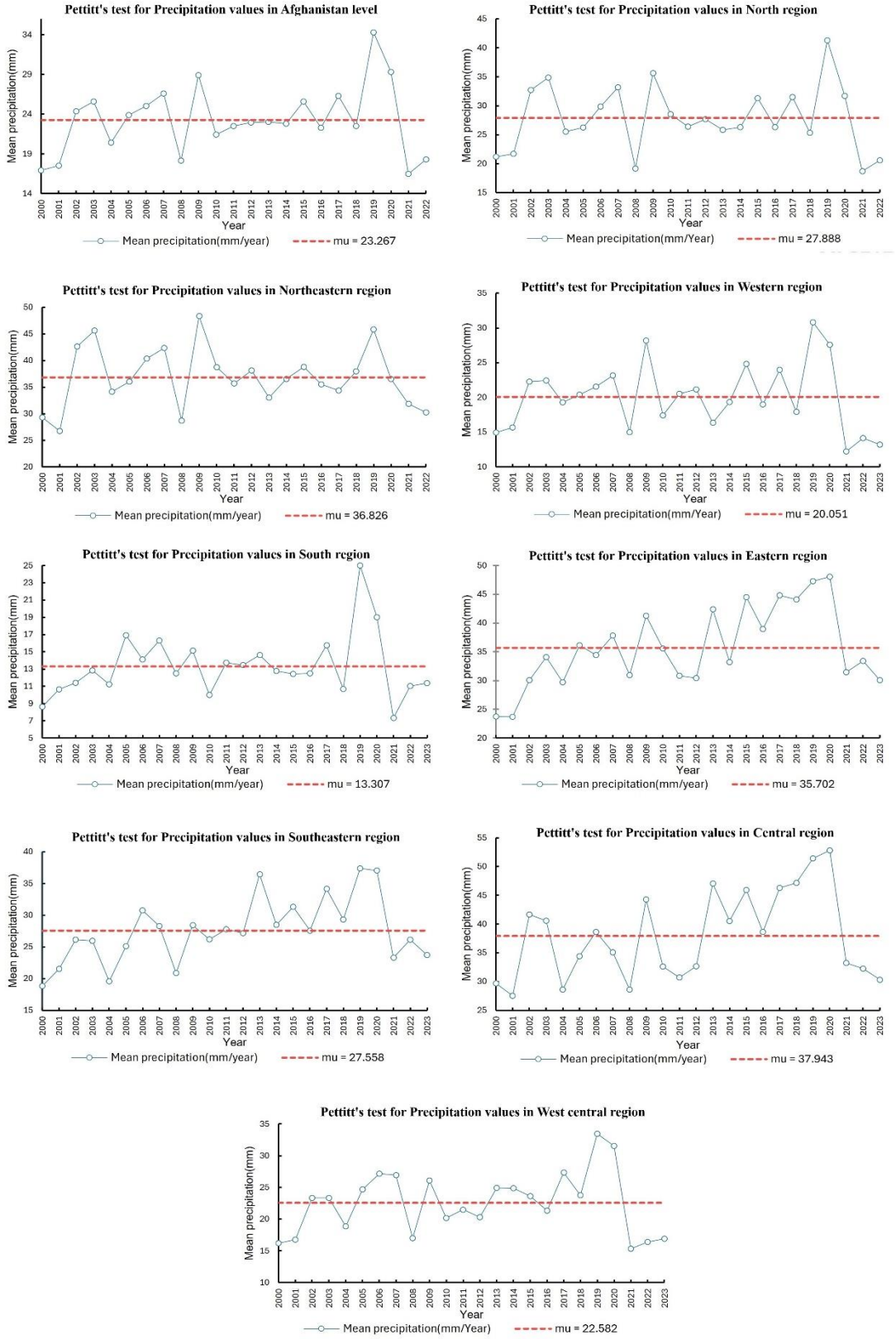

Figure 49. Significant change points based on the Pettitt's test in the mean of Precipitation values for annually (2000–2023).

Table 23. P-value of Homogeneity Test (Pettitt's test) for Soil Moisture Values.

Regions		Afghanistan	North	Northeastern	Western	South	Eastern	Southeastern	Central	West Central
Spring	P-value	0.619	0.264	0.121	0.768	0.958	0.320	0.314	**0.029**	0.640
	significant	H0	H0	H0	H0	H0	H0	H0	Ha	H0
	change point at year								2007	
Summe	P-value	0.875	0.140	0.698	0.945	0.860	0.420	0.234	0.852	0.942
	significant	H0	H0	H0	H0	H0	H0	H0	H0	H0
	Change point at year									
Fall	P-value	**0.025**	**0.010**	**0.007**	0.100	0.953	0.335	0.946	0.263	0.123
	significant	Ha	Ha	Ha	H0	H0	H0	H0	H0	H0
	Change point at year	2015	2015	2015						
Winter	P-value	**0.005**	**0.002**	**0.005**	0.102	0.481	0.079	0.270	**0.039**	**0.016**
	significant	Ha	Ha	Ha	H0	H0	H0	H0	Ha	Ha
	Change point at year	2015	2015	2016					2016	
Annual	P-value	**0.028**	**0.005**	**0.010**	0.260	0.991	0.325	0.854	0.408	**0.044**
	significant	Ha	Ha	Ha	H0	H0	H0	H0	H0	Ha
	Change point at year	2012	2015	2016						2016

As shown in Table 24, soil moisture during the summer season is homogeneous across all regions of Afghanistan, with no significant trends observed in this season. However, in the spring season, a change point in soil moisture is identified in the central region, indicating heterogeneity. Following 2007, soil moisture in this region has shown an increasing trend, while no change points were observed in other regions, which remain homogeneous. In addition, during the fall season, the soil moisture data across Afghanistan, as well as in the north and northeastern regions, supports the alternative hypothesis (H_1), indicating heterogeneity. The change point in these regions is noted in 2015, after which a decreasing trend was observed. In contrast, other regions exhibit homogeneous soil moisture data during the fall season.

Similarly, in the winter season, soil moisture demonstrates both homogeneity and heterogeneity. According to Table 24, a change point is recorded for soil moisture throughout Afghanistan and in the north, northeastern, and central regions, confirming heterogeneity. A significant change point is noted across Afghanistan and the north region in 2015, while the northeastern and central regions show a change point in 2016, both with decreasing trends. In other regions, the data remains homogeneous. Figure 50 further

illustrates that soil moisture experiences change points and is heterogeneous in Afghanistan, particularly in the north, northeastern, and western-central regions in 2012, 2015, and 2016. Following these years, soil moisture has begun to decline, while other regions have maintained homogeneity.

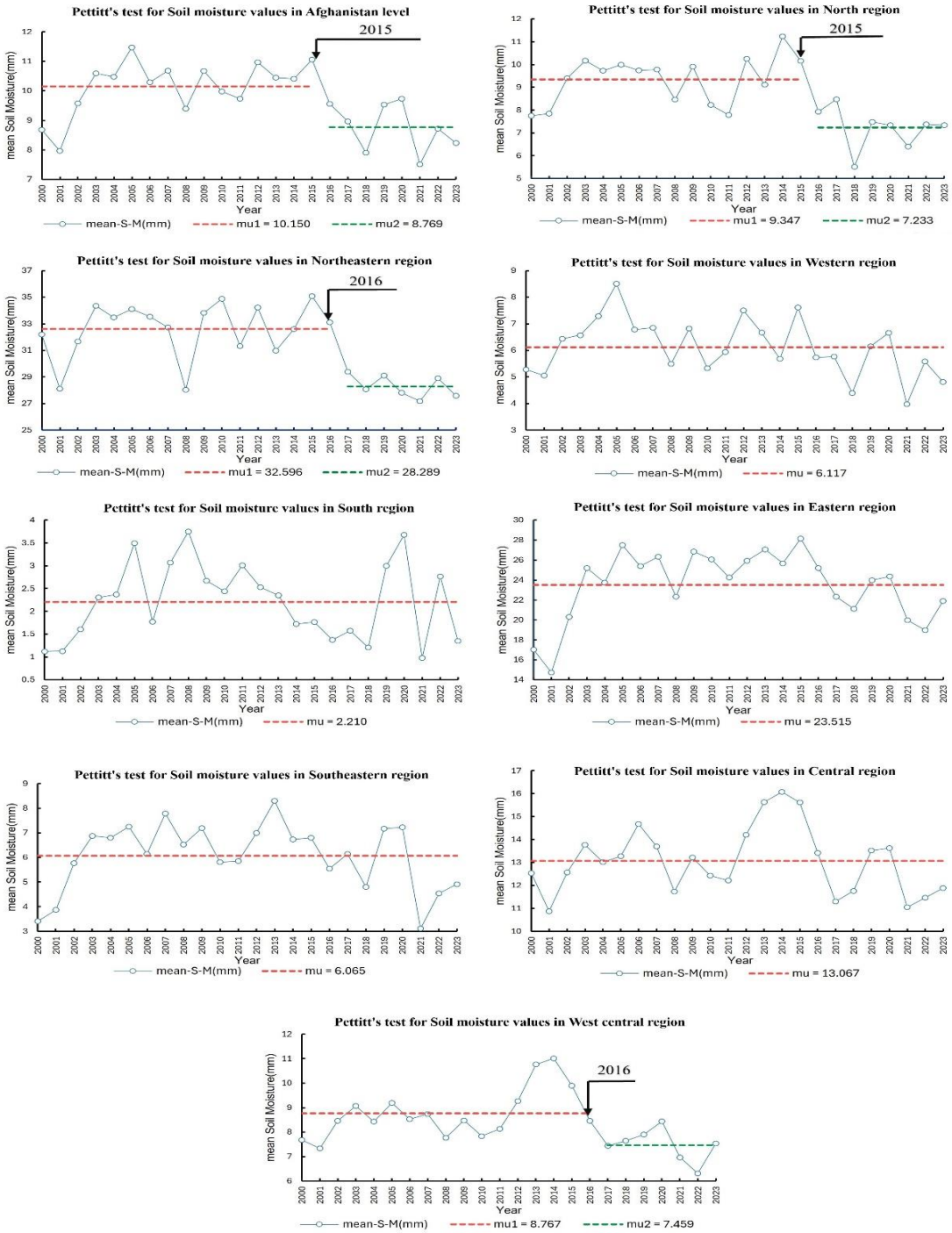

Figure 50. Significant change points based on the Pettitt's test in the mean of Soil Moisture values for annually (2000–2023).

Table 25 presents the results of the homogeneity test for the wind speed parameter across all regions of Afghanistan, both seasonally and annually. As indicated in Figure 51, wind speed shows no change point and is homogeneous on an annual basis. The data is also homogeneous seasonally in the fall and winter across all regions. However, during the spring season, heterogeneity is observed in the eastern and central regions. In the eastern region, the change point was recorded in 2004, while in the central region, it occurred in 2005. Following these years, wind speed in these areas has shown a significant downward trend. Similarly, in the summer season, the wind speed in the South region rejects the null hypothesis (H_0) and supports the alternative hypothesis (H_1), with 2008 identified as the change point for this region. After this year, the trend in summer wind speed has increased. In contrast, the data remains homogeneous in other regions, with no change points recorded.

Table 24. P-value of Homogeneity Test (Pettitt's test) for Wind Speed Values.

Regions		Afghanistan	North	Northeastern	Western	South	Eastern	Southeastern	Central	West Central
Spring	P-value	0.609	0.106	0.051	0.646	0.811	**0.039**	0.166	**0.032**	0.150
	significant	H0	H0	H0	H0	H0	Ha	H0	Ha	H0
	change point at year						2004		2005	
Summe	P-value	0.916	0.731	0.080	0.974	**0.026**	0.929	0.908	0.649	0.422
	significant	H0	H0	H0	H0	Ha	H0	H0	H0	H0
	Change point at year					2008				
Fall	P-value	0.250	0.616	0.498	0.261	0.988	0.336	0.339	0.061	0.416
	significant	H0	H0	H0	H0	H0	H0	H0	H0	H0
	Change point at year									
Winter	P-value	0.448	0.874	0.198	0.802	0.205	0.450	0.815	0.334	0.206
	significant	H0	H0	H0	H0	H0	H0	H0	H0	H0
	Change point at year									
Annual	P-value	0.954	0.912	0.421	0.720	0.864	0.328	0.175	0.419	0.084
	significant	H0	H0	H0	H0	H0	H0	H0	H0	H0
	Change point at year									

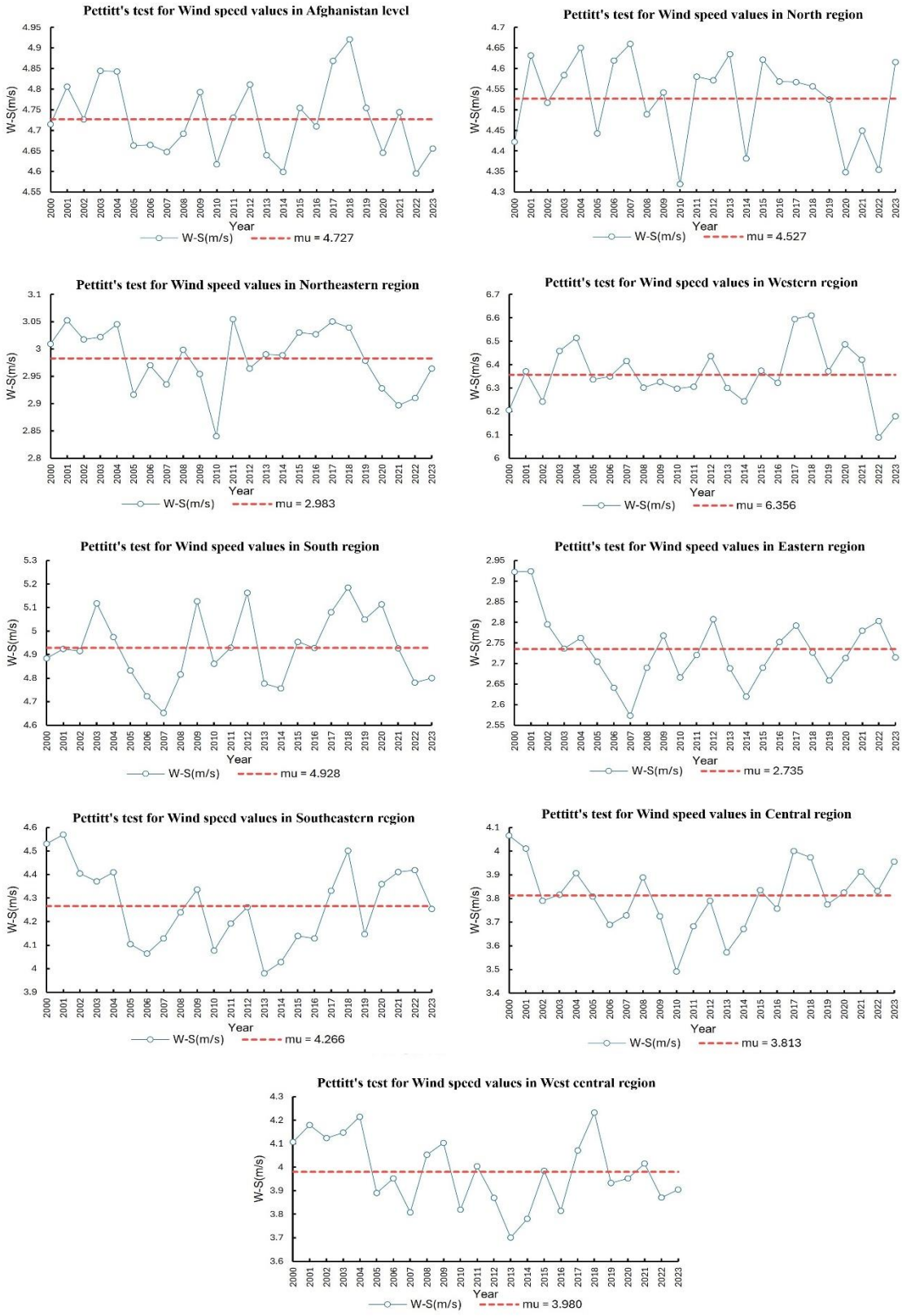

Figure 51. Significant change points based on the Pettitt's test in the mean of Wind Speed values for annually (2000–2023).

Table 25. P-value of Homogeneity Test (Pettitt's test) for VCI Values.

Regions		Afghanistan	North	Northeastern	Western	South	Eastern	Southeastern	Central	West Central
Spring	P-value	0.910	0.709	0.617	0.889	0.211	0.467	0.223	0.574	0.774
	significant	H0	H0	H0	H0	H0	H0	H0	H0	H0
	change point at year									
Summe	P-value	0.770	0.654	0.162	0.803	0.072	0.610	0.279	0.251	0.869
	significant	H0	H0	H0	H0	H0	H0	H0	H0	H0
	Change point at year									
Fall	P-value	0.457	0.138	0.231	0.881	0.344	0.802	0.941	0.613	0.625
	significant	H0	H0	H0	H0	H0	H0	H0	H0	H0
	Change point at year									
Winter	P-value	0.777	0.490	0.453	0.516	0.090	0.093	0.095	0.519	0.192
	significant	H0	H0	H0	H0	H0	H0	H0	H0	H0
	Change point at year									
Annual	P-value	0.668	0.287	0.578	0.340	0.134	0.978	0.955	0.701	0.483
	significant	H0	H0	H0	H0	H0	H0	H0	H0	H0
	Change point at year									

Table 26. P-value of Homogeneity Test (Pettitt's test) for TCI Values.

Regions		Afghanistan	North	Northeastern	Western	South	Eastern	Southeastern	Central	West Central
Spring	P-value	0.424	0.718	0.519	0.608	0.616	0.446	0.261	0.462	0.422
	significant	H0	H0	H0	H0	H0	H0	H0	H0	H0
	change point at year									
Summe	P-value	0.753	0.472	0.762	0.221	0.850	0.263	0.580	0.079	0.127
	significant	H0	H0	H0	H0	H0	H0	H0	H0	H0
	Change point at year									
Fall	P-value	0.764	0.396	0.523	0.783	0.397	0.921	0.243	0.770	0.764
	significant	H0	H0	H0	H0	H0	H0	H0	H0	H0
	Change point at year									
Winter	P-value	0.865	0.284	0.451	0.542	0.424	0.918	0.539	0.907	0.985
	significant	H0	H0	H0	H0	H0	H0	H0	H0	H0
	Change point at year									
Annual	P-value	0.682	0.728	0.957	0.691	0.541	0.781	0.174	0.705	0.544
	significant	H0	H0	H0	H0	H0	H0	H0	H0	H0
	Change point at year									

Figure 52. Significant change points based on the Pettitt's test in the mean of VCI values for annually (2000–2023).

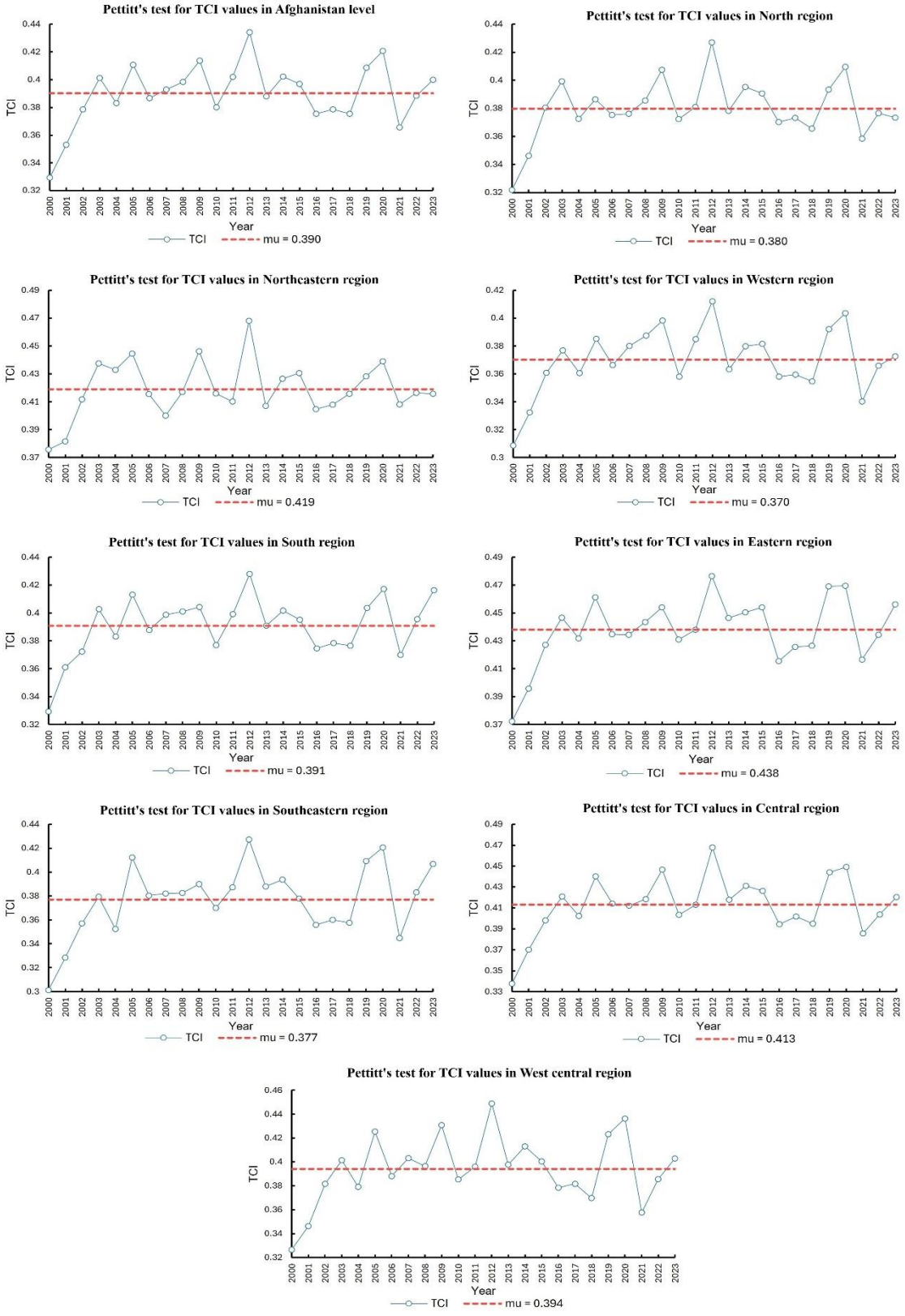

Figure 53. Significant change points based on the Pettitt's test in the mean of TCI values for annually (2000–2023).

The results of the homogeneity test for the VCI index are presented in Table 26. This index shows no change point seasonally, and the data is homogeneous across each season. Annually, as illustrated in Figure 52, the VCI index also lacks a change point and is considered homogeneous. Similarly, Table 27 indicates that the TCI index is seasonally homogeneous across all regions and exhibits no significant trend. Annually, as shown in Figure 53, the TCI index also lacks a change point, with the data demonstrating a homogeneous distribution.

In contrast, the VHI index is heterogeneous in the South and southeastern regions during the spring and winter seasons. According to Table 28, the VHI index exhibits a change point in the spring season of the southeastern region, which has shown an increasing trend since 2004. Additionally, the VHI index in the winter season of the South region experienced a change point in 2006, characterized by a decreasing trend. Furthermore, Figure 54 confirms that the VHI index remains homogeneous in other regions, both seasonally and annually.

Table 27. P-value of Homogeneity Test (Pettitt's test) for VHI Values.

Regions		Afghanistan	North	Northeastern	Western	South	Eastern	Southeastern	Central	West Central
Spring	P-value	0.754	0.711	0.545	0.700	0.688	0.668	**0.050**	0.301	0.715
	significant	H0	H0	H0	H0	H0	H0	Ha	H0	H0
	change point at year							2004		
Summe	P-value	0.874	0.463	0.290	0.547	0.287	0.521	0.366	0.166	0.770
	significant	H0	H0	H0	H0	H0	H0	H0	H0	H0
	Change point at year									
Fall	P-value	0.072	0.111	0.244	0.245	0.667	0.988	0.779	0.353	0.549
	significant	H0	H0	H0	H0	H0	H0	H0	H0	H0
	Change point at year									
Winter	P-value	0.560	0.967	0.760	0.686	**0.037**	0.410	0.146	0.357	0.684
	significant	H0	H0	H0	H0	Ha	H0	H0	H0	H0
	Change point at year					2006				
Annual	P-value	0.552	0.766	0.662	0.395	0.764	0.175	0.467	0.200	0.850
	significant	H0	H0	H0	H0	H0	H0	H0	H0	H0
	Change point at year									

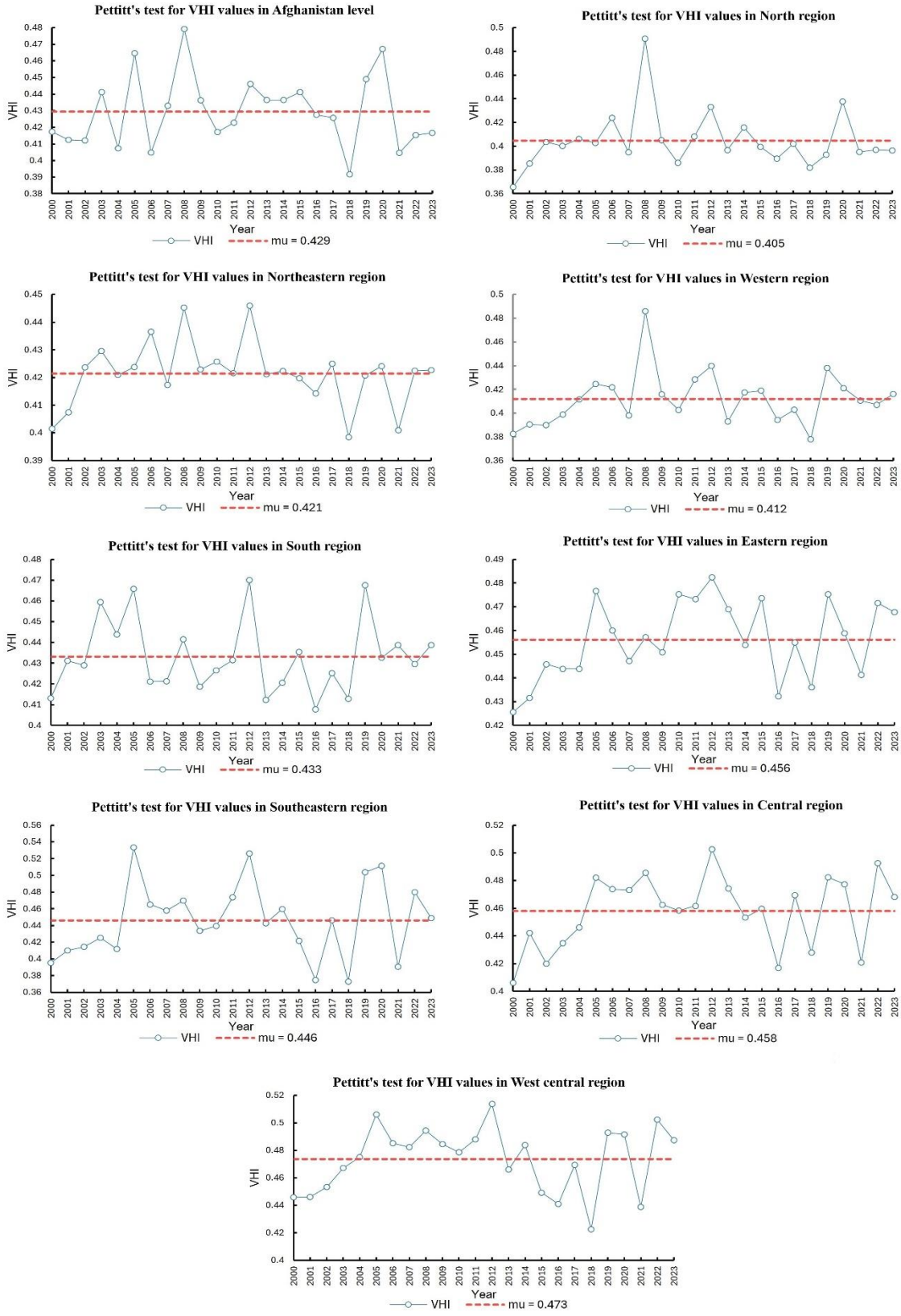

Figure 54. Significant change points based on the Pettitt's test in the mean of VHI values for annually (2000–2023).

The homogeneity test was applied to the HGFC data to assess the extent of forest loss, with the results presented in Table 29 and Figure 55. This test evaluates the homogeneity and heterogeneity of the HGFC data, specifically focusing on annual forest loss. As previously discussed, Afghanistan's forest areas are predominantly located in the eastern, southeastern, and northeastern regions.

Table 28. P-value of Homogeneity Test (Pettitt's test) for HGFC Values.

		Annual		
		P-value	significant	Change point at year
Climate Regions	**Afghanistan**	**0.004**	Ha	2011
	North	0.115	H0	
	Northeastern	**0.010**	Ha	2012
	Western	0.753	H0	
	South	**<0.0001**	Ha	2009
	Eastern	**0.044**	Ha	2011
	Southeastern	**0.035**	Ha	2011
	Central	**0.000**	Ha	2014
	West Central	**0.000**	Ha	2012

As indicated in Table 29 and Figure 55, the extent of forest loss is heterogeneous throughout Afghanistan, showing a downward trend in deforestation after 2011. In the northeastern region, forest loss has also decreased since 2012, establishing a downward trend. The eastern and southeastern regions exhibit the same change point, demonstrating heterogeneity and a decreasing trend after 2011. Similarly, the observed change points in the South, central, and west-central regions indicate heterogeneity, while the data from the north and western regions remains homogeneous.

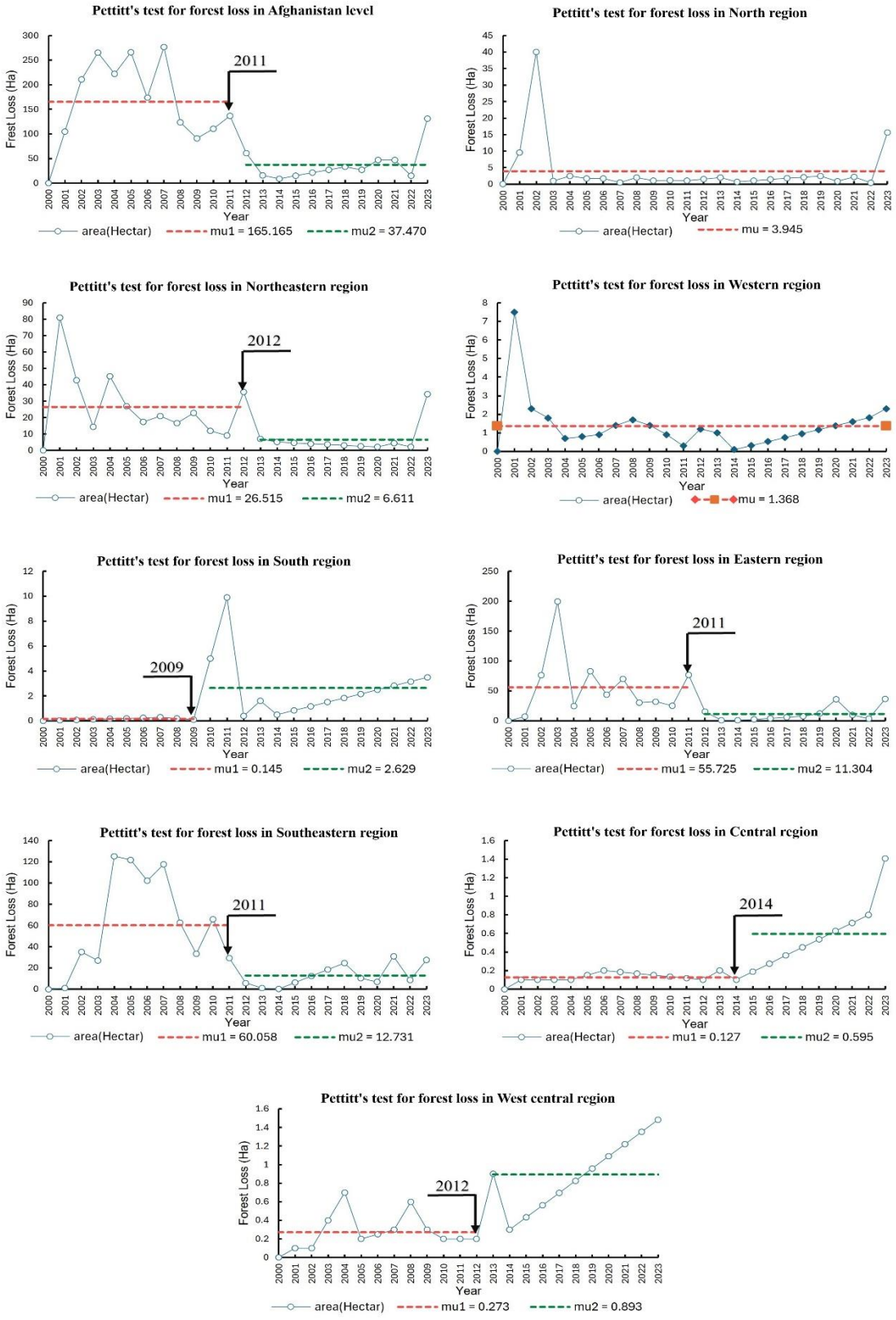

Figure 55. Significant change points based on the Pettitt's test in the mean of HGFC values for annually (2000–2023).

3.8. Results Based on ARIMA Model

In this section, the climate parameters examined are predicted using the Arima model. This model was created in the IBM SPSS program, as explained in the previous discussions of the ARIMA model. The ARIMA model has three main parameters (p, d, q) (sp, sd, sq) that these parameters should be identified before creating the model. The model parameters are selected based on Autocorrelation Function (ACF) and Partial Autocorrelation Function (PACF) analysis. ACF shows the relationship between a point and the previous point in the time series of data. And PACF calculates the direct correlation between one point and the previous point (Sabzevari and Islamian, 2024). The parameters of model for the climate parameters used in this thesis are listed in Tables 30 and 31, and the forecasting is done on data collected monthly data.

Table 29. Parameters of the model (p,d,q)(sp,sd,sq) for NDVI, LST, Ta, AET and PET parameters.

Climate region	NDVI	LST	Ta	AET	PET
Afghanistan	(17,0,13)(0,1,1)	(11,0,7)(0,1,1)	(7,0,89)(0,1,1)	(37,0,7)(0,1,1)	(17,0,3)(0,1,1)
North	(17,0,13)(0,1,1)	(96,0,83)(0,1,1)	(7,0,89)(0,1,1)	(17,0,13)(0,1,0)	(3,0,8)(0,1,1)
Northeastern	(24,0,17)(0,1,1)	(96,0,83)(0,1,1)	(3,0,17)(0,1,1)	(13,0,1)(0,1,1)	(5,0,21)(0,1,1)
Western	(24,0,17)(0,1,1)	(96,0,83)(0,1,1)	(7,0,89)(0,1,1)	(0,0,7)(0,1,1)	(51,0,26)(0,1,1)
South	(39,0,16)(0,1,1)	(11,0,7)(0,1,1)	(3,0,21)(0,1,0)	(5,0,47)(0,1,1)	(9,0,3)(0,1,1)
Southeastern	(7,0,43)(0,1,1)	(3,0,11)(0,1,1)	(3,0,21)(0,1,1)	(5,0,13)(0,1,1)	(3,0,9)(0,1,1)
Eastern	(39,0,16)(0,1,1)	(3,0,37)(0,1,1)	(3,0,21)(0,1,0)	(9,0,3)(0,1,1)	(1,0,7)(0,1,1)
Central	(7,0,56)(0,1,1)	(3,0,17)(0,1,1)	(3,0,21)(0,1,0)	(37,0,7)(0,1,1)	(9,0,3)(0,1,1)
West central	(7,0,43)(0,1,1)	(11,0,3)(0,1,1)	(3,0,27)(0,1,1)	(37,0,7)(0,1,1)	(17,0,03)(0,1,1)

Table 30. Parameters of the model (p,d,q)(sp,sd,sq) for precipitation, soil moisture, wind speed, VCI, TCI and VHI parameter.

Precipitation	Soil moisture	wind speed	VCI	TCI	VHI
(7,0,3)(0,1,1)	(24,0,17)(0,1,1)	(24,0,17)(0,1,1)	(24,0,17)(0,1,1)	(11,0,7)(0,1,1)	(24,0,17)(0,1,1)
(19,0,11)(0,1,1)	(24,0,17)(0,1,1)	(24,0,17)(0,1,1)	(93,0,21)(0,1,1)	(34,0,21)(0,1,1)	(24,0,17)(0,1,1)
(39,0,7)(0,1,1)	(24,0,17)(0,1,1)	(24,0,17)(0,1,1)	(24,0,17)(0,1,1)	(24,0,17)(0,1,1)	(31,0,24)(0,1,1)
(5,0,11)(0,1,1)	(37,0,11)(0,1,1)	(24,0,17)(0,1,1)	(93,0,21)(0,1,1)	(11,0,7)(0,1,1)	(31,0,24)(0,1,1)
(39,0,7)(0,1,1)	(37,0,11)(0,1,1)	(37,0,7)(0,1,1)	(21,0,97)(0,1,1)	(21,0,97)(0,1,1)	(21,0,97)(0,1,1)
(39,0,7)(0,1,1)	(49,0,27)(0,1,1)	(21,0,99)(0,1,1)	(93,0,21)(0,1,0)	(34,0,3)(0,1,1)	(91,0,13)(0,1,1)
(39,0,7)(0,1,1)	(37,0,11)(0,1,1)	(97,0,13)(0,1,1)	(93,0,21)(0,1,1)	(5,0,41)(0,1,1)	(91,0,13)(0,1,0)
(39,0,3)(0,1,1)	(37,0,11)(0,1,1)	(21,0,99)(0,1,1)	(93,0,21)(0,1,1)	(56,0,11)(0,1,1)	(91,0,13)(0,1,1)
(19,0,11)(0,1,1)	(49,0,11)(0,1,1)	(97,0,13)(0,1,1)	(24,0,17)(0,1,1)	(56,0,11)(0,1,1)	(91,0,13)(0,1,1)

3.8.1. Model Accuracy

In this model, the criteria of R^2, RMSE, and MAE are employed to evaluate its performance. The calculation methods for these criteria were explained in previous discussions. For forecasting the data trend from 2024 to 2035, data from 2000 to 2023 is utilized as the training dataset, while the most recent five years (2019-2023) serve as the testing dataset to evaluate the model's performance.

Table 31. ARIMA model accuracy.

Climate region	Accuracy	NDVI	LST (°C)	Ta (°C)	AET (mm)	PET (mm)	Precipit (mm)	S-M (mm)	W-S (m/s)	VCI	TCI	VHI
Afghanistan	R^2	0.92	0.97	0.98	0.87	0.99	0.68	0.92	0.78	0.88	0.97	0.94
	RMSE	0.01	2.23	1.77	4.67	6.47	13.25	1.43	0.33	0.04	0.04	0.02
	MAE	0.01	1.60	1.09	3.14	4.72	8.39	0.96	0.23	0.03	0.03	0.02
North	R^2	0.83	0.98	0.97	0.81	0.99	0.70	0.82	0.72	0.86	0.97	0.90
	RMSE	0.03	3.93	1.94	7.79	8.95	18.31	2.48	0.35	0.09	0.04	0.04
	MAE	0.02	1.69	1.21	5.16	6.40	10.19	1.47	0.24	0.05	0.03	0.03
Northeastern	R^2	0.97	0.98	0.98	0.93	0.99	0.66	0.93	0.68	0.95	0.97	0.69
	RMSE	0.01	3.30	1.57	4.82	6.45	19.98	3.59	0.21	0.05	0.04	0.02
	MAE	0.01	1.47	1.21	3.39	4.63	12.25	2.44	0.15	0.04	0.03	0.01
Western	R^2	0.85	0.97	0.98	0.78	0.99	0.66	0.85	0.89	0.87	0.97	0.90
	RMSE	0.00	3.72	1.83	6.14	9.23	14.24	1.68	0.51	0.87	0.04	0.04
	MAE	0.00	1.62	1.18	4.12	6.59	8.70	1.05	0.36	0.05	0.03	0.03
South	R^2	0.89	0.97	0.97	0.61	0.99	0.65	0.67	0.72	0.61	0.97	0.84
	RMSE	0.00	2.23	1.66	7.22	8.44	11.58	1.23	0.37	0.13	0.05	0.07
	MAE	0.00	1.66	1.24	4.65	6.15	6.52	0.61	0.27	0.08	0.03	0.04
Southeastern	R^2	0.88	0.95	0.96	0.74	0.99	0.61	0.86	0.62	0.84	0.95	0.71
	RMSE	0.02	2.87	1.87	10.31	7.69	16.62	2.14	0.50	0.12	0.05	0.06
	MAE	0.01	2.07	1.29	7.26	5.65	10.86	1.21	0.30	0.07	0.04	0.03
Eastern	R^2	0.95	0.97	0.97	0.82	0.99	0.60	0.92	0.63	0.94	0.97	0.75
	RMSE	0.02	1.99	1.52	9.64	6.60	21.97	4.36	0.25	0.06	0.04	0.04
	MAE	0.01	1.41	1.09	7.00	4.88	14.71	2.81	0.15	0.04	0.03	0.02
Central	R^2	0.95	0.97	0.97	0.92	0.99	0.71	0.91	0.81	0.96	0.97	0.78
	RMSE	0.02	2.54	1.76	6.71	7.09	24.08	2.29	0.49	0.07	0.05	0.03
	MAE	0.01	1.85	1.30	4.45	5.13	15.24	1.49	0.29	0.04	0.03	0.02
Westcentral	R^2	0.96	0.97	0.97	0.91	0.99	0.68	0.90	0.62	0.95	0.97	0.83
	RMSE	0.02	2.87	1.93	6.93	7.68	14.52	2.07	0.42	0.07	0.05	0.03
	MAE	0.01	54.09	1.39	4.09	5.40	9.25	1.29	0.26	0.05	0.03	0.02

3.8.2. Examining The Predicted Results of Climate Parameters

The RMSE value varies based on the scale of the data. If the data is expressed as a percentage (0-100), the RMSE is also calculated as a percentage; however, if the data is not in percentage form, the RMSE value is calculated according to the scale of that data. An acceptable RMSE value is one that is lower than the arithmetic mean of the data (Khan et al., 2023), and the same applies to MAE. As shown in Tables 30 and 31, the parameters of model for each climate parameters were configured in the IBM SPSS program prior to running the model, which was subsequently executed for each region. For the NDVI index across Afghanistan and the north region, the parameters (17,0,13)(0,1,1) were set, demonstrating good performance. According to Table 32, the R^2 values were 0.92 and 0.83, indicating a very high correlation between observed and predicted data, while the RMSE and MAE further illustrate the model's effectiveness in these regions.

In the northeast and western regions, the model parameters (24,0,17) (0,1,1) are set for the NDVI index, resulting in a strong model performance as indicated in Table 32. This demonstrates effective predictions. Similarly, the ARIMA model for the South and eastern regions is configured with parameters (39,0,16) (0,1,1), also achieving good predictions. Table 32 reveals that the model's performance is notably high, with close relationships between observed and predicted data. In the southeast, central, and west-central regions, the model parameters, as outlined in Table 30, indicate good performance, with a strong correlation between observed and predicted data, as well as a confirmed low error rate.

Figure 56 illustrates that NDVI data exhibits an increasing trend across Afghanistan and in all regions except the north region until 2035. Notably, the NDVI values in 2024 were high for all of Afghanistan, particularly in the northeastern, central, and South regions, attributed to significant precipitation in the spring of 2024, which boosted NDVI levels in these areas.

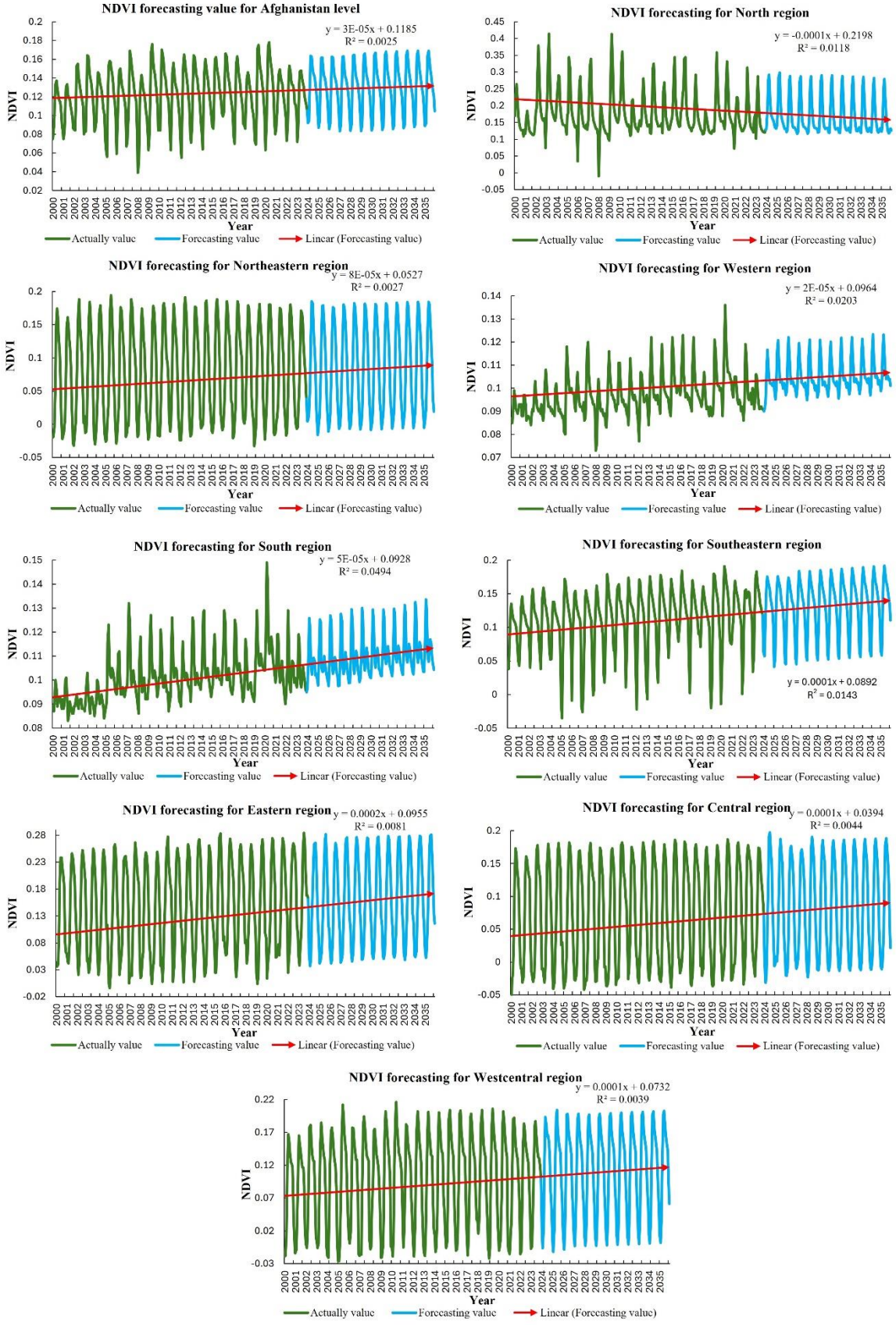

Figure 56. NDVI prediction values from 2024 to 2035.

Likewise, the LST parameter was predicted monthly for all regions of Afghanistan, and its trend was analyzed until 2035. Based on Table 30, the model parameters were adjusted to forecast LST data across all regions, as shown in Table 32, indicating good performance in the predictions. The model parameters for Afghanistan as a whole and the South region were set to (11,0,7) (0,1,1), yielding positive results and demonstrating high model performance. According to Figure 57, the LST in these areas is expected to remain stable from 2024 to 2035, which may correlate with the growth of NDVI.

Similarly, in the north, northeastern, and western regions, the model parameters were set to (96,0,83) (0,1,1). This configuration has resulted in better model performance compared to other regions, with a very high correlation between observed and predicted data. Figure 57 illustrates that the LST in the north and northeastern regions displays a different pattern through 2035, while in the western region, LST shows a decreasing trend during the same period. This decline may be linked to the projected growth of NDVI until 2035.

Moreover, the LST parameter in the east, southeast, central, and west central regions was configured with parameters as shown in Table 30, and its results were evaluated based on the criteria in Table 32. For instance, the R^2 value in the eastern region is 0.95, while in the southeastern, central, and west central regions, it is 0.97. The RMSE in the eastern region is 1.99, which is the lowest compared to other regions. The evaluation indicates a high accuracy between observed and predicted data in these regions. Figure 57 demonstrates that the LST in the south, east, southeast, central, and west central regions follow a decreasing trend until 2035, potentially due to climate change and the increase in NDVI.

Additionally, the parameters for the Ta parameter were set for all regions, as presented in Table 30, and prediction models were established for each region. Different parameters were assigned to each region, as seen in Table 30, and the prediction results are graphically displayed in Figure 58. According to Table 32, the Ta parameter predictions show strong model performance, with a high correlation (R^2) between observed and predicted data. The RMSE and MAE values are also within acceptable ranges for these predictions. Figure 57 illustrates a slight increasing trend in Ta until 2035, likely due to global climate changes.

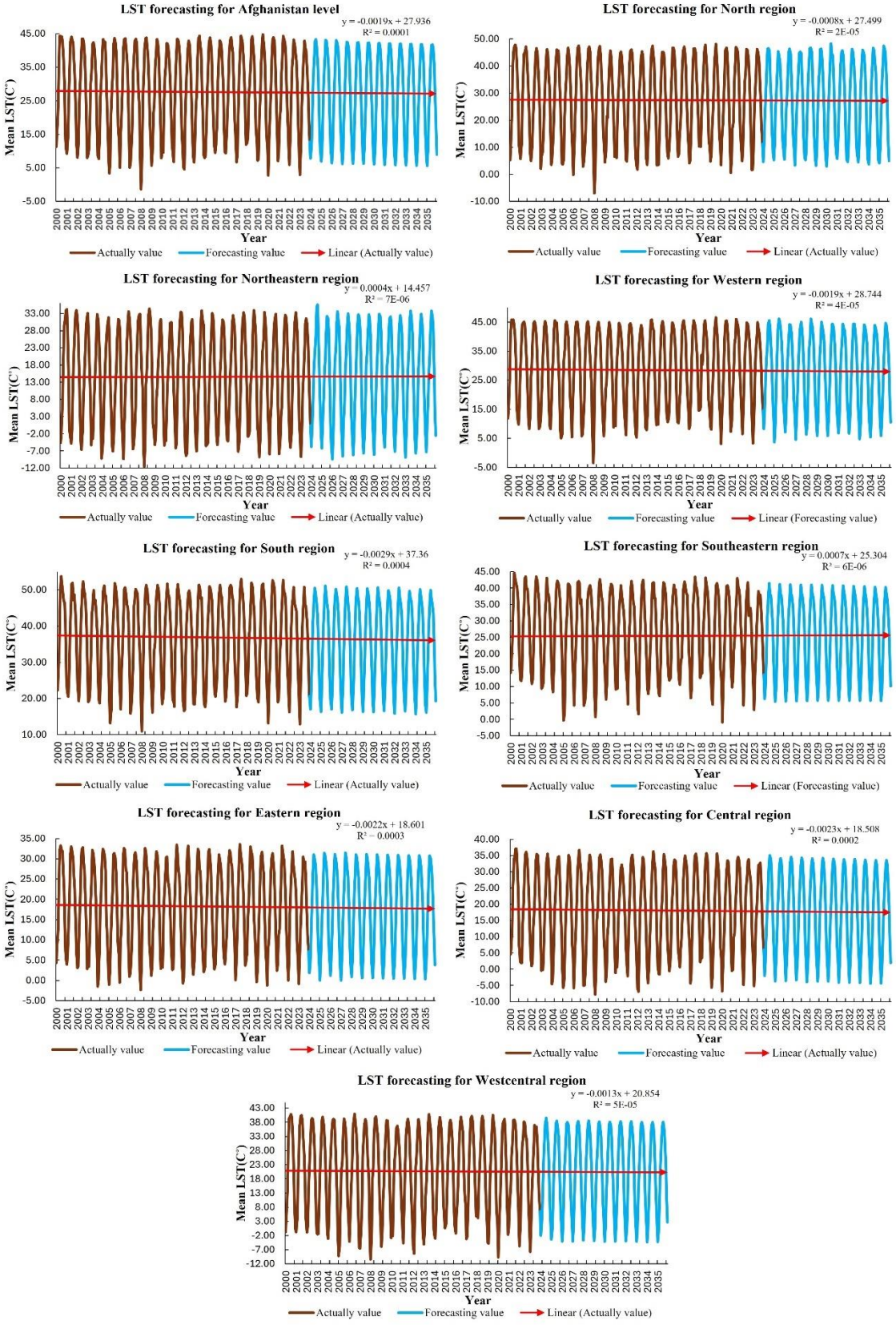

Figure 57. LST prediction values from 2024 to 2035.

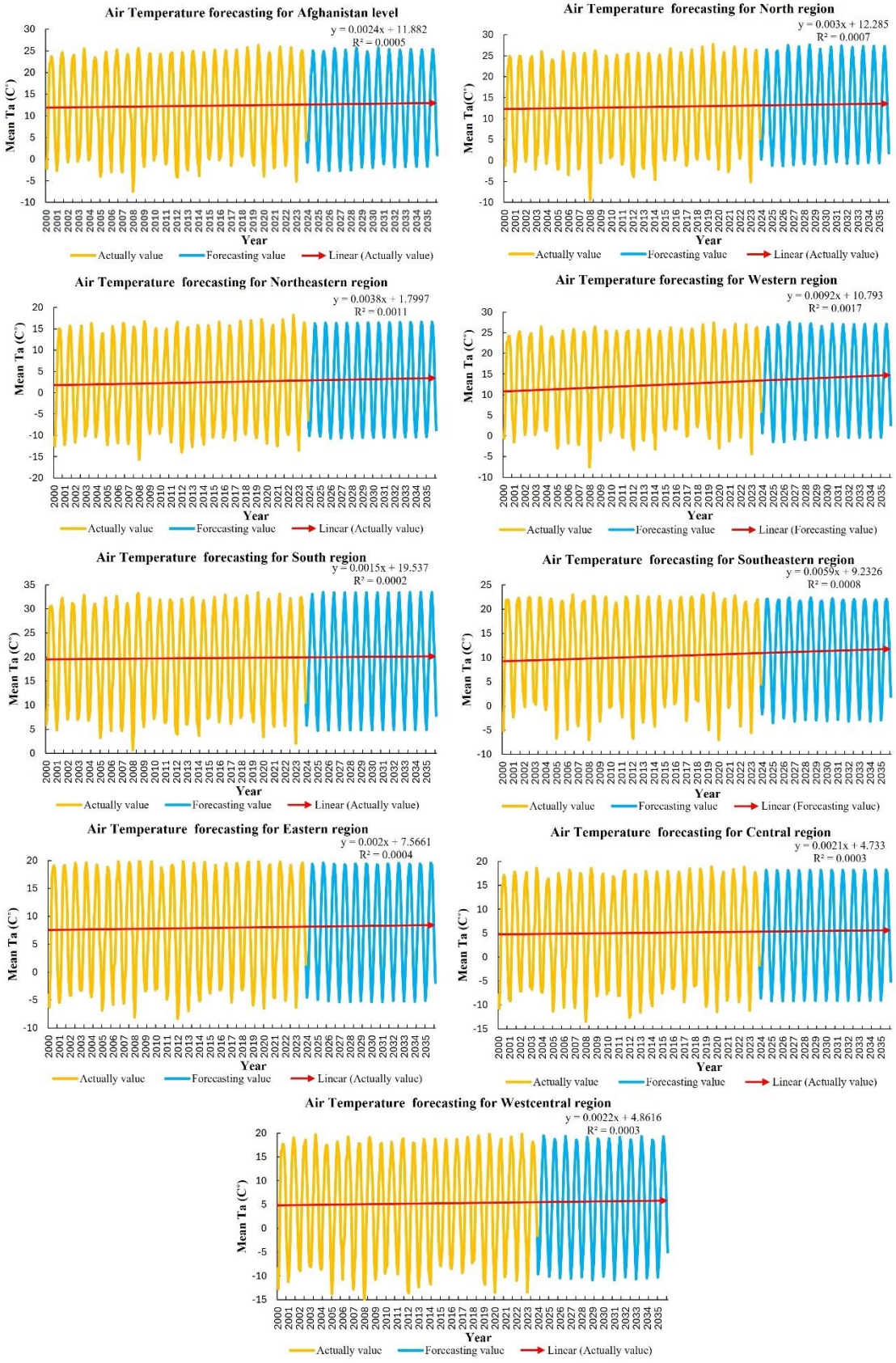

Figure 58. Ta prediction values from 2024 to 2035.

The AET parameter is also predicted using the ARIMA model. According to Table 30, the parameters of the model are set for each region, and then the prediction operation is performed. The AET parameter is also predicted using the ARIMA model. According to Table 30, the parameters of the model are set for each region, and then the prediction operation is performed. The parameter (37,0,7)(0,1,1) for all of Afghanistan and the central and west central regions, the parameter (17,0,13)(0,1,0) for the north region, (13,0, 1)(0,1,1) for the northeast region, (0,0,7)(0,1,1) for the west region, (5,0,47)(0,1,1) for the south region, (5,0,13)(0,1,1) is set for the southeast, and (9,0,3)(0,1,1) for the east region are adjusted. The performance results of the model show that the values of R^2, RMSE, and MAE have worked differently for all of Afghanistan and regions. As can be seen in table 32, the lowest value of R2 for the south region is 0.61 and the highest value for the northeast region is 0.93, which means that the correlation in the northeast region between the observed and predicted data is higher than in the south region. In the same way, the lowest value of RMSE is 4.67 for the whole of Afghanistan and the highest value is 10.31 for the southeast region, which means that the model has performed better in Afghanistan.

Likewise, the results of the monthly predicted values of the AET parameter can be seen in Figure 59: the predicted values across Afghanistan have shown a different pattern until 2035, and the trend is constant, but in the north, northeastern, and western regions. These patterns do not show much change during the projected years. In the same way, in the south and southeast region, the amount of AET was observed to be high in the early years of the forecast, and it has increased until 2035. In the east, central, and west central regions, the amount of AET has increased during the forecast period. As for the PET variable, it was predicted to use the ARIMA model. According to other climate parameters, in the PET parameter, the offending parameters were adjusted for each region, and by setting the parameters for the region, the prediction results were evaluated using the criteria of Table 32 and are satisfactory.

As seen in table 30, the parameter (17,0,3) (0,1,1) is set for data of throughout Afghanistan and the central west region, and in table 32, the performance of the model is evaluated. As shown in Table 32, $R^2 = 0.99$ was observed for Afghanistan and the central west region, which shows a very strong and significant correlation between the observed and predicted data, and the RMSE value for Afghanistan is 6.47 and it was 7.68 for the west-central region, which means that the performance of the model for the data of the entire Afghanistan was better than that of the west-central region, and the MAE criterion is also

smaller in the data of the entire Afghanistan compared to the west of the central region, indicating a better performance.

Also, the parameter (3,0,8)(0,1,1) is set for the north region to predict PET, which according to Table 32, R2 = 0.99, RMSE = 8.95, and MAE = 6.40. The calculated shows that the correlation between them is very good, but the RMSE amount does not seem too small, which has not reduced the difference between the observed and predicted data, and the MAE amount shows that the absolute average difference between the data is not high and has a good performance. Additionally, parameter (5,0,21) (0,1,1) is set for the northeast region and (51,0,26) (0,1,1) for the west region. According to Table 32, the correlation between observed and predicted data is very high in all regions, but the RMSE and MAE values are different in each region. The RMSE value is 6.45 in the northeast region and 9.23 in the west region; this shows that the difference between the observed and predicted data is greater in the west region, but still the model performance is acceptable. and the value of MAE in the northeast region is lower than in the west region. In general, the performance of the model in the northeast region was better than in the west region.

The parameter (9,0,3)(0,1,1) is set for the south and central regions, which indicates good model performance. However, according to Table 32, the model performs better in the central region compared to the South region because the difference between the data and the absolute mean is better preserved. Additionally, the parameter (3,0,9)(0,1,1) is set for the southeast region, and (1,0,7)(0,1,1) is set for the east region. Both performed well, but the model in the east region has performed better due to the lower RMS and MAE observed between smaller data values. In the parameter selection part of the model, since the amount of data differs by region, the selection of parameters also varies depending on the project location. As shown in Figure 60, PET has an increasing or constant trend in all regions for the predicted data. In regions where the predicted value of PET has decreased, climatic changes or the influence of other parameters may be involved.

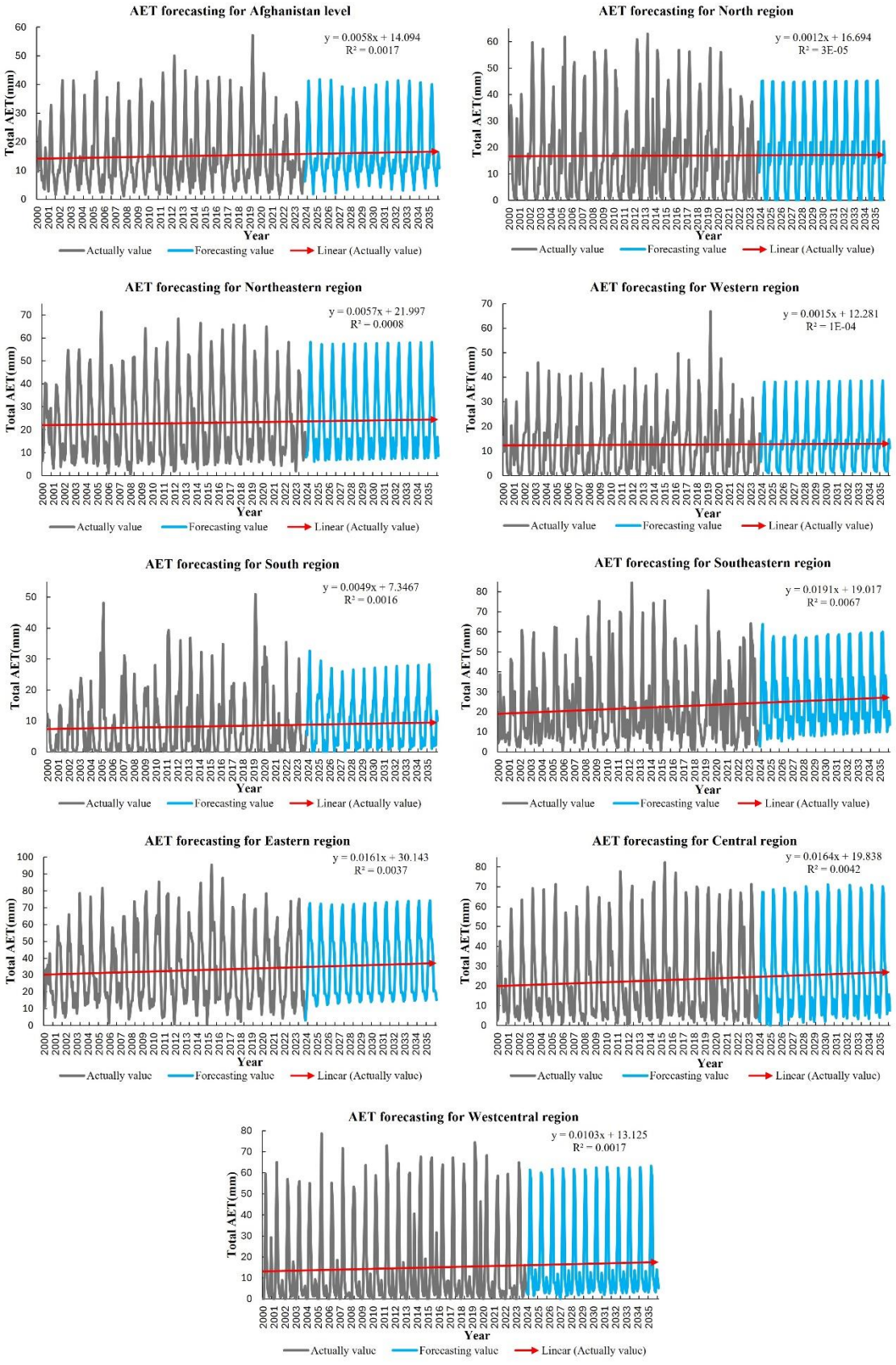

Figure 59. AET prediction values from 2024 to 2035.

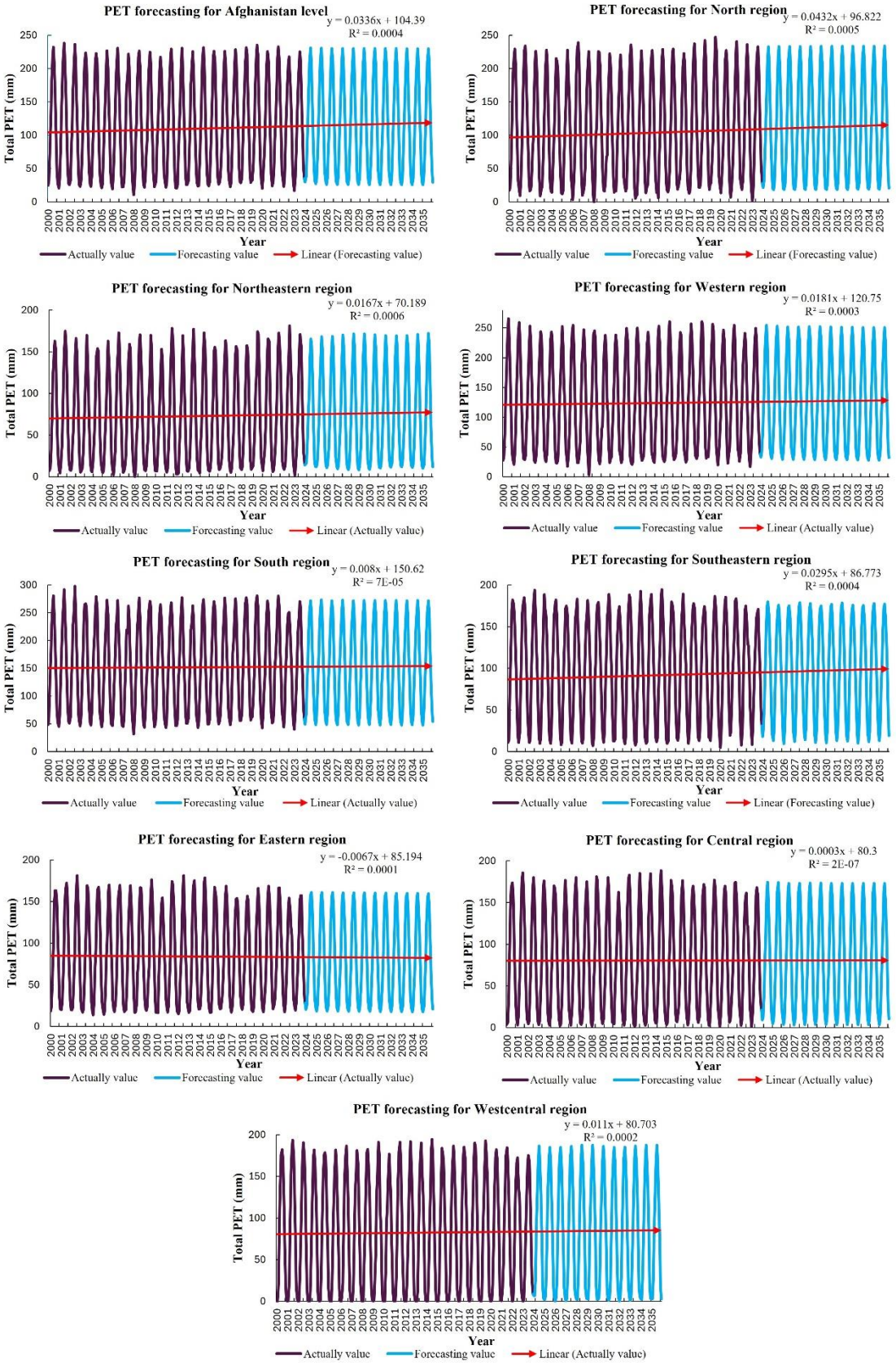

Figure 60. PET prediction values from 2024 to 2035.

Precipitation patterns in Afghanistan's regions vary significantly on monthly, seasonal, and annual scales. As illustrated in Figure 61, each region experiences different amounts and patterns of precipitation. According to the prediction results using the ARIMA model, accuracy tends to decrease when predicting monthly patterns, as noted by Sabzevari and Islamian (2024). In this study, the precipitation data exhibited distinct monthly patterns. Based on Table 31, the model parameters were set as follows: (7,0,3)(0,1,1) for the whole of Afghanistan, (19,0,11)(0,1,1) for the north and west-central regions, (39,0,7)(0,1,1) for the northeast, south, east, southeast, and central regions, and (5,0,11)(0,1,1) for the west region. As analyzed using the criteria in Table 32, the results indicate a correlation of over 60% between observed and predicted data. The central region showed the highest correlation of 0.71, while the eastern region had the lowest at 0.6. Table 32 also reveals that the north and central regions had stronger correlations, above 70%, whereas the other regions had correlations below 70%.

As shown in Table 32, the difference between observed and predicted precipitation data varies across regions. The lowest RMSE value of 11.58 was recorded in the South region, while the highest, at 24.08, was in the central region, indicating that the model did not perform well in this region. Similarly, an RMSE value of 21.97 was observed in the eastern region, which also suggests suboptimal model performance. However, despite this, the model performed better in the central region than in other regions. The RMSE values for Afghanistan as a whole, as well as the west-central and western regions, were within an acceptable range, indicating satisfactory model performance in these areas. Additionally, the MAE value in the South region was lower than in other regions, suggesting that the model performed better for precipitation data in the South region overall. As illustrated in Figure 61, the predicted precipitation across Afghanistan shows the highest value in 2025, though no consistent pattern is observed for the forecasted years. Similarly, precipitation in the eastern and southeastern regions is projected to increase between 2024 and 2035, while in other regions, the trend is either decreasing or stable.

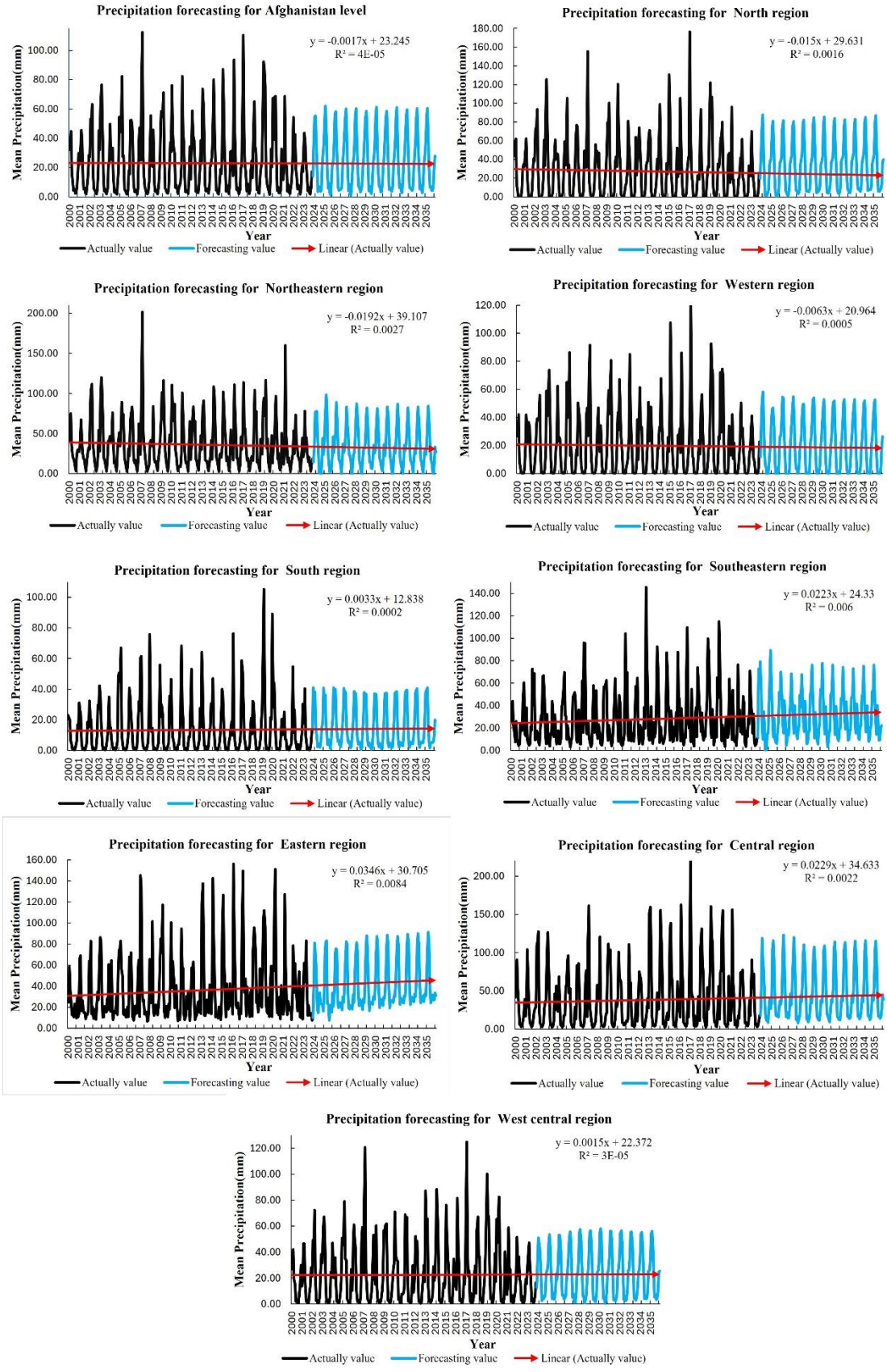

Figure 61. Precipitation prediction values from 2024 to 2035.

The soil moisture parameter is also predicted monthly using the ARIMA model. According to Table 31, the model parameters are set for the soil moisture parameter in each region, and the results are shown in Figure 62. The parameter (24,0,17) (0,1,1) is applied for the data covering Afghanistan as a whole, as well as the north and northeastern regions. As seen in Figure 62, the predicted soil moisture from 2024 to 2035 closely follows the pattern of observational data. By 2035, soil moisture shows an upward trend, and Table 32 indicates that the correlation between observed and predicted data is R = 0.92 for Afghanistan, R = 0.82 for the north region, and R = 0.93 for the northeastern region, demonstrating strong relationships across these areas. Additionally, the RMSE and MAE values for these regions reflect the model's high performance.

Similarly, the parameter (37,0,11) (0,1,1) was used for the western, South, eastern, and central regions, and the model performed well. As shown in Table 32, the correlation between observed and predicted data in these regions is high, though slightly lower in the South region at R = 0.67. However, the RMSE value of 1.43 in the South region indicates a relatively small difference between the observed and predicted data compared to other regions, and the MAE is also lower in the South region. Overall, the model performed effectively for the western, South, eastern, and central regions.

For the southeast region, the parameter (49,0,27) (0,1,1) was applied, and for the west-central region, (49,0,11) (0,1,1) was used. According to Table 32, the model performed well in both regions. The correlation between data and RMSE values in the west-central region were higher than in the southeast, indicating better model performance in the west-central region. As shown in Figure 62, soil moisture in the north region between 2024 and 2035 displays a fluctuating pattern, while in the northeastern region, soil moisture levels decrease over the same period. Similarly, a decrease is observed in the west region, but an increase in the south, likely due to increased use of surface water.

Wind speed predictions were also made, using different parameters as listed in Table 31. According to Table 32, the model evaluation criteria for wind speed indicate good performance and acceptable results. Figure 63 illustrates that wind speed will decrease in the southeastern, eastern, and west-central regions by 2035. The highest wind speeds in Afghanistan were observed in the western region, though this trend is expected to remain relatively stable through 2035.

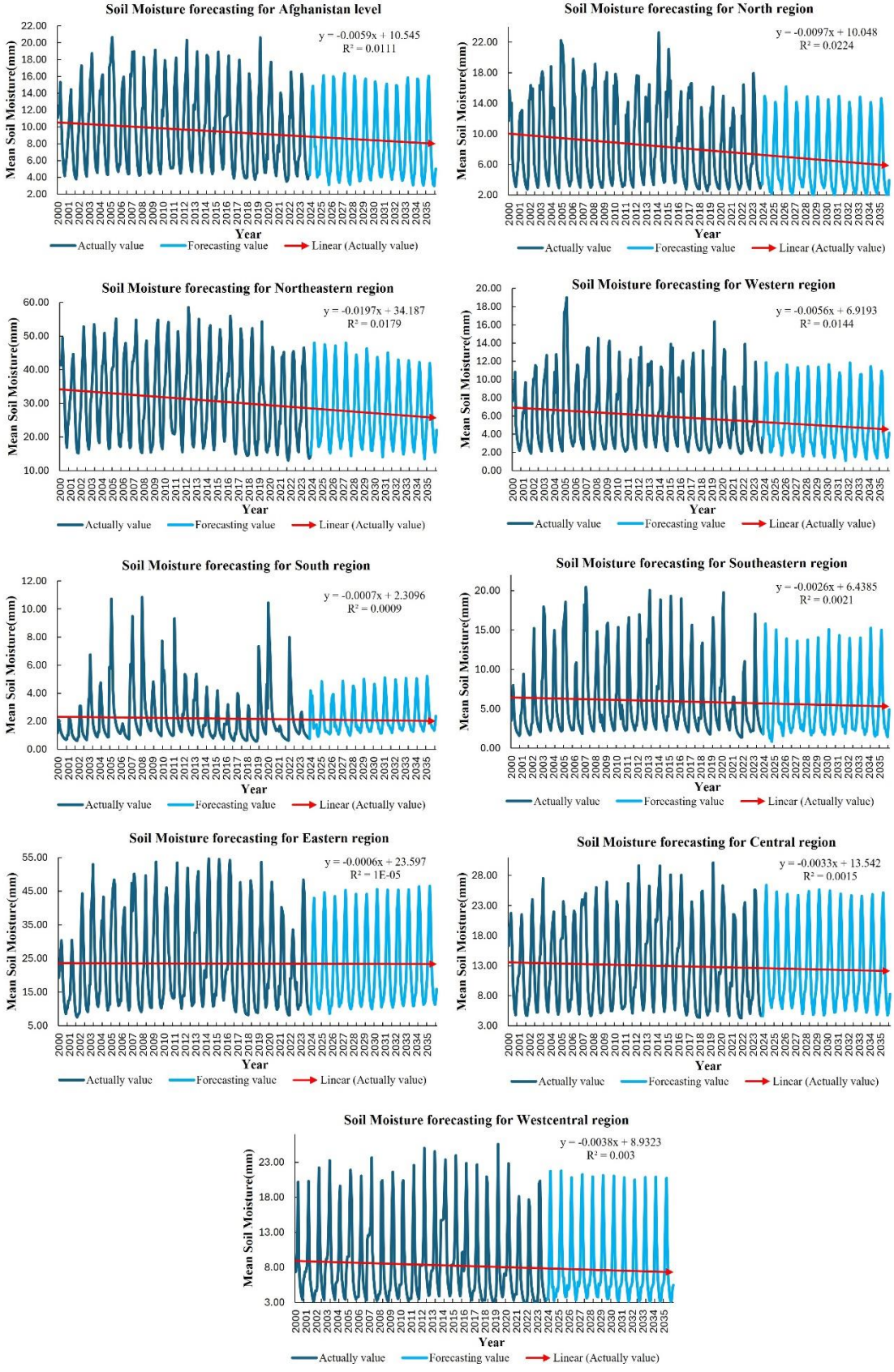

Figure 62. Soil moisture prediction values from 2024 to 2035.

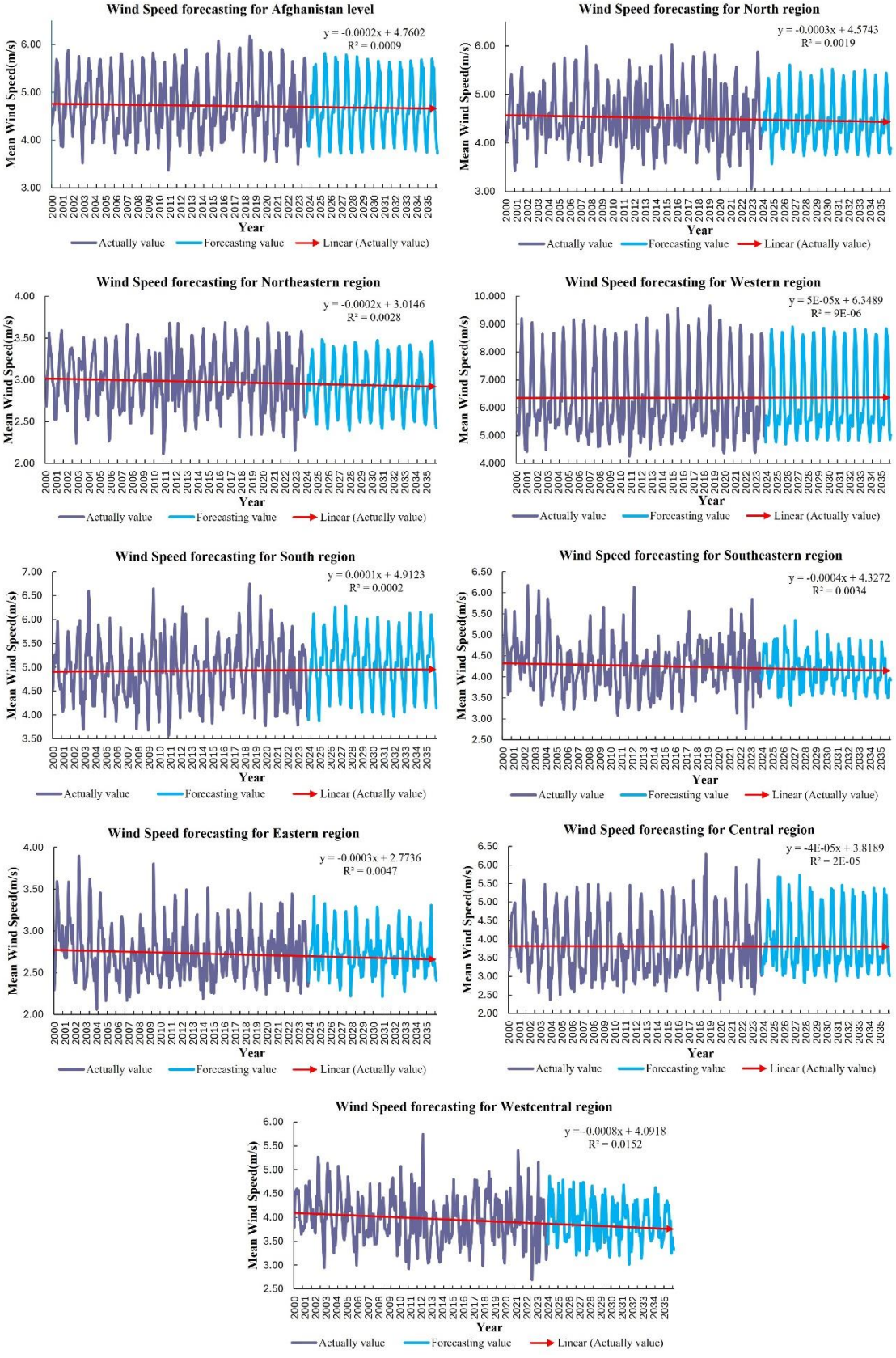

Figure 63. Wind speed prediction values from 2024 to 2035.

3.9. Drought Monitoring

In this section, drought monitoring is conducted using the VCI, TCI, and VHI indices. Previous discussions examined the trends of these indices on both a monthly and annual basis, but the annual drought conditions in each region were not analyzed. Therefore, this section provides a detailed analysis of drought and wet periods in each region from 2000 to 2023, followed by forecasts for these climate parameters using the ARIMA model. The annual average values of the VCI, TCI, and VHI indices were calculated for each region from 2000 to 2023 and similarly predicted from 2024 to 2035 and the red values in the tables indicate drought in that year. As shown in Table 33, the annual average values of the VCI index were computed to determine the drought conditions for each year. Based on the drought classifications in Table 1, we will analyze the drought conditions for each region and year.

According to Table 33, the VCI index for Afghanistan as a whole between 2000 and 2023 is above 0.4, indicating that no significant drought was observed nationwide. However, drought conditions were evident when examining specific regions. For instance, in the north region, the VCI index was below 0.4 in 2010, 2018, and 2019, indicating the presence of mild drought during these years. Similarly, mild drought was observed in the northeast region in 2018 and 2021 and in the southeast region in 2016 and 2018. This suggests that most regions in Afghanistan experienced mild drought in 2018. On the other hand, the western, South, eastern, central, and west-central regions did not experience consistent annual droughts, though seasonal droughts may have occurred.

The VCI index was forecasted using the ARIMA model up to 2035, with the predicted annual average values listed in Table 33. The model parameters for the VCI index are presented in Table 31, with different parameters set for each region. As indicated in Table 32, the model performed well in predicting the VCI index, as there is a strong correlation between the observed and predicted data, and the differences are minimal and within acceptable limits. The graph displaying the observed and predicted values of the VCI index is shown in Figure 64.

Table 32. Average annual VCI value.

Average Annual value of VCI for Drouth Monitoring in the All region of Afghanistan									
Year	**Afghanistan**	**North**	**Northeastern**	**Western**	**South**	**Eastern**	**Southeastern**	**Central**	**West central**
2000	0.505	0.410	0.427	0.457	0.497	0.479	0.489	0.475	0.565
2001	0.472	0.425	0.433	0.448	0.501	0.467	0.492	0.514	0.546
2002	0.446	0.427	0.436	0.419	0.486	0.464	0.472	0.442	0.525
2003	0.481	0.401	0.422	0.421	0.516	0.441	0.471	0.448	0.533
2004	0.432	0.439	0.409	0.463	0.504	0.456	0.471	0.490	0.571
2005	0.518	0.419	0.403	0.464	0.518	0.492	0.655	0.524	0.587
2006	0.423	0.472	0.458	0.477	0.454	0.485	0.550	0.534	0.582
2007	0.473	0.414	0.435	0.416	0.444	0.460	0.534	0.534	0.561
2008	0.560	0.596	0.474	0.585	0.482	0.471	0.557	0.553	0.592
2009	0.459	0.402	0.400	0.434	0.433	0.448	0.477	0.479	0.538
2010	0.454	0.399	0.436	0.448	0.476	0.519	0.509	0.513	0.572
2011	0.443	0.435	0.433	0.472	0.464	0.509	0.560	0.510	0.580
2012	0.458	0.439	0.424	0.468	0.512	0.488	0.625	0.537	0.578
2013	0.485	0.415	0.435	0.423	0.434	0.491	0.497	0.531	0.534
2014	0.471	0.436	0.418	0.455	0.439	0.457	0.526	0.476	0.554
2015	0.486	0.408	0.409	0.456	0.476	0.493	0.466	0.493	0.498
2016	0.480	0.409	0.424	0.431	0.441	0.449	0.394	0.439	0.503
2017	0.473	0.431	0.442	0.446	0.472	0.484	0.533	0.537	0.557
2018	0.408	0.398	0.381	0.401	0.449	0.446	0.388	0.461	0.475
2019	0.489	0.392	0.413	0.484	0.532	0.481	0.598	0.521	0.562
2020	0.513	0.466	0.409	0.439	0.448	0.448	0.602	0.506	0.547
2021	0.444	0.432	0.394	0.481	0.508	0.466	0.436	0.456	0.520
2022	0.442	0.417	0.429	0.448	0.463	0.509	0.577	0.582	0.619
2023	0.434	0.420	0.430	0.460	0.461	0.479	0.490	0.516	0.572
2024	0.490	0.424	0.412	0.470	0.479	0.496	0.410	0.552	0.569
2025	0.477	0.404	0.415	0.458	0.457	0.499	0.499	0.572	0.562
2026	0.463	0.406	0.416	0.445	0.440	0.495	0.541	0.524	0.566
2027	0.462	0.416	0.415	0.454	0.438	0.493	0.483	0.544	0.566
2028	0.463	0.419	0.415	0.467	0.483	0.493	0.518	0.533	0.567
2029	0.463	0.425	0.415	0.449	0.442	0.498	0.557	0.535	0.567
2030	0.462	0.414	0.414	0.450	0.451	0.483	0.438	0.535	0.567
2031	0.462	0.410	0.414	0.454	0.456	0.478	0.478	0.513	0.568
2032	0.461	0.409	0.414	0.454	0.449	0.474	0.506	0.509	0.568
2033	0.461	0.412	0.413	0.455	0.450	0.479	0.454	0.501	0.569
2034	0.460	0.412	0.413	0.454	0.449	0.481	0.509	0.512	0.570
2035	0.460	0.410	0.413	0.453	0.447	0.481	0.521	0.520	0.570

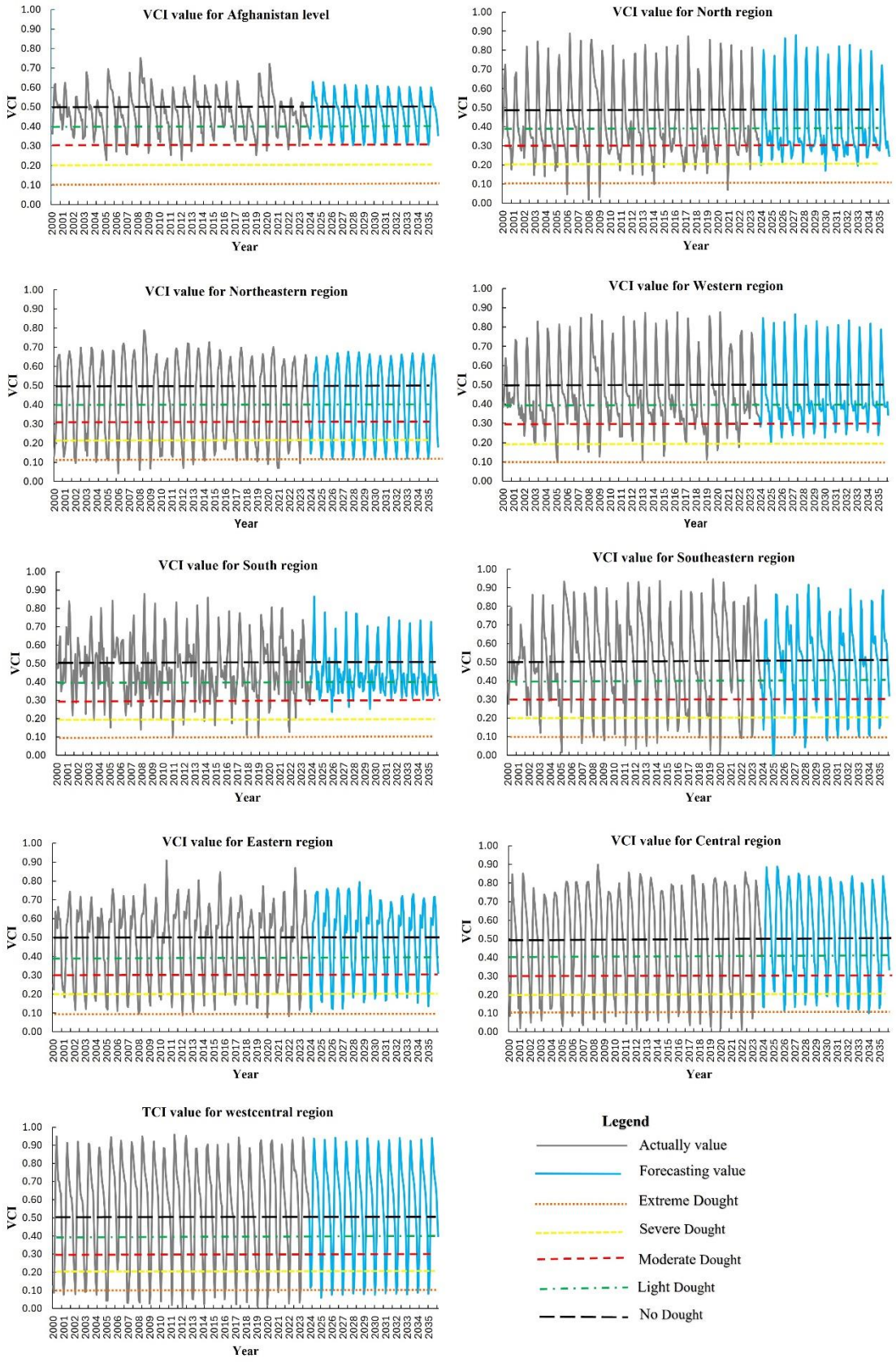

Figure 64. VCI prediction values from 2024 to 2035.

The dry condition of plants is monitored using the TCI index. As shown in Table 35, due to high temperatures in most years in Afghanistan, plants and crops have dried up, leading to drought. Between 2000 and 2023, consecutive droughts were observed in Afghanistan. In the north region, 2009, 2012, and 2020 were wet years, while the remaining years exhibited dry conditions, contributing to drought. Similarly, as shown in Table 34, the northeast region experienced drought in 2000 and 2001, with the other years being wet. In the western region, 2012 and 2020 were wet years, while other years were characterized by drought. The South region showed more frequent plant dryness across most years, indicating consecutive droughts. In contrast, the eastern region, like the northeast, witnessed plant dryness in 2000 and 2001, leading to drought, but the other years were wet. The southeast, central, and west-central regions experienced a decline in the TCI index between 2000 and 2023, indicating consecutive droughts in these areas.

The TCI index, like the VCI index, was predicted monthly using the ARIMA model for the period 2024-2035. The model parameters for each region were set, and the results evaluated using the criteria in Table 32, showing acceptable performance. In the southeast region, the R^2 value was 0.95, while in other regions, it was 0.97, indicating that the model explained more than 95% of the real data in the forecasts. The RMSE and MAE values in all regions were within acceptable limits, confirming the model's strong performance in predicting TCI values. The predicted annual TCI values are listed in Table 34, allowing observation of plant dryness in Afghanistan for 2024 and 2025. Additionally, drought conditions are forecasted for the north and western regions between 2024 and 2035, while wet conditions are predicted for the northeast, east, southeast, and central regions during the same period. In the South region, plant dryness is predicted for 2025, and in the west-central region, dryness is forecasted for 2024, 2025, 2026, and 2028, leading to potential droughts.

For agricultural drought monitoring, the VHI index performs better than the VCI and TCI indices because it is a combination of both (Zhao et al., 2021). As seen in Table 35, agricultural drought between the years 2000 and 2023 was identified using the VHI index. In 2018, drought affected all regions of Afghanistan, although the severity differed by region. The north region experienced mild to moderate droughts in the years 2000, 2001, 2007, 2010, 2016, 2018, 2019, 2021, 2022, and 2023. Likewise, the northeast region faced drought in 2018, while the western region saw drought in the years 2000, 2001, 2002, 2003, 2007, 2013, 2016, and 2018. The South, eastern, central, and west-central regions did not

face significant droughts, but the southeast region experienced mild drought in 2000, 2016, 2018, and 2021.

Table 33. Average annual TCI value.

Average Annual value of TCI for Drouth Monitoring in the All region of Afghanistan									
Year	Afghanistan	North	Northeastern	Western	South	Eastern	Southeastern	Central	West central
2000	0.329	0.322	0.376	0.309	0.329	0.372	0.301	0.338	0.327
2001	0.353	0.346	0.382	0.332	0.361	0.396	0.328	0.370	0.346
2002	0.378	0.381	0.412	0.361	0.372	0.427	0.357	0.398	0.382
2003	0.401	0.399	0.437	0.377	0.403	0.447	0.379	0.421	0.401
2004	0.383	0.373	0.433	0.360	0.383	0.432	0.352	0.402	0.379
2005	0.411	0.387	0.445	0.385	0.413	0.461	0.412	0.440	0.425
2006	0.387	0.375	0.416	0.366	0.388	0.435	0.380	0.414	0.388
2007	0.393	0.376	0.400	0.380	0.399	0.434	0.382	0.412	0.403
2008	0.398	0.386	0.417	0.387	0.401	0.443	0.383	0.418	0.397
2009	0.414	0.408	0.446	0.398	0.404	0.454	0.390	0.447	0.431
2010	0.380	0.372	0.416	0.358	0.377	0.431	0.370	0.403	0.385
2011	0.402	0.381	0.410	0.385	0.399	0.438	0.387	0.413	0.396
2012	0.434	0.427	0.468	0.412	0.428	0.476	0.427	0.468	0.449
2013	0.388	0.378	0.407	0.363	0.391	0.446	0.388	0.418	0.398
2014	0.402	0.395	0.426	0.380	0.402	0.451	0.394	0.431	0.413
2015	0.397	0.391	0.431	0.382	0.395	0.454	0.378	0.426	0.400
2016	0.375	0.370	0.405	0.358	0.375	0.416	0.356	0.394	0.378
2017	0.379	0.373	0.408	0.359	0.378	0.426	0.360	0.402	0.382
2018	0.375	0.366	0.416	0.355	0.376	0.427	0.358	0.395	0.370
2019	0.409	0.393	0.428	0.392	0.404	0.469	0.409	0.444	0.423
2020	0.421	0.410	0.439	0.404	0.417	0.469	0.421	0.449	0.436
2021	0.366	0.358	0.408	0.340	0.370	0.417	0.345	0.386	0.358
2022	0.388	0.377	0.416	0.366	0.396	0.434	0.383	0.404	0.386
2023	0.400	0.373	0.416	0.373	0.416	0.456	0.407	0.420	0.403
2024	0.396	0.383	0.419	0.374	0.415	0.470	0.401	0.418	0.399
2025	0.399	0.385	0.428	0.379	0.390	0.450	0.405	0.419	0.398
2026	0.400	0.382	0.426	0.380	0.415	0.449	0.400	0.417	0.397
2027	0.400	0.383	0.425	0.380	0.416	0.458	0.406	0.428	0.409
2028	0.401	0.383	0.424	0.380	0.409	0.456	0.404	0.423	0.399
2029	0.402	0.384	0.424	0.379	0.411	0.457	0.407	0.428	0.404
2030	0.403	0.385	0.425	0.380	0.413	0.458	0.410	0.428	0.403
2031	0.403	0.385	0.425	0.382	0.414	0.459	0.409	0.429	0.408
2032	0.404	0.385	0.426	0.383	0.416	0.460	0.414	0.432	0.410
2033	0.405	0.385	0.425	0.384	0.417	0.461	0.412	0.432	0.410
2034	0.405	0.385	0.426	0.384	0.418	0.462	0.416	0.435	0.410
2035	0.406	0.386	0.426	0.383	0.419	0.463	0.417	0.436	0.413

Table 34. Average annual VHI value.

Average Annual value of VHI for Drouth Monitoring in the All region of Afghanistan									
Year	**Afghanistan**	**North**	**Northeastern**	**Western**	**South**	**Eastern**	**Southeastern**	**Central**	**West central**
2000	0.417	0.366	0.401	0.383	0.413	0.426	0.395	0.406	0.446
2001	0.412	0.386	0.407	0.390	0.431	0.432	0.410	0.442	0.446
2002	0.412	0.404	0.424	0.390	0.429	0.446	0.414	0.420	0.453
2003	0.441	0.400	0.430	0.399	0.459	0.444	0.425	0.435	0.467
2004	0.407	0.406	0.421	0.412	0.444	0.444	0.412	0.446	0.475
2005	0.465	0.403	0.424	0.425	0.466	0.477	0.533	0.482	0.506
2006	0.405	0.424	0.437	0.422	0.421	0.460	0.465	0.474	0.485
2007	0.433	0.395	0.417	0.398	0.421	0.447	0.458	0.473	0.482
2008	0.479	0.491	0.445	0.486	0.442	0.457	0.470	0.485	0.494
2009	0.436	0.405	0.423	0.416	0.419	0.451	0.434	0.463	0.485
2010	0.417	0.386	0.426	0.403	0.427	0.475	0.439	0.458	0.479
2011	0.423	0.408	0.422	0.428	0.431	0.473	0.474	0.462	0.488
2012	0.446	0.433	0.446	0.440	0.470	0.482	0.526	0.503	0.514
2013	0.436	0.397	0.421	0.393	0.412	0.469	0.443	0.474	0.466
2014	0.436	0.416	0.422	0.418	0.421	0.454	0.460	0.453	0.484
2015	0.441	0.400	0.420	0.419	0.435	0.474	0.422	0.460	0.449
2016	0.428	0.390	0.414	0.394	0.408	0.432	0.375	0.417	0.441
2017	0.426	0.402	0.425	0.403	0.425	0.455	0.446	0.469	0.469
2018	0.392	0.382	0.398	0.378	0.413	0.436	0.373	0.428	0.422
2019	0.449	0.393	0.421	0.438	0.468	0.475	0.504	0.482	0.493
2020	0.467	0.438	0.424	0.421	0.433	0.459	0.511	0.477	0.491
2021	0.405	0.395	0.401	0.411	0.439	0.441	0.391	0.421	0.439
2022	0.415	0.397	0.422	0.407	0.429	0.472	0.480	0.493	0.502
2023	0.417	0.396	0.423	0.416	0.439	0.468	0.449	0.468	0.487
2024	0.443	0.404	0.415	0.422	0.447	0.483	0.406	0.485	0.484
2025	0.438	0.395	0.421	0.419	0.424	0.474	0.452	0.496	0.480
2026	0.431	0.394	0.421	0.413	0.427	0.472	0.470	0.471	0.481
2027	0.431	0.400	0.420	0.417	0.427	0.475	0.445	0.486	0.487
2028	0.432	0.401	0.420	0.424	0.446	0.475	0.461	0.478	0.483
2029	0.432	0.404	0.419	0.414	0.426	0.478	0.482	0.481	0.486
2030	0.432	0.399	0.420	0.415	0.432	0.471	0.424	0.481	0.485
2031	0.433	0.397	0.419	0.418	0.435	0.469	0.443	0.471	0.488
2032	0.433	0.397	0.420	0.418	0.432	0.467	0.460	0.470	0.489
2033	0.433	0.399	0.419	0.419	0.433	0.470	0.433	0.467	0.489
2034	0.433	0.399	0.420	0.419	0.433	0.471	0.463	0.474	0.490
2035	0.433	0.398	0.420	0.418	0.433	0.472	0.469	0.478	0.491

The VHI index is also predicted using the ARIMA model. As shown in Table 31, the model parameters were adjusted for each region, and the model's performance was evaluated using R^2, RMSE, and MAE criteria, as outlined in Table 32. The evaluation shows that the

model performed well in all regions. The predicted values of the VHI index up to 2035 indicate that the north region will experience agricultural drought in 2025, 2026, and from 2030 to 2035, unless effective action is taken by the Afghan government.

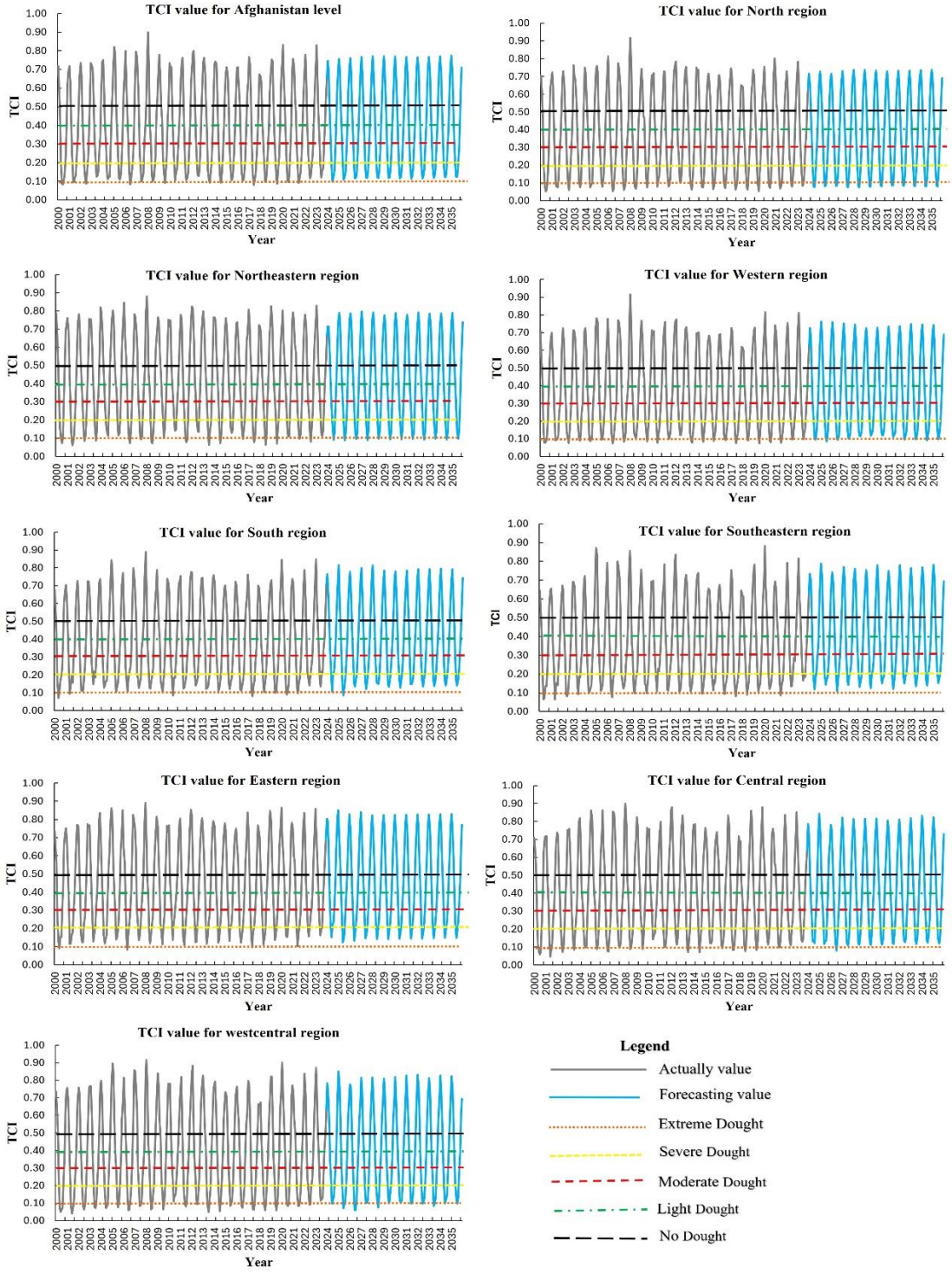

Figure 65. TCI prediction values from 2024 to 2035.

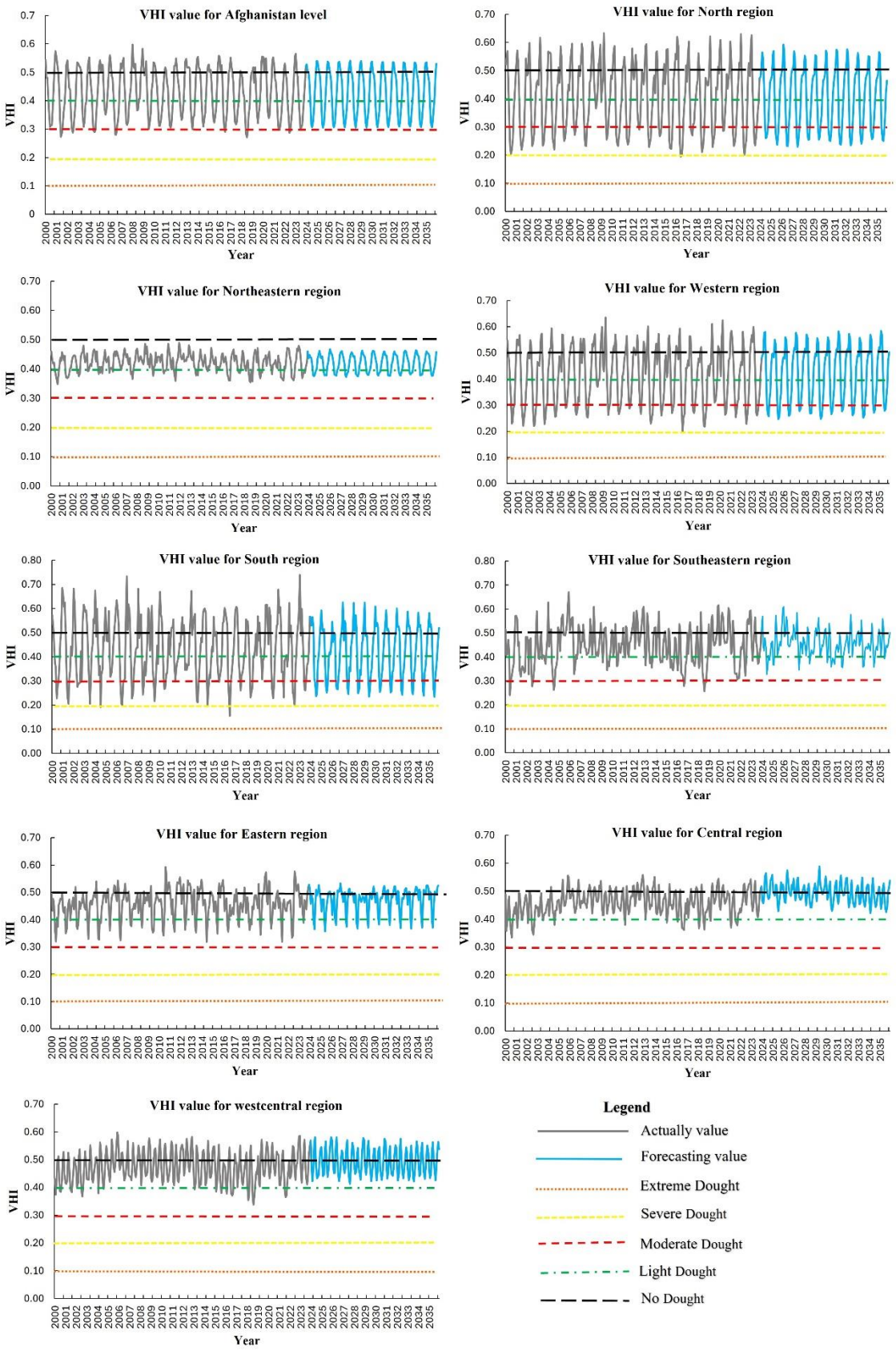

Figure 66. VHI prediction values from 2024 to 2035.

3.10. Results Based on The Regional Scale

In this section, the changes of the climate parameters are examined on a spatial scale. While the effects of climate parameters on climate change between 2000-2023 were analyzed on monthly, seasonal, and annual scales in previous sections, this section investigates these effects spatially. The maps of each climatic parameter were prepared for the years 2000, 2012, and 2023, allowing for an examination of the changes in each parameter annually and seasonally across different regions. As shown in Figure 1, Afghanistan's regional divisions are depicted, and the performance of each climate parameters can be observed for each region. The NDVI index values range between -1 and +1, where values between 0 and -1 indicate water, snow, or clouds; values near zero typically represent soil; values between 0.02 and 0.5 indicate scattered vegetation, such as agricultural areas with short vegetation; and values between 0.6 and 1 represent dense and healthy vegetation, such as forests or farmlands with dense vegetation (Nabizada et al., 2022).

As shown in Figure 67(a), the status of the NDVI index for the year 2000 is clearly visible. In that year, the north, South, western, and west-central regions were mostly within the range of 0.2, indicating soil and scattered vegetation. During the winter season, Figure 67(e) shows that parts of the north, northeastern, and western regions, where the LST ranges between 10-25℃ (as seen in Figure 70(e)), experienced exceptional NDVI growth. However, areas with values below 0 were covered with snow, which affected most of the northeastern and central regions of Afghanistan. The eastern and southeastern regions showed remarkably high NDVI levels due to forest cover. In the summer, the snow in these regions melts, leading to a significant increase in NDVI, as illustrated in Figure 67(c).

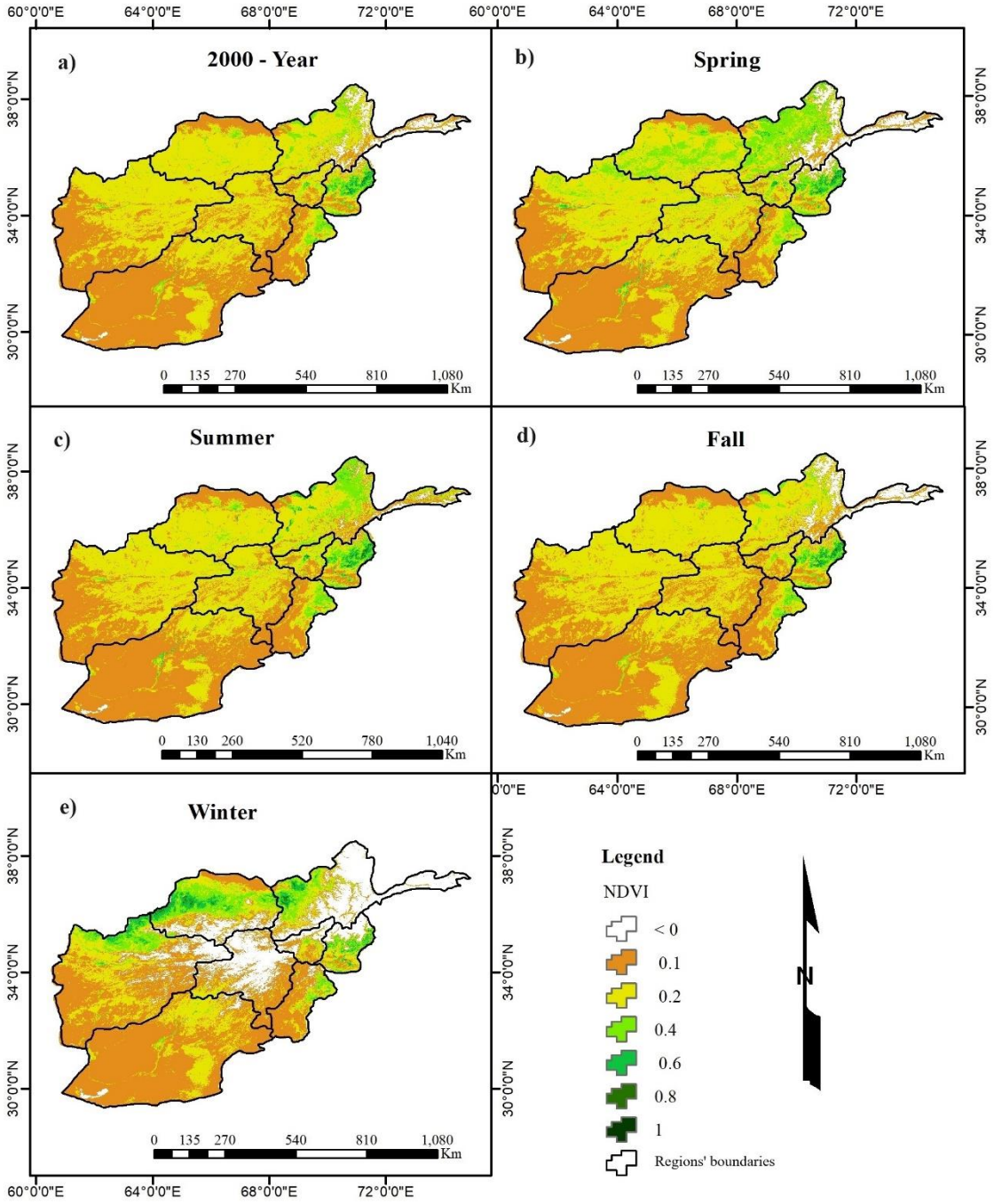

Figure 67. Spatial distribution of NDVI for 2000 year: 2000-year(a), Spring(b), Summer(c), Fall(d), Winter(e).

NDVI in 2012 shows significant growth compared to the year 2000 (as shown in Figure 68a). According to Figure 68b, during the spring season, the NDVI in the east, north, and northeast regions reaches the 0.8 range, which is higher than in 2000. Additionally, in the south, southeast, central, and west regions, NDVI has grown significantly compared to 2000. The increase in NDVI compared to 2000 is even more evident in the summer season

(as shown in Figure 68c). In the summer of 2000, NDVI was scattered across the north, northeast, south, west, and central areas, but it increased notably in the summer of 2012. Furthermore, during the winter of 2012, the central areas of Afghanistan had more snow cover compared to 2000, resulting in less vegetation (as shown in Figure 68e).

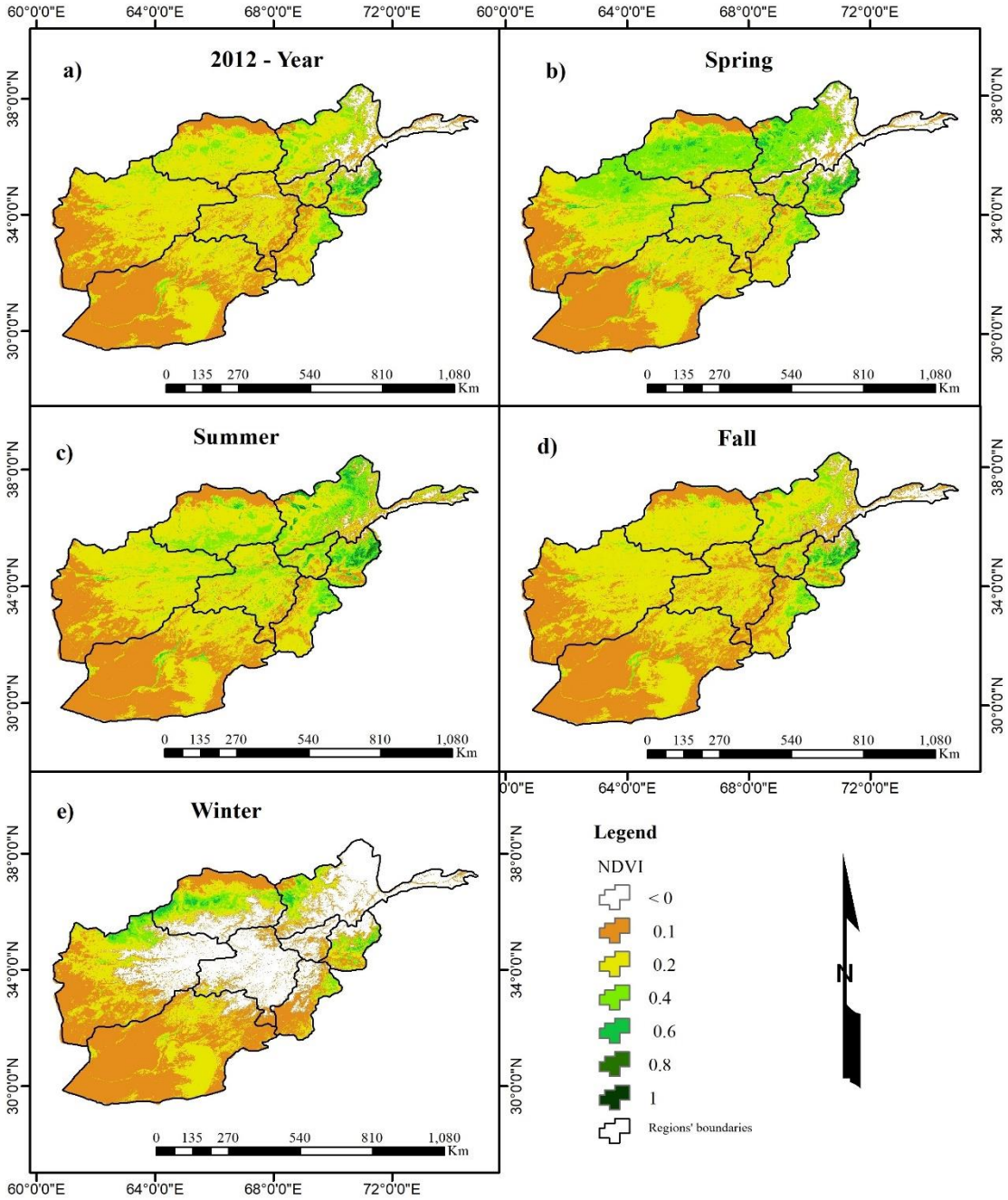

Figure 68. Spatial distribution of NDVI for 2012 year: 2012-year(a), Spring(b), Summer(c), Fall(d), Winter(e).

NDVI in 2023 decreased compared to 2012, but it is still higher than in 2000 (as shown in Figure 69). In the South region, NDVI has grown significantly in recent years compared to 2000. During the summer season, as depicted in Figure 69(c), NDVI increased in the east and southeast regions, possibly due to the forest cover.

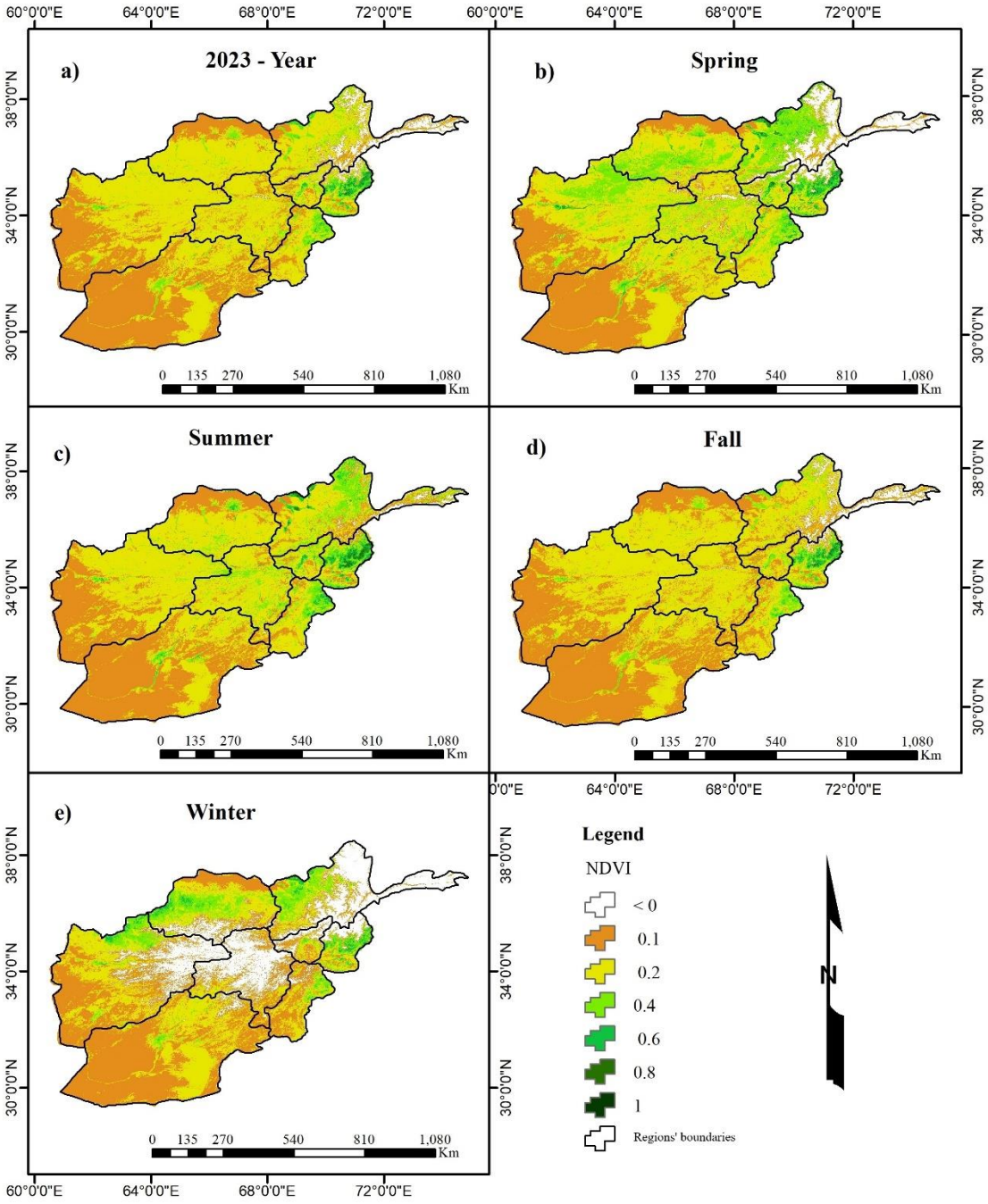

Figure 69. Spatial distribution of NDVI for 2023 year: 2023-year(a), Spring(b), Summer(c), Fall(d), Winter(e).

The average LST across Afghanistan was 31.5 °C in 2000, 25 °C in 2012, and 27 °C in 2023, as shown in Figure 25. In the seasonal and annual analysis of LST using charts, the highest LST was observed in 2000. As depicted in Figure 70, the South region recorded the highest LST values.

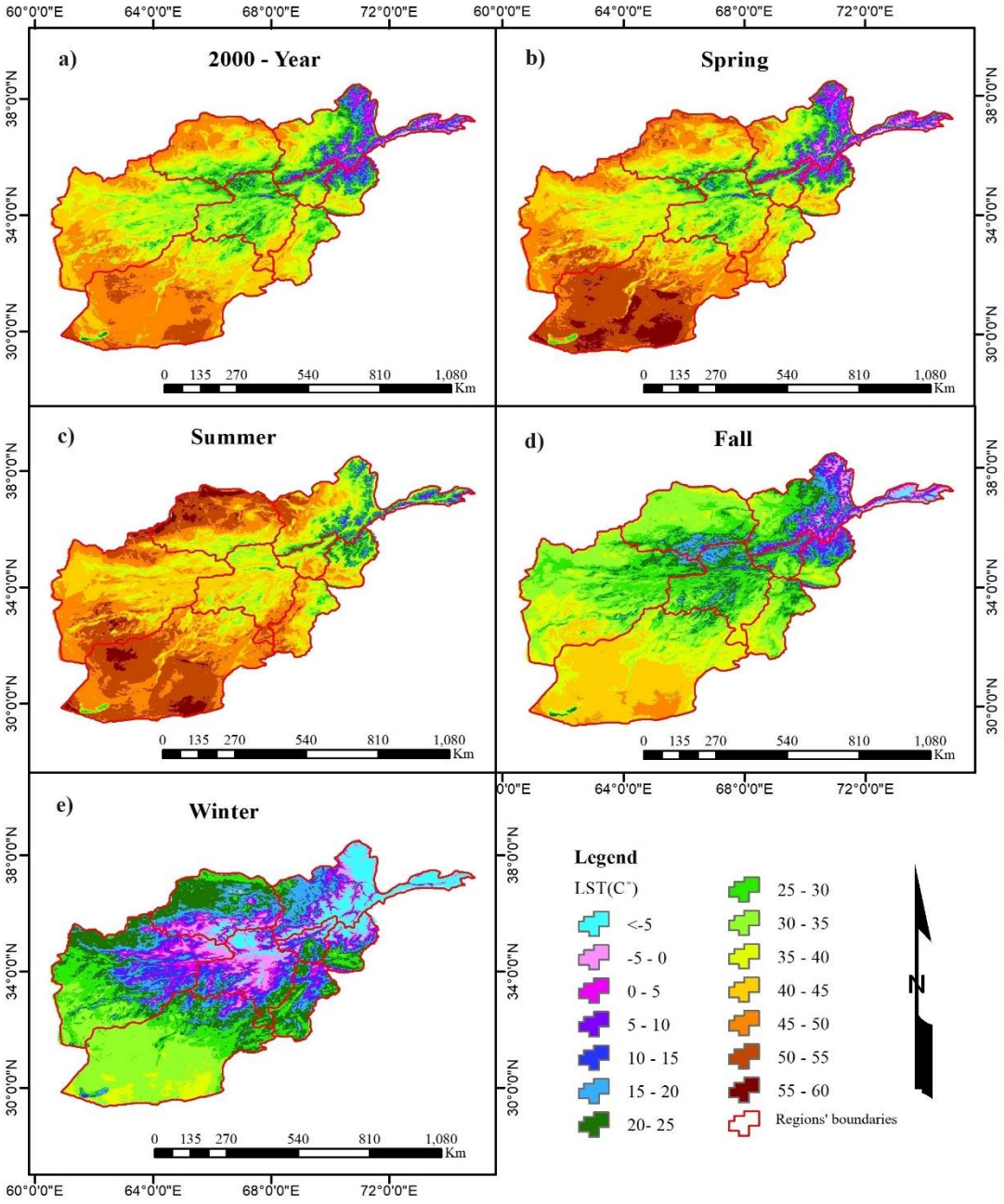

Figure 70. Spatial distribution of LST for 2000 year: 2000-year(a), Spring(b), Summer(c), Fall(d), Winter(e).

In the spring season, the highest LST was observed in the South region, while the lowest was recorded in the northeastern Pamir regions (Figure 70b). However, during the

summer, the LST increased in the north region (Figure 70c). In the winter season, the LST values were significantly low in the northeastern and central regions, whereas the South region experienced an increase up to 35°C (as shown in Figure 70e). In 2012, the overall LST levels decreased. On average, the highest LST in the South region was recorded in 2000 at 41.6°C, which then dropped to 35.2°C in 2012, before rising slightly to 35.5°C in 2023 (as shown in Figure 28).

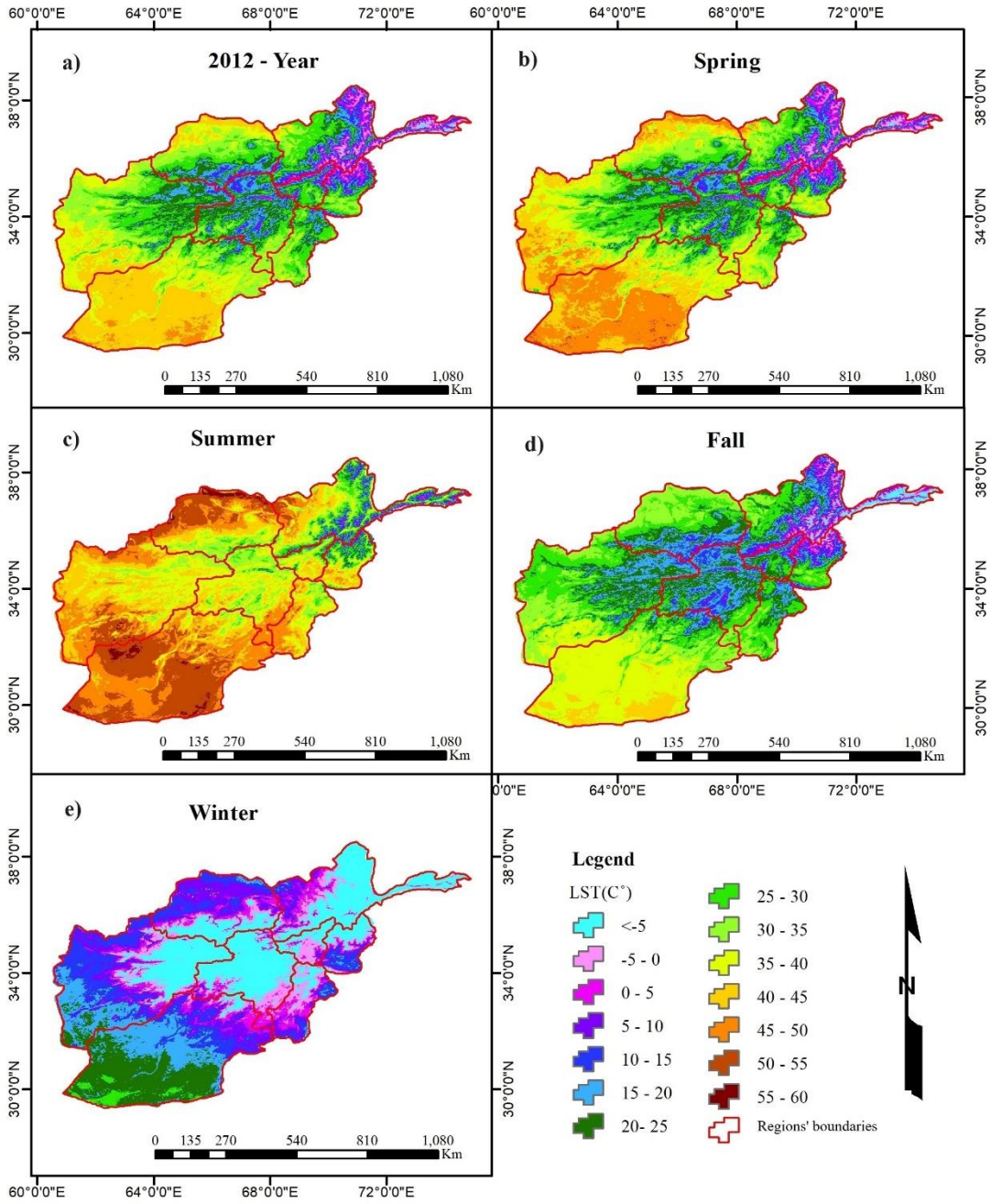

Figure 71. Spatial distribution of LST for 2012 year: 2012-year(a), Spring(b), Summer(c), Fall(d), Winter(e).

In addition, as shown in Figures 70, 71, and 72, the South region was the hottest in 2000 compared to other years, and other regions also experienced higher temperatures. The LST during the winter season of 2012 was lower than in 2000 and 2023 (as shown in Figure 71e). However, in recent years, the LST has increased once again.

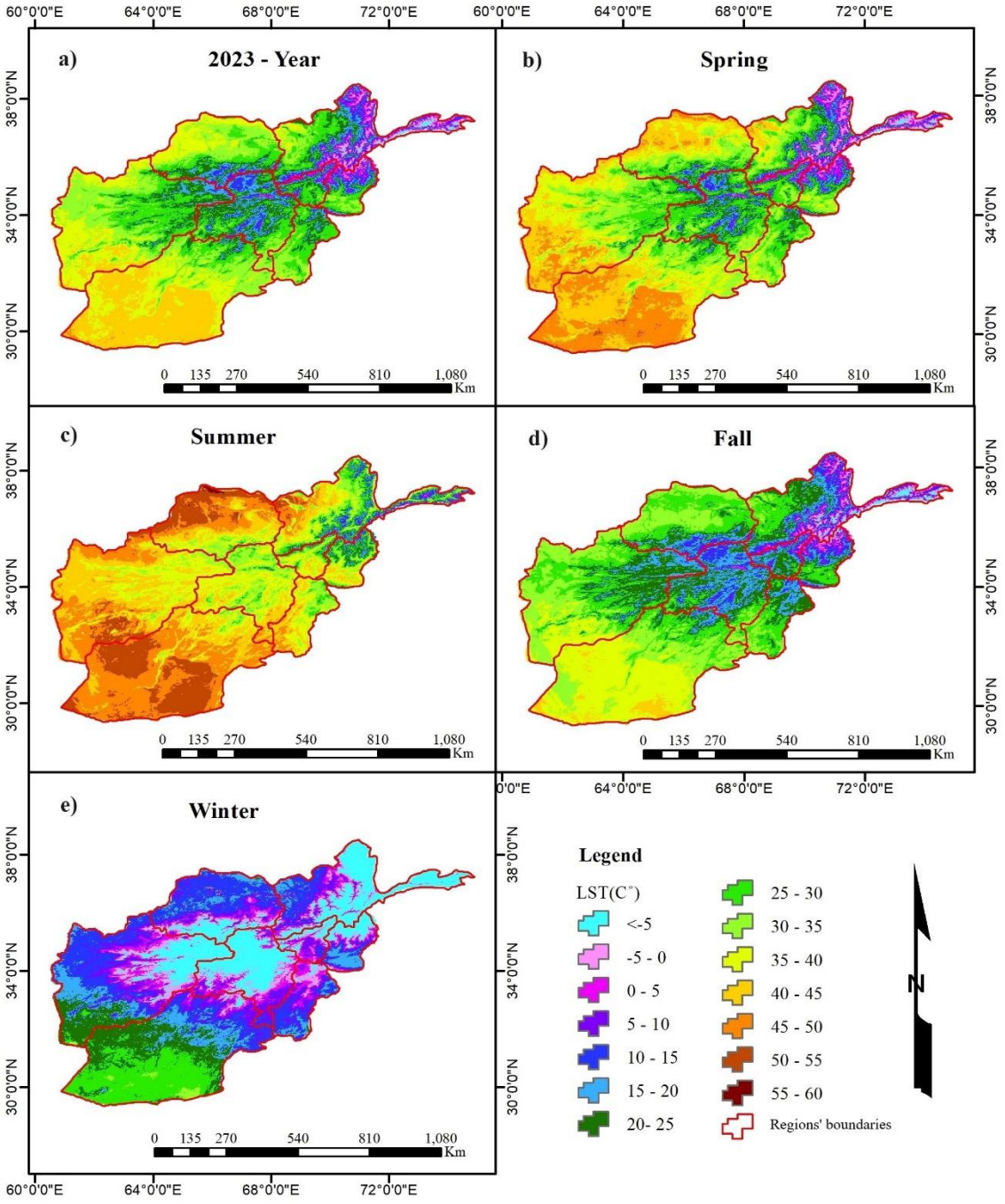

Figure 72. Spatial distribution of LST for 2023 year: 2023-year(a), Spring(b), Summer(c), Fall(d), Winter(e).

Figures 73, 74, and 75 illustrate the amount of AET for the years 2000, 2012, and 2023, with the highest AET observed in 2012. In the spring of 2000, AET levels were significantly higher compared to those in 2000 and 2023, particularly in the northeastern and central regions.

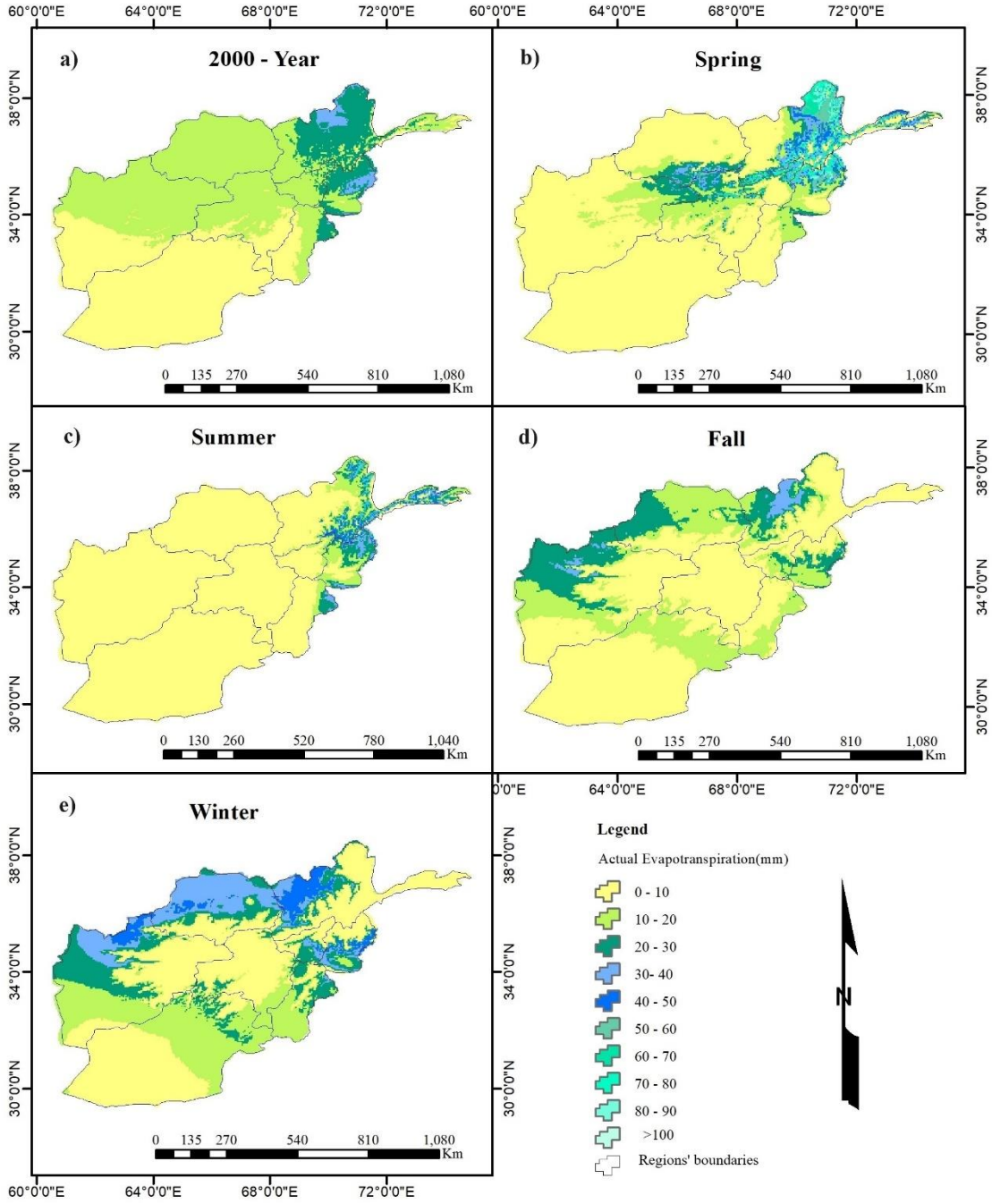

Figure 73. Spatial distribution of AET for 2000 year: 2000-year(a), Spring(b), Summer(c), Fall(d), Winter(e).

Also, in the spring season, the amount of AET in the north region and a part of the northeast region was very low in 2000 and 2023 compared to 2012 due to the decrease of NDVI.

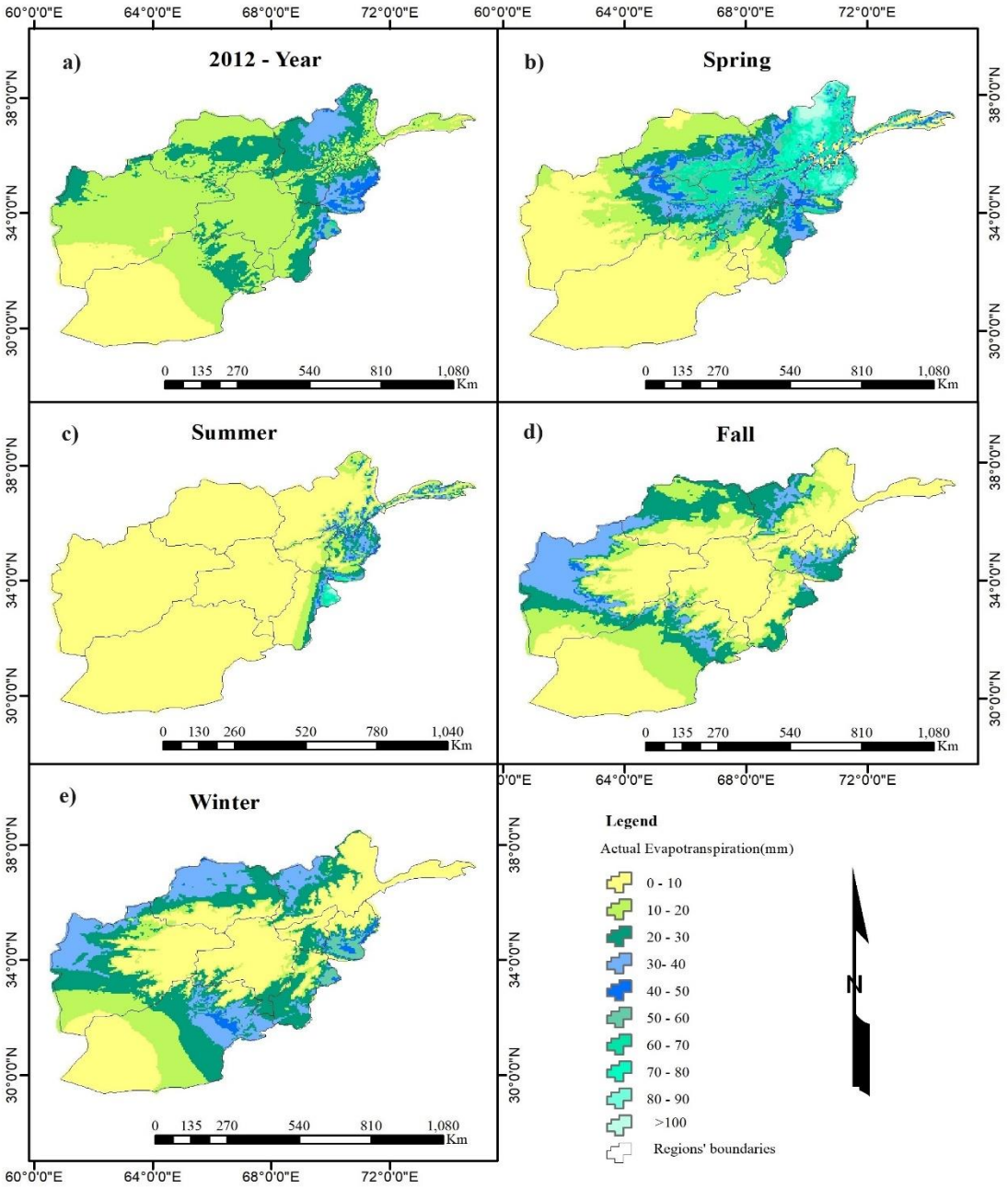

Figure 74. Spatial distribution of AET for 2012 year: 2012-year(a), Spring(b), Summer(c), Fall(d), Winter(e).

In the winter season, the northeastern and central regions, surrounded by the Hindu Kush and Pamir mountains, experience no AET due to heavy snowfall, as temperatures in these areas drop below 0°C. In contrast, AET is more prevalent in the north, western, South,

eastern, and southeastern regions during winter, where temperatures exceed 15°C (shown in Figures 73e, 74e, and 75e). Additionally, due to the increase in LST in 2000, AET in the eastern, southeastern, and Pamir regions rose during the summer season (shown in Figures 73c, 74c, and 75c). Although LST was high in 2000, AET levels were low due to lower NDVI values that year. Conversely, in 2012, LST decreased while AET increased, reflecting improvements in NDVI.

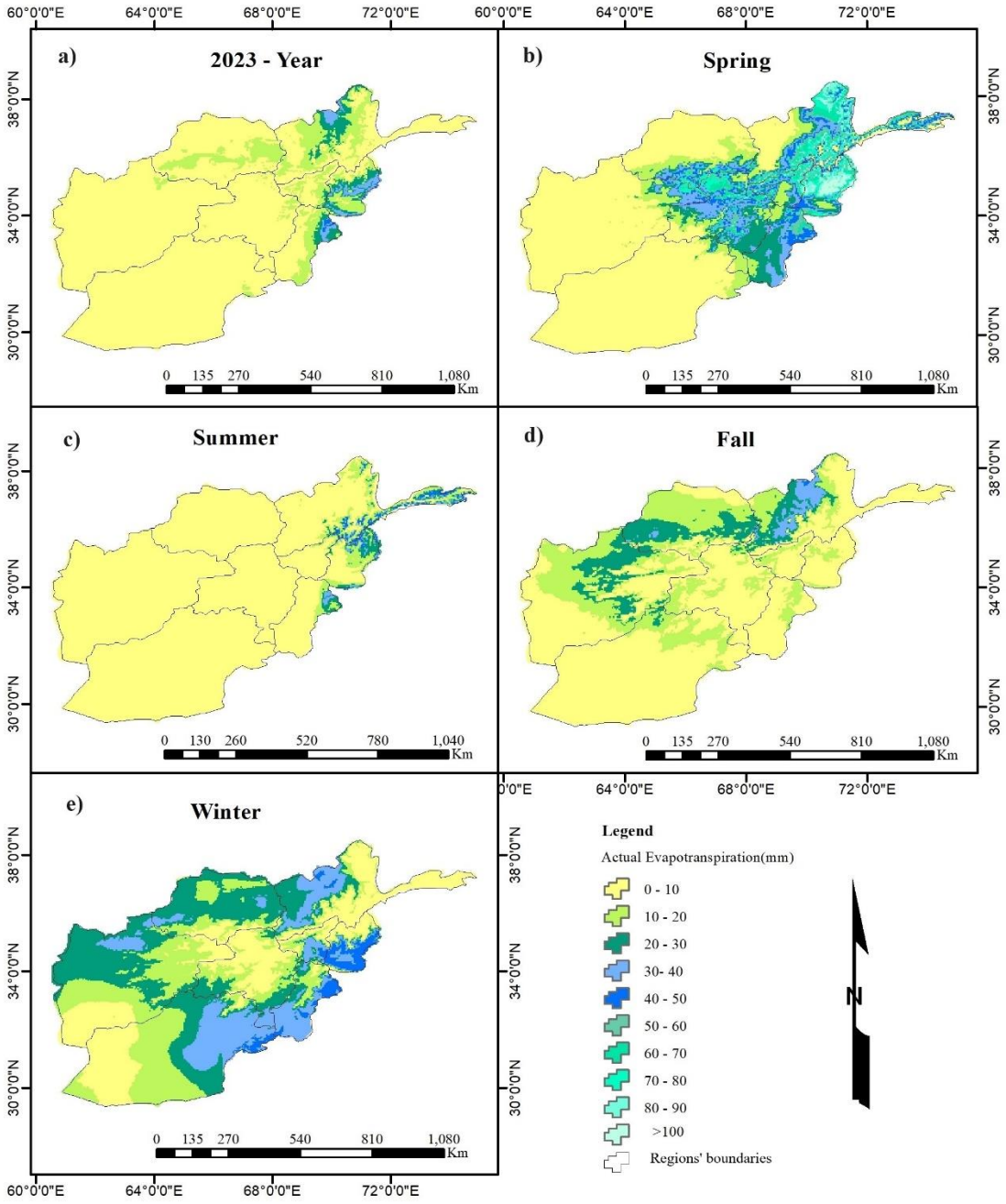

Figure 75. Spatial distribution of AET for 2023 year: 2023-year(a), Spring(b), Summer(c), Fall(d), Winter(e).

In Afghanistan, the highest amount of PET occurs in the spring and summer seasons, with the South, north, and western regions exhibiting the greatest levels due to elevated LST during these periods. As a result of this increase in LST, PET reached its peak in 2000 (shown in Figure 76a).

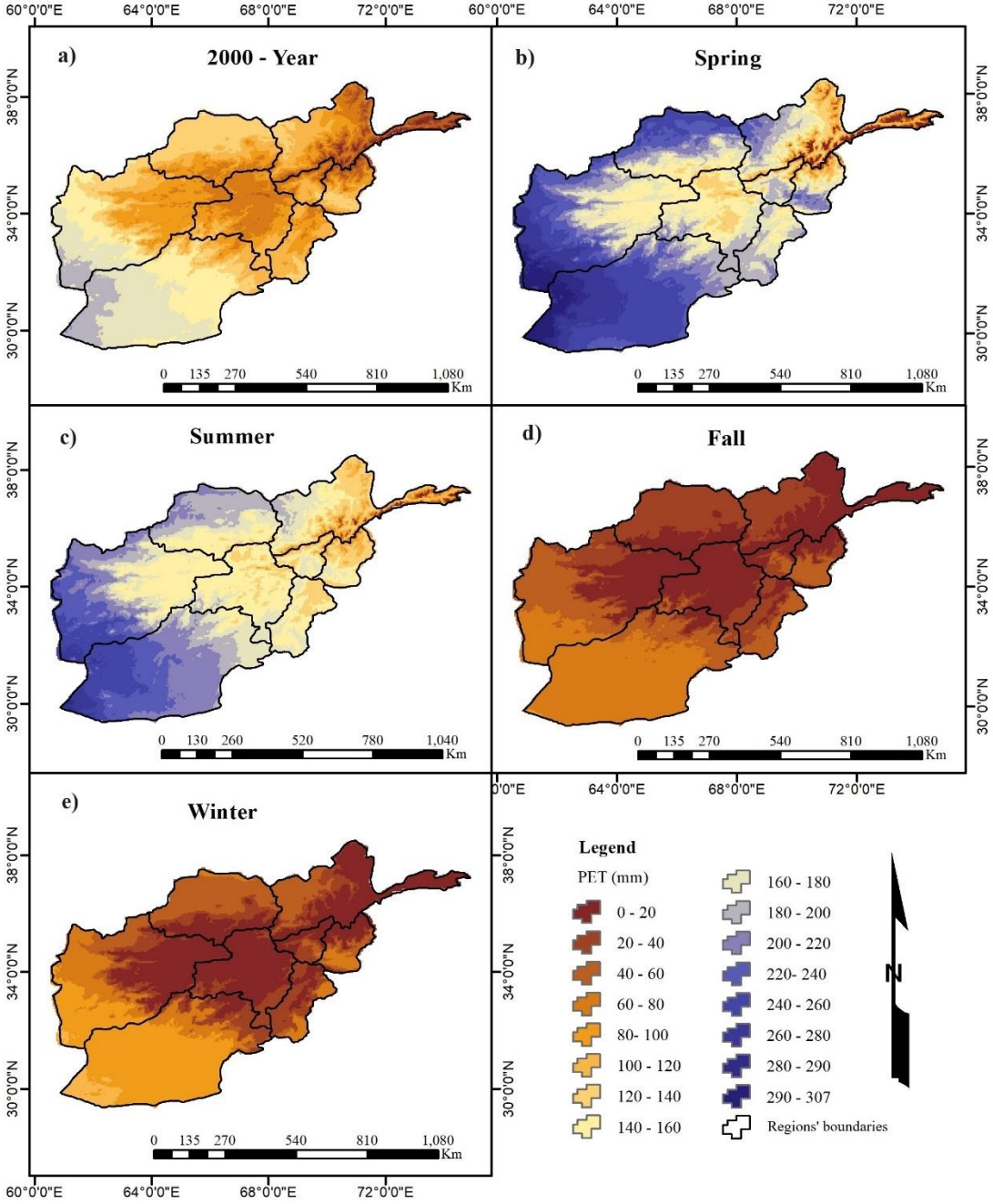

Figure 76. Spatial distribution of PET for 2000 year: 2000-year(a), Spring(b), Summer(c), Fall(d), Winter(e).

In the summer season, the highest amount of PET is produced in the South region due to rising temperatures. The production of PET in 2023 is greater than in 2000 and 2012, largely because the NDVI in the South region has significantly improved in recent years. Additionally, during the autumn season, the amount of PET in 2023 was also higher compared to 2000 and 2012.

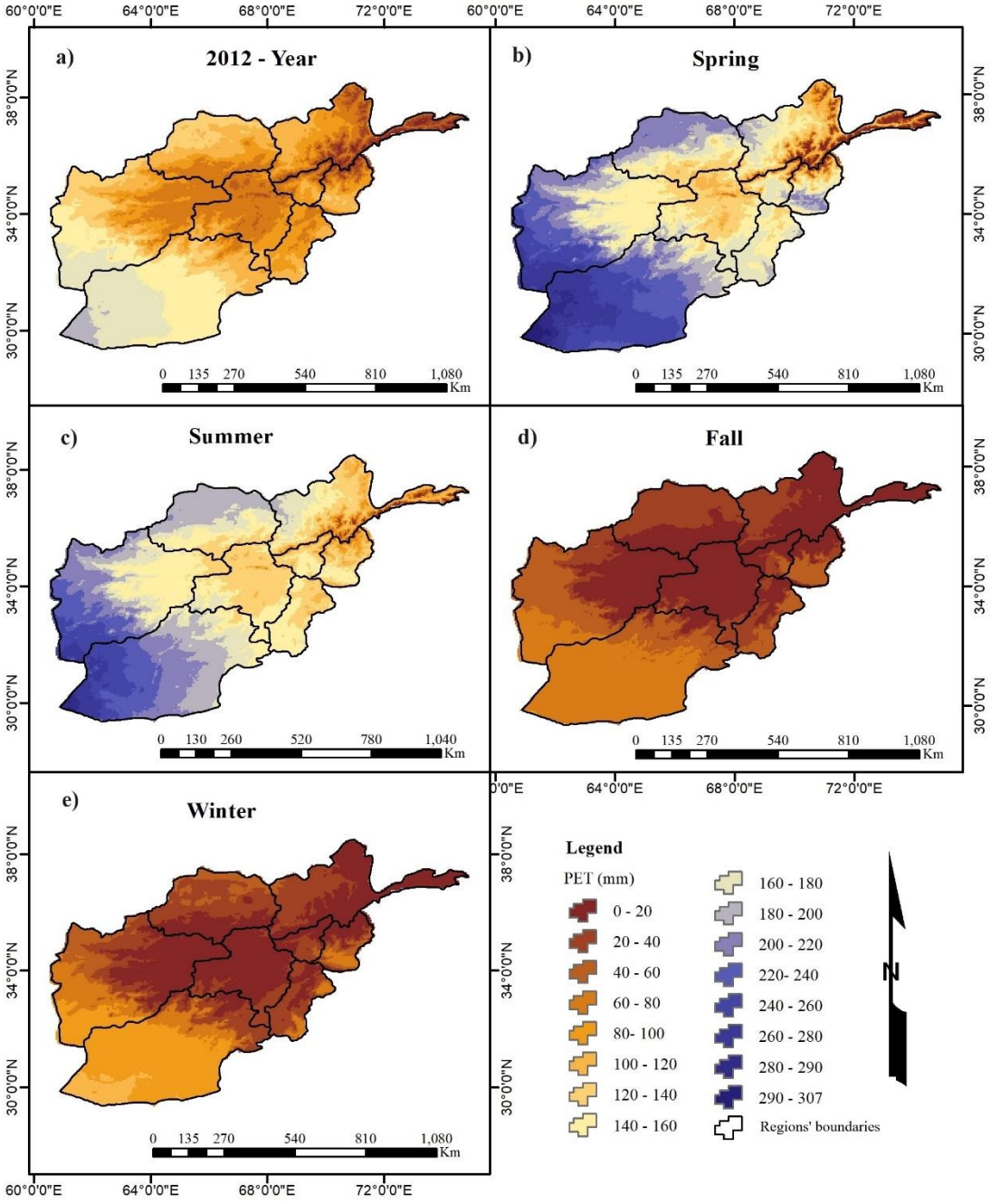

Figure 77. Spatial distribution of PET for 2012 year: 2012-year(a), Spring(b), Summer(c), Fall(d), Winter(e).

In 2012, the amount of PET in the north region was lower compared to 2000 and 2023. Although the rate of vegetation growth was high in 2012, a decrease in LST resulted in a lower observed PET (shown in Figure 78b).

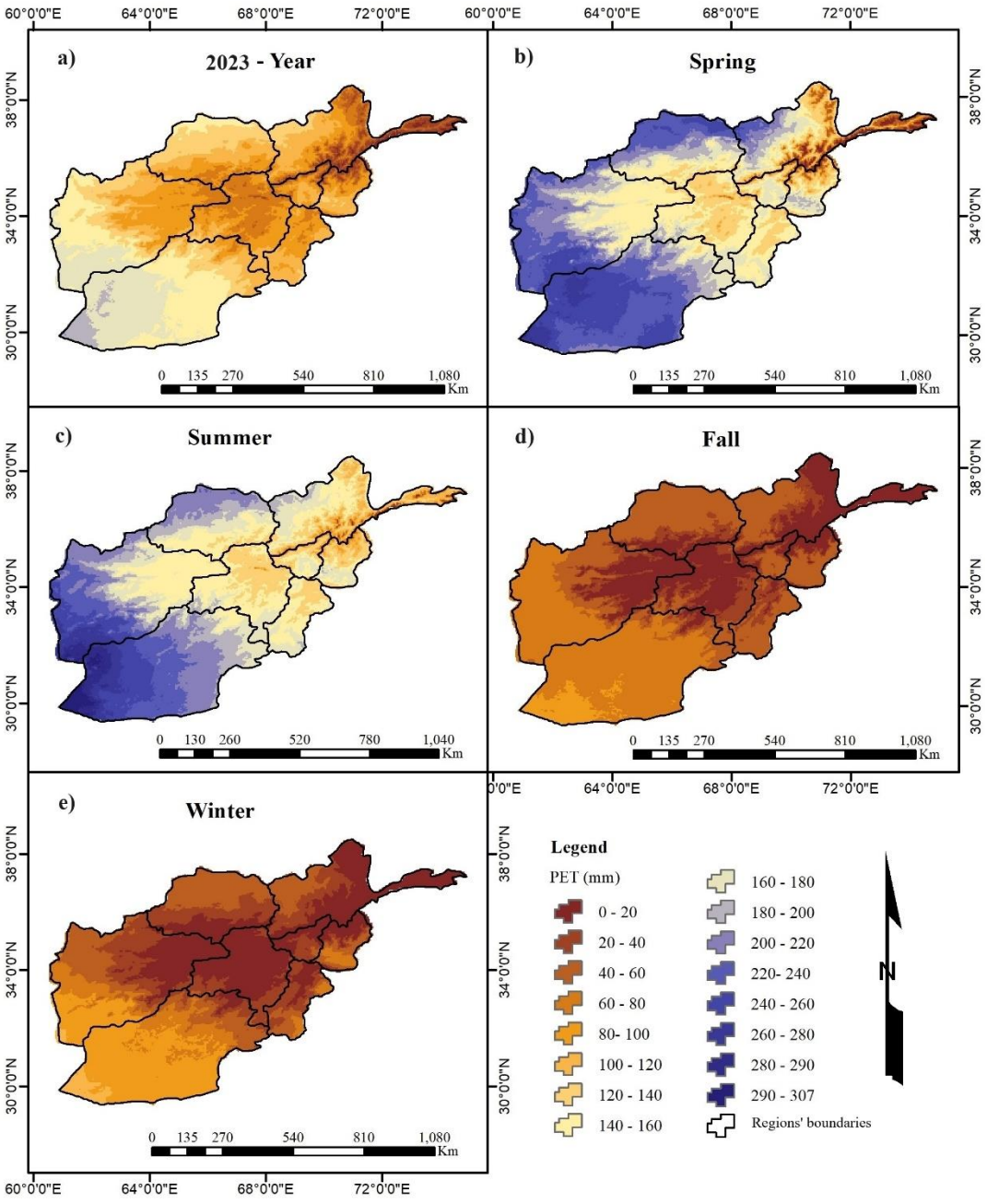

Figure 78. Spatial distribution of PET for 2023 year: 2023-year(a), Spring(b), Summer(c), Fall(d), Winter(e).

As shown in Figure 46, the precipitation levels in 2012 surpassed those recorded in both 2000 and 2023. In Afghanistan, the highest amount of precipitation is observed during

the winter and spring seasons. In this research, the unit of measurement for precipitation is mm/pentad, which indicates the amount of precipitation collected over a 5-day period (Zha et al., 2023). The highest levels of precipitation in Afghanistan occur in the Pamir and Hindu Kush mountains, while the South region experiences the lowest rainfall. In the spring season of 2023, the amount of precipitation in the South region was observed to be higher than in 2000 and 2012 (shown in Figure 81b).

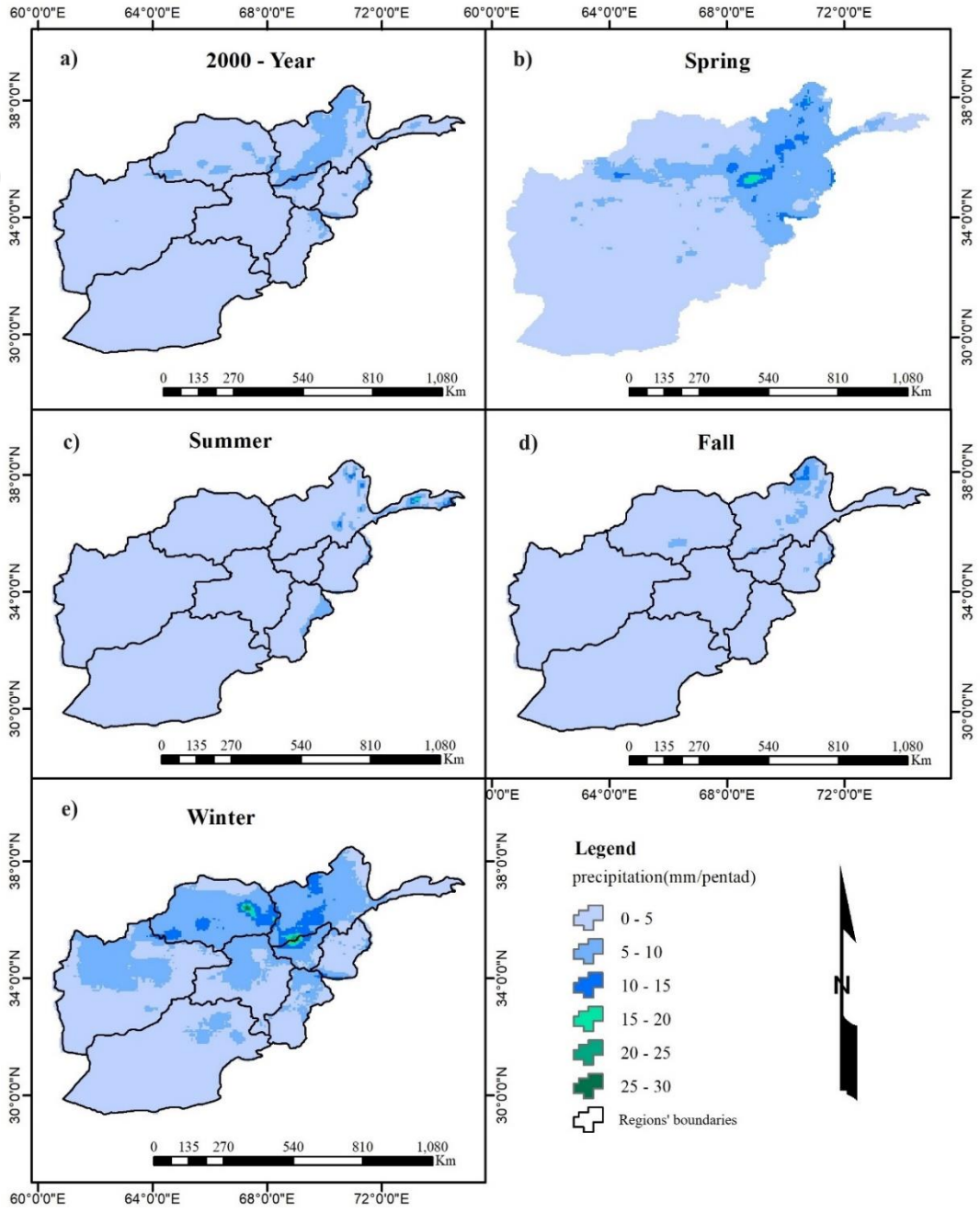

Figure 79. Spatial distribution of precipitation for 2023 year: 2023-year(a), Spring(b), Summer(c), Fall(d), Winter(e).

In the spring season of 2012, the amount of precipitation in the north and northeastern regions increased compared to 2000 and 2023 (shown in Figure 80b). Additionally, in 2023, higher precipitation levels were observed in the eastern and southeastern regions (shown in Figure 81b). Due to the Mediterranean climate, the eastern and southeastern regions occasionally experience rainfall in the summer; however, there is no significant difference in precipitation amounts across the years 2000, 2012, and 2023.

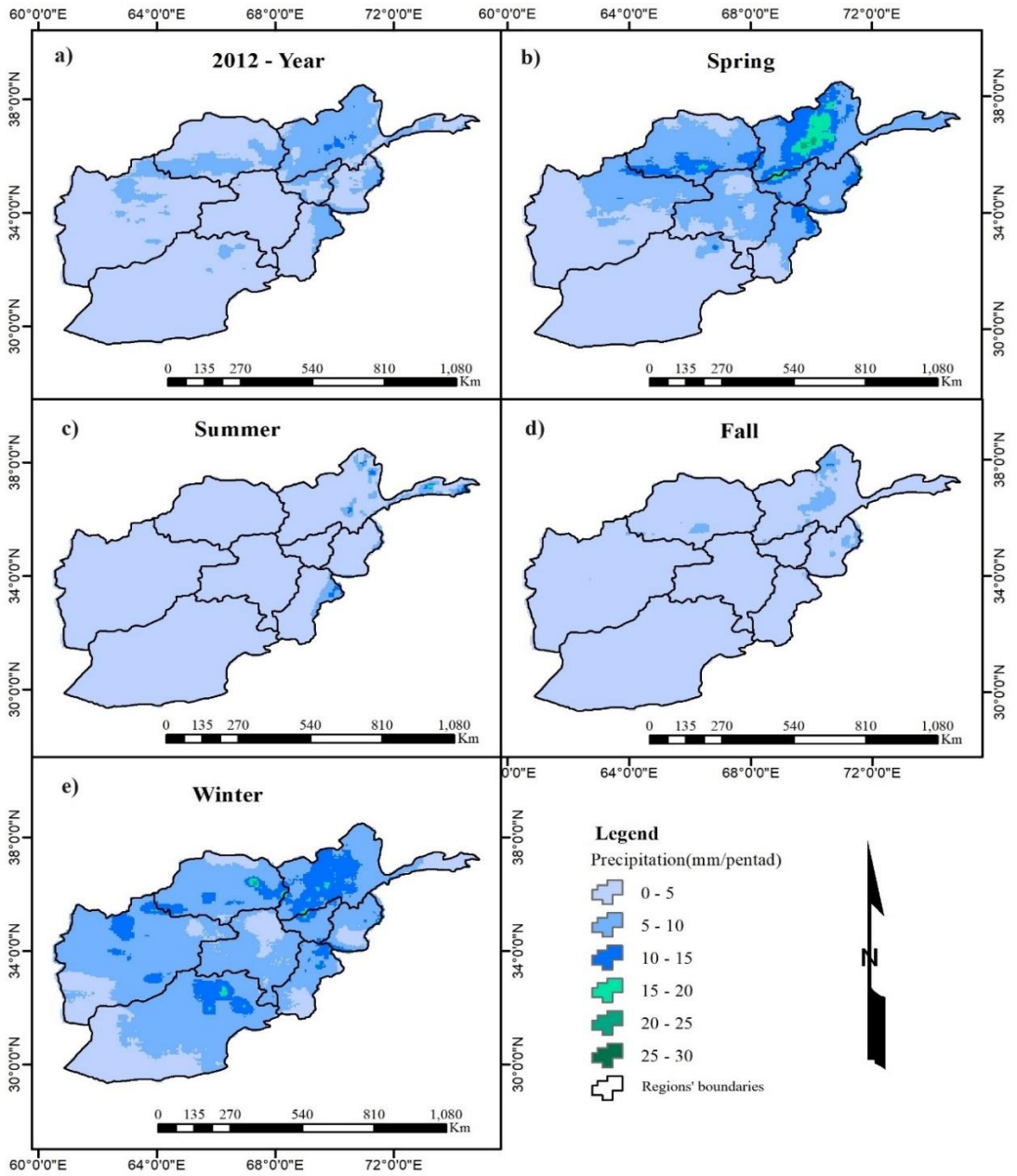

Figure 80. Spatial distribution of precipitation for 2012 year: 2012-year(a), Spring(b), Summer(c), Fall(d), Winter(e).

In the fall season of 2023, precipitation levels across Afghanistan were lower compared to 2000 and 2012 (shown in Figure 81d). Additionally, during the winter season of 2012, the highest amounts of precipitation were observed in the South, western, and west-central regions (shown in Figure 80e).

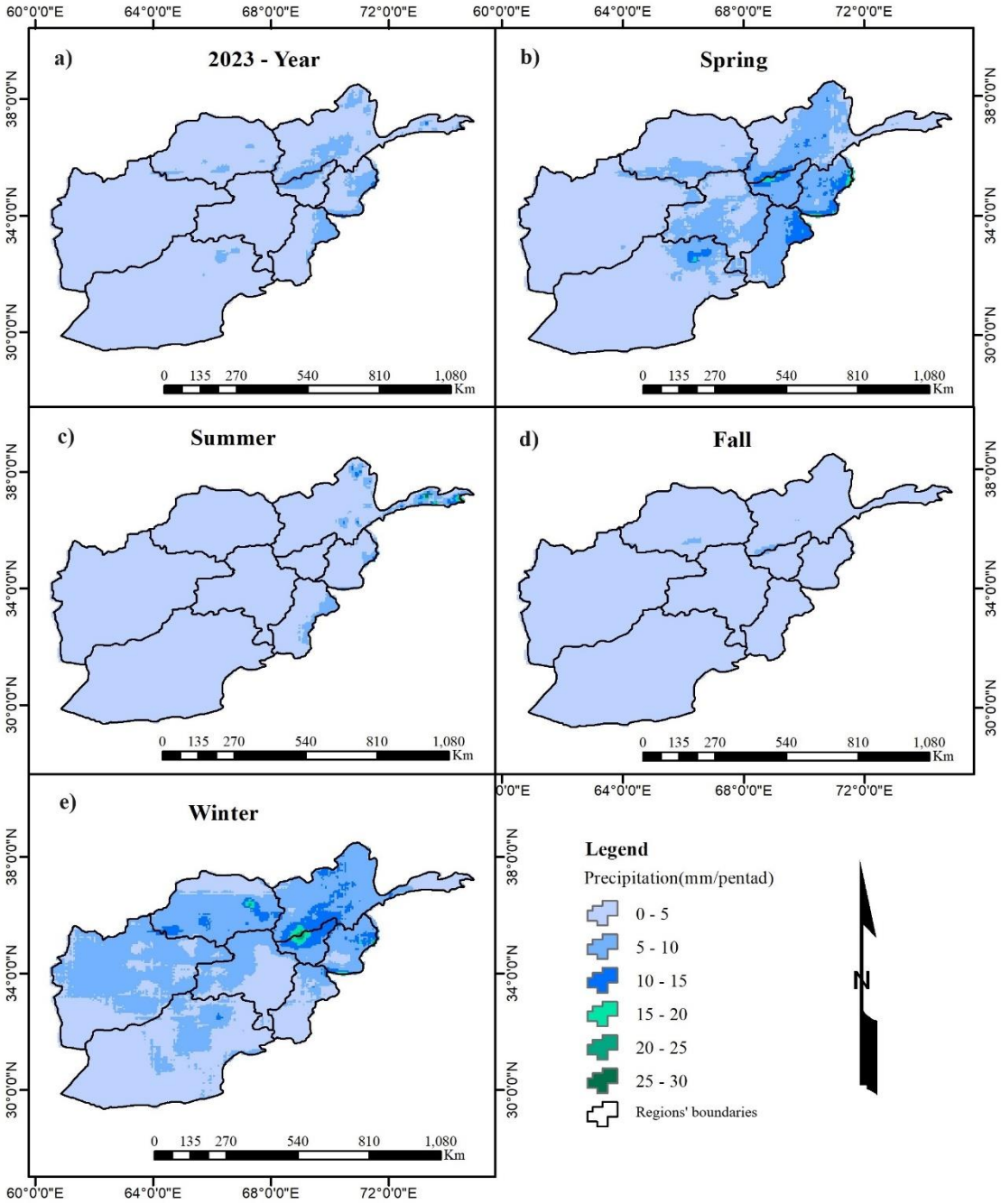

Figure 81. Spatial distribution of Precipitation for 2023 year: 2023-year(a), Spring(b), Summer(c), Fall(d), Winter(e).

In Afghanistan, the north, western, South, and southeastern regions experience high temperatures, leading to highly permeable soils and rocks that contribute to water loss. Consequently, soil moisture levels in these areas are low, ranging between 0-10 mm, and tend to dry up as LST increases. In 2000, due to a decrease in NDVI and an increase in LST, soil moisture levels in 2012 were observed to be higher than in both 2000 and 2023 (shown in Figure 83a).

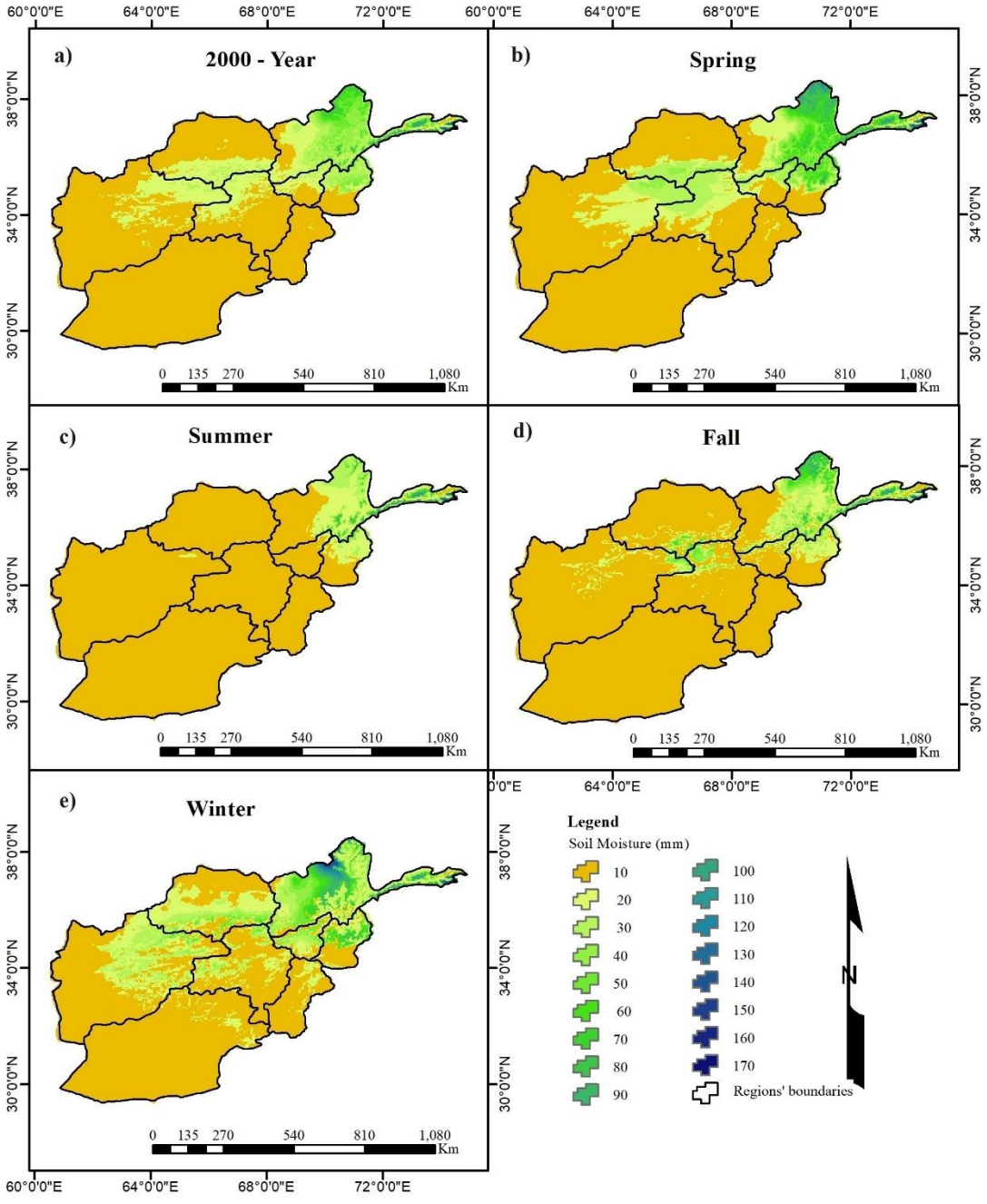

Figure 82. Spatial distribution of Soil Moisture for 2000 year: 2000-year(a), Spring(b), Summer(c), Fall(d), Winter(e).

The snow in the Pamir areas is more susceptible to heat during the summer season, leading to an increase in soil moisture levels as the snow melts. This increase was particularly pronounced in 2012. Additionally, the highest amount of soil moisture during the winter season was observed in the South region in 2012 (shown in Figure 83e).

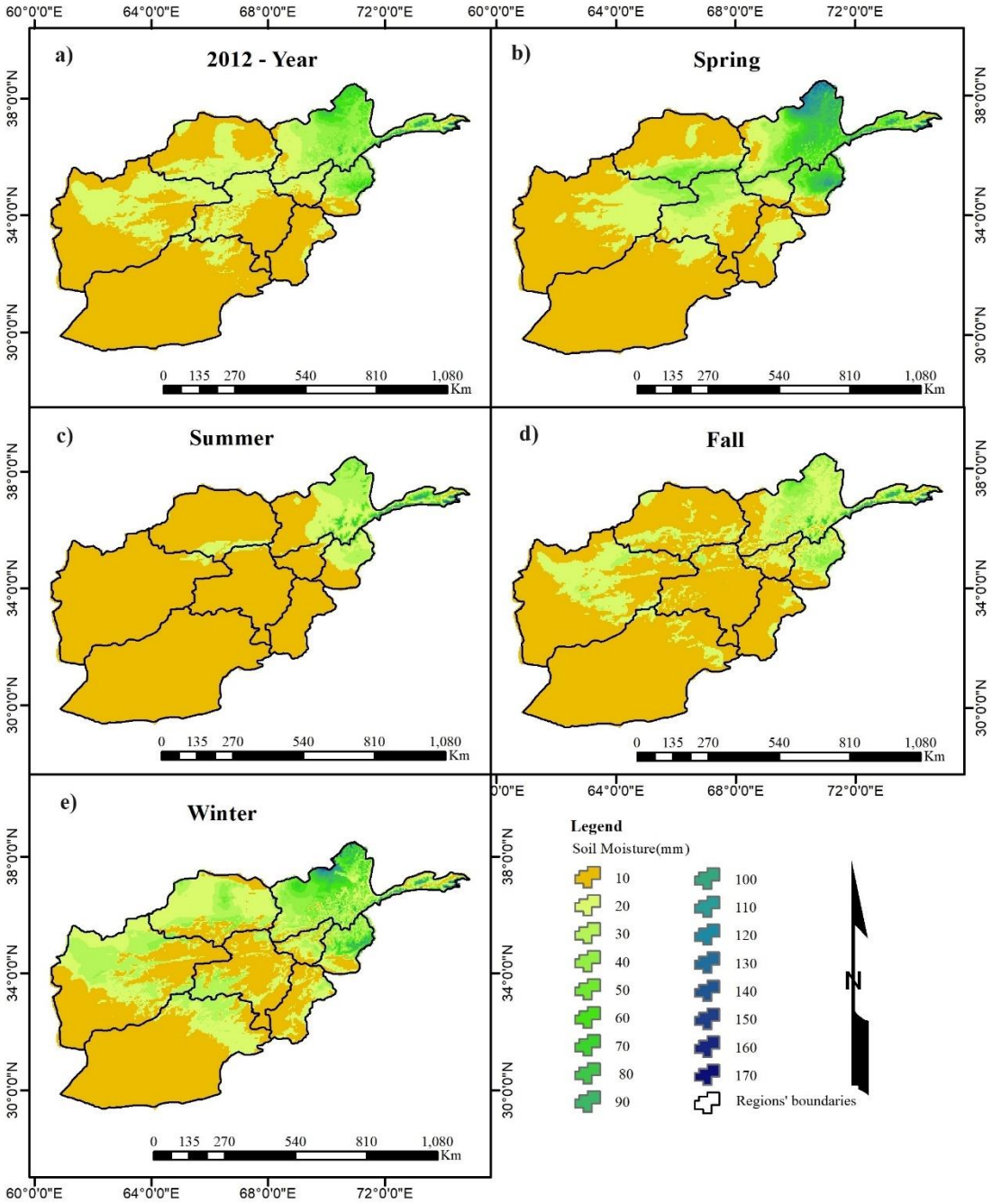

Figure 83. Spatial distribution of Soil Moisture for 2012 year: 2012-year(a), Spring(b), Summer(c), Fall(d), Winter(e).

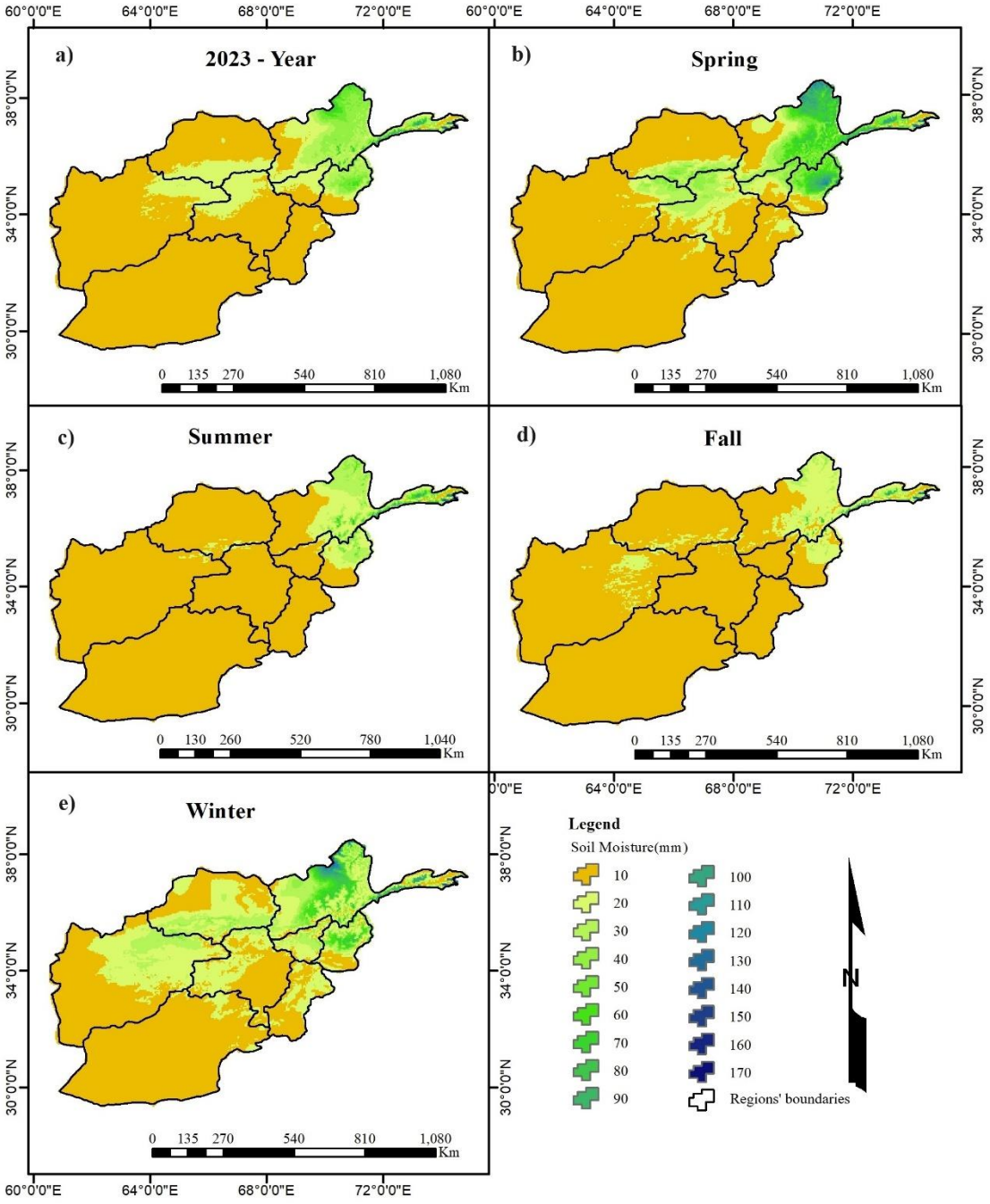

Figure 84. Spatial distribution of Soil Moisture for 2023 year: 2023-year(a), Spring(b), Summer(c), Fall(d), Winter(e).

In this research, the Ta paramerter was calculated as an average at 2 meters above the ground. As discussed regarding land surface temperature (LST), the hottest regions of Afghanistan are the South and north areas, where the highest Ta were recorded. As shown in Figure 85, the air temperature in 2000 was higher than in both 2012 and 2023. In the spring of 2000, the air temperature in the north region and parts of the northeastern region

reached an average of 30°C. However, this temperature decreased in 2012 and increased again in 2023, mirroring similar trends observed in the South region and parts of the western region.

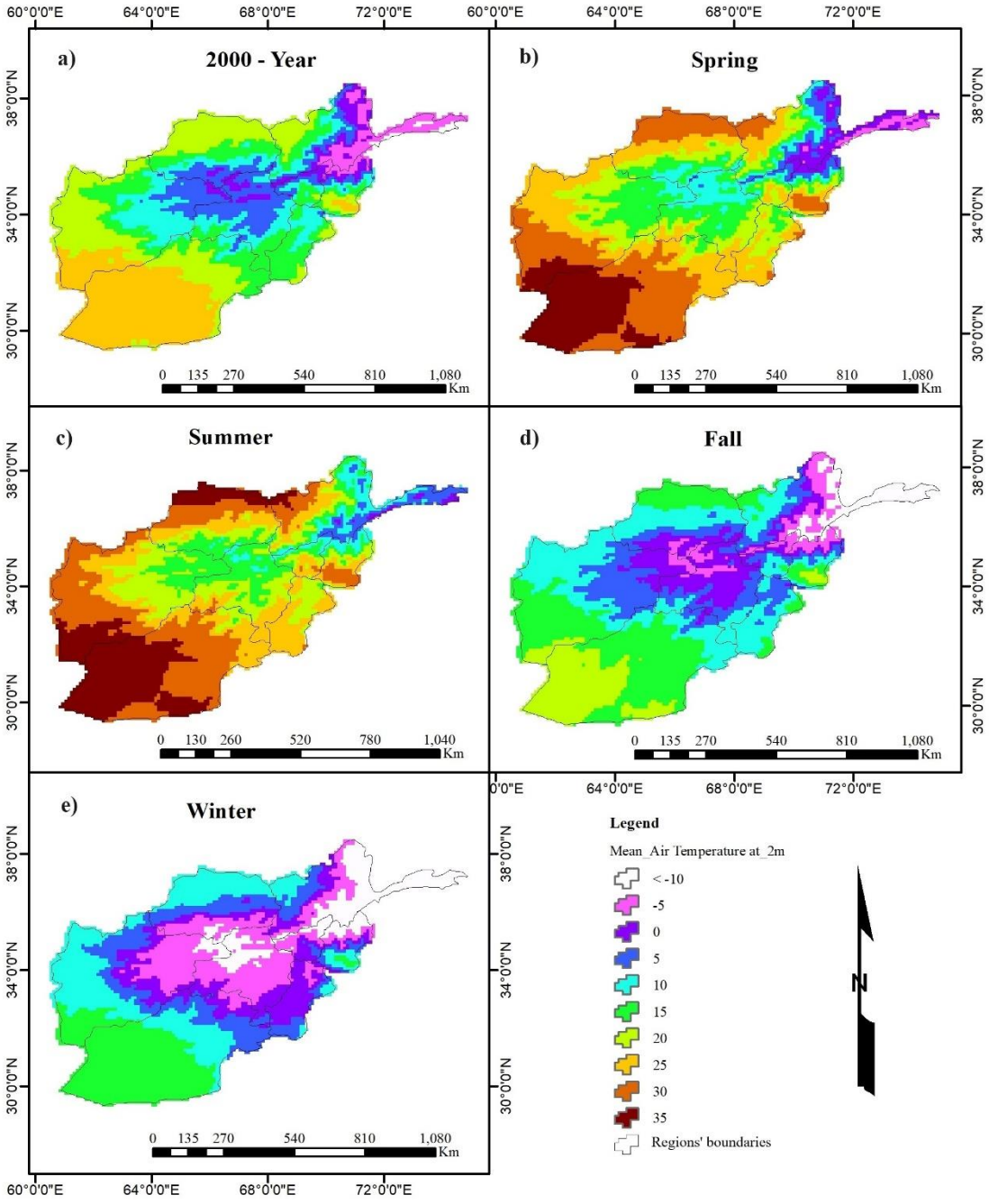

Figure 85. Spatial distribution of Ta for 2000 year: 2000-year(a), Spring(b), Summer(c), Fall(d), Winter(e).

In the summer season of 2023, the air temperature (Ta) in the eastern and South regions has slightly increased compared to 2000 and 2012 (shown in Figure 87c). Additionally, in

the fall of 2023, Ta has risen in the South, western, north, and southeastern regions compared to the same years. The air temperature in the central regions of Afghanistan during the winter of 2012 fell below -5°C, making it significantly colder than in 2000 and 2023. In contrast, the South region was warmer in the winter of 2023 compared to both 2000 and 2012 (shown in Figure 87e). Furthermore, the temperature in the Pamir region of the northeast was also warmer in the spring of 2023 than in 2000 and 2012.

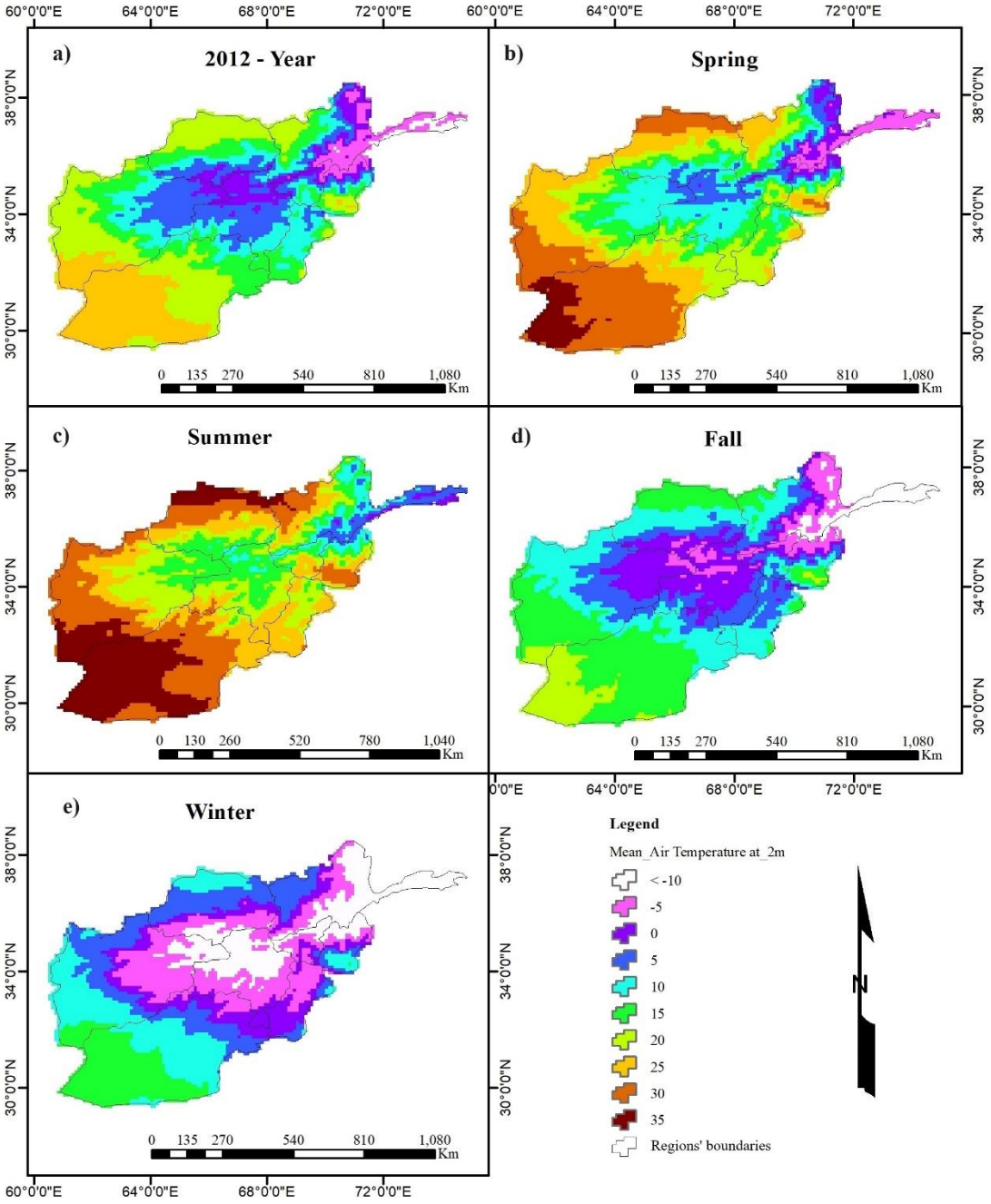

Figure 86. Spatial distribution of Ta for 2012 year: 2012-year(a), Spring(b), Summer(c), Fall(d), Winter(e).

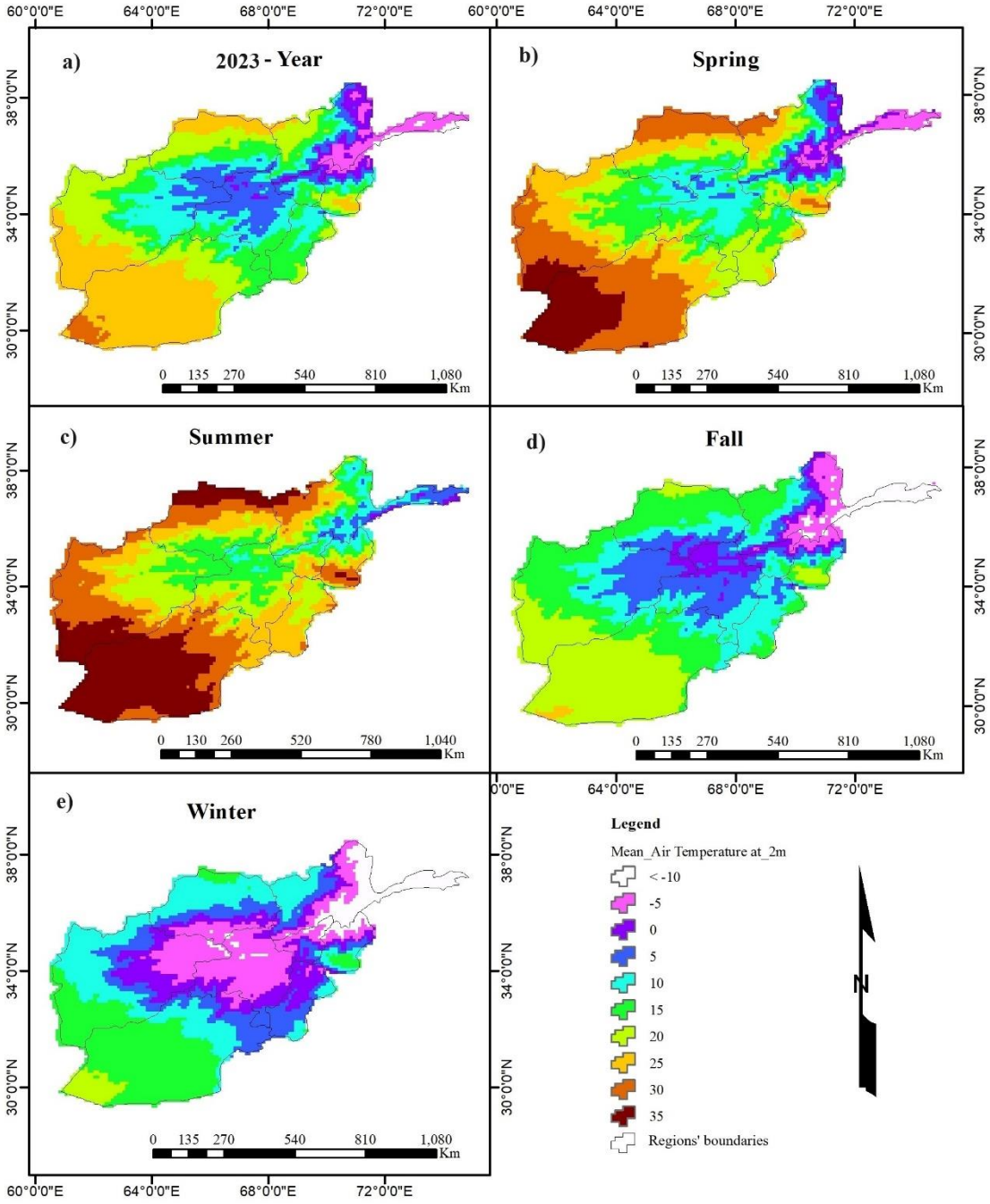

Figure 87. Spatial distribution of Ta for 2023 year: 2023-year(a), Spring(b), Summer(c), Fall(d), Winter(e).

In Afghanistan, the western region experiences the highest wind speeds, with mean values reaching up to 15 m/s. The peak wind speed was recorded in 2012 (shown in Figure 89). Wind speed plays a crucial role in reducing soil moisture; regions with higher wind speeds tend to show a decrease in soil moisture levels. Conversely, as soil moisture levels rise, NDVI levels tend to decline.

Wind speeds are typically higher during the warm season, making summer the period with the most significant wind activity. In the spring of 2000 and 2012, wind speeds in the western region peaked at 9-11 m/s, while in 2023, they decreased to 7-9 m/s. In contrast, wind speeds in the north region increased to 5-7 m/s in 2023 compared to 2000 and 2012 (shown in Figures 88b, 89b, and 90b).

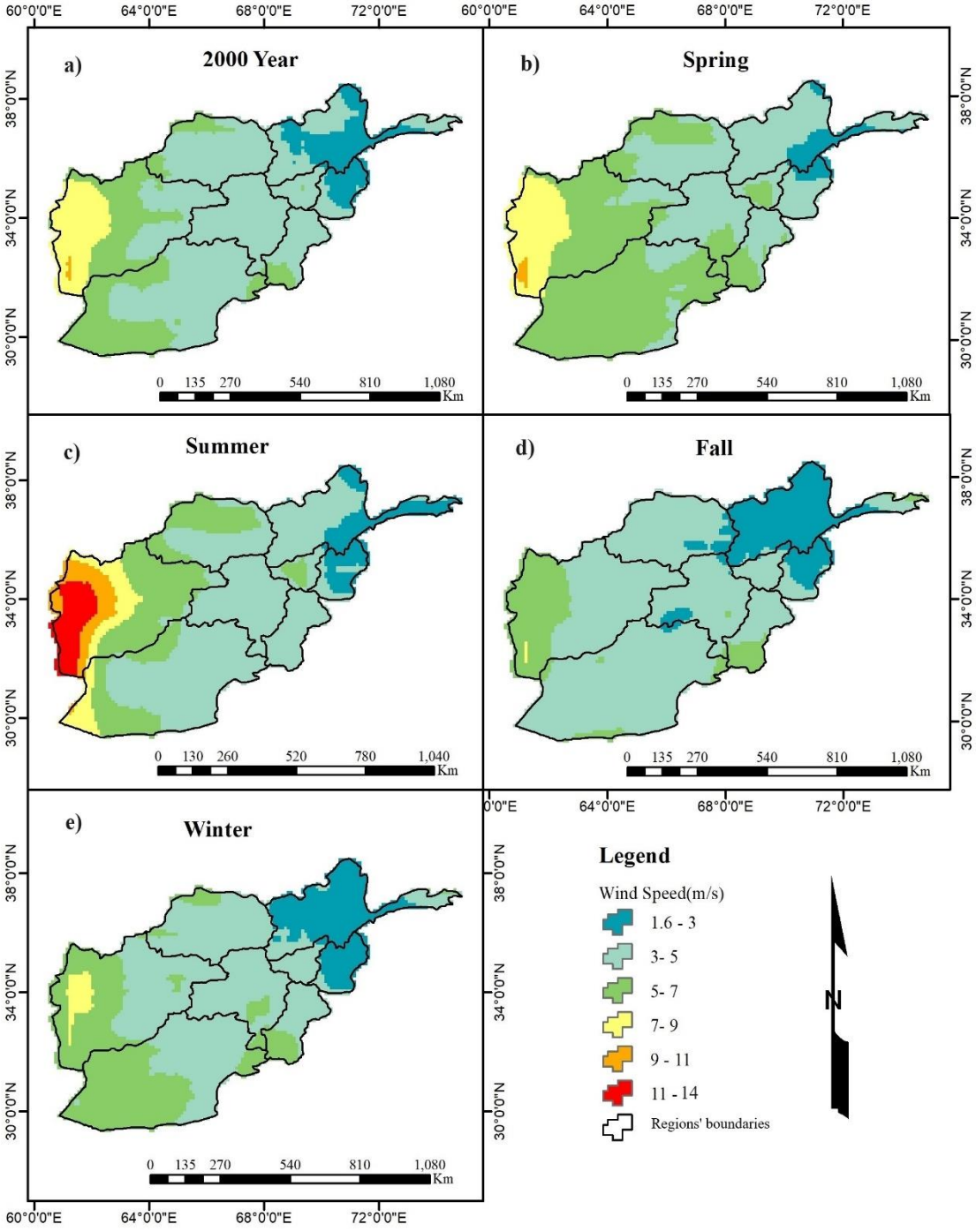

Figure 88. Spatial distribution of Wind Speed for 2000 year: 2000-year(a), Spring(b), Summer(c), Fall(d), Winter(e).

As shown in Figure 90, wind speeds across Afghanistan during the summer season of 2023 have increased compared to 2000 and 2012. This increase is particularly notable in the north and central regions, where wind speeds have risen to 7-9 m/s. In contrast, wind speeds on the slopes of the Pamir and Hindu Kush mountains remain very low due to the mountainous terrain.

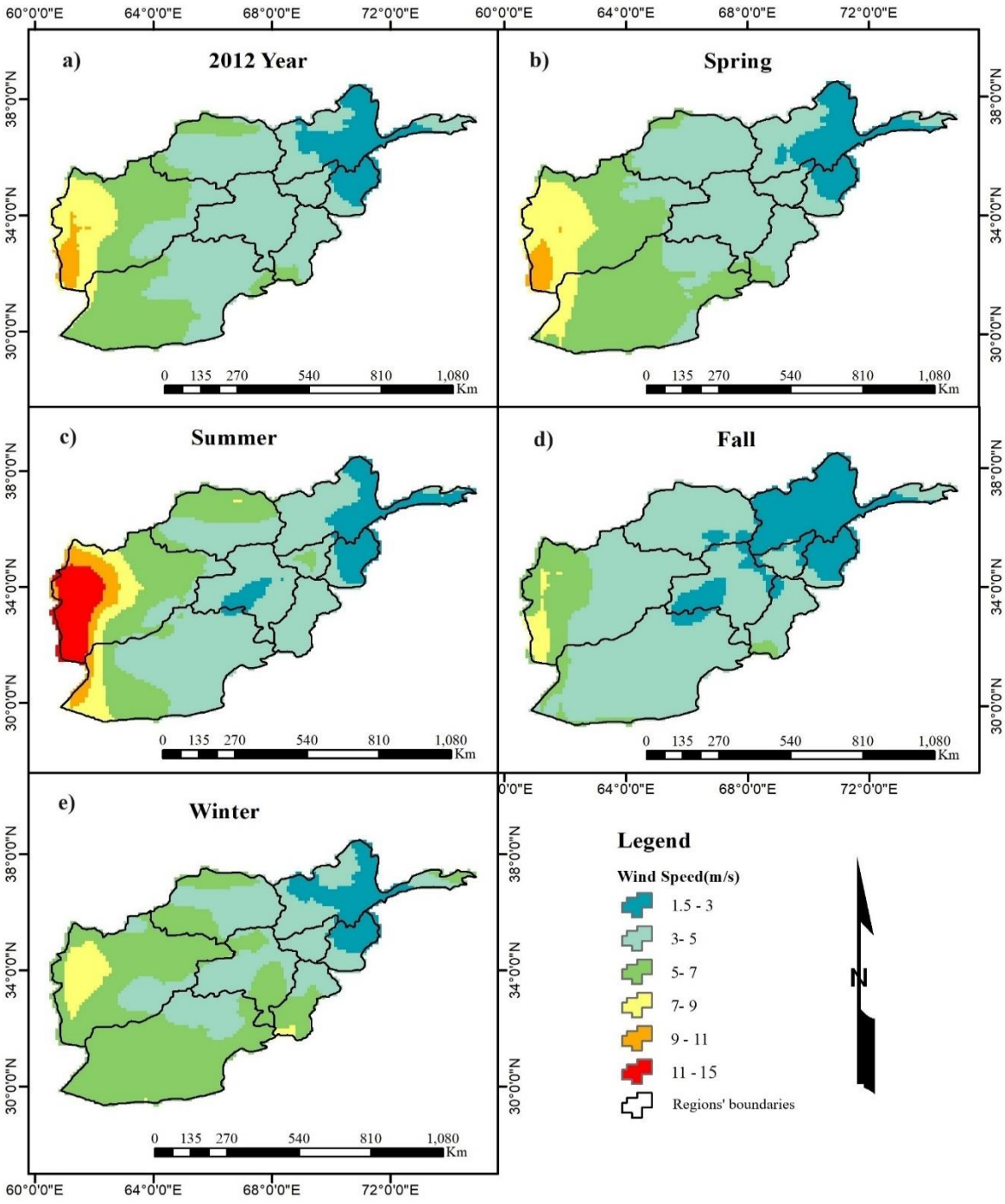

Figure 89. Spatial distribution of Wind Speed for 2012 year: 2012-year(a), Spring(b), Summer(c), Fall(d), Winter(e).

In the fall season of 2012, wind speeds in the western region increased to 9-11 m/s compared to 2000 and 2023 (shown in Figure 89d). Similarly, during the winter of 2012, wind speeds across Afghanistan were higher than in both 2000 and 2023 (shown in Figure 89e). In the winter of 2012, wind speeds in the north, South, and western regions were greater than those recorded in 2000 and 2023.

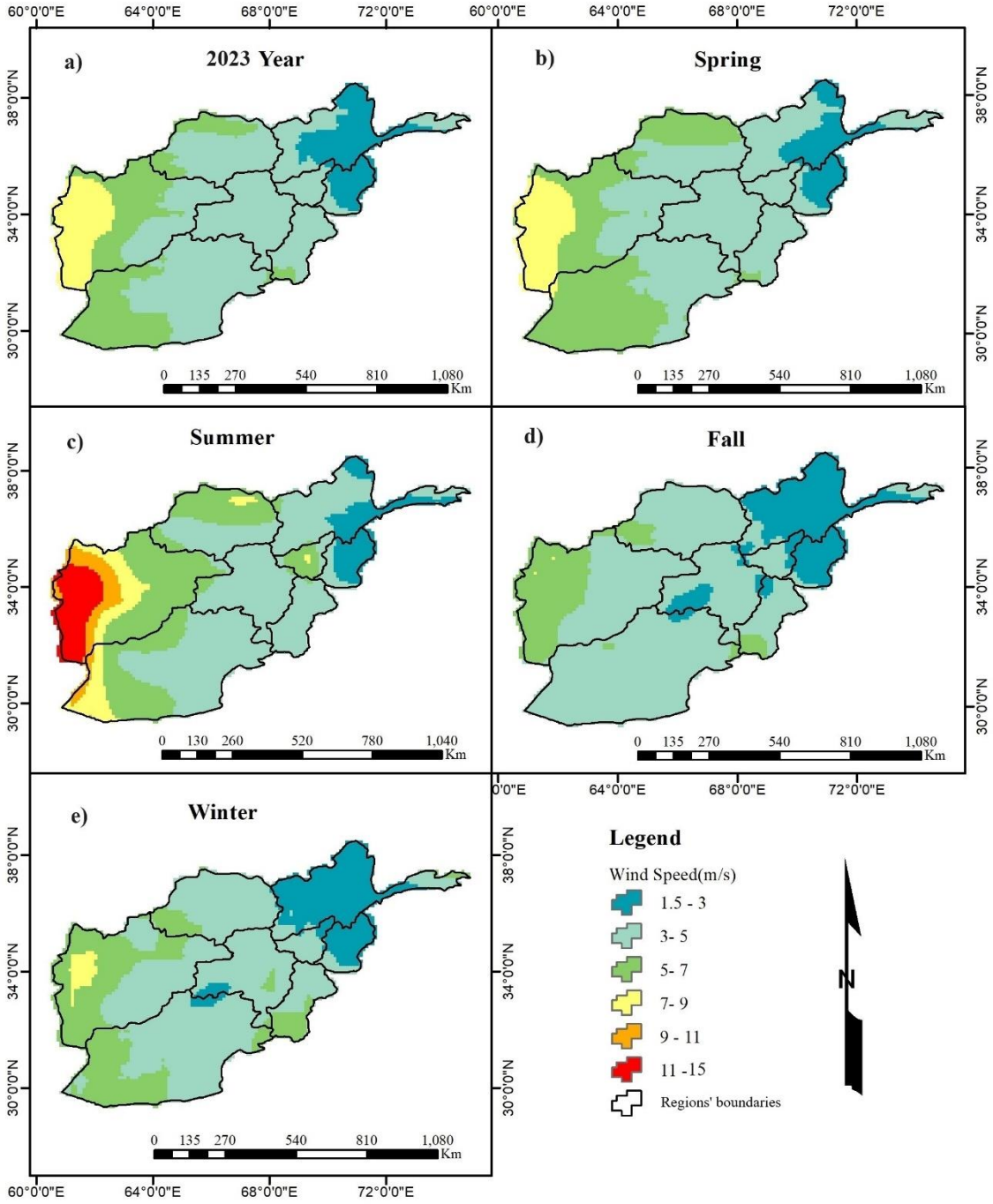

Figure 90. Spatial distribution of Wind Speed for 2023 year: 2023-year(a), Spring(b), Summer(c), Fall(d), Winter€.

In 2000, with the increase in LST, the amount of VCI decreased significantly, indicating that Afghanistan faced severe drought during those years. The most land of north and northeast region are agricultural land which is the faced drought in the spring and summer of 2000.

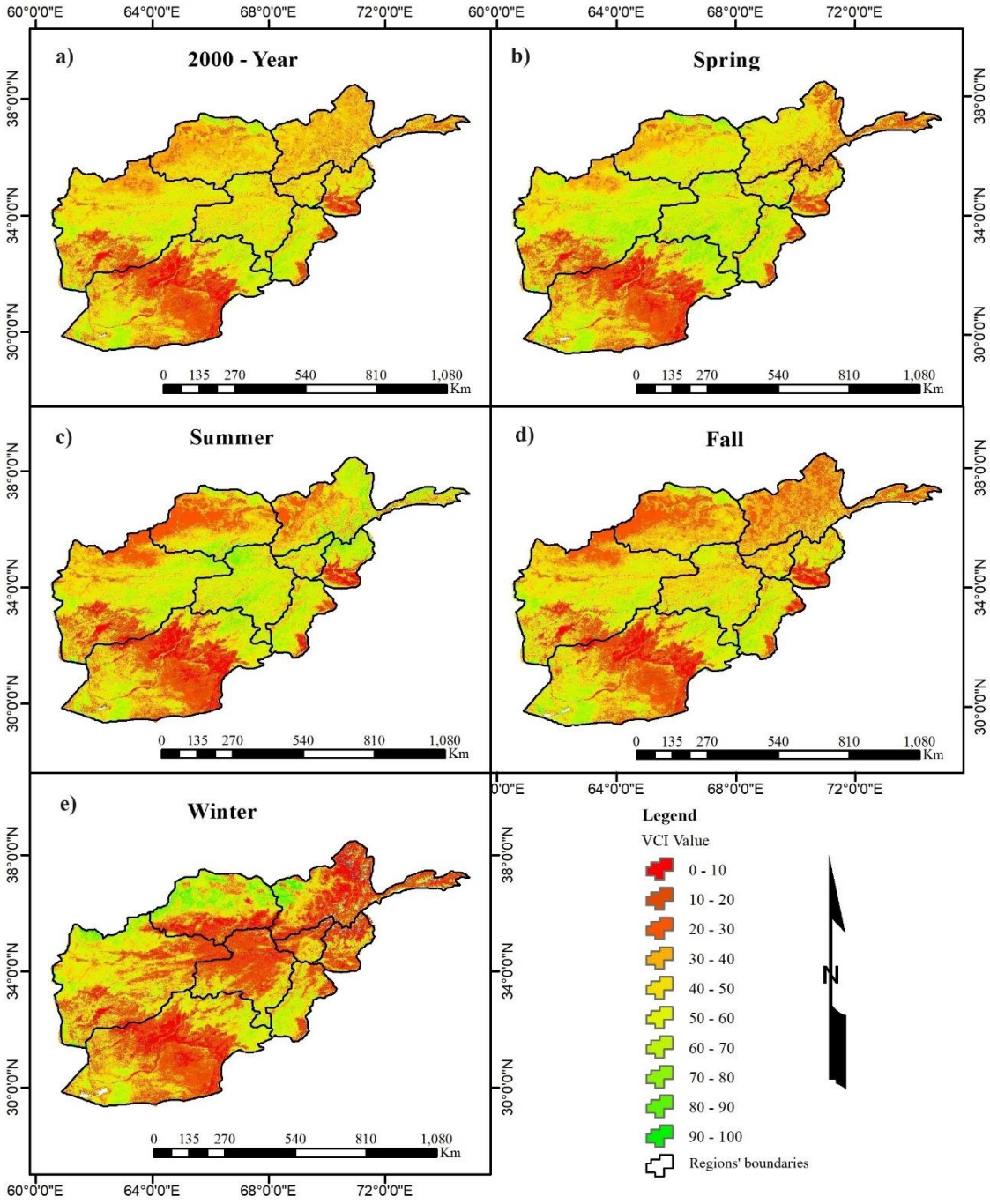

Figure 91. Spatial distribution of VCI for 2000 year: 2000-year(a), Spring(b), Summer(c), Fall(d), Winter(e).

Overall, the VCI in Afghanistan showed significant growth in 2012 compared to 2000 and 2023. In 2012, both NDVI and soil moisture levels were high, contributing to an increased VCI level, indicating a wet year. In the spring of 2012, the VCI notably increased in the north, northeastern, western, central-western, and southeastern regions (shown in Figure 92b).

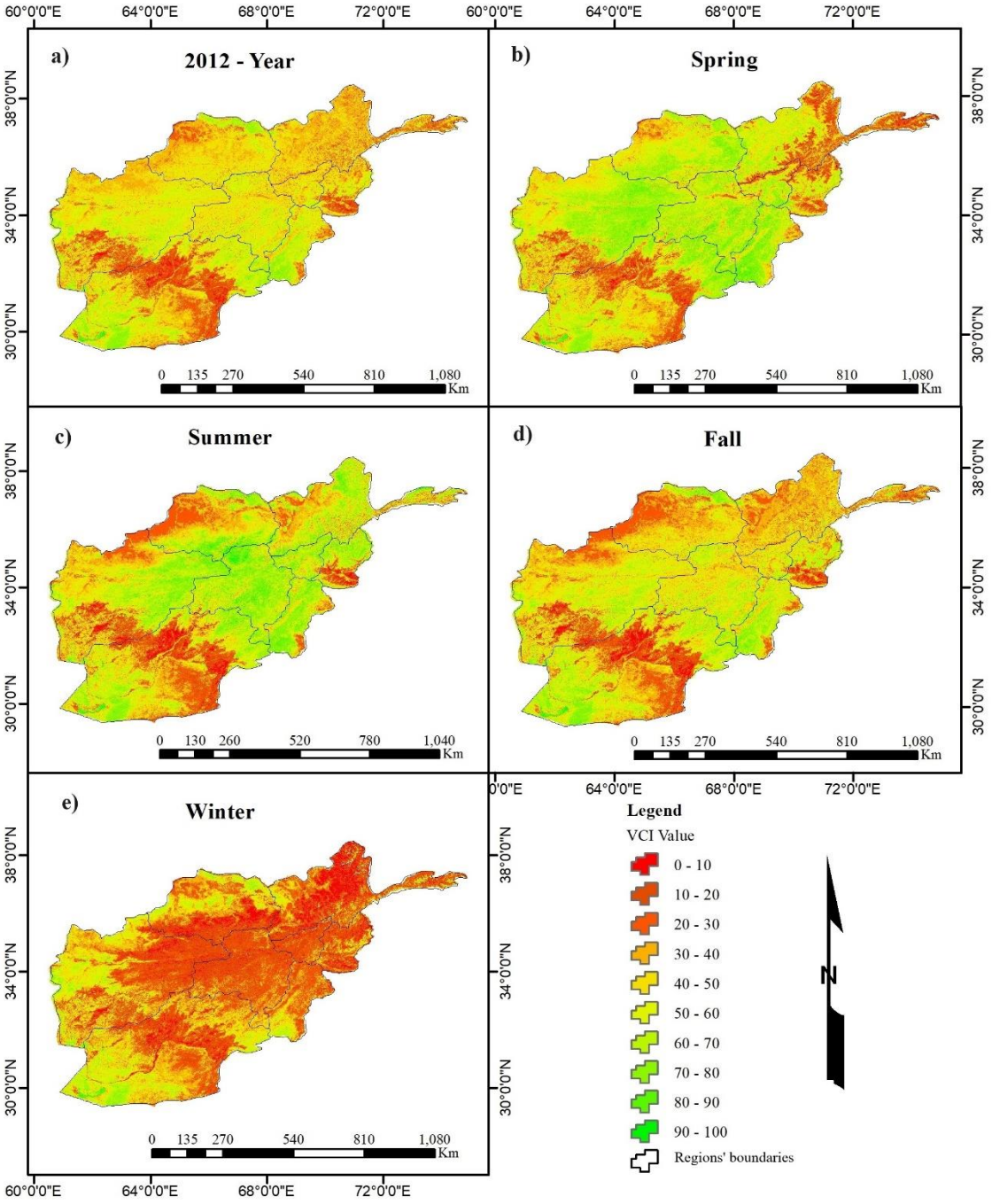

Figure 92. Spatial distribution of VCI for 2012 year: 2012-year(a), Spring(b), Summer(c), Fall(d), Winter.

The VCI in the South and western regions was very low in 2000, correlating with the increase in LST. However, it saw a significant increase in 2012 and 2023, attributed to the utilization of underground water by solar panels. During the summer, the melting snow in the northeastern regions (Pamir and Hindu Kush) leads to a decrease in LST, promoting the growth of NDVI and, consequently, an increase in VCI levels.

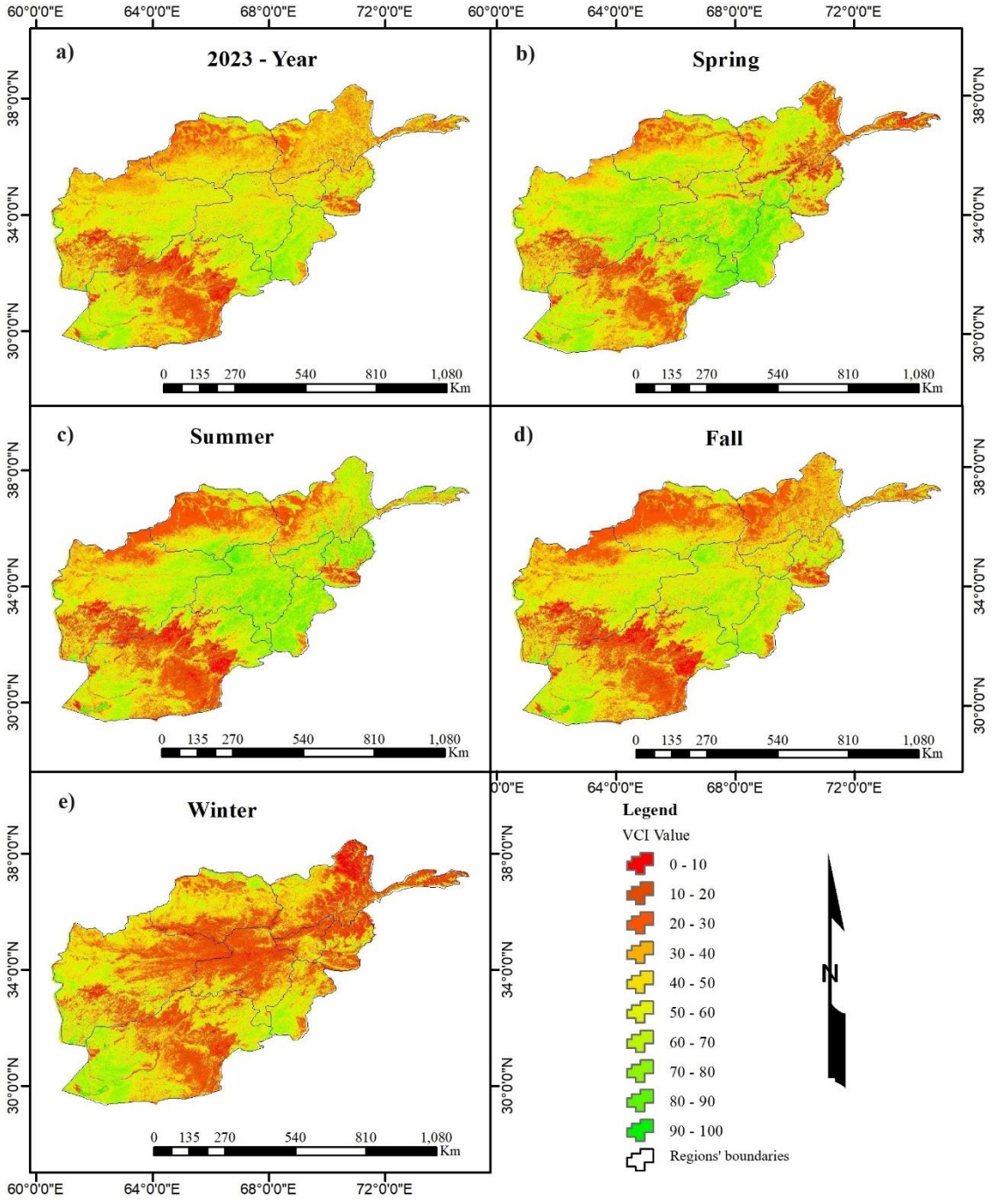

Figure 93. Spatial distribution of VCI for 2023 year: 2023-year(a), Spring(b), Summer(c), Fall(d), Winter(e).

The increase in LST led to a decrease in the TCI level for the year 2000 in Afghanistan, resulting in drought conditions. In the spring of 2000, drought was observed across all parts of Afghanistan. However, this trend shifted in 2012, when moderate to mild drought conditions emerged in the north, northeastern, western, and South regions. By 2023, the TCI levels increased in the South and southeastern regions, contributing to a greater incidence of wet years in these areas (shown in Figure 95 and Figure 96).

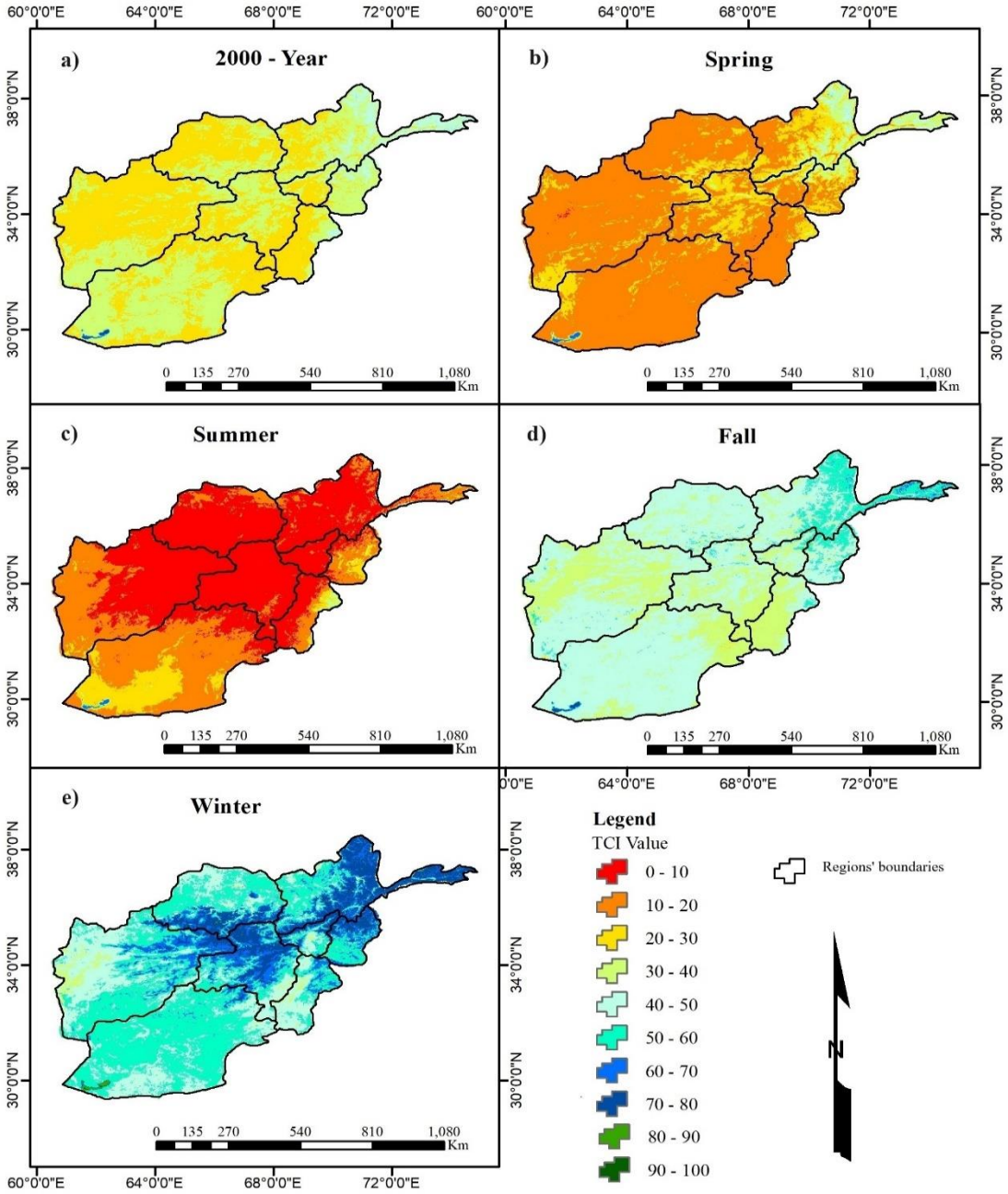

Figure 94. Spatial distribution of TCI for 2000 year: 2000-year(a), Spring(b), Summer(c), Fall(d), Winter(e).

In the summer season, some farms are harvested and the LST level continues to increase, resulting in a very low TCI. In the summer season, the TCI index has higher amount in the south, east and southeast regions than in other regions.

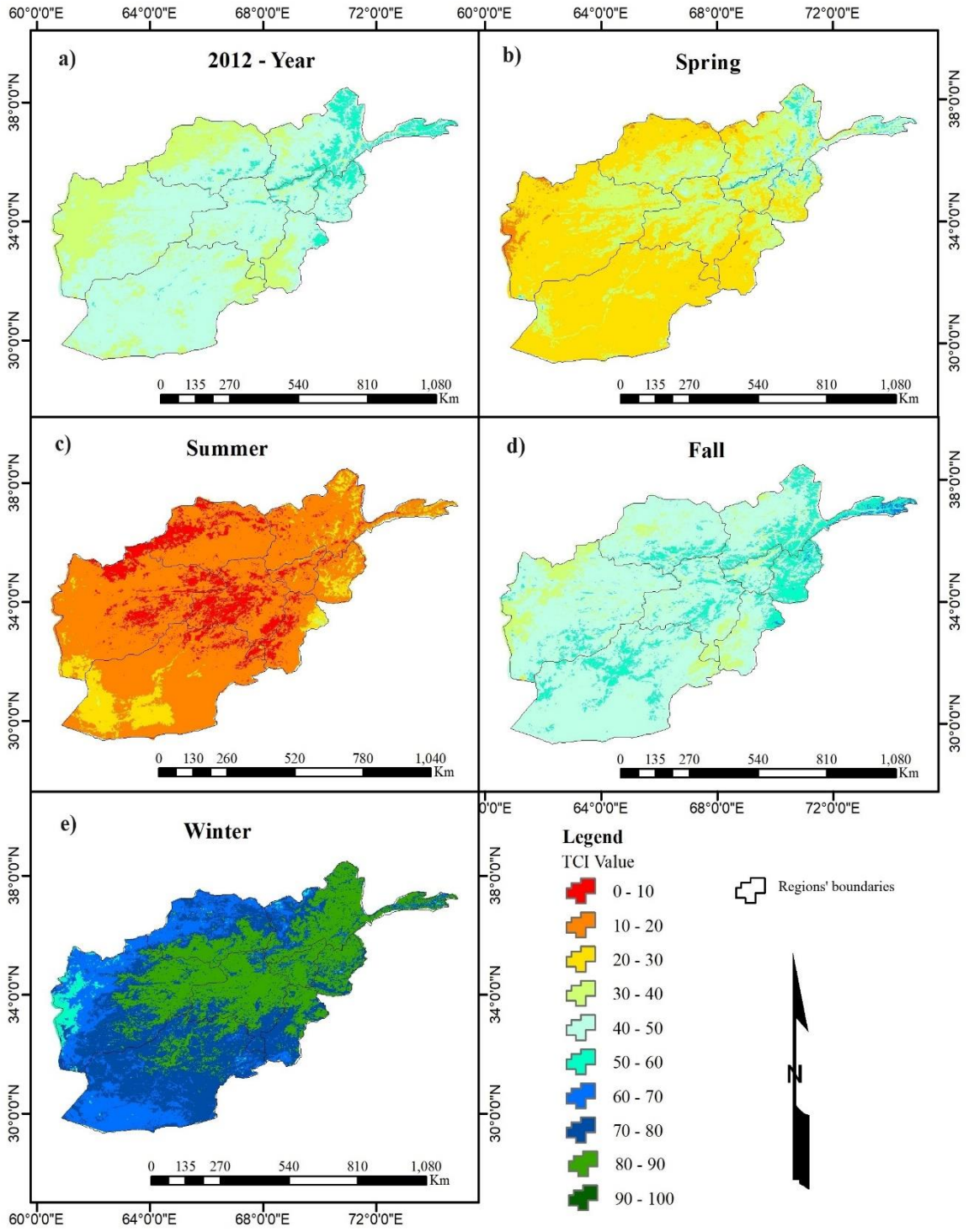

Figure 95. Spatial distribution of TCI for 2012 year: 2012-year(a), Spring(b), Summer(c), Fall(d), Winter(e).

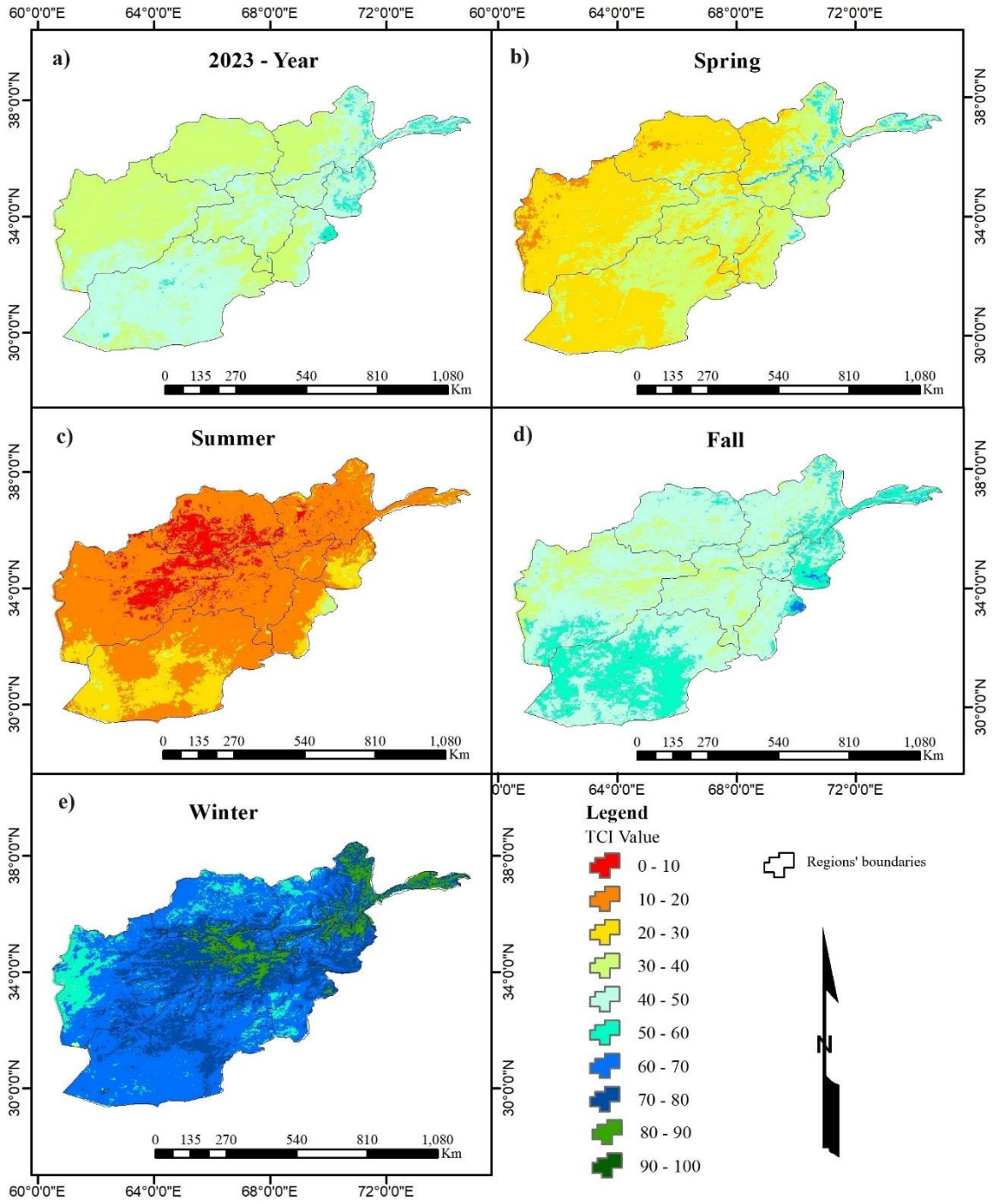

Figure 96. Spatial distribution of TCI for 2023 year: 2023-year(a), Spring(b), Summer(c), Fall(d), Winter(e).

To assess drought conditions, the VHI index, derived from both the TCI and VCI indices, is utilized. As illustrated by the VHI index, the value of VHI in 2012 was higher than in both 2000 and 2023, indicating that 2012 was a wetter year. In 2000, significant portions of the north, northeast, west, and south regions experienced drought. Specifically, in the spring of 2000, the VHI in the north region was low, contributing to severe drought in

that area. However, conditions improved in 2012, only for drought conditions to re-emerge in 2023. In the spring of 2000, the South region also exhibited low VHI levels, which improved in 2012, although some areas reverted to drought conditions by 2023 (shown in Figure 99c).

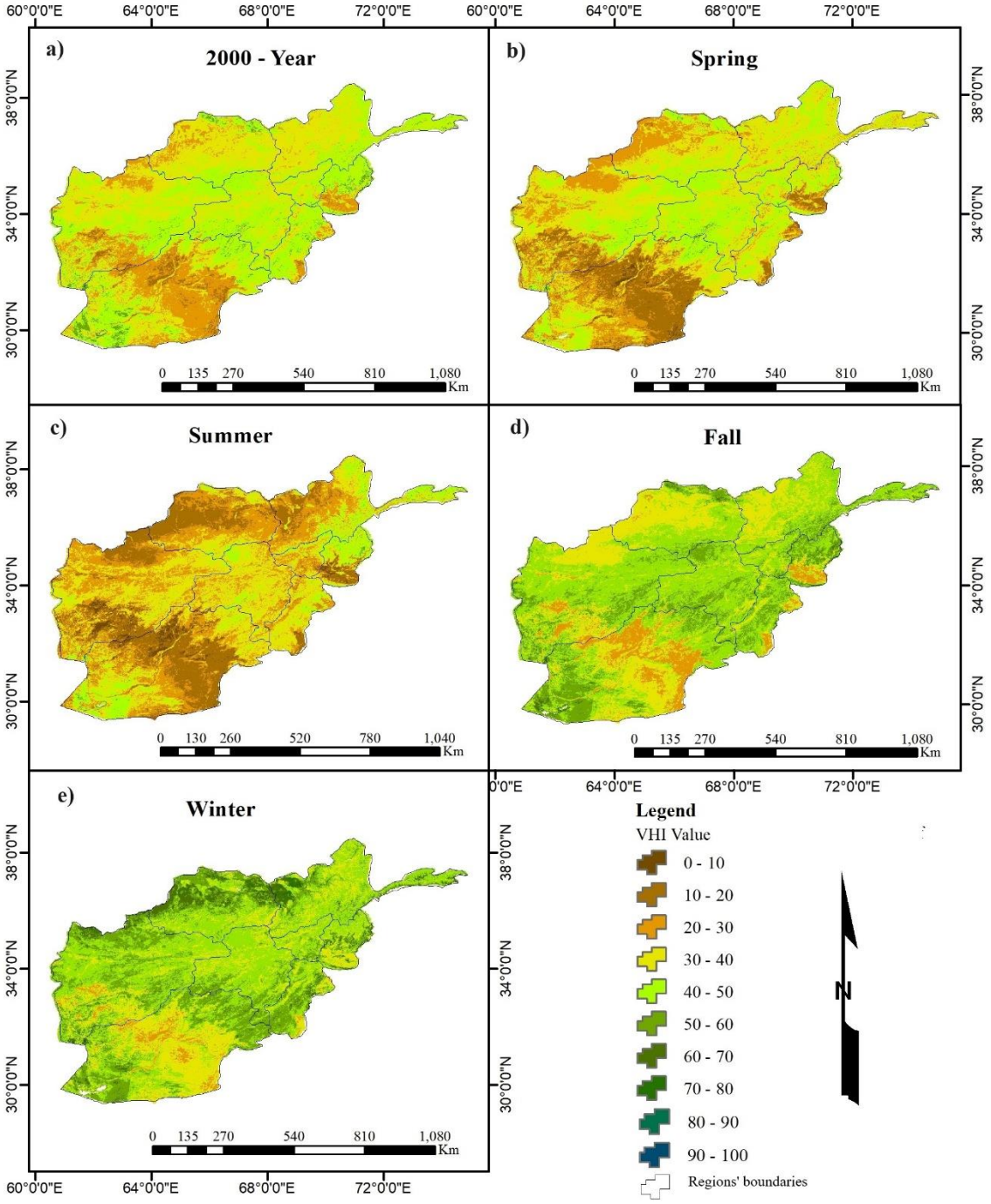

Figure 97. Spatial distribution of VHI for 2000 year: 2000-year(a), Spring(b), Summer(c), Fall(d), Winter(e).

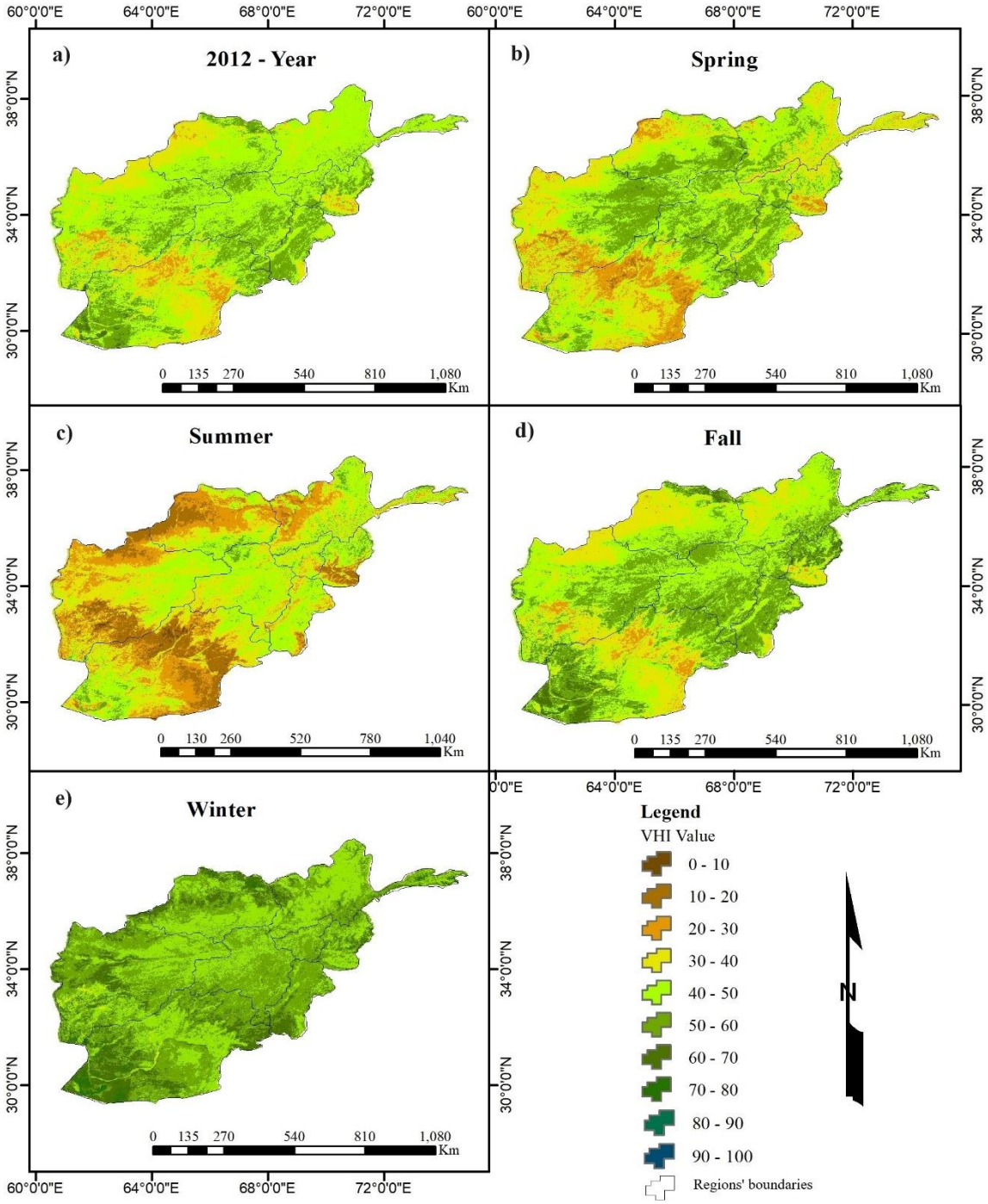

Figure 98. Spatial distribution of VHI for 2012 year: 2012-year(a), Spring(b), Summer(c), Fall(d), Winter(e).

In the summer season of 2000, the VHI level in the eastern region was very low; however, this level increased significantly in 2012 and showed further improvement in 2023 (shown in Figure 99c). Conversely, in the summer of 2023, the VHI in the north and northeast regions decreased compared to 2012, leading to increased exposure to drought conditions (shown in Figure 99c).

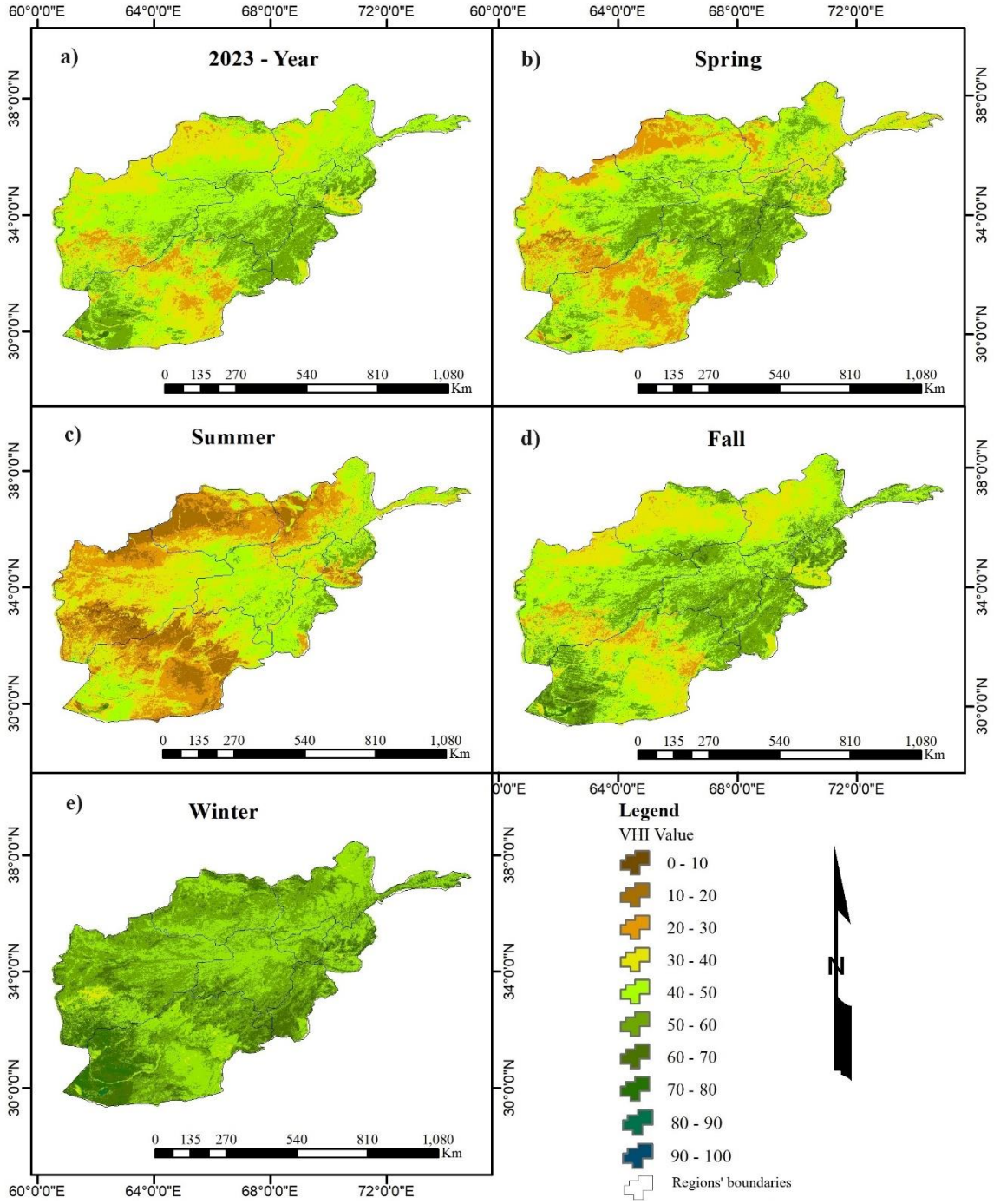

Figure 99. Spatial distribution of VHI for 2023 year: 2023-year(a), Spring(b), Summer(c), Fall(d), Winter(e).

The forests in the eastern and southeastern regions of Afghanistan predominantly consist of oak, juniper, and pine trees, which thrive in mountainous areas at elevations above 2,500 meters. As a resource-poor country with limited access to oil and gas, Afghanistan's population primarily relies on firewood for fuel. Consequently, there was an increase in deforestation, with more trees being cut for fuel in 2023 compared to previous years.

Although the largest forest cover is found in the eastern region, the highest rate of deforestation has occurred in the southeastern region (shown in Figure 100b).

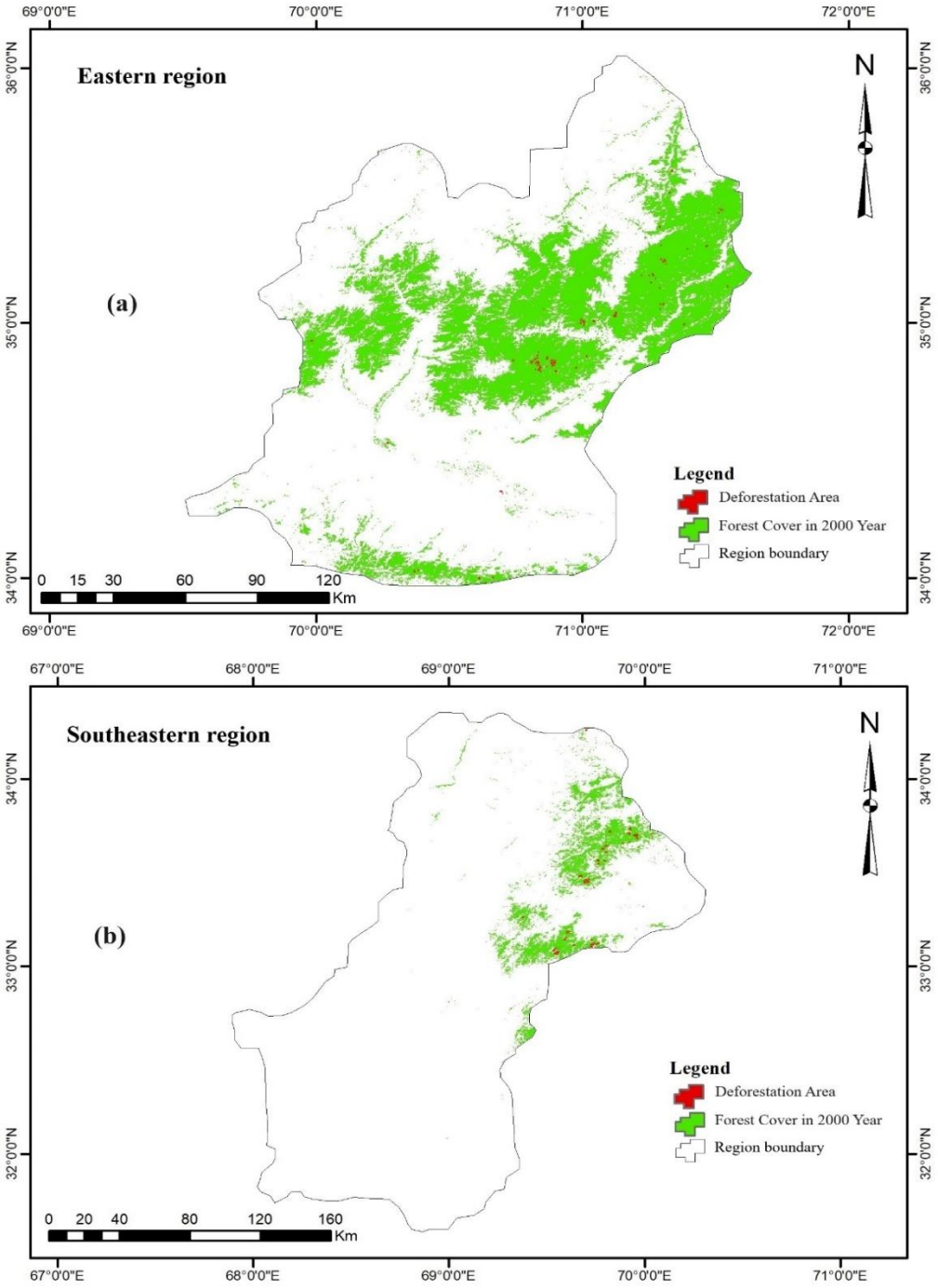

Figure 100. Forest areas: Eastern region(a), Southeastern region(b).

In the north region of Afghanistan, pistachio forests exist in certain areas, but their extent is considerably lower than that of the forests in the eastern region. Additionally, in

parts of the northeastern region, forests were significantly depleted in recent years, with many areas converted into agricultural or barren lands (shown in Figure 101).

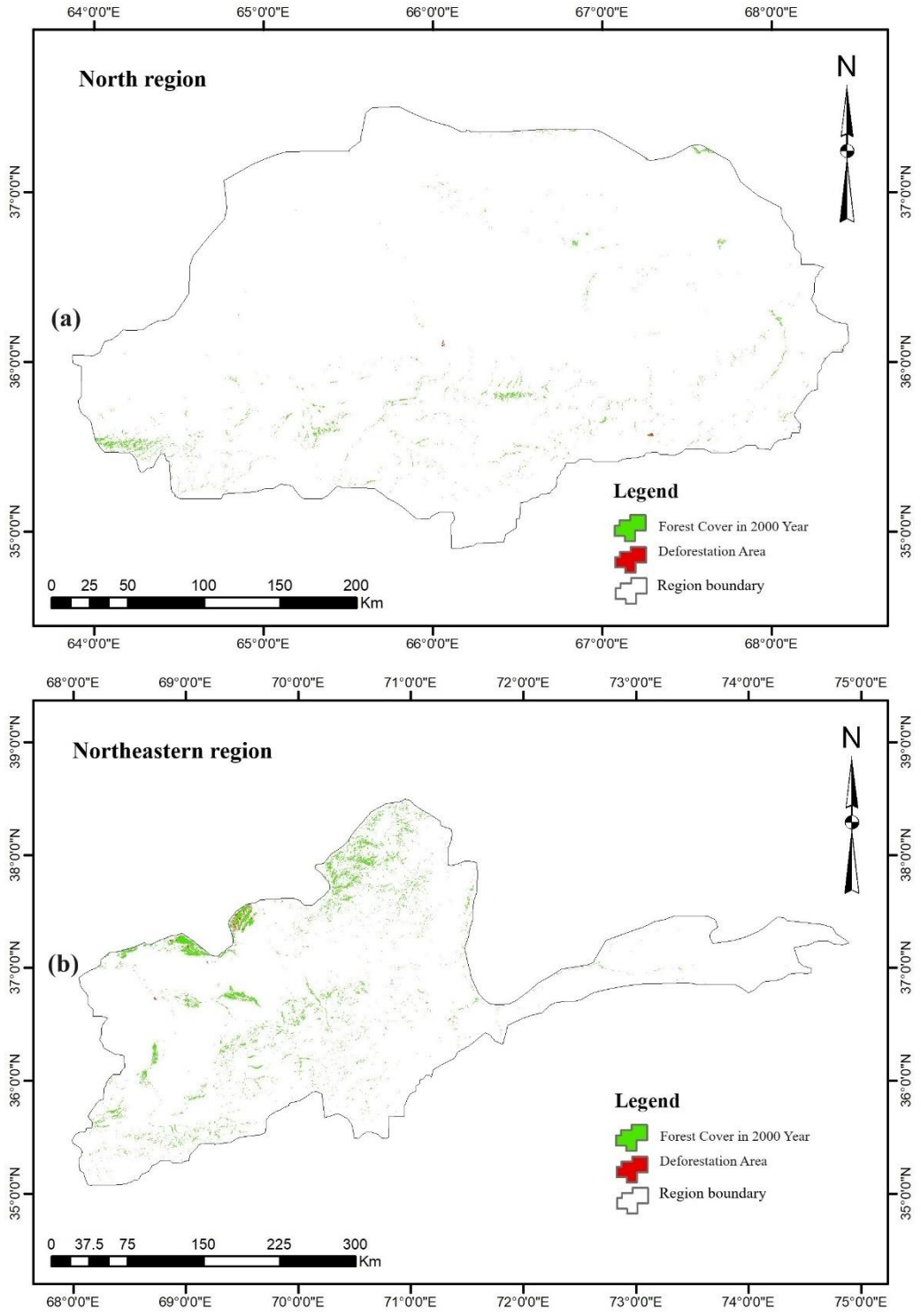

Figure 101. Forest areas: North region(a), Northeastern region(b).

The amount of natural forests in the central region is very low, with most trees being planted by people. However, some areas contain scattered forests. In the west-central region, there are also scattered trees, but these do not constitute forests.

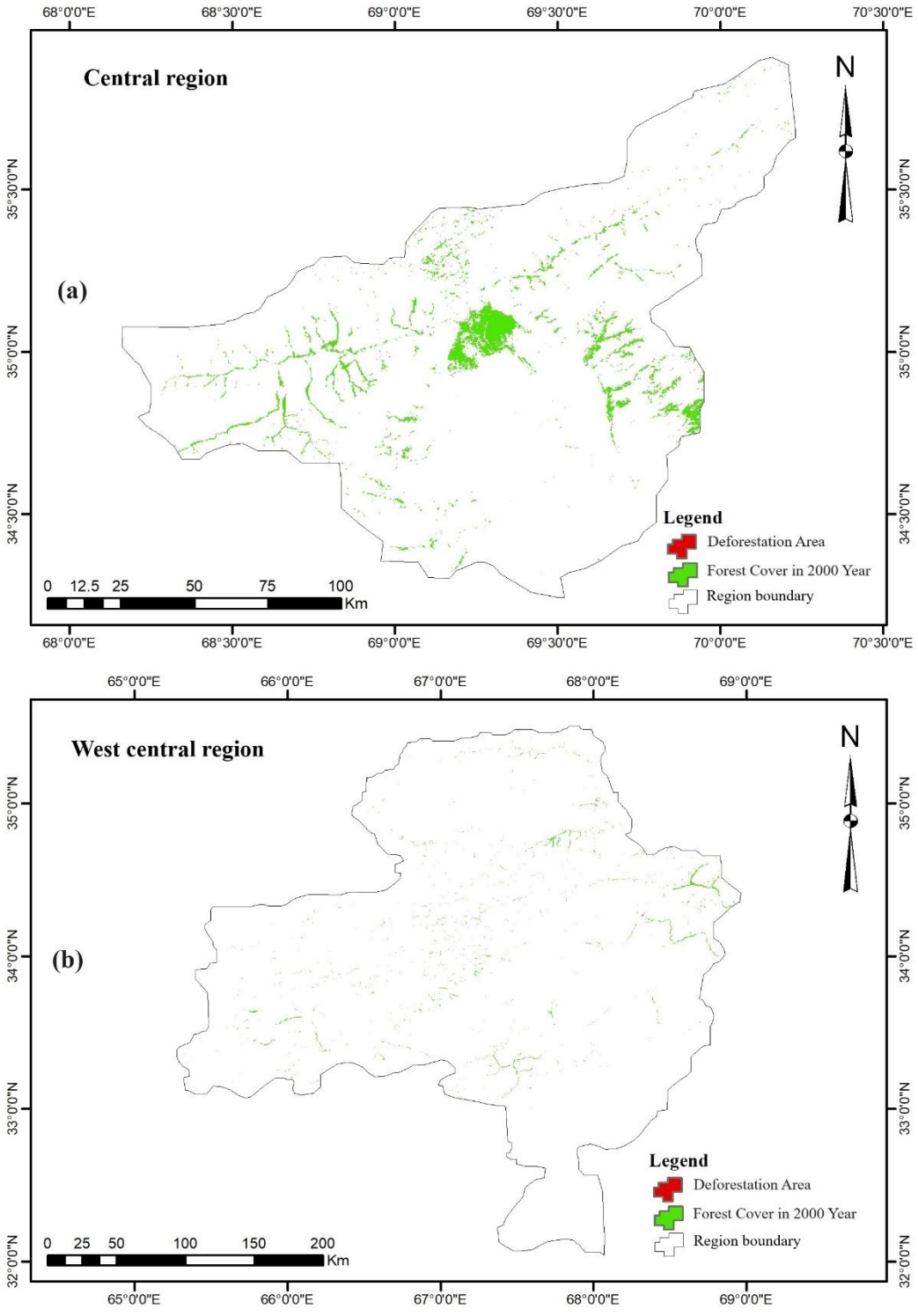

Figure 102. Forest areas: Central region(a), West Central region(b).

In the western region, pistachio forests can be found in parts of Badghis province. However, in recent years, sections of these forests were destroyed and cut down by people (shown in Figure 103a). There are no forested areas in other parts of this region, and the South region lacks any type of forest cover.

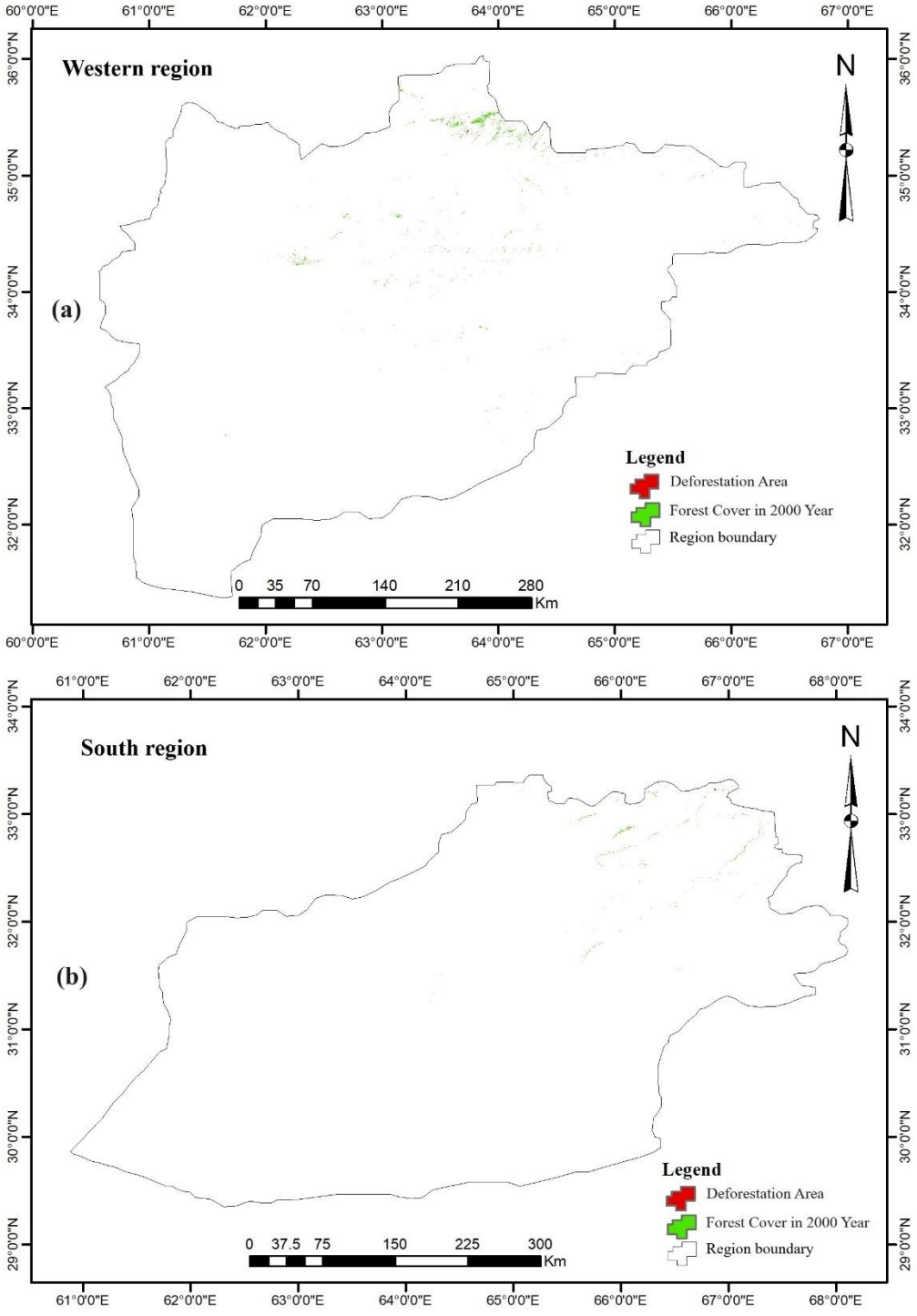

Figure 103. Forest areas: Western region(a), South region(b).

4. DISCUSSION

As stated at the beginning of this thesis, the primary objective of this study is to investigate the effects of climate change on various regions of Afghanistan. In this research, the climate parameters related to climate change were utilized and analyzed across three scales: monthly, seasonal, and annual. These analyses aimed to uncover the effects of each climate parameter on each region through statistical methods. In this section, the main findings of this research will be discussed and interpreted in relation to existing studies and climate effects. Initially, the key findings will be interpreted and discussed, followed by a comparison with previous research.

The NDVI index has shown an increasing trend monthly, seasonally, and annually across all regions of Afghanistan from 2000 to 2023, except for the north region. In Afghanistan, the peak of plant growth varies by region; in the north, northeast, west, and south regions, NDVI typically increases in spring and declines in summer and autumn due to rising LST. Conversely, in other regions, NDVI significantly rises during summer. The results of the Mann-Kendall test indicate that NDVI is significant in the months of each season, and the seasonal trends are also significant. Annually, NDVI exhibits a significant trend, except in the north and central regions. The homogeneity test confirms that NDVI data in Afghanistan has a significant increasing trend, excluding the north and central regions. After 2009, major changes in vegetation have occurred in the eastern and central regions, and after 2012 in the South and western regions, resulting in increased NDVI. The decrease in the NDVI trend in the north region may be attributed to rising LST, reduced rainfall, decreased soil moisture, and climate change. In contrast, the increase in NDVI in the South and western regions can be attributed to recent efforts by local populations to cultivate vegetation by utilizing underground water.

In Afghanistan, the LST parameter has a slightly decreasing but insignificant trend during the scope of this study. LST has shown a significant decreasing trend monthly in some regions and months, particularly in the summer season of the east, central, and west-central regions, as well as in the fall season of the south and southeast regions. However, the annual trend is slightly decreasing but insignificant. The highest amount of LST was observed in the South region, while the lowest is in the northeastern region.

The South region is primarily composed of sandy soil and plains, which increases the temperature. However, in recent years, underground water extraction in this area has led to an increase in NDVI. In contrast, most of the northeastern region remains covered with snow throughout the year, resulting in a decreased average temperature (shown in Figure 104).

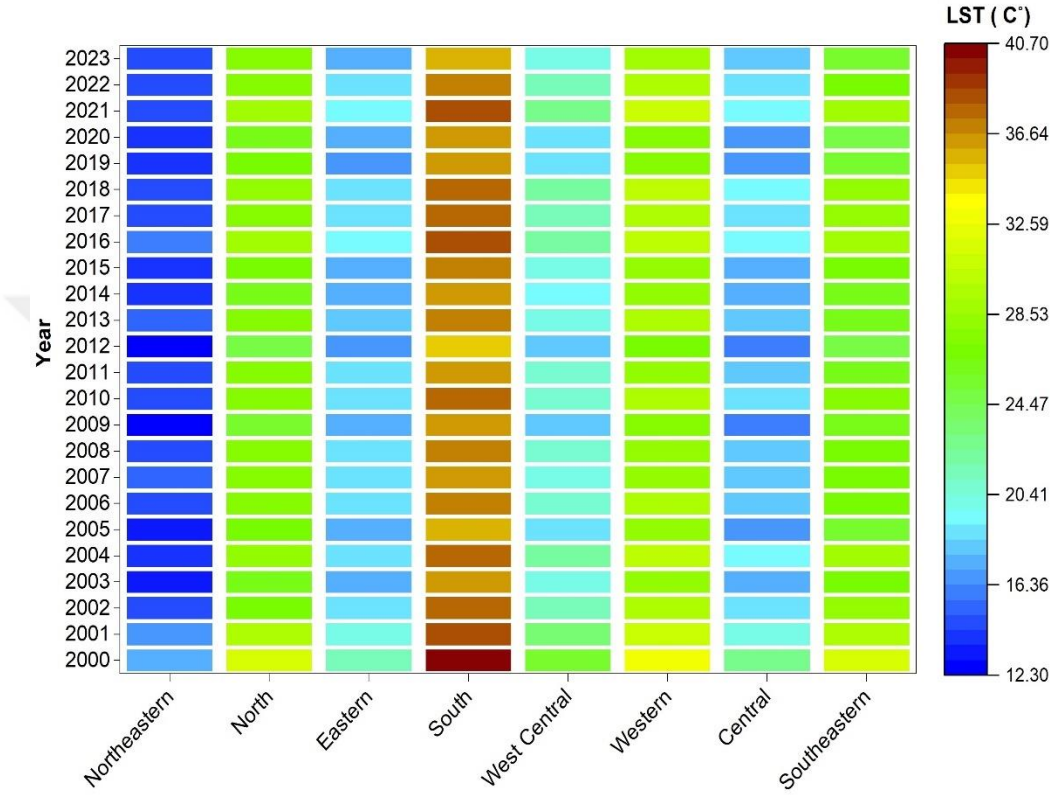

Figure 104. Mean LST difference in each region.

As illustrated in Figure 104, the LST values in 2000 were high across various regions of Afghanistan, with the South region exhibiting the highest LST values. Additionally, Figure 105 indicates a very strong correlation between air temperature and LST data, revealing that air temperatures were elevated in 2000 for all regions of Afghanistan, with the highest temperatures observed in the South region. However, NDVI values were low across all regions that year. Annually, LST has shown a decreasing trend in all regions of Afghanistan, while NDVI has demonstrated an increasing trend. Between 2000 and 2023, LST has slightly decreased, whereas air temperature has slightly increased. This increase in NDVI may be attributed to climatic and atmospheric effects, as well as greenhouse gas emissions. The rise in vegetation cover contributes to cooling the earth's surface through evapotranspiration, which subsequently has a reduced effect on Ta. The results of the

homogeneity test indicate that significant changes in the LST and Ta parameters have not occurred consistently in Afghanistan, and the temperature fluctuations were insignificant.

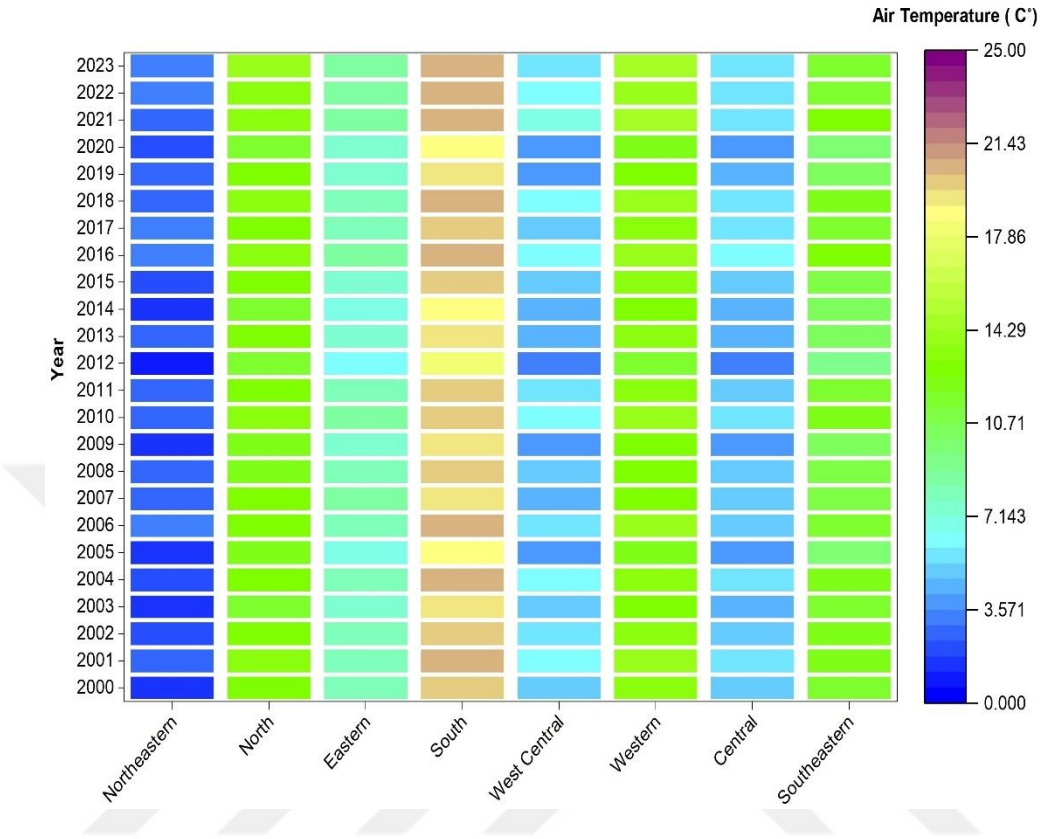

Figure105 Mean Ta difference in each region.

Additionally, the AET and PET parameters also influence climate change in Afghanistan. AET has shown a slight increasing trend monthly, seasonally, and annually across all regions, which can be attributed to the rise in NDVI. The AET homogeneity test indicates a significant increase in the Southeast and Central regions after 2007, and in the West Central region after 2010. While LST is high in the south, west, and north regions, AET is lower in these areas due to a lack of vegetation. However, in recent years, as vegetation has increased in these regions, AET has also seen a slight rise.

One reason for the increase in PET is the rise in air temperature and wind speed. In areas where PET has increased annually and LST, soil moisture and wind speed have decreased. This can be attributed to the overall increase in air temperature and changes in land use. The amount of precipitation has increased in the south, southeast, east, central, and west-central regions of Afghanistan, likely due to the expansion of vegetation and forests in the eastern and southeastern areas. Conversely, precipitation has decreased in the north, northeast, and west regions, which may be linked to the reduction of NDVI in those areas.

On the other hand, soil moisture has declined across all regions because Afghanistan is a mountainous country with predominantly stony and sandy soils. Given the soil type, water particles are quickly absorbed after rainfall, leading to rapid drying. Consequently, despite the increase in precipitation, soil moisture has decreased in some areas.

The results of the Mann-Kendall test indicate a significant increasing trend in annual precipitation in the eastern and southeastern regions of Afghanistan. Additionally, there is a significant upward trend in precipitation during the spring and summer seasons in the eastern and central regions. However, significant changes in precipitation have not been observed in any of the regions of Afghanistan.

According to the results of the homogeneity test, notable changes in soil moisture have occurred in the north regions after 2015 and in the northeastern and west-central regions after 2016, leading to a decline in soil moisture levels. This decrease is a crucial factor contributing to the reduction of vegetation in the north region. Furthermore, one significant reason for the decline in soil moisture in the western and north regions is the high wind speed, particularly pronounced in the western areas. Wind speed exhibits a consistent trend across all parts of Afghanistan, with no significant changes observed.

Similarly, the VCI, TCI, and VHI parameters were employed to monitor agricultural drought. These climate parameters have not exhibited a significant trend in most regions of Afghanistan between the years 2000 and 2023, primarily because much of Afghanistan's land is not suitable for agriculture, resulting in a lack of significant change trends. The calculation of these climate parameters has allowed for the assessment of drought conditions in each region. The annual results of the VHI index indicate that the north region has experienced the most droughts over the past 24 years. Likewise, the western, southeastern, and northeastern regions have encountered drought in some years, while the remaining regions have not experienced any drought. Predictions from the ARIMA model further suggest that the north region will continue to experience severe droughts from 2024 to 2035.

In this study, the effects of climate change were also assessed by calculating the amount of deforestation in each region and investigating its trend. Forest areas in Afghanistan are predominantly located in the eastern, southeastern, and northeastern regions, while the other regions have little to no forest cover, consisting instead of scattered trees. Deforestation data for the period from 2000 to 2023 reveal a declining trend overall, with the highest rates of deforestation occurring before 2010. However, there was an increase in deforestation in 2023. The main drivers of deforestation in Afghanistan are poverty and a

lack of fuel sources. In the northeastern region, 417.42 hectares of forest were cleared, with most deforestation occurring before 2012, as these areas were converted into agricultural land. Similarly, 804.35 hectares of forest was cut down in the eastern region, and 873.47 hectares were lost in the southeastern region. Overall, Afghanistan has seen a total loss of 2,431.62 hectares of forest over the past 24 years, with the southeastern region accounting for the majority of this loss.

The ARIMA model was employed to predict the data for this research, and the model's performance was evaluated using the R^2, RMSE, and MAE criteria, with values falling within acceptable limits. The NDVI index is projected to show an increasing trend in all regions until 2035, except for the north region. If the Afghan government does not take measures to prevent the reduction of vegetation in the north, this negative trend may continue. Conversely, the LST parameter is expected to display a decreasing trend across all regions until 2035. Additionally, the Ta parameter is forecasted to show an increasing trend in all regions until 2035, which directly influences the AET and PET parameters.

The AET parameter is projected to exhibit a slight increase in all regions except the north, while the PET parameter is also expected to rise until 2035. In contrast, the precipitation parameter in the north, northeastern, and western regions is predicted to decline until 2035, whereas it is expected to increase in other regions. This decrease in precipitation in the mentioned regions may be attributed to climate change. Furthermore, the soil moisture parameter is anticipated to show a declining trend across all regions until 2035, potentially due to rising Ta levels and climate change.

The main findings of this study are now compared with previous research. Nabizada et al. (2022) conducted a study to evaluate the spatial and temporal changes in land surface temperature (LST) in Afghanistan from 2000 to 2021. They assessed the impact of factors such as soil moisture, precipitation, and NDVI on LST using MODIS data for LST and NDVI, CHIRPS data for precipitation, and FLDAS data for soil moisture, which aligns with the data utilized in this thesis. The results of their research indicated that LST in Afghanistan showed a slightly decreasing but insignificant trend during the studied period, while NDVI, precipitation, and soil moisture exhibited an increasing trend. The decrease in LST was attributed to the influence of soil moisture, which is consistent with the findings of this thesis. In this study, NDVI increased across all regions of Afghanistan, except in the north region, from 2000 to 2023. Similarly, LST showed a slightly decreasing trend in all regions of Afghanistan. Furthermore, the monthly precipitation in Afghanistan exhibited a slight

decrease overall, with an annual slight increase. Specifically, the precipitation trend was slightly decreasing in the north, west, and northeast regions, while other regions displayed an increasing trend, corroborating the findings of the previous research. However, according to Nabizada et al., soil moisture did not increase in all regions of Afghanistan. This discrepancy may be due to the fact that with the increase in vegetation, plants absorb more water from the soil, resulting in decreased soil moisture. Additionally, much of Afghanistan's soil consists of sandy or stony materials, which can further contribute to this issue.

Similarly, the study conducted by Ganji and Kajisa (2018) indicates that in the western basin of Afghanistan, high temperatures, low humidity, and wind speed significantly impact evapotranspiration (ET). Their findings reveal that ET is elevated from June to September, which aligns with the results of this thesis. In this study, the correlation between wind speed and actual evapotranspiration (AET) in the western region of Afghanistan is 0.33, while the relationship between AET and LST is -0.44. This inverse relationship can be attributed to factors such as water shortages, plant stress, and dry soil in the region.

Additionally, research conducted by the Food and Agriculture Organization of the United Nations and the International Institute for Applied Systems Analysis, in collaboration with the government of Afghanistan, focused on climate change in the country. This study analyzed temperature, precipitation, humidity, and evapotranspiration climate parameters across eight regions of Afghanistan from 1981 to 2010, with predictions extending to 2070. The findings indicate that Afghanistan is likely to experience hotter and drier weather conditions in the future, which closely aligns with the results of this thesis.

This research highlights a pattern of decreasing precipitation extending from the northeastern to the southwestern regions of Afghanistan, consistent with the findings presented in this thesis. Specifically, the amount of precipitation decreased in the north, northeast, and west regions of Afghanistan (as shown in Figures 26, 27, and 30). Furthermore, the study indicates that the actual evapotranspiration (ETa) is significantly lower than the reference and potential evapotranspiration values, suggesting a notable deficiency in seasonal or year-round soil moisture across Afghanistan. This finding is also consistent with the results of this thesis, which demonstrate a decrease in soil moisture across all regions of the country.

In another study conducted by Alqasemi et al., (2010) regarding land surface temperature (LST) and air temperature in the United Arab Emirates, LST data were obtained from MODIS, while air temperature data were sourced from ground stations. The results

demonstrated a strong correlation between the two, with an $R^2 > 0.94$. In this thesis, a similarly strong correlation between LST and air temperature (Ta) is observed in each region.

5. CONCLUSION

In this thesis, the climatic effects of Afghanistan were investigated across eight distinct regions. The climate parameters used in this study included NDVI, VCI, TCI, VHI, LST, Ta, precipitation, soil moisture, AET, PET, wind speed, and deforestation areas. Each index was analyzed monthly, seasonally, and annually for each region between 2000 and 2023, and the trends were evaluated using the Mann-Kendall and homogeneity tests. The results obtained from these studies are summarized below:

- It was observed that with the increase of NDVI, LST has decreased in all regions of Afghanistan monthly, seasonally, and annually, except for the north region. This suggests a strong and inverse relationship between vegetation health and temperature regulation, indicating that areas with higher vegetation cover tend to maintain lower surface temperatures. Conversely, the Ta parameter increased across all three-time scales in all regions, revealing a warming trend that could be linked to broader climate change phenomena. While NDVI is decreasing in the north region, it is noteworthy that this region still exhibits the highest amount of NDVI compared to others.
- Monthly and seasonal precipitation has decreased in the north, northeast, and west regions, while it has increased in the remaining regions. However, despite some areas experiencing increased rainfall, soil moisture levels have declined across all regions. This indicates that the increased precipitation is insufficient to replenish soil moisture, likely due to higher evaporation rates influenced by rising temperatures.
- The western region recorded the highest wind speed, reaching an average of 11 m/s. This wind pattern has a direct impact on NDVI, soil moisture, and AET, highlighting the importance of wind dynamics in influencing local climatic conditions and vegetation health.
- The VCI, TCI, and VHI indices were utilized for monitoring agricultural drought. The results demonstrated that the north and west regions are more susceptible to drought, while the northeast and southeast region sexperience occasional agricultural drought as well. These findings emphasize the need for targeted agricultural policies to mitigate the impacts of drought, particularly in vulnerable regions.

- As noted, the highest forest cover was found in the eastern, southeastern, and northeastern regions of Afghanistan. Generally, deforestation in Afghanistan's forested areas has shown a decreasing trend between 2000 and 2023. However, in 2023, the rate of destruction has again increased, which significantly impacts the aforementioned indices aimed at examining climatic changes. This increase in deforestation can have profound effects on local climate patterns, biodiversity, and the livelihoods of communities dependent on these forests. The findings highlight the need for effective forest management strategies and conservation efforts to mitigate the adverse impacts of climate change and promote sustainable land use practices.
- The ARIMA model was employed to predict the time series data. Before implementation, the model's parameters (p, d, q) were analyzed using ACF (Autocorrelation Function) and PACF (Partial Autocorrelation Function), and adjustments were made for each climate parameters. The performance results of the model were subsequently evaluated using criteria such as R^2, RMSE and MAE ensuring a robust predictive framework.
- Lastly, a comprehensive mapping of each climate parameters were prepared for the years 2000, 2012, and 2023, providing valuable visual insights into the climatic variations over time. These maps serve as critical tools for stakeholders in understanding spatial patterns and facilitating data-driven decision-making in climate adaptation and resource management.

In conclusion, this study provides a nuanced understanding of the climatic dynamics affecting Afghanistan across various regions. The findings highlight the intricate relationships between vegetation, temperature, precipitation, and evapotranspiration, all of which are vital for developing effective climate adaptation strategies. As Afghanistan continues to face the challenges posed by climate change, the insights garnered from this research can inform policy initiatives aimed at enhancing resilience, promoting sustainable land use, and ensuring food security for its population. Future research should focus on integrating these findings with socio-economic data to develop comprehensive strategies that address both climatic and human factors affecting this region.

6. SUGGESTIONS

This study was accompanied by many limitations, the lack of ground data to validate the performance of the climate parameters, the low spatial resolution of some datasets and sensors, And the limitations of the predictive model, which was not suitable for some data, are among the most important limitations of this thesis.

The climate parameters that were examined in this study were not for climatic regions, my suggestion is that in the future, studies in this regard should be done separately for each city or climatic region, it will have better results. And ground data should also be available to evaluate the research findings. The climate parameters that are used to investigate the climate affects; the data should be processed once again to prevent an increase of errors. In the future, if similar research is done, a model should be used for forecasting where the climate parameters are entered into the model as a combination and then the forecast is made, because the climatic parameters have major effects on each other. In this study, VCI, TCI and VHI indices were used to investigate agricultural drought, but these indices were not enough, and other indices should also be studied to drought monitoring so that the drought situation in each region of Afghanistan is determined and measures are taken. Also, in this thesis, the amount of deforestation for each region of Afghanistan was investigated using the HGFC dataset. This dataset does not have data in some years and has a spatial resolution of 30 meters. Afghanistan's forests should be investigated separately, and high-resolution data should be used.

The studies conducted in this thesis revealed the effects of climate change in Afghanistan between the years 2000-2023 and predicted it until 2035, and my request to the Afghan government is to take the necessary measures for the consequences of these changes so that people are not exposed to natural disasters.

7. REFERENCE

Abbas, M. & Ahmad, B.B. (2014). Estimation of Land Surface Temperature using MODIS Thermal Infrared and weather station Data in Iraq. journal of kerbala university, 12(3), 113-118.

Ahlmer, A.K., Cavalli, M., Hansson, K., Koutsouris, A.J., Crema, S. & Kalantari, Z. (2018). Soil moisture remote-sensing applications for identification of floodprone areas along transport infrastructure. Environmental Earth Sciences, 77, https://doi.org/10.1007/s12665-018-7704-z

Aich, V., Akhundzadah, N.A., Knuerr, A., Khoshbeen, A.J., & Paton, E.N. (2017). Climate Change in Afghanistan Deduced from Reanalysis and Coordinated Regional Climate Downscaling Experiment (CORDEX)—South Asia Simulations. Climate, 5(2), http://dx.doi.org/10.3390/cli5020038

Akbari, E., Asadi, M.A.Z. & Moghadam, I.T. (2016). Monitoring land Use Changes Using Different Methods of Statistical Training Theory in Neishabur Region. Geographical Planning of Space Quarterly Journal, 6(20), 36-50.

Akbari, M., Seif, Z. & Zare Abyane, H. (2011). Estimation of Evapotranspiration by Remote Sensing Technique under Different Climate Condition. Journal of Water and Soil, 25(4), 835-844.

Akseer, N., Bhatti., Rizvi, A., Salehi, A.S., Mashal, T. & Bhutta, Z.A. (2016). Coverage and inequalities in maternal and child health interventions in Afghanistan. BMC Public Health, 16(2), 120-137.

Alahacoon, N. & Edirisinghe, M. (2022). Novel Index for Hydrological Drought Monitoring Using Remote Sensing Approach: Standardized Water Surface Index (SWSI). Remot Sensing, 14(21), https://doi.org/10.3390/rs14215324

Alqasemi, A., Hereher, M., Al-Quraishi, H., Saibi, H., Aldahan, A. & Abuelgasim, A. (2020). Retrieval of monthly maximum and minimum air temperature using MODIS aqua land surface temperature data over the United Arab Emirates. GEOCARTO INTERNATIONAL, 37(10), 2996-3013).

Arekhi, S., Savasari, M.B. & Emadaddian, S. (2022). Investigating the Indicators Resulting from Remote Sensing Technology in Drought Assessment using MODIS Images (Case Study: Qom, Isfahan, Chaharmahal and Bakhtiari, and Markazi Provinces). Journal of Geography and Environmental Hazards, 11(3), 189-224.

Azad, M.R.A. & Shabanzada, F. (2020). Investigating the trend of wind speed changes in Rasht's Hamdez station. Comprehensive humanities portal, 5(11), 1-11.

Balas, D.B., Tiwari, M.K., Trivedi, M. & Patel, G.R. (2023). Impact of Land Surface Temperature (LST) and Ground Air Temperature (Tair) on Land Use and Land Cover (LULC): An Investigative Study. International Journal of Environment and Climate Change, 13(10), 3117-3130.

Bazgir, S., Abasi, F., Oskoy, A., Haqiqat, M. & Rizazada, P. (2018). Analyzing the homogeneity of temperature and precipitation data in Iran with a climatic approach. Journal of Spatial Analysis of Environmental Hazards, 6(1), 51-70.

Bulut, B., Yilmaz, M.T., Afshar, M.H., Sorman, A.Ü., Yücel, T., Cosh, M.H. & Şimşek, O. (2019). Evaluation of Remotely-Sensed and Model-Based Soil Moisture Products According to Different Soil Type, Vegetation Cover and Climate Regime Using Station-Based Observations over Turkey. Remote Sensing, 11(16), http://dx.doi.org/10.3390/rs11161875

Byrne, G. (2007). A Statistical Primer: Understanding Descriptive and Inferential Statistics. Evidence Based Library and Information Practice, 2(1), 34-47, https://doi.org/10.18438/B8FW2H

DIMRI, T., AHMAD, Sh. and SHARIF, M. (2020). Time series analysis of climate variables using seasonal ARIMA approach. Journal of Earth System Science, 129, https://doi.org/10.1007/s12040-020-01408-x

Doe, J. (2021). Climate Change Impacts in Afghanistan. Norwegian Institute of International Affairs (NUPI).

Ejaz, N., Bahrawi, J., Alghamdi, KH. M., Rahman, KH. & Shang, S. (2023). Drought Monitoring Using Landsat Derived Indices and Google Earth Engine Platform: A Case Study from Al-Lith Watershed, Kingdom of Saudi Arabia. Remot Sensing, 15(4), https://doi.org/10.3390/rs15040984

ERDOĞAN, E. (2023). İKLİM DEĞİŞİKLİĞİNİN ÜLKEMİZE OLAN ETKİLERİNİN GOOGLE EARTH ENGİNE PLATFORMUNDA İNCELENMESİ. K.T.Ü.,Fen Bilimleri Enstitüsü, Y.Lisans Tezi, Trabzon.

Food and Agriculture Organization of the United Nations, and International Institute for Applied Systems Analysis. (2019). Agro-climatic indicators (Editors: G. Fischer, and H. Fischer). Rome, Italy: Food and Agriculture Organization of the United Nations.

GALLO, K., HALE, R., TARPLEY, D. & YU, Y. (2011). Evaluation of the Relationship between Air and Land Surface Temperature under Clear- and Cloudy-Sky Conditions. Journal of Applied Meteorology and Climatology, 50(3), 767–775.

Ganji, H. & Kajisa, T. (2018). ASSESSING REFERENCE EVAPOTRANSPIRATION USING PENMAN-MONTEITH AND PAN METHODS IN THE WEST REGION OF AFGHANISTAN. International Journal of GEOMATE, 16(56), 209-216.

Ganji, H. & Kajisa, T. (2019). Evaluation of FAO-56 Penman-Monteith Model Using Alternative Climatic Data Application to Afghanistan. Revista Brasileira de Meteorologia, 34(4), 481-486.

GILL, K.K., BHATT, K., KAUR, B. & SANDHU, S.S. (2023). ARIMA approach for temperature and rainfall time series prediction in Punjab. Journal of Agrometeorology, 25(4), 571-576.

GÜL, G.O. (2023). Monitoring of agricultural drought in Turkey with remote sensing data by use of Google Earth Engine. Pamukkale University Journal of Engineering Sciences, 30(1), 71-80.

Hess, A., Iyer, H. & Malm, W. (2001). Linear trend analysis: a comparison of methods. Atmospheric Environment, 35(30), 5211-5222.

Hidarnejad, M., Zarearnani, M. & Pakparvar, M. (2013). Determination Accuracy of SEBS Model in Estimating Actual Evapotranspiration in YAZD. The Journal of Geographical Research on Desert Areas, 1(1), 1-16.

Huacani, W., Meza, N.P., Aguirre, F., Sanchez, D.D. & Luque, E.N. (2022). Analysis of Deforested Area Using Google Earth Engine in The Period 2001-2020 In the Apurimac Region. Journal of Internet and e-Business Studies, https://ibimapublishing.com/articles/JIEBS/2022/988227/

Ilori, O.W. & Ajayi, V.O. (2020). Change Detection and Trend Analysis of Future Temperature and Rainfall over West Africa. Earth Systems and Environment, 4, 493-512.

Islami, N. & Zari, Kh. (2014). Forecasting monthly precipitation and temperature using time series models (ARIMA) (case study: Shiraz city). Journal of Civilica, https://civilica.com/doc/788391/

Jose, J. (2022). Introduction To Time Series Analysis and Its Applications. https://www.researchgate.net/publication/362389180_INTRODUCTION_TO_TIME_SERIES_ANALYSIS_AND_ITS_APPLICATIONS

Khan, M.K., Iqbal, M.F., Mahmood1, I., Shahzad, M.I., Zafar, Q. & Khalid, B. (2023). Evaluation of precipitation products over different climatic regions of Pakistan. Theoretical and Applied Climatology, 151, 1301-1321.

Khodaee, M., Shad, R. & Mqsudy, Y. (2017). Introducing drought satellite indicators and evaluating their performance. Journal of Civilica, https://civilica.com/doc/716864/

Kocsis, T., Székely, I.K. & Anda, A. (2019). Homogeneity tests and non-parametric analyses of tendencies in precipitation time series in Keszthely, Western Hungary. Theoretical and Applied Climatology, 139, 849-859.

Mahasa, P.S., Xulu, S. & Mbatha, N. (2023). Characterization of Evapotranspiration in the Orange River Basin of South Africa-Lesotho with Climate and MODIS Data. Water, 15(8), https://doi.org/10.3390/w15081501

Makari, M. & Abasnaya, M. (2020). Trends Analysis of Maximum Temperature by Using Mann-Kendall and Spearman Tests in Various Regions of Iran. journal of meteorological organization, 44, 33-47.

Masood, M., Naveed, M., Iqbal, M., Nabi, G., Kashif, H.M., Jawad, M. and Mujtaba, A. (2023). Evaluation of Satellite Precipitation Products for Estimation of Floods in Data-Scarce Environment. Advances in Meteorology, https:// doi.org/10.1155/2023/1685720

McNally, A., Jacob1, J., Arsenault, K., Slinski, K., Sarmiento, D.P., Hoell, A., Pervez, SH., Rowland, J., Budde, M., Kumar, S., Lidard, Ch. & Verdin, J.P. (2022). A Central Asia hydrologic monitoring dataset for food and water security applications in Afghanistan. Earth System Science Data, 14(7), 3115-3135.

Mehrabi, A. (2019). Monitoring Vegetation Changes (pistachio orchards) Using Multi-Temporal Satellite Image Processing. Geography and Development, (56), 21-38.

Modaresi, F., Araghinejad, SH., Ebrahimi, K. & Kholghy, M. (2019). Regional Assessment of Climate Change Using Statistical Tests:Case Study of Gorganroud-Gharehsou Basin. Journal of Water and Soil, 24(3), 476-489.

Mojaradi, B., Mirmiri, J. & Hosein, A. (2020). Assessment of Vegetation Condition Index Using Modified Standard Precipitation Index to Monitor and zoning Drought. Journal of Watershed Engineering and Management, 12(3), 725-736.

Mostarshed, M. (2014). on precipitation climatology of Afghanistan. Geographical research, 3(114), 191-202.

Nabizada, A.F., Rousta, I., Dalvi, M., Olafsson, H. & Siedliska, A. (2022). Spatial and Temporal Assessment of Remotely Sensed Land Surface Temperature Variability in Afghanistan during 2000–2021. Climate,10(7), http://dx.doi.org/10.3390/cli10070111

Nascimento, A.C.L., Galvani, E., Gobo, J.P.A. & Wollmann, C.A. (2022). Comparison between Air Temperature and Land Surface Temperature for the City of São Paulo, Brazil. Atmosphere, 13(3), https://doi.org/10.3390/atmos13030491

National Environmental Protection Agency. (n.d.). Afghanistan Initial National Communication to the United Nations Framework Convention on Climate Change. Kabul, Afghanistan: National Environmental Protection Agency.

Neideen, T. & Brasel, K, (2007). Understanding Statistical Tests. Journal of Surgical Education, 64(2), 93-96.

Pahlevanzadeh, N., Janalipour, M., Tehrani, N.A. & Farhanj, F. (2019). Accuracy Improvement of Land Surface Temperature Extracted from Thermal Bands of Landsat Satellite using Linear Regression and Ground Observations. Journal of Geography and Environmental Planning, 30(3), 59-78.

PEARCE, N.E. and CRYER, P. C. (1986). ANALYSIS OF THE COMPONENTS OF A LINEAR TREND IN PROPORTIONS. American Journal of Epidemiology, 124(1), 127-133.

Prasad, R., Bhimala, K.R., Patra, G.K., Himesh, S. & Goroshi, SH. (2023). Annual and seasonal trends in actual evapotranspiration over different meteorological sub-divisions in India using satellite-based data. Theoretical and Applied Climatology, 152, 999-1017.

Qu, C. & Hao, X. (2018). Agriculture Drought and Food Security Monitoring over the Horn of Africa (HOA) from Space. IEEE Xplore, https://ieeexplore.ieee.org/document/8476128

Rahimpour, M., Karimi, N., Rouzbahan, R. & Eftekhari, M. (2018). Validation and Calibration of FAO's WaPOR Product (Actual Evapotranspiration) in Iran Using In-Situ Measurements. Iran-Water Resources Research, 14(2), 249-262.

Sabzevari, Y. & Islamian, S. (2024). Forecasting the State of Climate Warming Using Time Series Analysis (Case Study: Aligudarz). Applied Researches in Water Engineering, 1(1), 85-98.

Salik, A.W. & Karacabey, E. (2019). Application of Landsat 8 Satellite Image – NDVI Time Series for Crop Phenology Mapping: Case Study Balkh and Jawzjan Regions of Afghanistan. Çanakkale Onsekiz Mart University, Journal of Graduate School of Natural and Applied Sciences, 5(1), 49-62.

Sarmento, R.P. & Costa, V. (2019). An Overview of Statistical Data Analysis. Arxiv, https://arxiv.org/abs/1908.07390

Sayah, M. J., Abdallah, Ch., Khouri, M., Nedjai, R. & Darwich, T. (2020). A framework for climate change assessment in Mediterranean data-sparse watersheds using remote sensing and ARIMA modeling. Theoretical and Applied Climatology, 143, 639-658.

Sayemuzzaman, M. & Jha, M.K. (2014). Seasonal and annual precipitation time series trend analysis in North Carolina, United States. Atmospheric Research, 137, 183-194.

State of Idaho. (2011). Idaho land cover dataset standard, (Version 1.0), State of Idaho.

Suryavanshi, SH., Joshi, N., Maurya, H.K., Gupta, D. & Sharma, K.K. (2022). Understanding precipitation characteristics of Afghanistan at provincial scale. Theoretical and Applied Climatology, 150, 1775-1791.

Tang, W., Zhou, Ji., Ma, J., Wang, Z., Ding, L., Zhang, X. & Zhang, X. (2024). RIMS LST: A daily 1-km all-weather land surface temperature dataset for the Chinese landmass and surrounding areas (2000-2021). Earth System Science Data, 16(1), 387-419.

Tehrani, N.A., Janalipour, M. & Bagheri, M. (2022). Drought Potential Mapping using Remote Sensing Indices and Artificial Neural Networks (Case study: Kermanshah Province, Iran). Iranian Journal of ECO HYDROLOGY, 9(2), 387-402.

Thilagaraj, P., Masilamani, P., Venkatesh, R. & Killivalavan, J. (2021). GOOGLE EARTH ENGINE BASED AGRICULTURAL DROUGHT MONITORING IN KODAVANAR WATERSHED, PART OF AMARAVATHI BASIN, TAMIL NADU, INDIA. The International Archives of the Photogrammetry, Remote Sensing and Spatial Information Sciences, https://doi.org/10.5194/isprs-archives-XLIII-B5-2021-43-2021

United Nations Environment Programme. (2023). Afghanistan's climate change vulnerability assessment. UNEP.

Xu, H., Ge, Zh. & Ao, W. (2024). Research on Climate Change Prediction based on ARIMA Model and its Impact on Insurance Industry Decision-Making. Frontiers in Computing and Intelligent Systems, 8(1), https://doi.org/10.54097/3r7nkd35

YAMAN, Ş. (2023). Orman Sağlığının Google Earth Engine İle İzlenmesi. K.T.Ü.,Fen Bilimleri Enstitüsü, Yüksek Lisans Tezi, Trabzon.

Yu, T., Jiapaer, G., Bao, A., Zhang, J., Tu, H., Chen, B., Maeyer, P. & Voorde, T.V.D. (2022). Evaluating surface soil moisture characteristics and the performance of remote sensing and analytical products in Central Asia. Journal of Hydrology, 617, https://doi.org/10.1016/j.jhydrol.2022.128921

Zha, X., Xiong, L., Liu, CH., Shu, P. & Xiong, B. (2022). Identification and evaluation of soil moisture flash drought by a nonstationary framework considering climate and land cover changes. Science of the Total Environment, 856(2), http://dx.doi.org/10.1016/j.scitotenv.2022.158953

Zhao, B., Mao, K., Cai, Y., Shi, J., Li, Zh., Qin, Zh., Meng, X., Shen, X. & Guo1, Zh. (2020). A combined Terra and Aqua MODIS land surface temperature and meteorological station data product for China from 2003 to 2017. Earth System Science Data, 12(4), 2555-2577.

Zhao, X., Xia, H., Pan, L., Song, H., Niu, W. & Qin, Y. (2021). Drought Monitoring over Yellow River Basin from 2003–2019 Using Reconstructed MODIS Land Surface Temperature in Google Earth Engine. Remot Sensing, 13(18), https:// doi.org/10.3390/rs13183748

Zo, H., Ge, Zh. & Ao, w. (2024). Research on Climate Change Prediction based on ARIMA Model and its Impact on Insurance Industry Decision-Making. Frontiers in Computing and Intelligent Systems, 8(1), https://doi.org/10.54097/3r7nkd35

URL-1. (2024, July 05). Afghanistan Information Network: https://cl.gy/wAJkR.

URL-2. (2024, July 28). Iranian Students Nwes Agency: https://rb.gy/c1ylxa.

URL-3. (2024, July 28). Iran Remote Sensing Academy Company: https://rb.gy/6t268e.

URL-4. (2024, July 29). School of Remote Sensing: https://rb.gy/zgwo9f.

URL-5. (2024, July 30). Wikipedia: https://rb.gy/47us84.

URL-6. (2024, July 31). Mahamax: https://rb.gy/k5ch4m.

URL-7. (2024, July 31). https://cl.gy/mNoSh.

URL-8. (2024, August 02). Mohammad Mohammad Khani: https://cl.gy/XdGoN.

URL-9. (2024, July 31). National Weather Service: https://cl.gy/rjJmw.

URL-10. (2024, July 31). Google Earth Engine: https://earthengine.google.com/.

URL-11. (2024, August 01). Wikipedia: https://cl.gy/SGOlg.

URL-12. (2024, August 01). Analytics Vidhya: https://cl.gy/ccfaY.

URL-13. (2024, August 02). Consulate General of the Islamic Republic of Iran: https://cl.gy/tQOLc.

URL-14. (2024, August 02). Climate Change Adaptation: https://cl.gy/qkazd.

URL-15. (2024, August 06). ARM Weblog: https://cl.gy/iBpLw.

URL-16. (2024, August 25). https://tinyurl.com/39v5nsdn

RESUME

I am Abdul Basit YARASH. I started school in 2000 year, and I graduated from Kaftar Ali High School, Yangi Qala District, Takhar Province in 2013. In the same year, I passed the university entrance exam, and entered the Department of Geodesy, Jawzjan University. Then in 2018 year, I graduated from Jawzjan University. After graduating from university, I worked in the surveying and design departments of both governmental and private institutions. In 2019, I started teaching in the academic field. And in 2021, I received the Turkish scholarship to continue my studies in geomatics engineering at Karadeniz Technical University. After entering the field of geomatics engineering, I was very interested in remote sensing, and in this sense, with the guidance of Assoc. Prof. Dr. Volkan YILMAZ, I prepared my Master Thesis with the title "Investigation of The Effects of Climate Change in Afghanistan Using Remote Sensing Techniques".